Discrete Modeling and Sliding Mode Control of Piezoelectric Actuators

A Thesis Submitted to the College of

Graduate Studies and Research

In Partial Fulfillment of the Requirements

For the Degree of Doctor of Philosophy

In the Department of Mechanical Engineering

University of Saskatchewan

Saskatoon

By

Yu Cao

Permission to Use

In presenting this thesis in partial fulfillment of the requirements for a Postgraduate degree from the University of Saskatchewan, I agree that the Libraries of this University may make it freely available for inspection. I further agree that permission for copying of this thesis in any manner, in whole or in part, for scholarly purposes may be granted by the professor or professors who supervised my thesis work or, in their absence, by the Head of the Department or the Dean of the College in which my thesis work was done. It is understood that any copying or publication or use of this thesis or parts thereof for financial gain shall not be allowed without my written permission. It is also understood that due recognition shall be given to me and to the University of Saskatchewan in any scholarly use which may be made of any material in my thesis.

Requests for permission to copy or to make other use of material in this thesis in whole or part should be addressed to:

Head of the Department of Mechanical Engineering

University of Saskatchewan

Saskatoon, Saskatchewan S7N 5A9

Abstract

With the ability to generate fine displacements with a resolution down to sub-nanometers, piezoelectric actuators (PEAs) have found wide applications in various nano-positioning systems. However, existence of various effects in PEAs, such as hysteresis and creep, as well as dynamics can seriously degrade the PEA performance or even lead to instability. This raises a great need to model and control PEAs for improved performance, which have drawn remarkable attention in the literature. Sliding mode control (SMC) shows its potential to the control of PEA, by which the hysteresis and other nonlinear effects can be regard as disturbance to the dynamic model and thus rejected or compensated by its switching control. To implement SMC in digital computers, this research is aimed at developing novel discrete models and discrete SMC (DSMC)-based control schemes for PEAs, along with their experimental validation.

The first part of this thesis concerns with the modeling and control of one-degree of freedom (DOF) PEA, which can be treated as a single-input-single-output (SISO) system. Specifically, a novel discrete model based on the concept of auto-regressive moving average (ARMA) was developed for the PEA hysteresis; and to compensate for the PEA hysteresis and improve its dynamics, an output tracking integrated discrete proportional-integral-derivative-based SMC (PID-SMC) was developed. On this basis, by making use of the availability of PEA hysteresis models, two control schemes, named “the discrete inversion feedforward based PID-SMC” and “the discrete disturbance observer (DOB)-based PID-SMC”, were further developed. To illustrate the effectiveness of the developed models and control schemes, experiments were designed and conducted on a commercially available one-DOF PEA, as compared with the existing ones.

The second part of the thesis presents the extension of the developed modeling and control methods to multi-DOF PEAs. Given the fact that details with regard to the PEA internal

configurations is not typically provided by the manufacturer, a state space model based on the black box system identification was developed for the three-DOF PEA. The developed model was then integrated in the output tracking based discrete PID-SMC, with its effectiveness verified through the experiments on a commercially available three-DOF PEA. The superiority of the proposed control method over the conventional PID controller was also experimentally investigated and demonstrated. Finally, by integrating with a DOB in the discrete PID-based SMC, a novel control scheme is resulted to compensate for the nonlinearities of the three-DOF PEA. To verify its effectiveness, the discrete DOB based PID-SMC was applied in the control experiments and compared with the existing SMC.

The significance of this research lies in the development of the discrete models and PID-based SMC for PEAs, which is of great help to improve their performance. The successful application of the proposed method in the control of multi-DOF PEA allows the application of SMC to the control of complicated multi-inputs-multi-outputs (MIMO) systems without details regarding the internal configuration. Also, integration of the inversion based feedforward control and the DOB in the SMC design has been proven effective for the tracking control of PEAs.

Acknowledgements

I would like to express my sincere and earnest gratitude to my supervisor, Prof. Daniel Chen, for the guidance and support he showed to me throughout my PhD program. His patient encouragement enabled me continuously reach my research goals. His immense knowledge and enthusiasm inspired me to explore each challenge in my research. I can hardly imagine a successful research without the help from my supervisor.

I also would like to take this opportunity to express my sincerest appreciation to my family, my father and mother, Hongxin Cao and Jiaming Dong, and to my grandma, Cuilian Si. They have continuously been supported with me their love and patience. I will always be grateful that they offer me with confidence, whenever I encountered problems in my life. I hope that I have made them proud. They deserve it.

I am sincerely and heartily grateful to the members of my Advisory Committee: Prof. Richard Burton, Prof. Fangxiang Wu and Prof. Aryan Saadat Mehr for their examination and advices in my research program. Their gifted and enthusiastic teaching grants me inspiration in my research.

My thanks also extend to Mr. Doug Bitner in the Department of Mechanical Engineering for his technical assistance for my experiments.

Special thanks to my honorific classmate Dr. Jinyang Peng, who helped me a lot in writing my dissertation. It is also my great pleasure to thank my friends for their help and support during my research. They are Lezhi Yang, Jianwei Li, Lu Wang, Zhen Wang and Ning Zhu.

Finally, I gratefully acknowledge the financial support from the Chinese Scholarship Council (CSC) and Natural Science and Engineering Research Council (NSERC)

Contents

Permission to Use i
Abstract ii
Acknowledgements iv
List of Figures x
List of Tables xiii
List of Abbreviations xv
1 Introduction and Objectives 1
1.1 Introduction 1
1.2 Literature Review 4
1.3 Objectives 5
1.4 Organization of the Dissertation 6
1.5 Contribution of the Primary Investigator 10
2 A Survey of Modeling and Control Issues for Piezoelectrc Actuators 11
2.1 Abstract 11
2.2 Introduction 12
2.3 Piezoelectric Actuators 14
2.3.1 One-DOF Piezoelectric Actuators 14
2.3.2 Multi-DOF Piezoelectric Actuators 15
2.4 Model and Control Issues of Piezoelectric Actuators 16
2.4.1 Creep 17
2.4.2 Hysteresis 17
2.4.3 Dynamics 25
2.4.4 Model Uncertainty 27
2.5 Control Approaches for Piezoelectric Actuators 30
2.5.1 Charge Control 31
2.5.2 Feedback Control 32
2.5.3 Inverse Feedforward Control 33
2.5.4 Iterative Learning Control 35
2.6 Emerging Issues in Control of Piezoelectric Actuators 36
2.6.1 Disturbance Rejection 36
2.6.2 Discrete Controller Design 43
2.6.3 Controller for Multi-DOF Piezoelectric Actuators 45
2.7 Summary 49
2.8 Acknowledgement 52
3 Model of One-DOF Piezoelectric Actuators 53
3.1 Introduction and Objectives 53

3.2 Methods 53
3.3 Results 54
3.4 Contributions 55
3.5 Paper: A Novel Discrete ARMA-based Model for Piezoelectric Actuator Hysteresis 55
3.5.1 Abstract 55
3.5.2 Introduction 56
3.5.3 DiscreteARMA-based Hysteresis Model 58
3.5.4 Parameter Identification 64
3.5.5 Experiments and Results 65
3.5.6 Conclusions and Discussions 73
3.5.7 Acknowledgment 74
4 Discrete Sliding Mode Control for One-DOF Piezoelectric Actuators 75
4.1 Introduction and Objectives 75
4.2 Methods 76
4.3 Results 78
4.4 Contributions 78
4.5 Paper: An Output Tracking Integrated Discrete PID-based Sliding Mode Control on SISO Systems 79
4.5.1 Abstract 79
4.5.2 Introduction 80
4.5.3 Output Tracking Integrated PID-based Sliding Mode Control 82
4.5.4 Experiments 94
4.5.5 Conclusion 106
4.5.6 Acknowledgment 107
5 Inversion-based Sliding Mode Control and Disturbance Observer based Sliding Mode Control for One-DOF Piezoelectric Actuators 108
5.1 Introduction and Objectives 108
5.2 Methods 108
5.3 Results 110
5.4 Contributions 110
5.5 Paper: Two Modified Discrete PID-based Sliding Mode Controllers for Piezoelectric Actuators 111
5.5.1 Abstract 111
5.5.2 Introduction 112
5.5.3 Discrete PID-based SMC 115
5.5.4 Inversion based PID-SMC for Piezoelectric Actuator Hysteresis 119
5.5.5 DOB-based PID-SMC for Piezoelectrc Actuator Hysteresis 120
5.5.6 Experiments and Results 122
5.5.7 Conclusions and disscussions 132
5.5.8 Appendix 133
5.5.9 Acknowledgment 135

6 Model of the Multi-DOF Piezoelectric Actuators....136
6.1 Introduction and Objectives....136
6.2 Methods....136
6.3 Results....137
6.4 Contributions....137
6.5 Paper: State Space System Identifcation of three-DOF Piezo-actutator Driven Stages with Unknown Configuration....138
6.5.1 Abstract....138
6.5.2 Introduction....139
6.5.3 Black Box System Identification....141
6.5.4 Experiments and Results....147
6.5.5 Conclusions and Discussions....160
6.5.6 Acknowledgment....161
7 Discrete Sliding Mode Control for Multi-DOF Piezoelectric Actuators....162
7.1 Introduction and Objectives....162
7.2 Methods....163
7.3 Results....163
7.4 Contributions....164
7.5 Paper: An Output Tracking based Discrete PID-Sliding Mode Control on MIMO Systems....164
7.5.1 Abstract....164
7.5.2 Introduction....165
7.5.3 Output Tracking based Discrete PID-SMC for MIMO systems....168
7.5.4 Experiments....181
7.5.5 Conclusion....194
7.5.6 Acknowledgment....194
7.5.7 Appendix....195
8 Disturbance Observer based Sliding Mode Control for Multi-DOF Piezoelectric Actuators 198
8.1 Introduction and Objectives....198
8.2 Methods....198
8.3 Results....200
8.4 Contributions....200
8.5 Paper: Disturbance Observer based Sliding Mode Control for a Three-DOF Nano-positioning Stage....200
8.5.1 Abstract....201
8.5.2 Introduction....201
8.5.3 DOB-SMC for the Three-DOF Nano-positioning Stage....204
8.5.4 Experiments and Results....213
8.5.5 Conclusions and Discussion....221
8.5.6 Acknowledgment....222

9 Conclusions and Future Work 223
9.1 Concluding Remarks 224
9.2 Future Work 226
References 229
Copyright permission 252

List of Figures

Figure 1. 1 Diagram of the general idea and major steps of the present research 7

Figure 2. 1 Typical structure of PEAs 15
Figure 2. 2 Hysteresis and the memory effect [12] 18
Figure 2. 3 Hysteresis mappling [33] 20
Figure 2. 4 PI operator [34] 21
Figure 2. 5 Initial loading curve [34] 22
Figure 2. 6 Series of rate-independent hysteresis and linear dynamics 26
Figure 2. 7 Grounded load charge amplifier [70] 31
Figure 2. 8 Inverse feedforward control 33
Figure 2. 9 Inverse feedforward based feedback control 34
Figure 2. 10 Iterative control [76] 35
Figure 2. 11 Structure of a disturbance observer-based controller [81] 37
Figure 2. 12 Schematic of a system that considers hysteresis to be a disturbance to the dynamics of a PEA [82] 38
Figure 2. 13 Control scheme of sliding mode 40
Figure 2. 14 Comparison of discrete and continuous controllers 44
Figure 2. 15 Quantization error in sampling and holding module 45
Figure 2. 16 Difference between the continuous and discrete SMC systems [100] 45
Figure 2. 17 Schematic of a PID controller combined with linearized feedback and a repetitive controller [17] 47
Figure 2. 18 Control system structure with control allocation performing separately [112] 49

Figure 3. 1 ARMA-based hysteresis model 54
Figure 3. 2 Quadratic estimation of the integral term 61
Figure 3. 3 Experimental settings on the piezoelectric driven stage 66
Figure 3. 4 Input voltage for the model verification 67
Figure 3. 5 Comparsion of experimental results and simulation results under inputs with a fixed amplitude of 70 V and different frequencies 69
Figure 3. 6 Comparison of experimental results and simulation results and the errors 72

Figure 4. 1 Inversion based approach for the discrete PID-based SMC 77
Figure 4. 2 Decomposition of the discrete SISO plant 83
Figure 4. 3 Equivalent plant for the design of $\Delta v(k)$ 85
Figure 4. 4 Model reference approach of the SMC design 88

Figure 4. 5 Step tracking performance (20000 Hz sampling rate) of the proposed method designed by the inversion approach 97
Figure 4. 6 Step tracking performance (1000 Hz sampling rate) of the proposed method designed by the inversion approach 98
Figure 4. 7 Step tracking performance of the proposed method designed by model reference approach at the 20000 Hz sampling rate 100
Figure 4. 8 Reference signals in the control verification 101
Figure 4. 9 Tracking performance of the proposed method and the continuous PID-based SMC at 5000 Hz sampling rate for different reference signals 103
Figure 4. 10 Comparison of tracking errors as controlled by the discrete and continuous PID-based SMC with different sampling rates 106

Figure 5. 1 Inversion based PID-SMC 109
Figure 5. 2 DOB-based PID-SMC 110
Figure 5. 3 Block diagram of a discrete *n*th order SISO system: $f(z)$ and $y(z)$ is the input and output of the dynamics respectively, $v(z)$ is a middle variable 115
Figure 5. 4 Cascade model of PEA 119
Figure 5. 5 Hysteresis of PEA 120
Figure 5. 6 Experimental settings on the piezoelectric driven stage 123
Figure 5. 7 Hysteresis identification 125
Figure 5. 8 Comparison of the tracking performance controlled by different methods 129
Figure 5. 9 Hysteresis compensation by the inversion feedforward control (Sinusoidal input with 10 um amplitude and 1 Hz frequency) 130

Figure 6. 1 Experimental settings on the piezo-actuator driven stage 148
Figure 6. 2 Linearity of the 3-DOF piezo-actuator driven stage 149
Figure 6. 3 Flow chart of black box system identification 151
Figure 6. 4 Estimation error changes with *p* when reference input was applied in Channel 1 152
Figure 6. 5 Comparison of experimental results and model prediction under 10 um 10 Hz sinusoidal input in Channel 1 158
Figure 6. 6 Comparison of experimental results and model prediction from combined inputs to all three channels 159

Figure 7. 1 Equivalent plant for SMC 178
Figure 7. 2 Step tracking performance of the 3-DOF nano-positioning stage 187
Figure 7. 3 Tracking performance of the discrete PID-based SMC designed by model reference approach for the 2 Hz 10 μm sinusoidal input in Z direction and 5 Hz 50 μrad sinusoidal input in *Rx* direction 192

Figure 7. 4 Tracking performance of the discrete PID-based SMC designed by mode reference approach for the 5 Hz 10 μm PWSW input in Z direction and 10 Hz 50 μrad SW input in *Ry* direction 193

Figure 8. 1 Control scheme of the DOB-based SMC 199
Figure 8. 2 Control scheme with the disturbance observer..... 205
Figure 8. 3 Block diagram of a discrete *n*th order SISO system..... 209
Figure 8. 4 Tracking performance of the discrete PID-based SMC designed by model reference approach as compared with the three nominal PID-based SMC (stated as 3-SMC) introduced in [13]..... 219
Figure 8. 5 Tracking performance of the discrete PID-based SMC designed by model reference approach as compared with the three nominal PID-based SMC (3-SMC) introduced in [13]... 220

List of Tables

Table 3- 1 Identifcation results of the discrete ARMA based hysteresis model developed by trapezoid equation estimation based on the least square method 68
Table 3- 2 Identification results of the discrete ARMA based hysteresis model developed by trapezoid equation estimation based on the online estimation method..... 68
Table 3- 3 Identification results of the discrete ARMA based hysteresis model developed by quadratic equation estimation based on the least square method 68
Table 3- 4 Identification results of the discrete ARMA based hysteresis model developed by quadratic equation estimation based on the online estimation method..... 68
Table 3- 5 Inputs used for model verification 71
Table 3- 6 Error estimated from the discrete ARMA-based hysteresis model developed by trapezoid equation and the existing discrete model 71
Table 3- 7 2-norm error for the discrete ARMA-based hysteresis model developed by using different discrete method 73

Table 4- 1 Identified parameters for the dynamic model 95
Table 4- 2 Parameters adjusted in the proposed method for different sampling rates (traditional SMC design approach)..... 96
Table 4- 3 Parameters adjusted in the proposed method for different sampling rates (model reference approach)..... 99
Table 4- 4 Parameters adjusted in the proposed method for different sampling rates (model reference approach)..... 102
Table 4- 5 Comparison of the tracking performance between the proposed method and the continuous PID-based SMC at 20000 Hz sampling rate 104
Table 4- 6 Comparison of the tracking performance between the proposed method and the continuous PID-based SMC at 5000 Hz sampling rate 104

Table 5- 1 Inputs in the experiments..... 124
Table 5- 2 Parameters in the experiments for the first part..... 127
Table 5- 3 Comparison of the tracking performance controlled by different methods in the experiments for the first part..... 127
Table 5- 4 Parameters in the experiments for the second part 131
Table 5- 5 Comparison of the tracking performance controlled by different methods in the experiments for the second part 132

Table 6- 1 Motion range and resolution in each DOF 148
Table 6- 2 Model prediction error if chirp inputs were applied 153
Table 6- 3 Model prediction error if random inputs were applied 153
Table 6- 4 Estimation error from the chirp input in channel 1 154
Table 6- 5 Estimation error from the chirp input in channel 2 155
Table 6- 6 Estimation error from the chirp input in channel 3 155
Table 6- 7 Estimation error by applying the online estimation method 157
Table 6- 8 Estimation error by applying the identification method introduced in [16] 157

Table 7- 1 Notations used in the equations 171
Table 7- 2 Estimation error under chirp inputs in each channel 185
Table 7- 3 PID parameters adjusted for the PID controller 189
Table 7- 4 Comparison of the tracking performance between the discrete PID-based SMC and PID controller 189

Table 8- 1 PID parameters adjusted for the DOB-based SMC and nominal SMC 216
Table 8- 2 Tracking error by means of the DOB-based SMC 217
Table 8- 3 Tracking error by means of the nominal PID-based SMC 217

List of Abbreviations

3D	Three dimensional
AFM	Atomic force microscope
ARMA	Auto-regressive moving average
ARX	Auto-Regressive Exogenous
CLS	Canadian Light Source
CSC	China Scholarship Council
CSMC	Continuous SMC
DOB	Disturbance observer
DOF	Degree of freedom
DSMC	Discrete SMC
DVD	Digital video disc
HOSMC	High order sliding mode control
ILC	Iterative learning control
MAP	Maximum-a-posteriori
MIMO	Multi-inputs-multi-outputs
MOESP	Multivariable output-error state space
N4SID	Numerical algorithms for subspace state space system identification
NARMAX	Nonlinear auto-regressive moving average model with exogenous inputs
NSERC	Natural Sciences and Engineering Research Council
P	Proportional
PEA	Piezoelectric actuator
PI	Prandtl-Ishlinskiĭ
PI	Proportional-integral
PID	Proportional-integral-derivative
PID-SMC	PID-based SMC
PZT	Lead zirconate titanate
RGA	Real-coded genetic algorithm
SISO	Single-input-single-output
SMC	Sliding mode control
STM	Scanning tunnelling microscope
SVD	Singular value decomposition

1 Introduction and Objectives

1.1 Introduction

Piezoelectric actuators (PEAs) have been widely used in nano-positioning applications due to their high stiffness, fast response and the capability to produce extremely small displacement down to 0.1 nm as well as large force [1]. However, the positioning precision can be greatly degraded by their nonlinear behavior such as hysteresis [2]. To successfully exploiting the full potential of PEAs in nano-positioning applications, modeling and control for PEAs have drawn considerable attention [3]-[83]. The models developed to describe the PEA hysteresis can be generally divided into two categories: the physical based models and the phenomenon based models. The physical based models are derived from the laws with clear physical meaning [25]. But due to their complicated forms, they are limited as applied to the control of PEAs. The phenomenon based models, such as Prandtl-Ishlinskiĭ (PI) model [34], Preisach model [26]-[32] and Duhem model [11], utilize mathematical methods to describe the hysteresis based on the experimental data, regardless of their physical meaning. These models have relatively simple forms compared to the physical models and have been applied in the control of PEA.

The hysteresis effect greatly deteriorates the performance of PEAs, for example, the tracking error can reach to 15%-20% of the stroke in the open-loop operation [2]. As a result, closed loop controllers are used in nano-positioning applications to improve their tracking performance. Among them, Proportional-integral-derivative (PID) controllers are simple and commonly

employed in PEA-driven nano-positioning systems to compensate for their nonlinear effects, including hysteresis and creep [2], [23]. The challenge to apply the PID controller is the improvement of performance while maintaining the system stability with the presence of parameter uncertainty and disturbance, and its low gain margin problem in high frequency operation. To improve the robustness of the control system, advanced feedback controllers such as the H_∞ and H_2 controller have been developed in nano-positioning control systems [4], [47], [72]. As an alternative method to compensate for the hysteresis, feedforward control, which is model based, does not share the stability problem of the feedback approach. Therefore, significant improvement can be made at high frequencies. However, this approach cannot account for the external disturbance and modeling uncertainties [2], [7], [10], [12], [34].

Sliding mode control (SMC) becomes the subject of research due to its great promising performance, even with the presence of system nonlinearity and uncertainty [84]-[93]. However, chattering, caused by the discontinuous switching control in SMC, may excite the high frequency resonant vibration, thereby degrading control performance and potentially even damaging the actuators being controlled. To resolve the chattering problem, boundary layer control has been employed by researchers [94], in which a saturation function is used to replace the discontinuous 'bang-bang' switching control. If the unknown disturbance is significant, a sufficiently high gain control is needed. To alleviate this problem, one alternative way is to use a high order sliding surface instead of the first order one in the nominal SMC. With the merits of the SMC, the high order sliding mode control (HOSMC) can reduce the chattering effect [95], [96], which, however, is limited by the increased sliding information for its implementing. A new continuous PID-based

SMC (PID-SMC) for PEAs is recently developed, in which the discontinuous 'bang-bang' switching function is replaced by a PID regulator to eliminate chattering. Experimental results demonstrate that the PID-based SMC can effectively compensate for the hysteresis existing in a PEA, thus leading to an improved PEA performance [98].

Although the advances have made in the past decades with regard to the modeling and control of PEA, there are still a number of issues that need to be addressed by research. The present study is aimed to address some of them, particularly in the discrete domain. These issues are briefly outlined as follows, with details discussed in the literature review.

SMC stands out for its merits in the uncertainty and disturbance rejection, as well as the improved control efficiency over the feedforward controller. The issue here is whether it is effective to use SMC in conjunction with the feedforward control or the disturbance observer (DOB) to reduce the effects caused by the disturbance and uncertainties.

Second, it is noted that the existing PID-based SMC is essentially a state tracking control scheme. In some applications, the system states might not be readily or even impossibly obtained due to system complexity. In such case, the application of the existing PID-based SMC is challenged due to the lack of system states information.

Third, when implemented in a digital computer, the existing continuous SMC (CSMC) may not work as expected due to quantization error made by data sampling. For discrete SMC (DSMC), if the switching time doesn't match the sampling time, the state will not stay on the sliding surface and the trajectory appears like a zigzag motion around the sliding surface, which suggests that the sampling itself also induces the chattering problem in the DSMC. Moreover, if

the mean of zigzag motion deviates from the sliding surface, steady state error will exist. Therefore, the appropriate forms of DSMC are desirable to alleviate the aforementioned problems, especially for the applications where the sampling rate is limited.

Fourth, the existing PID-based SMC for the single-input-single-output (SISO) system is developed based on the one-DOF dynamic performance. Its application can be extended to the control of multi-inputs-multi-outputs (MIMO) system with one PID-based SMC designed for each pair of input and output independently. However, adjusting controller parameters of one loop affects the performance of another, sometimes even to the extent of destabilizing the entire system. The cross-coupling effects caused by the multivariable interactions accounts for essential difference in design methodologies between single variable and multi-variable control systems. Inspired by this, it is desired to extend the application of PID-based SMC to the control of MIMO systems.

1.2 Literature Review

A manuscript on the literature review was appended with this thesis in Chapter 2, which was recently submitted to *ASME Journal of Dynamic System, Measurement and Control* for possible publication. This manuscript presents a review on the recent achievements in modeling and control techniques for PEAs. Particularly, the existing methods for modeling hysteresis, creep, and vibration dynamics in PEAs are examined. Issues associated with the modeling errors are discussed along with the justification of the need of present research. Discussions are also given to various control schemes developed for PEAs. The literature review is essential for the author

to understand the current challenges in the control of PEAs, and establish the objectives of the present research as given in the following section.

1.3 Objectives

This research is aimed at developing a discrete feedforward or DOB-based SMC to improve the PEA performance and implementing it digitally. To fulfill this requirement, the following objectives are set.

① Model the PEAs to describe their behavior.

Hysteresis is an important nonlinear effect exhibited by PEAs. To develop the control scheme for the PEA, a phenomenon based hysteresis model will be developed and then combined with the models for their dynamics, forming an integrated model for the one-DOF PEA behavior. For the multi-DOF PEA with available information regarding its internal configuration, the one-DOF model can be extended to the multi-DOF PEA application by means of physical laws. If such details are not available, a state space model based on the black box system identification will be employed to describe the dynamic performance, with its parameters estimated from the Hankel matirx.

② Develop output tracking integrated discrete PID-SMC for PEAs.

To compensate for the hysteresis and improve the performance of PEA, an output tracking integrated discrete PID-SMC along with the controller design approach will be developed for the one-DOF PEA. Without the need of system states, this method allows for eliminating chattering problem and the steady state error that may exists in such control methods as the continuous

PID-based SMC. Then the aforementioned method will be extended to the control of a three-DOF piezoelectric-driven stage. Cross-coupling effects among the inputs and outputs are to be considered in the design of the equivalent control. Using the model reference approach, the output tracking problem is transferred to a sub-state tracking problem on which the general SMC design approach can apply. The stability and zero steady state error of the proposed method will be theoretically proven. To demonstrate the effectiveness of the developed methods, experiments will be carried out on the commercially available piezoelectric actuators with varying sampling rates, as compared to other methods.

③ Develop a discrete feedforward or DOB based SMC by integrating the feedforward control or DOB in the DSMC developed previously.

The feedforward controller will be strategically combined with the DSMC developed previously to control the PEA. By employing the feedforward control, the low gain margin problem of the feedback approach can be alleviated. The feedforward control error caused by the model uncertainty will be considered as the disturbance to the dynamics of the PEA and rejected by means of the switching control in DSMC. Another approach to improve the performance of the discrete PID-based SMC is to integrate the DOB with the DSMC, in which the disturbance is partially predicted and compensated by the equivalent control, thus reducing the disturbance rejected by the switching control.

1.4 Organization of the Dissertation

Figure 1.1 shows the diagram of the general idea and major steps of the present research.

Based on the desired steps, this dissertation is comprised of eight chapters. Each of the first seven chapters mainly consists of a manuscripts appended with this thesis; and the last chapter presents the conclusions drawn from this research, followed by suggestions and recommendations for possible future work.

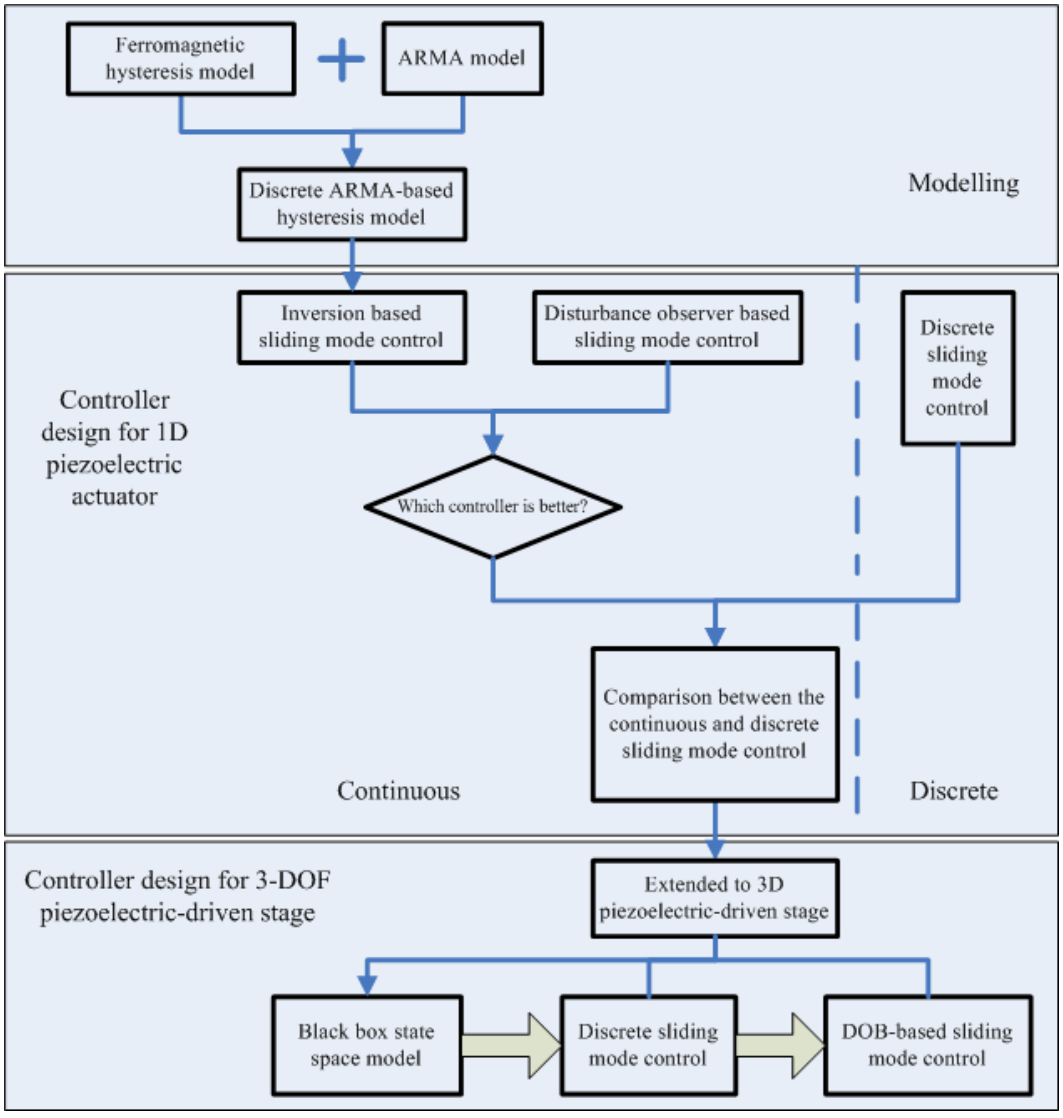

Figure 1. 1 Diagram of the general idea and major steps of the present research

Specifically, a discrete ARMA based hysteresis model was developed for a one-DOF PEA, as detailed in Chapter 3, where the performance was considered as a cascade of the hysteresis nonlinearity and the dynamics. Both the trapezoid estimation and the quadratic estimation were employed in the discretization of the hysteresis model. They are finally compared in the model verification experiments and the superiority of the proposed discrete model over the existing model is demonstrated.

Based on the dynamic model, Chapter 4 concerned with the development of an output tracking based DSMC for the control of one-DOF PEA, in which the hysteresis and other nonlinearities were regarded as the disturbance rejected by the switching control of the DSMC. In order to eliminate chattering, a PID regulator was applied instead of the 'bang-bang' switching control. The effectiveness of the proposed method was verified through the experiments carried on the commercially available one-DOF PEA by comparing the tracking error with the continuous PID-based SMC. Control effects under varying sampling rates are investigated and compared as well.

It is noted that if the hysteresis can be modeled or partially modeled, integration of hysteresis models into control schemes may improve the performance of the controller. Inspired by this, DSMC was combined with the inversion feedforward control and the DOB respectively to control the PEA in Chapter 5. Improvement over the nominal DSMC was illustrated through verification experiments and comparison between these modified DSMCs was made as well.

Then, research work based on the one-DOF PEA was extended to the three-DOF PEA. As the detail information with regard to the internal mechanical configuration of the three-DOF PEA

was not provided by the manufacture, the straightforward modeling method by means of physical laws is not applicable. Instead, the three-DOF PEA is regarded as a black box system, with its state space model obtained by system identification. Online estimation was integrated, further improving the parameter estimation. The effectiveness of the developed model and the corresponding identification method and its superiority over the conventional identification were verified experimentally, as shown in Chapter 6.

In Chapter 7, the output tracking integrated discrete PID-SMC developed in Chapter 4 was extended to the control of the three-DOF PEA. Static decoupling was employed in the equivalent control design. The remaining dynamic decoupling was considered as disturbance to be rejected by the discrete PID-based SMC. Due to the ingenious design of the sliding surface, coupling effect between variables can be diminished to an acceptable extent. To verify the effectiveness of the output tracking integrated discrete PID-SMC, experiments were carried out on the three-DOF PEA, with its model being identified in Chapter 6. The control results were compared to the conventional PID controller.

The disturbance can also be pre-rejected by the use of DOB, leading to the development of the discrete DOB-based SMC for the three-DOF piezoelectric driven stage, which is the major work presented in Chapter 8. By integration with DOB, the plant can be decoupled as three independent SISO systems and controlled by the corresponding discrete PID-based SMC. Since the coupling effect was compensated by the use of DOB, the disturbance to be rejected by the discrete PID-based SMC was reduced. Therefore, the tracking error was expected less in comparison to the nominal SMC which had been verified in the experiments.

The verification experiments for the models and control schemes developed in the present research were carried on commercially-available PEAs (P-753 and P-558.TCD, Physik Instrumente).

1.5 Contribution of the Primary Investigator

All papers are co-authored; however it is mutual understanding of the authors that Yu Cao, as the first author, is the primary investigator of the research work. The contributions of other authors are limited to an advisory and editorial capacity and they are acknowledged.

2 A Survey of Modeling and Control Issues for Piezoelectrc Actuators

Authors: Y. Cao, X. B. Chen[1]

Index Terms: Piezoelectric Actuators, SISO, MIMO, Hysteresis, Model, Sliding Mode Control, Discrete Control

2.1 Abstract

Piezoelectric actuators (PEAs) have been widely used in nano-positioning applications due to their high stiffness, fast responses, and large actuating forces. However, the existence of its nonlinearities such as hysteresis greatly deteriorates their performance and as such model and control of PEAs have drawn remarkable attention in the literature. This paper reviews the recent achievements in modeling and control of PEAs. Specifically, the various existing methods for modeling hysteresis, creep, and vibration dynamics in PEAs are examined, followed by the discussions on the issues leading to the modeling errors. In the control of PEAs, the various

Manuscript received October 10, 2012. This work was supported by the China Scholarship Council (CSC) and the Natural Science and Engineering Research Council (NSERC) of Canada.

Y. Cao is with the Department of Mechanical Engineering, 57 Campus Drive, University of Saskatchewan, Saskatoon, SK, S7N 5A9 (e-mail: yuc150@ mail.usask.ca).

X. B. Chen is with the Department of Mechanical Engineering, 57 Campus Drive, University of Saskatchewan, Saskatoon, SK, S7N 5A9 (phone: 1-306-966-1267; e-mail: xbc719@ mail.usask.ca).

control schemes are introduced along with their corresponding advantages and disadvantages. The challenges associated with the control problem are also discussed.

2.2 Introduction

An increasing demand for high accuracy in production manufacturing and other devices has led to the rapid development of precision engineering. From its origin in mechanical engineering, it evolved into micro-mechanics and then nanotechnology [1]. Nanotechnology is the study of controlling matter on an atomic and molecular scale. Generally, nanotechnology deals with structures that are sized between 1 and 100 nanometers and it involves developing materials or devices within that size. The past two decades have witnessed a huge growth of nanotechnology. Invention of the scanning tunnelling microscope (STM) and the atomic force microscope (AFM) have fundamentally changed research in many areas, such as chemistry, biology, medical science, physics and mechatronic manufacturing [2]. Nanopositioning is the core of these nanotechnologies. In the Canadian Light Source (CLS), for example, the monochrometer must be controlled precisely on a nanometer scale in the diffraction enhanced imaging process [3]. Therefore, high precision manipulation plays an important role in the imaging-based research at the CLS.

PEAs have been widely used in nanopositioning applications, such as the aforementioned, due to their fast response, high stiffness and ability to generate large forces [4]. PEAs utilise the piezoelectric effect of piezoelectric ceramic materials. One commonly-used material for PEAs is lead zirconate titanate (PZT) [5]. The dipoles in PZT are randomly distributed in various

directions and, as such, the total force generated by each dipole balances out. If PZT is exposed to a DC electric field, the directions of the dipoles are aligned regularly, referred to as the polarization process. As a result, most of the dipoles align in the same direction as the electric field and a net force is generated. This causes a change in the length of the crystal elements in the piezoelectric crystal material. The typical change in length is less than 100 nm. Based on the polarization process, PEAs are used to move the stage in STM with a high resolution [6]-[9]. Unlike other actuators such as electric motors, PEAs can be configured so that there is no friction between moving parts.

The performance of PEAs can be, however, degraded by hysteresis, creep and vibration [10]. Hysteresis is a memory effect of various systems, occurring in such phenomena as plasticity friction and ferromagnetic superconductivity. The hysteresis exhibited at a given time instant depends not only on the input at the present time, but also on the operational history of the system [11]. If displacement of the PEA is plotted versus the input voltage, the hysteresis loop appears to have a shape similar to phase lag, which is not nonlinearity and exists in many linear systems. One of the most important characteristics that makes hysteresis different from phase lag is the memory effect [12].

Creep is another undesirable property of PEAs which results in loss of positioning precision when the PEAs are used for a long period of time. In particular, during slow operation or scanning in a monochrometer, creep can cause significant distortion in the image generated [3].

Vibration occurs when the input frequency is close to the resonant frequency of the PEA, which is typically quite high. Therefore, tracking precision is seriously deteriorated by vibration

in high frequency manipulation. In applications such as SPM, the scanning speed is typically chosen to be 10-100 times lower than the first resonant frequency of the PEA in order to reduce the vibration effect [2].

In the aforementioned properties, hysteresis is considered to be the most important nonlinear effect of PEAs. It can cause a tracking error of 15% in the total displacement range [2]. Therefore, the modeling and control of hysteresis has drawn considerable attention and a number of control schemes were developed for reducing the hysteresis effect. The aim of this review paper is to help the readers obtain a better understanding of the modeling and control issues for PEAs. To this end, it will be organized as follows. In section 2, categories and mechanical configuration of PEAs will be introduced. Creep, hysteresis and vibration, which present challenges to the control of PEAs, will be discussed in section 3, followed by control approaches in section 4 and emerging control issues in section 5. Finally, modeling and control issues will be summarized in section 6.

2.3 Piezoelectric Actuators

2.3.1 One-DOF Piezoelectric Actuators

A PEA is an electromechanical device that undergoes a dimensional change when a voltage is applied to both sides of the PEA. Due to the polarization process, the generated displacement is approximately proportional to the applied voltage and, therefore, can be adjusted with an extremely high resolution. One of the disadvantages of PEAs is the limited amount of

dimensional change. In order to extend the motion range, PEAs are commonly constructed by stacking piezoelectric slices. Figure 2.1 shows the typical configuration of a one-degree of freedom (DOF) PEA which is widely used in nano-positioning. The PEA is connected to a driven stage which moves by means of the deformation of the flexible hinges. As a result, friction and clearances in the macro-mechanical systems are avoided.

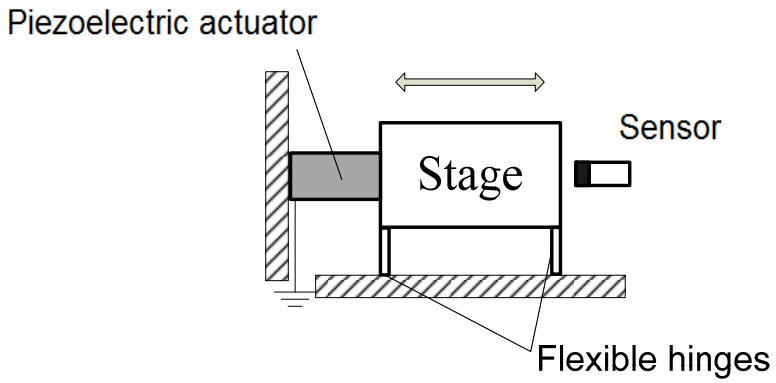

Figure 2. 1 Typical structure of PEAs

2.3.2 Multi-DOF Piezoelectric Actuators

Multi-DOF piezoelectric positioning systems are configured by means of several PEAs, which are connected through flexible joints. There are several studies on the design of three dimensional (3D) piezoelectric positioning systems. A three-DOF flexure-based parallel mechanism for nano-positioning was designed and fabricated in [13]. In that research, three PEAs were distributed symmetrically around a moving platform which was connected to the PEAs by flexure hinges. The translational and rotational displacement of the flexure based

mechanism reached 3 nm and 0.4 μrad, respectively. With the help of PID control, the dynamic overshoot of the positioning system was greatly reduced. A flexure-based XY stage for fast nano-positioning was described in [14]. Two PEAs were employed to actuate the nano-positioning stage. With special design of the flexure hinge, cross coupling of the XY axles was reduced to -35 dB. Similar designs can also be found in [15] and [16].

As an efficient approach to removing singularities over the workspace in parallel systems [17], redundancy actuation is being used more often in multi-DOF PEAs [18] - [21].With advantages of improving Cartesian stiffness, achieving uniform output forces and optimizing internal and external forces, it provides the positioning system with the ability of fault tolerance [22] so as to increase the availability and reliability of multi-DOF PEAs. However, the control of actuation redundant multi-DOF PEA is much more complicated than that of non-actuation redundant systems because the control of each actuator must be coordinated with the others to avoid the deformation or internal stress of the multi-DOF PEAs.

2.4 Model and Control Issues of Piezoelectric Actuators

As stated previously, the performance of PEAs can be greatly degraded by creep, hysteresis and vibration. An increased interest in using model-based control design techniques to improve the precision of the PEAs has been reported in the literature. The challenges of modeling and control of PEAs are discussed in this section.

2.4.1 Creep

Creep is an undesirable property of PEAs. It occurs when the input voltage is kept constant and the output displacement increases or decreases with time. As such, creep can result in significant tracking error if the PEAs are used for an extended period of time.

Piezoelectric creep is related to the effect of the applied voltage on the remnant polarization of the piezoceramic actuator [2]. When the operating voltage of a PEA is kept constant, remnant polarization continues which results in a slow displacement increase of the PEA. A negative change in the applied voltage would have the opposite effect.

Creep can be physically modelled as an infinite cascade of mass-spring-damper systems [6] or as a phenomenon-based model. For example, an exponential equation was used to represent the creep nonlinearity in [23] and [24]. Feedback control for hysteresis reduction can be employed to compensate for the creep effect and, as such, control for creep only is seldom reported in the literature.

2.4.2 Hysteresis

Hysteresis is a memory effect of PEAs. The hysteresis exhibited at a given time instant depends not only on the input at the present time, but also on the operational history of the system. One of the most important characteristics of hysteresis that differs from phase lag is the memory effect, as shown in Figure 2.2. As the input signal varies from point 1 to point 7 in Figure 2.2(a), one major and two minor loops are generated in the displacement/voltage

hysteretic domain as the result of these alternations. Then from point 7 to point 8, the input voltage increases and passes the point with the same magnitude as the extreme point 6, where the effect of turning points 6 and 7 and the properties of the inner loop are no longer useful for the remaining hysteresis and are wiped out. Instead, the hysteresis trajectory follows the path of the previously rising curve between points 5 and 6 towards the turning point 4.

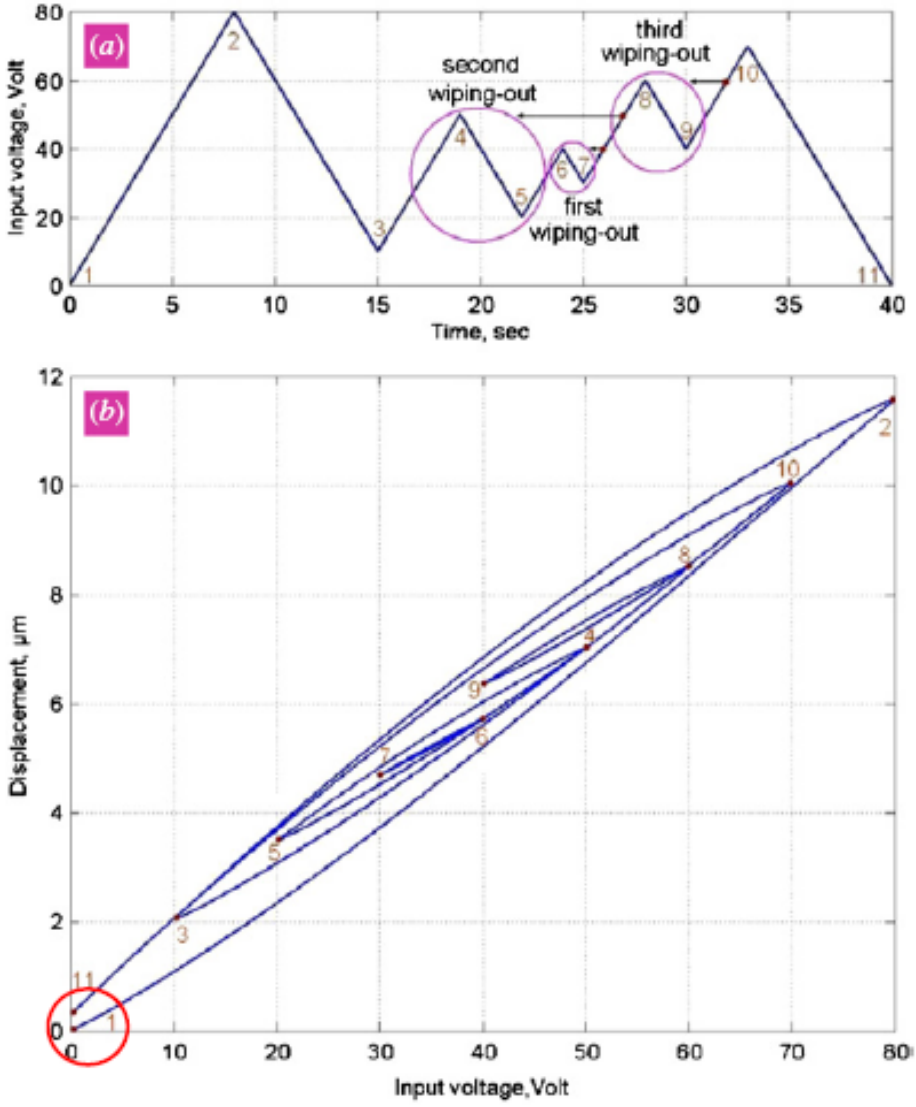

Figure 2. 2 Hysteresis and the memory effect [12]
(a) the input voltage to the PEA and (b) the output displacement versus the input voltage

The second wiping out happens when the input voltage exceeds the extreme point 4 and the internal loop associated with points 4 and 5 is no longer useful. Similarly, the trajectory continues along the path of the rising curve between points 3 and 4. The direction of input voltage change is reversed at point 8 and the trajectory goes down towards the turning point 3. The input voltage decreases from point 8 to 9, and then increases to a value equal to that of extreme point 8. At this point, the third wiping-out effect occurs with the trajectory following the path of the curve 3-8 up to point 10, where the direction of input voltage is changed one more time. The trajectory initiates from turning point 10, approaches and hits point 3 and continues along the path of curve 2-3 until the input voltage reaches its zero ending value.

In order to understand the performance of PEAs, several models have been developed to describe hysteresis, which can be divided into two categories: the physical-based model and the phenomenon-based model. The physical-based models are derived from the physical means of hysteresis and can be strictly verified [25]. One of the advantages of the physical-based models is their clear physical meaning. However, due to their complicated form, physical-based models are not commonly used in the control of PEAs. Phenomenon-based models for describing hysteresis, such as the Preisach, Prandtl-Ishlinskiĭ (PI) and Duhem models [11] utilize mathematical methods directly based on experimental data, regardless of the physical meaning. They are suitable for predicting the hysteresis performance of several materials and are widely used in research. However, the lack of physical meaning makes them difficult to understand. The following sections introduce hysteresis models typically used in the control of PEAs.

2.4.2.1 Preisach model

The Preisach model is a commonly used hysteresis model [26]-[32]. It employs a simple integral formula to describe the hysteresis effect,

$$H(t) = \iint \mu(\alpha, \beta)\hat{\gamma}_{\alpha,\beta}[u(t)]d\alpha d\beta \tag{2.1}$$

where $\mu(\alpha, \beta)$ is the weighting function of the hysteresis operator with two parameters α and β, $\hat{\gamma}_{\alpha,\beta}[u(t)]$ is the hysteresis operator and $u(t)$ is the input voltage. The hysteresis can be regarded as the integral of the hysteresis operator in the α-β plane, as shown in Figure. 2.3.

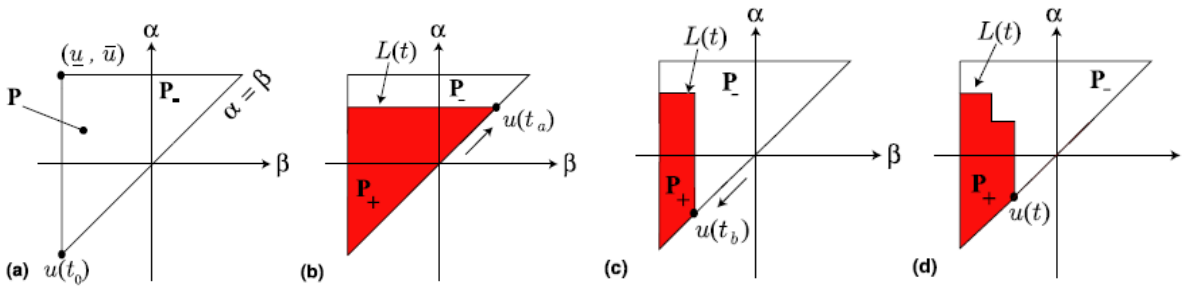

Figure 2. 3 Hysteresis mappling [33]

When the input voltage increases monotonically from $u(t_0)$ to $u(t_a)$, the interference line $L(t)$ moves horizontally from $\alpha = \alpha_{\min}$ to $\alpha = u(t_a)$. In the integral region below the interference line, $\hat{\gamma}_{\alpha,\beta}[u(t)] = 1$; and above this line, $\hat{\gamma}_{\alpha,\beta}[u(t)] = 0$. Therefore, the output displacement $H(t)$ can be written as

$$H(t) = \iint_{p+} \mu(\alpha, \beta)d\alpha d\beta . \tag{2.2}$$

As the input voltage decreases monotonically from $u(t_a)$ to $u(t_b)$, the interference line $L(t)$ moves vertically from $\beta = u(t_a)$ to $\beta = u(t_b)$. To the left of the interference line, $\hat{\gamma}_{\alpha,\beta}[u(t)] = 1$;

and to the right, $\hat{\gamma}_{\alpha,\beta}[u(t)] = 0$. In general, the output of the hysteresis equals the integral of the hysteresis weighting function in the *P*+ region. and this leads to the memory effect of hysteresis. The Preisach model can describe a wide range of hysteresis accurately, but the lack of physical meaning makes it difficult to understand. Also, compared to the differential model (mentioned in Section (d)), digital implementation requires more calculations.

2.4.2.2 Prandtl-Ishlinskiĭ model (PI model)

The Prandtl-Ishlinskiĭ model was introduced in [34] to describe the hysteresis performance of smart materials. In contrast to the Preisach model, the PI model uses the PI operator (Backlash) as the basic element of the hysteresis, as shown in Figures 2.4 and 2.5.

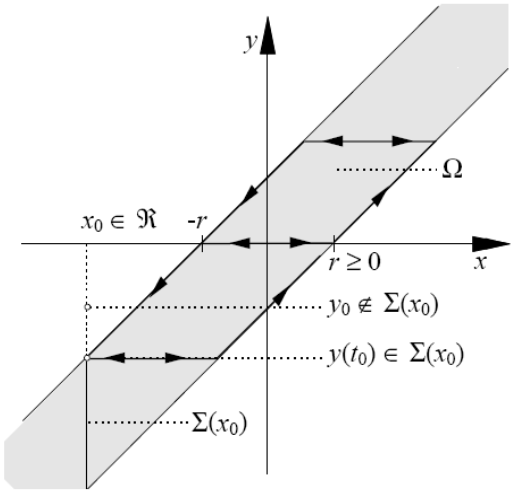

Figure 2. 4 PI operator [34]

The PI model can be regarded as the superposition of different PI hysteresis operators with corresponding weights as

$$H[x(t)] = w^T H_r[x, z_0](t) \tag{2.3}$$

where w^T is the vector of weight, H_r is the PI hysteresis operator, $\boldsymbol{r}$ is the vector of thresholds. It has been mathematically verified that the PI model is a subset of the Preisach model [11]. Compared to the Preisach model, less research has applied the PI model for improving the performance of PEAs.

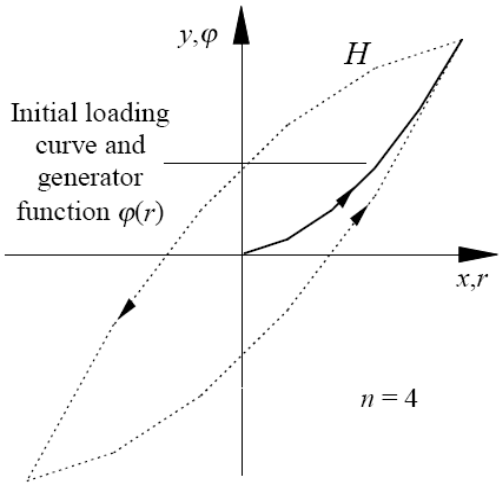

Figure 2. 5 Initial loading curve [34]

2.4.2.3 Duhem model

The generalized Duhem model is also a candidate for hysteresis. It can be described by [35]-[37]

$$\begin{aligned} \dot{x}(t) &= f[x(t), u(t)]g[\dot{u}(t)], x(0) = x_0, t \geq 0 \\ y(t) &= h[x(t), u(t)] \end{aligned} \tag{2.4}$$

where x is the state, x_0 is the initial state, u and y are respectively the input and output of the hysteresis, f, g and h are continuous functions. The state space Equation (2.4) is a closed curve if

there exists a continuous piecewise, periodic map $\gamma:[0,+\infty)\to R^2$ such that $\gamma([0,+\infty))=\text{Hysteresis}$, and γ belongs to a first order derivative continuous function space. If the following parameters are given: $f[x(t),u(t)]=[-\gamma x(t)+\frac{d\phi[u(t)]}{du(t)},\gamma x(t)+\frac{d\phi[u(t)]}{du(t)}]$; $g[\dot{u}(t)]=[\dot{u}_+(t),\dot{u}_-(t)]^T$; $y(t)=x(t)+\mu u(t)+h_0[u(t)]$; where $\dot{u}_+(t)\triangleq\max\{0,\dot{u}\}$ and $\dot{u}_-(t)\triangleq\min\{0,\dot{u}\}$, then the Duhem model can be changed into the Bouc-Wen model [35].

2.4.2.4 Bouc-Wen model

The Bouc-Wen model has received an increased interest in recent years. Due to its capability to form a range of shapes of hysteretic cycles which match the behavior of a wide class of hysteretic systems, it has been applied in varies applications such as modeling the piezoelectric elements, control of magnetorheological dampers, developing wood joints and base isolation devices for buildings [38]-[42].

The normalized Bouc-Wen moel can be expressed as [39]

$$\begin{aligned}\Phi(x)(t)&=k_x x(t)+k_w w(t)\\ \dot{x}(t)&=\rho[\dot{x}(t)-\sigma|\dot{x}(t)||w(t)|^{n-1}w(t)+(\sigma-1)\dot{x}(t)|w(t)|^n]\end{aligned}\tag{2.5}$$

where w is the input, $\Phi(x)(t)$ is the output of the hysteresis, $n\in\{\lambda\mid\lambda\in Z,\lambda\geq 1\},\rho>0,\sigma>0.5,\ \ k_x>0$ and $k_w>0$ are the parameters.

Bouc-Wen model presents a good matching with specific experimental input data. However, its matching performance might be greatly deteriorated in the model prediction applications where the system input is independently provided [38]. Moreover, the Bouc–Wen class models are not in agreement with the requirements of classical plasticity theory, such as Drucker's

postulate, and may produce negative energy dissipation when the unloading–reloading process occurs without load reversal [40].

2.4.2.5 Differential model

Another frequently used hysteresis model is a differential equation induced from the ferromagnetic material model [35], [43],

$$\dot{y} = \alpha |\dot{x}|[f(x) - y] + \dot{x}g(x) \tag{2.6}$$

where x is the input of the hysteresis, y is the output, and $f(x)$ and $g(x)$ are real valued functions of x which determine the shape of the hysteresis loop [44].

Commonly, $f(x)$ and $g(x)$ are chosen such that $f(x) = ax/\alpha$, $g(x) = b$, $c = -1/\alpha$ and then Equation (2.6) can be rewritten as

$$\dot{y} = |\dot{x}|(ax + cy) + b\dot{x} \tag{2.7}$$

The differential equation of the ferromagnetic material hysteresis model is readily implemented in computer simulation due to its simple mathematical form. The challenge for applying the ferromagnetic hysteresis model to PEA applications is choosing suitable shape functions $f(x)$ and $g(x)$.

2.4.2.6 Other models

According to the wiping-out property of hysteresis, Bashash and Jalili [12] introduced an intelligence rule for representing piecewise hysteresis. They used an exponential expression to describe the hysteresis curve between two extreme points in the voltage-displacement plane,

$$x(v) = F(v, v_1, x_1, v_2, x_2) = k(1 + \alpha e^{-\tau(v - v_1)})(v - v_1) + x_1 \tag{2.8}$$

where $k = \frac{x_2 - x_1}{v_2 - v_1}(1 + \alpha e^{-\tau(v - v_1)})^{-1}$, and (v_1, x_1) and (v_2, x_2) are the two arbitrary extreme points. The predicted ascending hysteresis path can be represented as

$$x_A(v) = F(v, v_{L1}, x_{L1}, v_{U1}, x_{U1})H(v, v_{L1}, v_{U1}) + \sum_{i=1}^{n} F_{A_i}(v)H(v, v_{U_i}, v_{U_{i+1}}) \tag{2.9}$$

where H is the Heaviside function. The same equation predicts the descending hysteresis path. When the intelligence rule is applied to feedforward control, determining the inverse of the intelligence hysteresis model is not difficult. Bashash and Jalili reduced the nonlinearity of hysteresis from 14 to 1%. However, all of the extreme points must be considered in predicting the hysteresis path. Therefore, its implementation is difficult.

2.4.3 Dynamics

The above mentioned models are rate-independent hysteresis models whose loops do not vary with the frequency of the input voltage. In reality, the displacement/voltage loops of PEAs are rate-dependent. If the PEA is used at the resonant frequency, vibration occurs, which might destroy the mechanical configuration of the PEA. For this reason, PEAs are always used at an input frequency that is 10-100 times lower than their first resonant frequency.

A common method used to describe the performance of PEAs is regarding the PEA as the series connection between the rate-independent hysteresis and the dynamics [6], [43], [45], as shown in Figure 2.6. For example, the voltage v is the input to the ferromagnetic material hysteresis sub-model **H** and its output u is the effective mechanical force applied to the

subsequent dynamic model that predicts the displacement y. Cascading with the dynamics of the PEA, the rate-independent hysteresis model can be the Preisach model, ferromagnetic material model or one of the other models mentioned above. A transfer function can be used to represent linear dynamics. In [46], it was mathematically verified that when the mass ratio between the stage and the PEA increases, the dynamics of a PEA can be approximated as a second order system. Several studies have identified the dynamic model parameters [4], [7], [47]-[51]. In the majority of those studies, the use of Bode Plots is the preferred identification method.

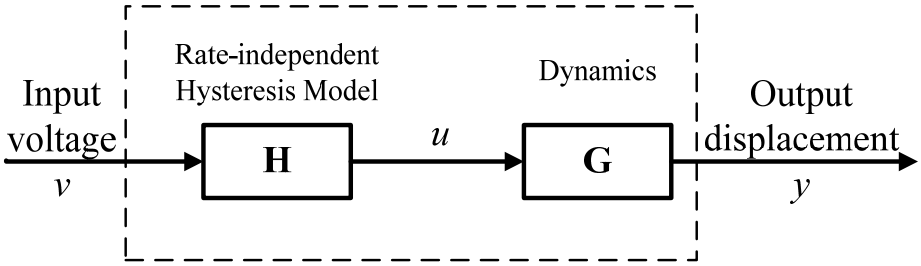

Figure 2. 6 Series of rate-independent hysteresis and linear dynamics

The rate-independent hysteresis model can also be combined with the nonlinear auto-regressive moving average model with exogenous inputs (NARMAX) to describe the rate-dependent performance of PEAs. For example, in [52], an empirical operator was employed to connect with the NARMAX model, and a model fit error of less than 0.1% was finally obtained.

A rate-dependent weighting function was developed in [53] to take place of the rate-independent weighting function in the Preisach model as

$$H(t) = \iint \mu[\alpha, \beta, \dot{u}(t)]\hat{\gamma}_{\alpha,\beta}[u(t)]d\alpha d\beta . \quad (2.10)$$

Through the aid of learning algorithms in neural networks, the hysteresis output was shown to vary with the frequency of the input voltage.

Other rate-dependent models that considered the effects of dynamics included the neural network model [54]-[56] and the wavelet model [57]-[59]. However, the wavelet models were seldom employed in studies for control.

2.4.4 Model Uncertainty

To successfully exploit the full potential of PEAs in control schemes, it is necessary to develop accurate hysteresis models for PEAs. The challenge is to minimize the effect of model uncertainty caused by parameter change, unmodeled dynamics, the coupling effect in multi-DOF PEAs and discrete model error.

2.4.4.1 Parameter Change

A major difficulty in modeling a PEA is that parameters are not known accurately. Even when the parameters are identified with low estimation error, they can change over long time intervals due to aging effects. Moreover, piezoelectric parameters are very sensitive to environmental conditions such as temperature change [60]. Therefore, making robust, adaptive and learning techniques are important aspects of controller design for PEA-based systems.

2.4.4.2 Unmodeled Dynamics

In order to obtain a simplified model for controller design, high frequency vibration modes are often neglected. This conveys model uncertainties to the control system which greatly limits the achievable performance of the closed-loop system. In addition, high frequency vibration modes can affect the stability of the closed-loop system. Therefore, the effects of these unmodeled modes should be considered in controller design [2].

2.4.4.3 Model for the Multi-DOF PEAs

Due to the ingenious design of flexible hinges, friction and backlash clearance issues can be avoided, which leads to further improvement in the performance of multi-DOF PEAs. However, the cross-coupling effect of the parallel mechanism together with nonlinear effects in each PEA, such as creep and hysteresis, can greatly degrade the positioning accuracy of the stages [61] - [63]. To develop control schemes in nano-positioning, modeling of piezoelectric stages has been reported in the literature with increasing frequency.

In [15], a three-by-three transfer function matrix and a physical model were built for a three-DOF precision micro-stage. Empirical transfer function estimation was employed to identify the dynamic effect. Comparison with experimental data showed that both of these models were able to predict the performance of the micro-stage with acceptable accuracy.

An Auto-Regressive Exogenous (ARX) model was developed in [64] to describe the dynamic performance of a biaxial piezo-stage. The model was integrated in a feedforward compensator for precision tracking control and experimental results proved its effectiveness. However,

cross-coupling between the two axes was not considered in the ARX model potentially causing a negative effect to the performance of the controller.

In [65], a fourth order linear transfer function was identified for a piezoelectric stage. Since the cross-coupling effect was neglected here as well, a chirp signal was applied to each of the axes independently. From the measured outputs, the parameters in each transfer function were estimated using the subspace system identification method integrated in the MATLAB command n4sid.

In [66], the dynamic equations of a plane-type three-DOF precision positioning table were combined with Bouc-Wen model for each PEA. The resultant model was applied to a contour tracking controller design. The parameters of the model were optimized based on the real-coded genetic algorithm (RGA) method. From numerical simulations and experimental results, it was shown that the three-DOF cross-coupling was reduced by the proposed control method. Good contour tracking performance was obtained due to successful identification of the dynamic models.

If the controller is designed for each input/output pair of the multi-DOF PEA, the cross-coupling effect between axles can be regarded as unmodeled dynamics. In particular, this effect becomes significant if the PEAs are used with high frequency inputs. Therefore, it is necessary to consider the cross-coupling between axles in the controller design for multi-DOF PEAs.

2.4.4.4 Discrete Models

The models mentioned above are considered to be continuous hysteresis models because the controllers are designed in the continuous time domain. With the advance of computer technology, controllers have been mostly implemented either digitally or in a discrete domain. It is well-known that not all continuous controllers work on digital systems as desired, since errors due to quantization can degrade the control performance and make the system unstable [67]. Reducing the sampling time period could improve the system performance, but this is at a cost of requiring more expensive hardware and faster data processing for implementation. Therefore, it is desirable to develop discrete models for PEAs hysteresis in order to facilitate digital controller design. Vörös discretized the ferromagnetic hysteresis model as [68]

$$y(k+1)-y(k)=\alpha\{f[x(k)]-y(k)\}\left|x(k+1)-x(k)\right|+g[x(k)][x(k+1)-x(k)] \qquad (2.11)$$

He used the difference equation directly to estimate the derivative term from Equation (2.6). Unfortunately, this model was rate-independent and was not suitable for describing PEA hysteresis.

2.5 Control Approaches for Piezoelectric Actuators

As mentioned above, the hysteresis effect greatly deteriorates the performance of PEAs. In open loop manipulation, the tracking error can reach 15-20% of the stroke of PEAs. Closed loop control is used to compensate for the hysteresis effect. Several kinds of controllers have been developed and reported in the literature for improving the performance of PEAs.

2.5.1 Charge Control

In 1981, a patent was granted for the use of charge control to reduce the hysteresis effect of PEAs [69]. Stemming from this idea, many researchers combined the use of charge control with other feedback control methods to reduce hysteresis nonlinearity [44], [49], [70], [71]. A grounded load charge amplifier is illustrated in Figure 2.7, where R_s and R_L are resistances, C_s and C_L are capacitors, v_{ref} is the applied reference voltage, q_L and q_{Lc} represents the load charge and actual charge respectively.

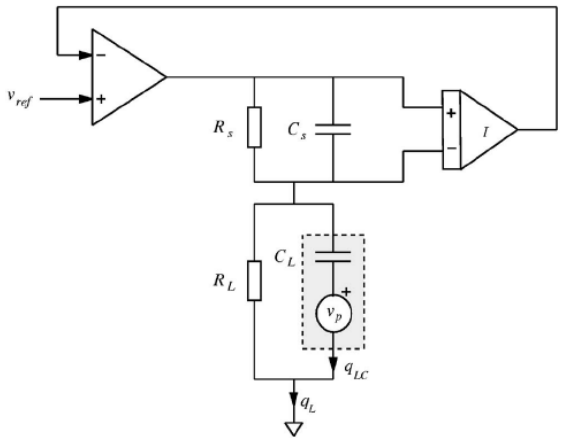

Figure 2. 7 Grounded load charge amplifier [70]

The transfer function between the load charge and the reference voltage is:

$$\frac{q_L(s)}{v_{ref}(s)} = C_s \frac{s + \dfrac{1}{C_s R_s}}{s} \tag{2.12}$$

Thus, $\frac{q_{L_C}(s)}{v_{ref}(s)} = \frac{q_L(s)}{v_{ref}(s)} \frac{q_{L_C}(s)}{q_L(s)} = C_s \frac{s + \frac{1}{C_s R_s}}{s} \frac{s}{s + \frac{1}{C_L R_L}}$. Setting $C_s R_s = C_L R_L$, $\frac{q_{L_C}(s)}{v_{ref}(s)} = C_s$.

At frequencies above 1/RC, the amplifier is charge dominant which can be used to reduce the hysteresis effect. The results show an 89% reduction in the hysteresis. However, charge control requires hardware support which increases the difficulty and cost of use in applications.

2.5.2 Feedback Control

As a simple feedback controller, the proportional-integral-derivative controller (PID)/ proportional-integral controller (PI) is well suited for nanopositioning. It was applied in [23] to compensate for the nonlinear effect of PEAs, such as creep and hysteresis, which were shown to be greatly reduced. The challenges of PID controller application are the improvement of performance while maintaining the stability of the overall system in the presence of parameter uncertainty and disturbance, and the low gain margin problem in high frequency manipulation [2]. To improve the robustness of control, advanced feedback controllers, such as the H_∞ and H_2 robust controllers, were designed to compensate for the hysteresis effect of PEAs. Their tracking errors were between 0.7 and 2% given a 50Hz sinusoidal input signal [4], [47], [72].

Little work has been reported which uses phase compensation for hysteresis compensation. In [73], hysteresis was regarded as a transfer function whose amplitude and phase vary with both the input signal frequency and the magnitude of the input signal, i.e.,

$$|P(j\omega)| = f_m(j\omega, |u|), \angle P(j\omega) = f_p(j\omega, |u|) \tag{2.13}$$

where $P(j\omega)$ and $\angle P(j\omega)$ is the amplitude and phase of the transfer function, ω is the round frequency, u is the input signal. A nonlinear phaser with a positive phase can be added ahead of the plant to balance out the hysteresis phase. The results showed that the phase control is effective under a certain range of input amplitude and frequency. The phase difference was decreased from 38° to approximately zero. However, phase compensation was only reported in low frequency applications. For example, in [73], the frequencies of the input signals given in the experiments range only from 0.05Hz to 5Hz. The effect of phase compensation in high frequency applications has not been verified yet.

2.5.3 Inverse Feedforward Control

Another control method which is frequently used in PEAs is inverse feedforward control [7], [10], [12], [34]. The basic idea of inverse feedforward control is shown in Figure 2.8, where the inverse of the transfer function is cascaded with the plant. The performance of this control scheme is sensitive to errors in the plant transfer function, leading to problems like divergence and instablity.

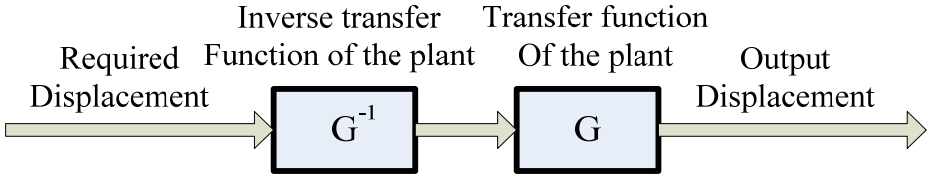

Figure 2. 8 Inverse feedforward control

In practice, feedforward control is commonly combined with feedback control, as shown in Figure 2.9. It does not share the low gain margin problem of the feedback approach leading to significant improvement of PEAs at high frequencies. However, determining the inverse of the hysteresis, as in the Preisach model, is still a significant burden on computer calculations.

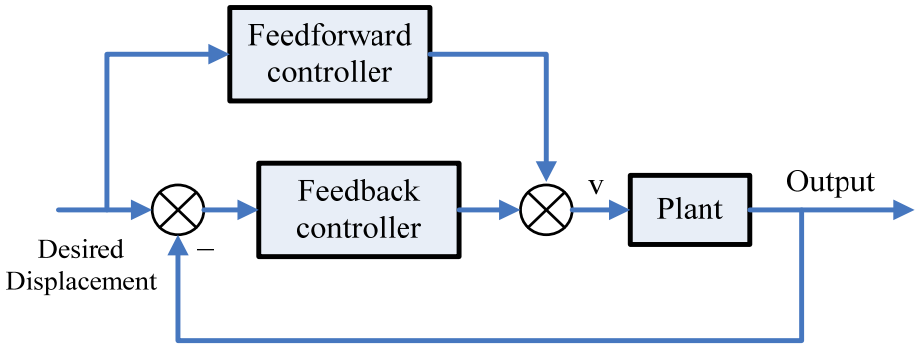

Figure 2. 9 Inverse feedforward based feedback control

Researchers have reported promising results in the literature combining feedforward with feedback. In [74], an adaptive control method combined with inverse feedforward was presented in which the inverse hysteresis model was updated online by means of an adaptive parameter controller. A tracking error of 1% was achieved. Using a similar method, hysteresis nonlinearity was reduced in [75]. A high gain feedback controller was employed for the tracking performance of the PEA in [7]. It used only the inverse of the linear dynamic part of the plant and a tracking error below 1.54% from a 50Hz sinusoidal input signal resulted. In [61], a PID controller combined with an inverse hysteresis model was introduced to control a PEA. The maximum tracking error was less than 0.45μm for a given 20 Hz sinusoidal input signal with a magnitude

of 15μm.

2.5.4 Iterative Learning Control

Compared with inverse feedforward control, iterative learning control (ILC) does not require accurate, typically complicated, hysteresis models. An iterative controller generates the control action at present based on the tracking error and the control action of the previous iteration, as shown in Figure 2.10 [76]-[79].

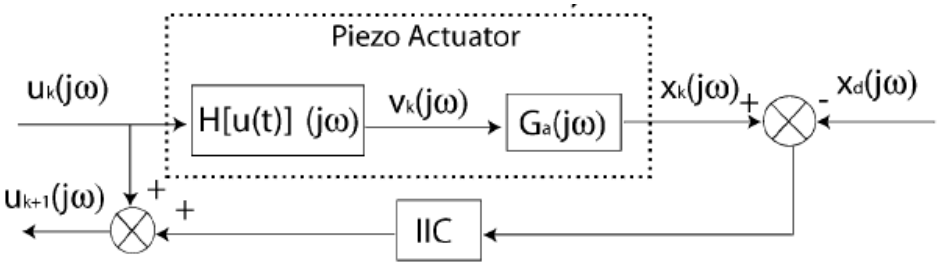

Figure 2. 10 Iterative control [76]

The control action of ILC is given by

$$u_0(j\omega) = 0, u_{k+1}(j\omega) = u_k(j\omega) + \rho(j\omega)G_{a.m}^{-1}(j\omega) \times [x_d(j\omega) - x_k(j\omega)] \quad (2.14)$$

where $G_{a.m}^{-1}(j\omega)$ is the frequency response model of the system, $\rho(j\omega)$ is the frequency-dependent iterative coefficient, $u_k(j\omega)$ and $x_k(j\omega)$ are the Fourier transform of the input and output at the *k*th iteration respectively. The goal of ILC is to generate a feedforward control that tracks a specific reference signal and rejects the repeating disturbance [79]. As such, the control performance is highly robust for system uncertainties. Moreover, it can significantly increase the manipulation bandwidth without reducing the positioning precision. However, ILC

is an open-loop control. For non-repeating disturbance or system uncertainties, a feedback controller is required as well. In spite of this, ILC has been widely used in nanopositioning, such as in the control of ATM, because a plant model is not required, it has self-learning adaptability, and it is robust.

2.6 Emerging Issues in Control of Piezoelectric Actuators

In this section, emerging applications and control issues in PEA-based nanopositioning will be discussed.

2.6.1 Disturbance Rejection

Since uncertainties are inevitable in the model of PEAs, maintaining the performance of the controller is necessary in the presence of disturbance and uncertainties.

2.6.1.1 Disturbance Observer

Disturbance observer-based control (DOB) is an advanced control which has disturbance attenuation performance [80]. The general structure of a DOB controller is shown in Figure 2.11, where δ represents the disturbance of the plant system, and Q is a low pass filter that is used for the causality and determines several characteristics of the DOB system.

DOB control is aimed at estimating the system disturbance by taking the inverse of the plant model and subtracting the output from the input of the plant. The estimated disturbance is then fed back to the system input and subsequently eliminated by the controller. DOB has been widely

used in various motion control systems [80].

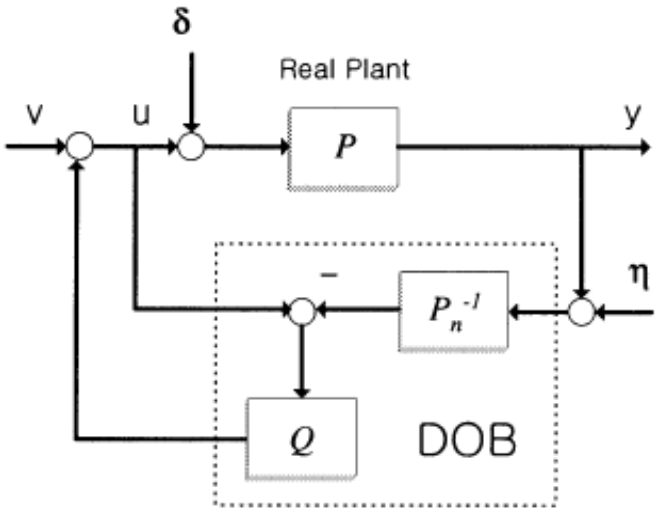

Figure 2. 11 Structure of a disturbance observer-based controller [81]

Chang et. al. applied DOB in the control system of PEAs [82]. The significance of their proposed DOB hysteresis compensator is its simple form that is implemented in the computer and its robustness due to independence from any mathematical model of hysteresis. They considered hysteresis to be a disturbance to the dynamics of the PEA, as shown in Figure 2.12 and represented mathematically as

$$Q(t) = \alpha v(t) + d(t) \tag{2.15}$$

where $Q(t)$ and $v(t)$ are the input and output of the hysteresis respectively, $d(t)$ represents the hysteresis considered as a disturbance. Their experimental results showed successful compensation of hysteresis at an input frequency of 200 Hz.

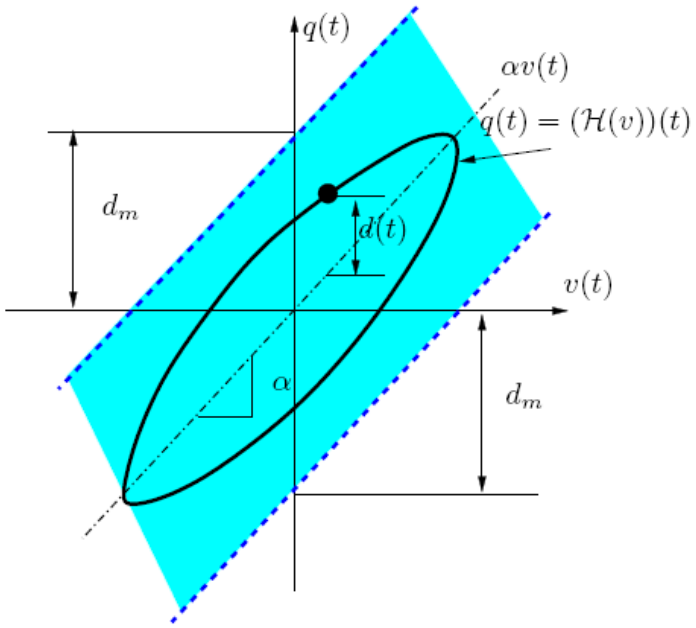

Figure 2. 12 Schematic of a system that considers hysteresis to be a disturbance to the dynamics of a PEA [82]

The Q filter in DOB greatly affects the performance of DOB. There are three important factors in designing the Q filter: the time constant, numerator order and denominator order. Ideally, from Figure 2.11, if the nominal plant $Pn = P$, then the output of the DOB w is

$$w = -uQ + QP^{-1}(\eta + y) = -uQ + QP^{-1}[\eta + P(u + \delta)] = QP^{-1}\eta + Q\delta \qquad (2.16)$$

where v is the main controller output, u is the control input, δ is the external disturbance, y is the plant output and η is the sensor noise.

Based on Equation (2.16), three conditions that must be satisfied for the Q filter design were given in [83]: i.e.,

Condition 1: All unstable zeroes of the plant must be zeroes of Q such that the output of the DOB is stable;

Condition 2: The relative degree of Q must be larger than the relative degree of P to ensure reality of the DOB.

Condition 3: To completely compensate for hysteresis nonlinearity, the steady state gain of the Q filter should be 1.

In [80], a robust measure was introduced to combat the external perturbation and sensor noise for a DOB system. A lower robust measure requires a larger denominator order, a smaller relative degree and a smaller time constant. However, this makes the DOB system more sensitive to sensor noise. Therefore, a design which is aimed at reducing the sensitivity of DOB to disturbance and sensor noise is a contradiction [80].

2.6.1.2 Sliding Mode Control

Sliding mode control (SMC) is an attractive method for control applications in the presence of nonlinearity and system uncertainty. It has been successfully used in many studies [84]-[91]. Consider a second order system, for example, if the state error e is defined as the difference between the desired state X_d and the actual state X such that

$$e = X - X_d , \tag{2.17}$$

then the state error of the system can be regarded as a point in the phase plane. When the desired state error trajectory is given by

$$\dot{e} = ke , \tag{2.18}$$

then as long as all eigenvalues of matrix k stay in the left half complex plane, e will exponentially converge to zero, as shown in Figure 2.13. The initial state error is not on the

desired trajectory. Therefore, a control action is desired that forces the system state error to reach the desired trajectory. If there exists a switching rule which limits the system state to the boundary layer region after the desired trajectory is reached, the state will follow a zig-zag motion around the desired trajectory and will finally converge to zero. The desired trajectory is called the sliding surface ($S = 0$).

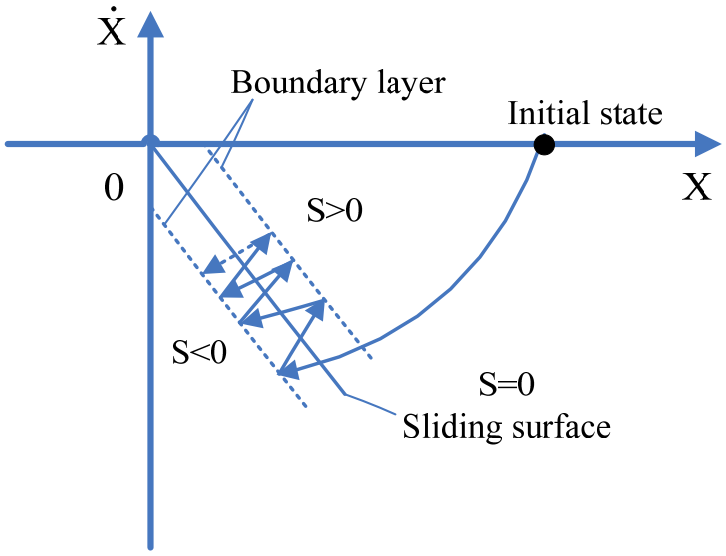

Figure 2. 13 Control scheme of sliding mode

Generally, the aim of SMC is to design a switching law which limits the system state in the boundary layer around the sliding surface [92]. For a system described by

$$\dot{e} = Ae + Bu + w \tag{2.19}$$

where A and B are the system matrices of the state space model, w represents the matched uncertainties, the sliding surface is usually chosen to be $s = Ce$. The controller can be divided

into two parts

$$u = u_{eq} + \Delta u \tag{2.20}$$

where $u_{eq} = (CB)^{-1} CAe$ is the equivalent control which is utilized to maintain the state of the system on the desired trajectory without any disturbance and $\Delta u = K \operatorname{sgn}(s)$, $K \geq -(CB)^{-1} C w_{\max}$ is the switching rule for rejecting the uncertainties of the control system [93].

The advantages of SMC are its robustness when subjected to system uncertainties and disturbances and the reduced order convergence to the zero state. However, due to the discontinuous characteristics of Δu, the state will switch around the sliding surface rather than lie directly on it. Switching can occur at high frequency, called chattering, which can excite an undesired high resonance mode which deteriorates the system tracking performance.

One solution to the chattering problem is the use of boundary layer control [94], in which a saturation switching control replaces the discontinuous switching control. If the unknown disturbance is significant, a sufficiently-high gain in the controller is always required and such a control scheme behaves like a high-gain proportional (P) controller. As a result, steady state error may exist. An alternative method for solving the chattering problem is to enlarge the width of the boundary layer and reduce the effective linear gain in order to reduce the state oscillation around the sliding surface. However the state can no longer strictly locate on the ideal sliding surface due to the wider boundary layer and the system will never behave as described by the sliding mode.

In [95] and [96], a high order sliding surface was designed instead of using a first order one

as in the nominal SMC design. While maintaining the main advantages of the nominal SMC, the high order sliding mode control (HOSMC) reduced the chattering effect and provided even higher accuracy [97]. The drawback to using HOSMC is the requirement of increased sliding information in its implementation. For example, the *r*-sliding controller keeping $S = 0$ requires $s', s'', \cdots, s^{r-1}$ to be available.

Recently, a new continuous PID-based SMC was developed in which the discontinuous 'bang-bang' switching function is replaced by a PID regulator to eliminate the chattering problem [98]. Due to the integral effect of the PID regulator, zero steady state error can be achieved in the tracking performance of the plant. The continuous PID-based SMC was implemented in the tracking control of a commercially available PEA at a 20000 Hz sampling rate. The PEA was modeled as a second order system and other nonlinear effects, such as the hysteresis, were treated as uncertainties and disturbances which were rejected by the SMC. The results showed that with a 50 Hz sinusoidal input reference signal, the tracking error was reduced by 30% compared to the traditional PID controller.

The continuous PID-based SMC developed in [98] is actually a state tracking control scheme. For its application to second order mechanical systems, the states can be estimated from the output and its derivatives. The error state can then be evaluated by subtracting the desired state from the estimated one. The aim of a continuous PID-based SMC is to force the state error to be zero. However, for high order systems with zeros in their transfer functions, e.g., mechanical accelerometer systems and satellite rotation control systems, the states cannot be simply represented by the output and its derivatives. As a result, the design method developed in [98]

may not be applicable for these systems.

2.6.2 Discrete Controller Design

With the advance of computer technology, controllers are mostly implemented digitally or in a discrete domain. Figure 2.14(b) shows, schematically, a continuous controller, represented by Figure 2.14(a), implemented in a real system. Blocks **H** and **S** represent the holding and sampling modules. Due to the quantization error of sampling, the control signal transferred to the plant is not exactly the same as calculated by the continuous controller, as illustrated in Figure 2.15. This error can degrade the control performance and even make the system unstable, especially at low sampling rates [99]. For example, if the continuous SMC controller is directly implemented in the digital computer, the chattering problem will not be resolved by employing boundary layer control. Figure 2.16 shows the difference between the trajectories of a continuous sliding mode control system (CSMC) and a discrete sliding mode control system (DSMC). If the uncertainties are not considered and it is assumed that the discontinuous control can be implemented ideally, then the state of the CSMC, starting from any initial position, will move towards the sliding surface and arrive in a finite time, as shown in Figure 2.16(a). For DSMC, if the states arrive at the sliding surface at the sampling time instant, the trajectory will follow the sliding surface. This is called a type-I trajectory which is an ideal trajectory, as shown on the left side of Figure 2.16(b). If the switching time does not exactly match the sampling time, the state will not lay on the sliding surface and the trajectory will appear as a zigzag motion around the sliding surface. This is called type-P trajectory, as shown in the right side of Figure 2.16(b). This

indicates that the sampling itself can induce the chattering problem in DSMC.

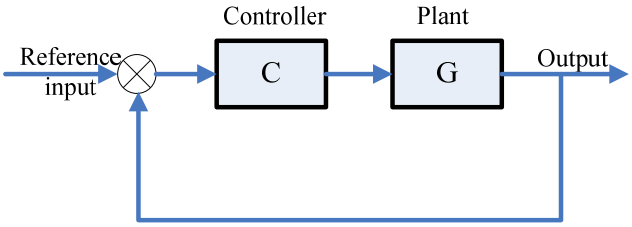

(a) Controller designed in continuous time domain

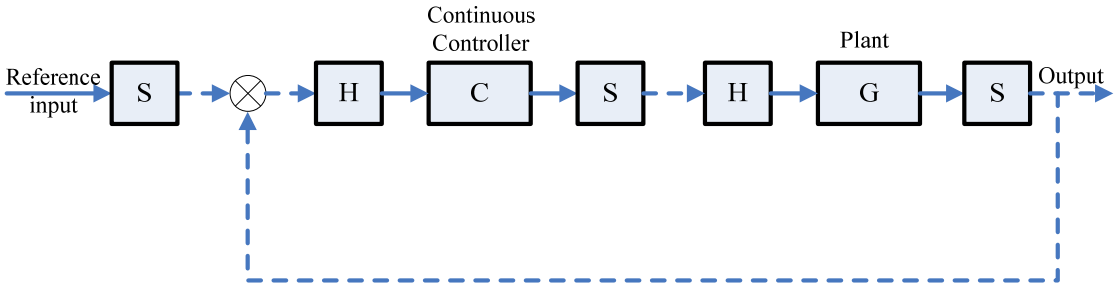

(b) Continuous controller implemented in real systems

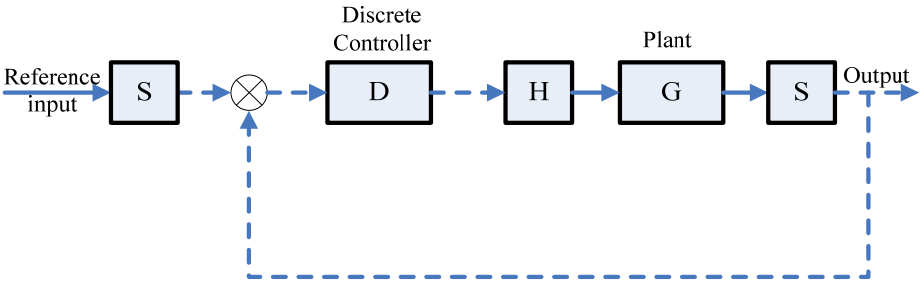

(c) Discrete controller implemented in real systems

Figure 2. 14 Comparison of discrete and continuous controllers
The solid line represents the continuous signal and the dashed line represents the discrete signal.

Increasing the sampling frequency could improve control performance, but at a cost of requiring more expensive hardware and faster data processing for implementation [54]. Therefore, it is necessary to develop a discrete hysteresis model for PEAs, as shown in Figure 2.14(c), and their digital controllers as well. Some DSMC design methods may be found in [101]

- [103].

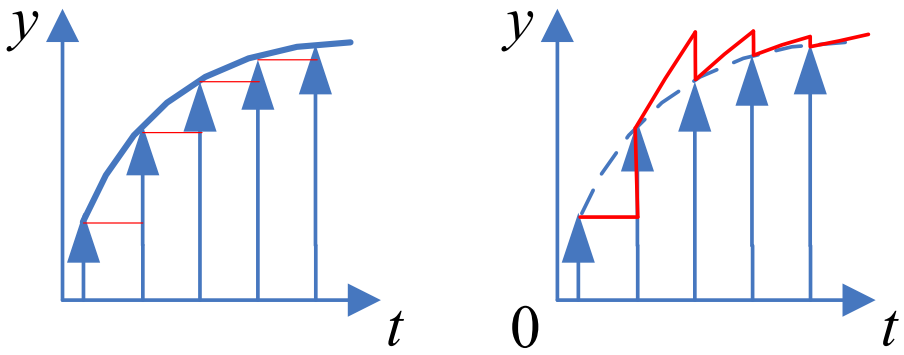

(a) Sampling and zero hold (b) First order hold

Figure 2. 15 Quantization error in sampling and holding module

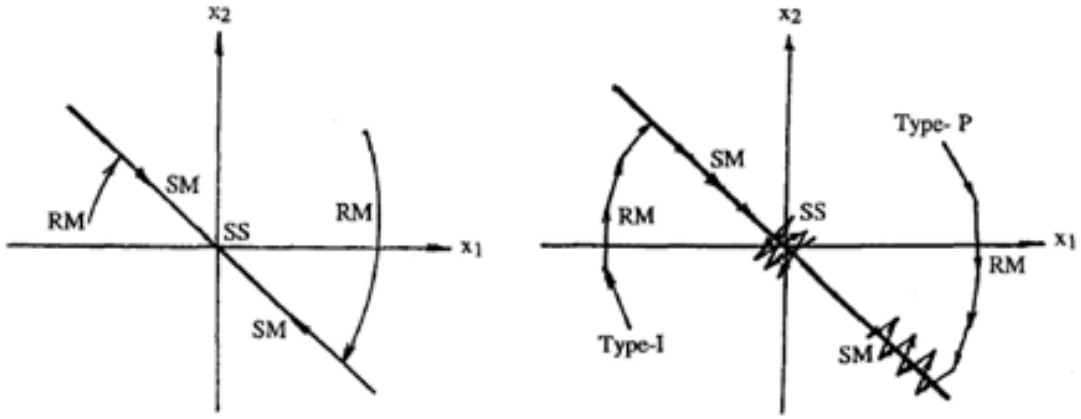

(a) (b)

Figure 2. 16 Difference between the continuous and discrete SMC systems [100]
(a) Trajectories of continuous SMC; (b) Trajectories of discrete SMC

2.6.3 Controller for Multi-DOF Piezoelectric Actuators

One of the most important characteristic of a multi-DOF system is the cross-coupling effect

or interaction between variables. For example, one input variable can lead to outputs of all variables. Commonly, each input/output pair is controlled separately without considering the coupling effects between variables. However, coupling greatly degrades the performance of the controller in many systems, in particular, parallel mechanics and chemical engineering systems with significant interactions [104]. Since the pioneering research of the early sixties [105], control of multi-DOF systems has received increased attention not only in the control research area but also in industry. Generally, controllers for single-DOF systems cannot be extended to multi-DOF systems due to the cross-coupling effect of multi-DOF systems [106]. Therefore, new controllers must be designed which consider the coupling effect [107]-[111].

Compared to the controller design for the one-DOF PEA mentioned above, much less work has been reported on the control of multi-DOF piezo-positioning systems. In [15], integral resonant control (IRC) was combined with inverse feedforward control to increase the damping ratio and ensure good performance at high frequency. The tracking error was reduced to 1.92% from a 400Hz input signal. In [16] an extended Coleman-Hodgdon model was introduced to represent the hysteresis effect of each axis in an AFM. The transfer matrix of the multi-input-multi-output (MIMO) system was identified by the non-parametric open-loop identification method and Welch's averaged periodogram method. Robust inverse feedforward control was applied on each PEA and the tracking error was reduced to ±5nm with a scanning velocity of 3.6μm/s. A PID controller combined with a linearized feedback controller and a repetitive controller was developed in [17] for the tracking performance of an XY piezoelectric driven stage, as shown in Figure 2.17. The PEAs on both axes were controlled separately with a

capacitive sensor on each axis. The error was reduced to 0.51μm after 30 periodic iterations while tracking a sinusoidal path with amplitude of 150μm and frequency of 1Hz.

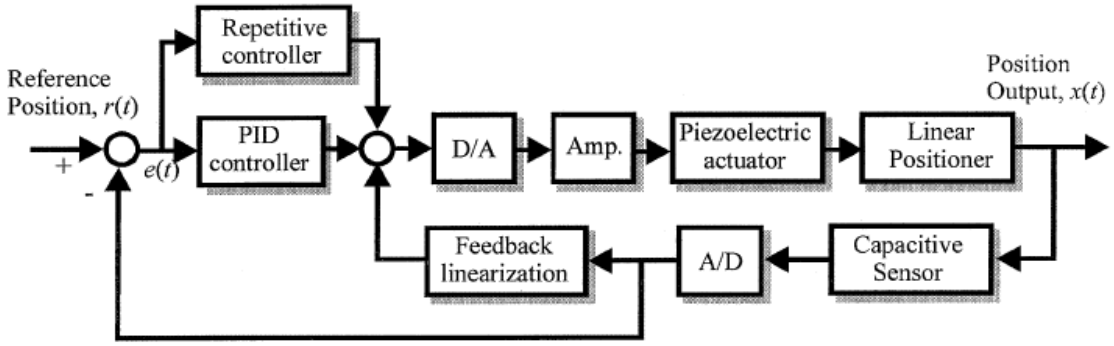

Figure 2. 17 Schematic of a PID controller combined with linearized feedback and a repetitive controller [17]

Another issue of concern in the control of multi-DOF piezoelectric positioning systems is actuation redundancy (i.e., the number of actuators is larger than the degrees of freedom of the mechanism). For example, assume that the plant in sliding mode control can be represented by the state space model $\dot{x} = Ax + Bu, y = Cx$ where A is the state matrix, B is the input matrix, C is the output matrix, x is the state, u and y are the input and output of the plant respectively. If the number of inputs is less than or equal to the number of outputs, the B matrix in the state space model will be a full rank matrix. As such, there exists a solution to the equivalent control by taking the inverse of the matrix SB, where S is the hyperplane defined by the switching function. However, if the number of inputs is greater than the outputs, actuation redundancy exists in the system and B will not be a full rank matrix. As such, SMC for one-DOF PEAs cannot be extended to the control applications of multi-DOF PEAs.

A common approach for eliminating actuation redundancy is to use optimal control design methods, such as linear quadratic control which shapes the closed loop dynamics as well as actuator control distribution in one-step [112] - [114]. Consider a steady state model where (*A*, *B*, *C*, *D*) represent the system matrices, the optimal steady state x^* and the control signal u^* are derived by solving $\min(u^*)^T Ru^*$ subject to the constraints $Ax^* + Bu^* = 0$ and $Cx^* + Du^* = 0$. If any actuator is broken or mis-controlled, the model should be changed because configuration of optimal control is not possible under conditions of a faulty actuator or incorrect control. Alternatively, the closed-loop chain mechanism could be transformed into several open-loop chain mechanisms by making a virtual cut and representing the joint torques of the original closed chain mechanism as open loop chain torques by taking account of the constraint. As a result, the dynamic model for the closed loop mechanism can be found [115]-[118]. Based on this model, controllers can be designed and a pseudo inverse is employed to solve the actuator redundancy [119], [120]. However, to find the dynamic model, the configuration of the parallel system is desired.

Another frequently used method for actuation redundancy control reported in the literature is control allocation [112], [113], [121], [122]. Control allocation is a control distribution module which is used to resolve actuation redundancy in parallel mechanisms. Figure 2.18 shows the scheme of the control system when control allocation performs separately. The control allocation is located between the controller and the plant, resolving the actuation redundancy such that no actuation redundancy exists in the control law. The distribution rule in the control allocation module is defined by certain optimal control methods such as the linear quadratic method. The

advantages of using control allocation module include tuning facility, ease of reconfiguration and actuator constraint consideration.

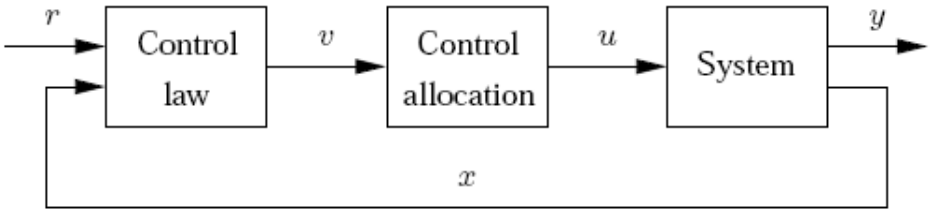

Figure 2. 18 Control system structure with control allocation performing separately [112]

2.7 Summary

PEAs have been widely used in nanopositioning applications due to their ability to produce displacements as small as 0.01 nm, as well as their high stiffness, fast response and large force. However, positioning precision can be greatly degraded by nonlinear behaviour such as hysteresis. With the purpose of successfully exploiting the full potential of PEAs in nanopositioning applications, modeling and control of PEAs has drawn considerable attention. To understand their behaviour, several models have been developed to describe hysteresis, which can be divided into two categories: phenomenon-based models and physically-based models. The phenomenon based models, such as the Prandtl-Ishlinskiĭ (PI), Preisach and Duhem models utilize mathematical methods to describe the hysteresis based on experimental data, regardless of physical meaning. These models have relatively simple forms compared to the physical models and as such, have been widely used in the control of PEAs.

The hysteresis effect greatly deteriorates the performance of PEAs. Therefore, closed-loop controllers are used in nanopositioning applications to improve tracking performance. Among them, PID/PI controllers are simple and commonly employed in PEA-driven nanopositioning systems to compensate for nonlinear effects like hysteresis and creep. The challenge that exists in PID controller application is improving performance while maintaining the stability of the overall system in the presence of parameter uncertainties and disturbances In addition, it has low gain margin in high frequency manipulation. Therefore, advanced feedback controllers such as H_∞ and H_2 controllers, charge control and DOB have been developed for nanopositioning control systems. Feedforward control, which is model-based, does not share the stability problem of the feedback approach. So, significant improvement can be made at high frequencies. However, this approach cannot account for external disturbance and modeling uncertainties.

SMC became the subject of much research due to its success in the presence of nonlinearities and system uncertainty. However, chattering, caused by discontinuous switching control may excite high frequency resonant vibrations, thereby degrading control performance and potentially damaging the actuators being controlled. To resolve the chattering problem, boundary layer control has been employed by researchers in which a saturation function is used to replace the discontinuous 'bang-bang' switching function. If the unknown disturbance is significant, a significantly high gain in control is needed and, as such, steady state error may exist. Alternatively, a high order sliding surface is designed instead of the first order one used in the nominal SMC design. While keeping the main advantages of the nominal SMC, HOSMC reduces the chattering effect and provides even higher accuracy. The main drawback is the

increased sliding information required for implementing the HOSMC.

A new continuous PID-based SMC for PEAs was recently developed, in which the discontinuous ‘bang-bang’ switching function was replaced by a PID regulator to eliminate the chattering problem. Experiments were implemented on a commercially available PEA and it was proven that use of a continuous PID-based SMC effectively compensates for the hysteresis that exists in the PEA thereby leading to a great improvement in PEA performance. Moreover, due to the integration effect of the PID regulator, zero steady state error was achieved in the tracking performance.

The positive effect of combining feedforward control with the feedback approach has been shown in the literature. Therefore, it is reasonable to assume that better control performance will be obtained by combining a feedforward controller with SMC if model uncertainty must be considered in the controller design. This potentially leads to the development of a new controller called feedforward-based SMC. However, a discrete version of this new controller has not been reported in the literature. In addition, general SMC design, including the developed PID-based SMC, is actually a state tracking control approach which cannot be applied to the control of complicated PEA systems that must be identified as black box models. Therefore, development of a new SMC design approach is desired for these types of systems. Moreover, when SMC is implemented in a MIMO system, cross-coupling effects between variables can greatly affect the calculations of the equivalent inputs. As a result, it is still a challenge to extend the application of SMC to MIMO systems. Unfortunately, control of multi-DOF PEAs by SMC has not been reported in the literature.

2.8 Acknowledgement

The support to the present study from the China Scholarship Council (CSC) and the Natural Sciences and Engineering Research Council (NSERC) of Canada is acknowledged.

3 Model of One-DOF Piezoelectric Actuators

The work presented in this chapter was published in the following paper appended.

Y. Cao and X. B. Chen, "A Novel Discrete ARMA-based Model for Piezoelectric Actuator Hysteresis," *IEEE/ASME Transactions on Mechatronics*, Vol. 17, No. 4, pp. 737-744, August 2012.

3.1 Introduction and Objectives

The performances of PEAs are greatly affected by hysteresis. Therefore, modeling and control for PEA hysteresis have drawn remarkable attention in the literature. There are several hysteresis models which are developed and successfully applied in the continuous controllers for PEAs, which, however, might not work as expected in the digital system, especially in the applications where the sampling rate is limited. As a result, it is desirable to develop discrete hysteresis model as well as the corresponding discrete controller to improve the PEA performance. To meet this need, this paper aims at developing a discrete model to describe the hysteresis and dynamic behavior of one-DOF PEA.

3.2 Methods

The performance of PEA was modeled by cascading the ARMA model with the ferromagnetic material hysteresis model, resulting in the so-called "ARMA-based hysteresis model". Figure 3.1 is the schematic of the model, in which the output of the ferromagnetic material hysteresis model is the input to the ARMA model.

The ferromagnetic material hysteresis model is given by [35], [43]

$$\dot{y} = \alpha \left|\dot{x}\right|[f(x) - y] + \dot{x}g(x) \tag{3.1}$$

where α is the parameter which determines the shape of the hysteresis loop, x is the input, y is the hysteresis output, $f(x)$ and $g(x)$ are functions of x, with which one can "shape" the hysteresis loop as well.

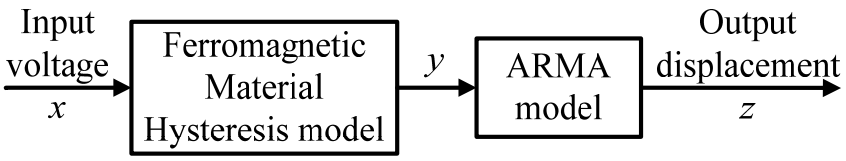

Figure 3. 1 ARMA-based hysteresis model

If define

$$f(x) = \frac{ax}{\alpha} \tag{3.2}$$

$$g(x) = b \tag{3.3}$$

and $c = -1/\alpha$, taking integration on Equation (3.1) in one sampling interval yields

$$y(k+1) - y(k) = \frac{1}{2}a[x^2(k+1) - x^2(k)] + c\int_{x(k)}^{x(k+1)} y\,dx + b[x(k+1) - x(k)] \tag{3.4}$$

The integral term in the right side of Equation (3.4) can be estimated by trapezoid estimation and quadratic estimation, leading to different discrete hysteresis model. Since the hysteresis dominates in the performance of PEA under a low frequency input voltage x, parameters of the hysteresis model can be determined first, and the effective mechanical force y can be estimated from the identified hysteresis model. The dynamic model is to be identified from the estimated y and the measured displacement z.

3.3 Results

Experiment results showed that the discrete ARMA-based hysteresis model predicts the performance of the PEA with higher accuracy. Moreover, the online estimation method leads to

better parameter identification for the discrete ARMA-based hysteresis model than the least square method. The model shows larger prediction error at high frequencies due to the estimation error caused by the integral term. Employing the quadratic equation can reduce the discrete estimation error at high input frequencies. However, the complexity of the model increases.

3.4 Contributions

The contribution of this paper rests on the development of such a comprehensive discrete model to predict the performance of piezoelectric actuators, which can be of great help in the controller design.

3.5 Paper: A Novel Discrete ARMA-based Model for Piezoelectric Actuator Hysteresis

Authors: Y. Cao and X. B. Chen, *Member, IEEE*[2]

Index Terms: Autoregressive moving average process, Hysteresis, Piezoelectric devices

3.5.1 Abstract

Hysteresis is an important nonlinear effect exhibited by piezoelectric actuators and its modeling has been drawing considerable attention. This paper presents the development of a novel discrete model based on the concept of auto-regressive moving average (ARMA) for the piezoelectric-actuator hysteresis, and its parameter identification method as well. Experiments

---

Manuscript received October 4, 2010. This work was supported by the China Scholarship Council (CSC) and the Natural Science and Engineering Research Council (NSERC) of Canada.

Y. Cao is with the Department of Mechanical Engineering, 57 Campus Drive, University of Saskatchewan, Saskatoon, SK, S7N 5A9 (e-mail: yuc150@ mail.usask.ca).

X. B. Chen is with the Department of Mechanical Engineering, 57 Campus Drive, University of Saskatchewan, Saskatoon, SK, S7N 5A9 (phone: 1-306-966-1267; e-mail: xbc719@ mail.usask.ca).

were carried out to verify the effectiveness of the developed model. The result obtained shows that the developed model can well represent the piezoelectric actuator hysteresis, with improved performance over an existing discrete hysteresis model.

3.5.2 Introduction

Due to their fast response and large force generated, piezoelectric actuators (PEA) have been widely used in nano-positioning technologies, such as atomic force microscope (AFM), scanning tunnel microscope (STM), digital video disc (DVD) reading and writing, diamond lathe machine, lithography, X-ray imaging and microfactory [123]. It has been shown that the hysteresis existed in a PEA can greatly degrade its performance [61], [124], [125]. Hysteresis is a memory effect [11], occurring in such phenomena as plasticity friction, ferromagnetism, superconductivity. The hysteresis exhibited at a given time instant depends on not only the input at the present time but also the operational history of the system considered. In order to develop control schemes on PEA, modeling of PEA has been drawing considerable attention and several models have been resulted to describe the hysteresis effect. In the study [29], the Preisach model was developed by integrating hysteresis operators in the Preisach plane. Since then, the Preisach model has been used in the PEA controller design, showing varying degrees of success [6], [62], [74]. The shortage of this model is the significant burden of calculation [63]. Prandtl-Ishlinskiĭ model (PI model) was developed to describe the hysteresis effect of a magneticostrictive actuator and was applied to the development of inverse control for improved performance [34], [126]. It is a kind of modified form of the Preisach model [11]. Limited work was found in the literature to use the PI model for the control of the PEA performance. Bouc-Wen model is a state space model to describe the hysteresis nonlinearity [127], which has been shown to have the ability to represent the behavior of a wide class of hysteresis systems [39]. Because of the introduction of an extra

state variable, difficulty increases in parameter identification and controller design [128]. A first order differential equation was used in the ferromagnetic material model [35], [43] to describe the hysteresis effect. Due to its simplicity, it is easy to be implemented in computer simulation. However like the other models mentioned above, this model cannot describe the rate-dependent characteristic of the PEA as well.

In contrast to the rate-independent hysteresis model, the shape of the rate-dependent hysteresis loop varies with the input frequency. It was reported in the literature [6], [43], [45], [82] that the hysteresis effect can be modeled in series with the dynamics of the actuator, i.e., the output of the rate-independent hysteresis model is the input of the dynamics model. Based on this concept, the Bouc-Wen model and the state space model were combined to describe the hysteresis and dynamics of a 6-DOF precision positioning system and the parameters of the combined model were identified by means of the Genetic Algorithm [129]. Similar method is also employed in [52] where a nonlinear auto-regressive moving average model with exogenous input (NARMAX model) is used to describe the input and output relationship of PEA. The hysteresis effect is considered as a hysteresis operator which is the input of the NARMAX model in the study.

It is noted that all the models aforementioned, including both rate-independent and rate-dependent hysteresis model, were developed in the continuous domain. Accordingly, the controller designs based on these models were then performed in the continuous time domain too. With the advance of computer technology, nowadays controllers have been mostly implemented digitally or in a discrete domain. It is known that not all the continuous controllers can work on the digital system as desired since the error due to quantization can degrade the control performance and even make the system unstable [67]. Reducing the sampling time period

could improve the performance, but at a cost of requiring more expensive hardware and faster data processing for implementation. Therefore, it is desirable to develop discrete models for the PEA hysteresis in order to facilitate the digital controller design. The ferromagnetic material hysteresis model was discrete by using difference equation in [68]. Unfortunately, the model was rate-independent and was not suitable to describe the PEA hysteresis.

To meet this need, this paper presents the development of a novel discrete model based on the concept of auto-regressive moving average (ARMA) for the piezoelectric-actuator hysteresis, and a method to identify the model parameters as well. In order to verify the effectiveness of the developed model, experiments were carried out on a typical PEA. Also, the results obtained from the discrete ARMA-based hysteresis model were compared to those from an existing discrete hysteresis model reported in [68].

3.5.3 DiscreteARMA-based Hysteresis Model

In this study, the hysteresis is to be modeled by combining the ARMA model and the ferromagnetic material hysteresis model, resulting to the so-called "the ARMA-based hysteresis model". Figure 3.1 is the schematic of the model, in which the output of the ferromagnetic material hysteresis model is the input to the ARMA model.

3.5.3.1 Discrete form of the Ferromagnetic Material Hysteresis Model

The first order hysteresis differential equation in the ferromagnetic material hysteresis model [35] is given by Equation (3.1) where α is the parameter which determines the shape of the hysteresis loop, x is the magnetic field strength, y is the magnetic flux density, $f(x)$ and $g(x)$ are functions of x, with which one can "shape" the hysteresis loop as well. It has been experimentally verified that this differential equation is also promising to describe the electric

hysteresis exhibited by PEAs.

According to the previous study [44], it is reasonable to choose $f(x) = ax/\alpha, g(x) = b$ for the shape functions. Thus Equation (3.1) can be rewritten as

$$\dot{y} = |\dot{x}|(ax + cy) + b\dot{x} \tag{3.5}$$

for a PEA, where x is the voltage input and y is the corresponding displacement, $c = -1/\alpha$. By integrating both sides of Equation (3.5) in a time interval, the continuous derivative term can be transferred to the discrete one. If the input signal is monotonically increasing, i.e. $\dot{x} > 0$, taking integration on both sides of Equation (3.5) in one sampling interval yields

$$\int_{kT}^{(k+1)T} \dot{y}dt = a\int_{kT}^{(k+1)T} \dot{x}xdt + c\int_{kT}^{(k+1)T} \dot{x}ydt + b\int_{kT}^{(k+1)T} \dot{x}dt \tag{3.6}$$

where T is the sampling interval.

Equation (3.6) can also be rewritten as Equation (3.4).which is the discrete form of the first order hysteresis differential Equation (3.5). However, it is noted this equation cannot be directly used as the integral term $\int_{x(k)}^{x(k+1)} ydx$ is unknown, which needs to be determined or estimated. One solution to this is to estimate the value of the integral term from the data of the adjacent points. For this, different methods can be used and discussed as follows.

A. Trapezoid Estimation

By using trapezoid estimation, the integral term is given by

$$\int_{x(k)}^{x(k+1)} ydx = \frac{1}{2}[x(k+1) - x(k)][y(k+1) + y(k)] \tag{3.7}$$

Substituting Equation (3.7) into (3.6) yields

$$y(k+1) = a\frac{\alpha(k+1)}{2 - c\beta(k+1)} + \frac{2 + c\beta(k+1)}{2 - c\beta(k+1)}y(k) + b\frac{2\beta(k+1)}{2 - c\beta(k+1)} \tag{3.8}$$

where

$$\alpha(k+1) = x^2(k+1) - x^2(k),\ \beta(k+1) = x(k+1) - x(k) \tag{3.9}$$

For the zero initial condition, i.e., $y(1) = 0$, one can have $y(2) = a\frac{\alpha(2)}{2 - c\beta(2)} + b\frac{2\beta(2)}{2 - c\beta(2)}$,

$$y(3) = a[\frac{\alpha(3)}{2 - c\beta(3)} + \frac{2 + c\beta(3)}{2 - c\beta(3)} \cdot \frac{\alpha(2)}{2 - c\beta(2)}] + b[\frac{2\beta(3)}{2 - c\beta(3)} + \frac{2 + c\beta(3)}{2 - c\beta(3)} \cdot \frac{2\beta(2)}{2 - c\beta(2)}] \cdots$$

It is seen from the above equations that the output *y* can be represented by the combination of $a[\cdot] + b[\cdot]$. Denoting the terms in the brackets by y_1 and y_2 respectively, one then has the following expression at $t = kT$,

$$y(k) = ay_1(k) + by_2(k) \tag{3.10}$$

It is noted that both $y_1(k)$ and $y_2(k)$ are still functions of *x*.

Substituting Equation (3.10) at $t = kT$ into Equation (3.8) yields:

$$y(k+1) = a[\frac{\alpha(k+1)}{2 - c\beta(k+1)} + \frac{2 + c\beta(k+1)}{2 - c\beta(k+1)} y_1(k)] + b[\frac{2\beta(k+1)}{2 - c\beta(k+1)} + \frac{2 + c\beta(k+1)}{2 - c\beta(k+1)} y_2(k)] \tag{3.11}$$

Thus,

$$y_1(k+1) = \frac{\alpha(k+1)}{2 - c\beta(k+1)} + \frac{2 + c\beta(k+1)}{2 - c\beta(k+1)} y_1(k) \tag{3.12}$$

$$y_2(k+1) = \frac{2\beta(k+1)}{2 - c\beta(k+1)} + \frac{2 + c\beta(k+1)}{2 - c\beta(k+1)} y_2(k) \tag{3.13}$$

If the input signal is monotonically decreasing, $\dot{x} < 0$, repeating the above process, one can have

$$y(k+1) = ay_1(k+1) + by_2(k+1) \tag{3.14}$$

where

$$y_1(k+1) = \frac{-\alpha(k+1)}{2 + c\beta(k+1)} + \frac{2 - c\beta(k+1)}{2 + c\beta(k+1)} y_1(k) \tag{3.15}$$

$$y_2(k+1) = \frac{2\beta(k+1)}{2 + c\beta(k+1)} + \frac{2 - c\beta(k+1)}{2 + c\beta(k+1)} y_2(k) \tag{3.16}$$

B. Quadratic Estimation

In the quadratic estimation, a quadratic curve $f(x)$ is used to represent the hysteresis curve between k and k+1 approximately, as shown in Figure 3.2.

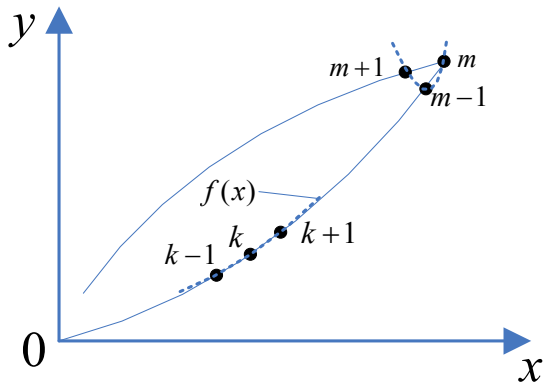

Figure 3. 2 Quadratic estimation of the integral term

Suppose $f(x)$ is described by

$$y = f(x) = d_1 x^2 + d_2 x + d_3 \tag{3.17}$$

The integral term can be estimated as:

$$\int_{x(k)}^{x(k+1)} y dx = \int_{x(k)}^{x(k+1)} (d_1 x^2 + d_2 x + d_3) dx = \frac{1}{3} d_1 [x^3(k+1) - x^3(k)] + \frac{1}{2} d_2 [x^2(k+1) - x^2(k)] + d_3 [x(k+1) - x(k)] \tag{3.18}$$

where d_1, d_2, d_3 are determined from the data at $k-1$, k, $k+1$,

$$\begin{bmatrix} d_1 \\ d_2 \\ d_3 \end{bmatrix} = \begin{bmatrix} x^2(k-1) & x(k-1) & 1 \\ x^2(k) & x(k) & 1 \\ x^2(k+1) & x(k+1) & 1 \end{bmatrix}^{-1} \begin{bmatrix} y(k-1) \\ y(k) \\ y(k+1) \end{bmatrix} = \begin{bmatrix} m_{11} & m_{12} & m_{13} \\ m_{21} & m_{22} & m_{23} \\ m_{31} & m_{32} & m_{33} \end{bmatrix} \begin{bmatrix} y(k-1) \\ y(k) \\ y(k+1) \end{bmatrix} \tag{3.19}$$

Substituting Equation (3.18) into (3.4), one has

$$(1-q_3)[y(k+1)-y(k)]=\frac{1}{2}a[x^2(k+1)-x^2(k)]+b[x(k+1)-x(k)]+q_1y(k-1)+q_2y(k) \quad (3.20)$$

where $q_i=\frac{1}{3}cm_{1i}[x^3(k+1)-x^3(k)]+\frac{1}{2}cm_{2i}[x^2(k+1)-x^2(k)]+cm_{3i}[x(k+1)-x(k)]$(i=1,2,3$\cdots$)

Similarly, using Equation (3.10), one can have

$$y_1(k+1)=\frac{\alpha(k+1)}{2(1-q_3)}+\frac{q_1}{1-q_3}y_1(k-1)+\frac{1+q_2}{1-q_3}y_1(k) \quad (3.21)$$

$$y_2(k+1)=\frac{\beta(k+1)}{1-q_3}+\frac{q_1}{1-q_3}y_2(k-1)+\frac{1+q_2}{1-q_3}y_2(k) \quad (3.22)$$

If the input signal is monotonically decreasing, $\dot{x}<0$, repeating the above process, one can have

$$y_1(k+1)=-\frac{\alpha(k+1)}{2(1+q_3)}-\frac{q_1}{1+q_3}y_1(k-1)+\frac{1-q_2}{1+q_3}y_1(k) \quad (3.23)$$

$$y_2(k+1)=\frac{\beta(k+1)}{1+q_3}-\frac{q_1}{1+q_3}y_2(k-1)+\frac{1-q_2}{1+q_3}y_2(k) \quad (3.24)$$

There are two special cases that need to be addressed when discreting Equation (3.5) by means of the quadratic curve estimation.

① Estimation of the output at certain time instant $y_i(k+1),\ i=1,2$ is based on the output of $y_i(k)$ and $y_i(k-1)$, as indicated by Equation (3.21)~(3.24). If $k=2$, $y_i(1)$ and $y_i(2)$ needs to be known. It is reasonable to set $y_i(1)=0$ at the beginning, but $y_i(2)$ is unknown. In such a case, one has to use the trapezoid method to estimate $y_i(2)$. The use of Equations (3.12) and (3.13) as well as Equation (2.9) can yield

$$y_1(2)=\frac{x^2(2)}{2-cx(2)},\ y_2(2)=\frac{2x(2)}{2-cx(2)} \quad (3.25)$$

② At the extreme points where the derivative of the input voltage $\dot{x}$ changes its sign, the hysteresis loop starts from $m-1$, then goes through m and arrives at $m+1$, as shown in

Figure 3.2. It is noted that the hysteresis loop between $m-1$ and $m+1$ is not a one-to-one mapping. Instead, the fitted quadratic curve (3.17) may start from m, go through $m-1$ and arrive at $m+1$, shown as the dash line in Figure 3.2. Moreover, if $x(m-1)=x(m+1)$, it is impossible to take the inverse of matrix in Equation (3.19). As such, the quadratic equation cannot be used at the extreme point. Given the output at the extreme point m, the output of the next point $m+1$ can be estimated by using the trapezoid estimation. Thus, the use of Equation (3.10)~(3.16) yields

if $x(m+1) \geq x(m)$,

$$y_1(m+1) = \frac{\alpha(m+1)}{2-c\beta(m+1)} + \frac{2+c\beta(m+1)}{2-c\beta(m+1)} y_1(m) \tag{3.26}$$

$$y_2(m+1) = \frac{2\beta(m+1)}{2-c\beta(m+1)} + \frac{2+c\beta(m+1)}{2-c\beta(m+1)} y_2(m) \tag{3.27}$$

if $x(m+1) < x(m)$,

$$y_1(m+1) = \frac{-\alpha(m+1)}{2+c\beta(m+1)} + \frac{2-c\beta(m+1)}{2+c\beta(m+1)} y_1(m) \tag{3.28}$$

$$y_2(m+1) = \frac{2\beta(m+1)}{2+c\beta(m+1)} + \frac{2-c\beta(m+1)}{2+c\beta(m+1)} y_2(m) \tag{3.29}$$

3.5.3.2 Discrete ARMA-based Hysteresis Model

In the literature, the ARMA model has been widely applied to auto-correlated time series data. Given a time series of data z_t, the ARMA model is used to predict the future values by taking the following form

$$z(t) = \sum_{i=1}^{N_z} a_i z(t-i) + \sum_{i=0}^{N_y} b_i y(t-i) \tag{3.30}$$

In our previous study [46], it was concluded for a PEA-driven positioning stage that if the

mass ratio of the stage to the PEA is big enough that the system can be approximated by using a second order system. By utilizing a second order ARMA model, one can have the following equation.

$$z(t) = a_1 z(t-1) + a_2 z(t-2) + b_0 y(t) + b_1 y(t-1) + b_2 y(t-2) \tag{3.31}$$

Substituting the discrete hysteresis Equation (3.10) and (3.14) into Equation (3.31), one can obtain the discrete ARMA-based hysteresis model, which will be used to describe the rate-dependent PEA hysteresis, i.e.,

$$\begin{aligned} z(t) &= a_1 z(t-1) + a_2 z(t-2) + b_0[a y_1(t) + b y_2(t)] \\ &\quad + b_1[a y_1(t-1) + b y_2(t-1)] + b_2[a y_1(t-2) + b y_2(t-2)] \\ &= a_1 z(t-1) + a_2 z(t-2) + b_0' y_1(t) + b_0'' y_2(t) \\ &\quad + b_1' y_1(t-1) + b_1'' y_2(t-1) + b_2' y_1(t-2) + b_2'' y_2(t-2) \end{aligned} \tag{3.32}$$

3.5.4 Parameter Identification

Given a series of known data sets $\{y_{1i}, y_{2i}, z_i\}$, Equation (3.32) can be rewritten as

$$\mathbf{Z} = \mathbf{W}\boldsymbol{\theta} \tag{3.33}$$

where $\mathbf{Z} = [z_3, z_4, \cdots, z_i]^T$; $\boldsymbol{\theta} = [a_1, a_2, b_0', b_0'', b_1', b_1'', b_2', b_2'']$ is the parameter vector which is to be identified; $\mathbf{W} = \begin{bmatrix} z_2, & z_1, & y_{13}, & y_{23}, & y_{12}, & y_{22}, & y_{11}, & y_{21} \\ z_3, & z_2, & y_{14}, & y_{24}, & y_{13}, & y_{23}, & y_{12}, & y_{22} \\ & & & & \cdots & & & \\ z_{i-1}, & z_{i-1}, & y_{1i}, & y_{2i}, & y_{1(i-1)}, & y_{2(i-1)}, & y_{1(i-2)}, & y_{2(i-2)} \end{bmatrix}$; i represents the number of the data points.

Equation (3.33) is linear, so the vector of $\boldsymbol{\theta}$ can be readily identified by using the least square method. Online estimation method can be applied as well to continuously update parameters as new data become available. However, in the present study as suggested by Equation (3.12) (3.13) (3.15) (3.16), the data sets $\{y_{1i}, y_{2i}\}$ are calculated from the measured

input voltage $\{x_i\}$ and the value of *c* which is an unknown parameter. It is required to obtain the value of parameter *c* firstly in order to use the ordinary parameter identification methods.

Consider the model error, Equation (3.33) can be rewritten as

$$\mathbf{Z} = \mathbf{W}\boldsymbol{\theta} + \boldsymbol{\varepsilon} \tag{3.34}$$

where $\boldsymbol{\varepsilon}$ is an error vector which follows a normal distribution. The parameter vector $\boldsymbol{\theta}$ can be identified by using least square method as

$$\boldsymbol{\theta} = (\mathbf{W}^T\mathbf{W})^{-1}\mathbf{W}^T\mathbf{Z} \tag{3.35}$$

If there is an uncertainty of parameter *c*, it will induce an error in the estimation of $y_1(k+1)$ and $y_2(k+1)$ to the estimation of matrix **W**. Suppose the estimation error of **W** is **M**, then Equation (3.35) becomes:

$$\boldsymbol{\theta} = [(\mathbf{W}+\mathbf{M})^T(\mathbf{W}+\mathbf{M})]^{-1}(\mathbf{W}+\mathbf{M})^T\mathbf{Z} \tag{3.36}$$

The expectation of the estimated parameter $\boldsymbol{\theta}$ is given by, if $\mathbf{W}+\mathbf{M} \neq 0$ and $\mathbf{M} \neq 0$

$$E(\boldsymbol{\theta}) = \boldsymbol{\theta} - [(\mathbf{W}+\mathbf{M})^T(\mathbf{W}+\mathbf{M})]^{-1}(\mathbf{W}+\mathbf{M})^T\mathbf{M}\boldsymbol{\theta} \tag{3.37}$$

which indicates that with the error in estimating *c*, the estimated parameters will be biased. To address this issue, a straight forward method is to adjust the value of *c* in the parameter identification until the difference between model predictions and experimental results is minimum, which is detailed in the following section.

3.5.5 Experiments and Results

The experiments presented in this section were implemented on a PEA (P-753, Physik Instrumente), shown in Figure 3.3. The actuator can generate displacement in a range of 15 μm with a resolution of 0.5 nm. For displacement measurements, a capacitive displacement sensor with a resolution of 50 nm, which is a built-in sensor of the P-753 PEA, was used. Both the

actuator and the sensor were connected to a host computer via an I/O board (PCI-DAS1602/16, Measurement Computing Corporation) and controlled via SIMULINK programs. All displacements were measured with a sampling interval of 0.05 ms. The mass ratio of the stage to the PEA is 49.8, suggesting that the dynamics of the piezoelectric driven stage can be regarded as a second order system approximately according to the previous study [46], [130].

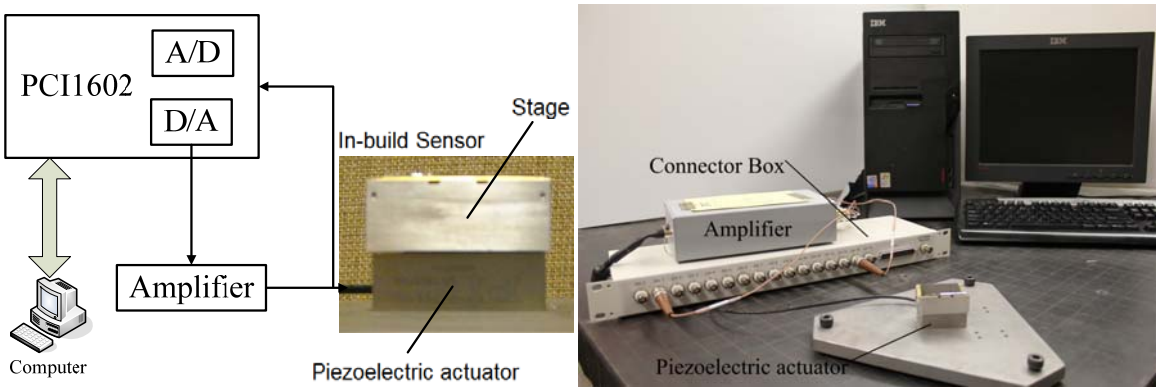

(a) (b)

Figure 3. 3 Experimental settings on the piezoelectric driven stage (a) schematic and (b) picture.

In the experiments, three types of inputs were used to excite the system. One type is the sinusoidal inputs with amplitude of 70 V and varying frequencies from 1 Hz to 200 Hz. These sinusoidal inputs and the measured outputs were used in the parameter identification. The second type of inputs is the piecewise continuous combination of different-amplitude sinusoidal inputs with the same frequency, as shown in Figure 3.4*a*. The last type is the superposition of four sinusoidal inputs with different frequency, amplitude and phase delay, as shown in Figure 3.4*b*. The latter two types of inputs were mainly used in model verification.

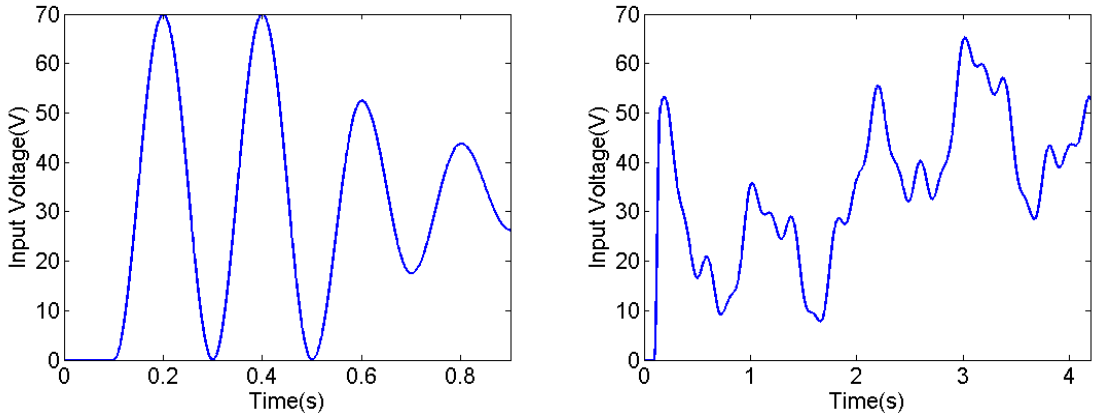

(a) (b)

Figure 3. 4 Input voltage for the model verification
(a) the piecewise continuous combination of different-amplitude sinusoidal inputs with the same frequency and (b) the superposition of four sinusoidal input with different frequency, amplitude and phase delay.

3.5.5.1 Parameter Identification

The values of parameters *a, b* and *c* were initially identified from the 1 Hz 70 V sinusoidal input and the measured output by using least square method, which gives $a = 0.0064$, $b = 0.1144, c = -0.0378$. With the value of *c*, data sets $\{y_{1i}, y_{2i}\}$ were produced for identifying the parameters involved in the linear model (3.33) and the estimation errors were calculated in terms of the 2-norm of the error vector. By adjusting the value of c around the above initially-identified value (i.e., -0.0378), the estimation errors were obtained and it was found that the minimum error occurs at $c = -0.0305$. On this basis, the least square method and online estimation method was used, respectively, to identify other parameters of the discrete ARMA-based hysteresis model by employing the trapezoid estimation. The identified results are summarized in Table 3-1 and Table 3-2 along with the calculated 2-norm errors. From Table 3-1 and Table 3-2, it is seen that the online estimation method can get a better estimation than the least square method.

Table 3- 1 Identifcation results of the discrete ARMA based hysteresis model developed by trapezoid equation estimation based on the least square method

Parameters	a_1	a_2	b_0'	b_0''	c
Value	0.0725	0.7577	-0.0703	-1.4122	-0.0305
Parameters	b_1'	b_1''	b_2'	b_2''	$Error(\mu m)$
Value	0.1448	2.9350	-0.0732	-1.5032	0.0451

Table 3- 2 Identification results of the discrete ARMA based hysteresis model developed by trapezoid equation estimation based on the online estimation method

Parameters	a_1	a_2	b_0'	b_0''	c
Value	1.6531	-0.6758	-0.002759	-0.07323	-0.0305
Parameters	b_1'	b_1''	b_2'	b_2''	$Error(\mu m)$
Value	0.006409	0.1736	-0.003526	-0.09756	0.0309

Table 3- 3 Identification results of the discrete ARMA based hysteresis model developed by quadratic equation estimation based on the least square method

Parameters	b_1'	b_1''	b_2'	b_2''	$Error(\mu m)$
Value	0.0592	0.7413	-0.0763	-2.4981	-0.029
Parameters	b_1'	b_1''	b_2'	b_2''	$Error(\mu m)$
Value	0.1539	5.0563	-0.0766	-2.5343	0.1323

Table 3- 4 Identification results of the discrete ARMA based hysteresis model developed by quadratic equation estimation based on the online estimation method

Parameters	b_1'	b_1''	b_2'	b_2''	$Error(\mu m)$
Value	1.6522	-0.6751	-0.0027	-0.0748	-0.029
Parameters	b_1'	b_1''	b_2'	b_2''	$Error(\mu m)$
Value	0.0063	0.1766	-0.0035	-0.099	0.0309

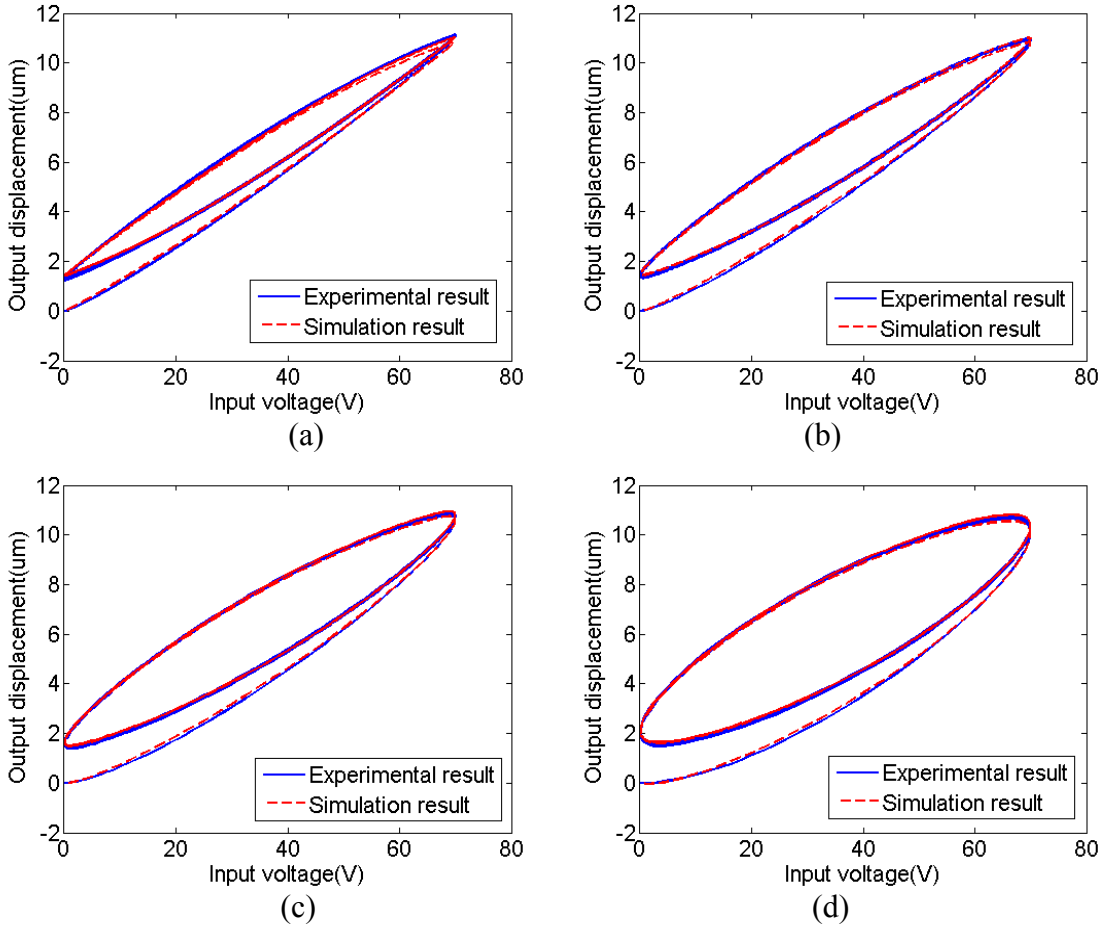

Figure 3. 5 Comparsion of experimental results and simulation results under inputs with a fixed amplitude of 70 V and different frequencies
(a) 10 Hz, (b) 50 Hz, (c) 100 Hz, and (d) 200 Hz.

Using the same method, Table 3-3 and Table 3-4 show the estimation results for the discrete ARMA-based hysteresis model developed by using the quadratic estimation based on least square method and online estimation method, respectively. As an example, Figure 3.5 shows the online estimation result for the discrete ARMA-based hysteresis model developed by using quadratic equation, under inputs with a fixed amplitude of 70 V and different frequencies of 10, 50, 100, and 200 Hz. It can be seen that the simulation results are in agreement with the experimental results.

3.5.5.2 Model Verification

The inputs shown in Figure 3.4 and the recorded output were used for the model verification. Table 3-5 shows each type of input data and their abbreviation.

A. Comparison between the discrete ARMA-based hysteresis model developed by trapezoid equation and an existing discrete hysteresis model

In order to verify the effectiveness of the discrete ARMA-based hysteresis model, a comparison was made with an existing discrete hysteresis model reported in [68]. As the discrete hysteresis model developed in [68] is rate-independent, it was combined with the ARMA model to represent the rate-dependent performance of the PEA and the same parameter identification method was applied. With the identical input, the corresponding output predicted by both the discrete ARMA-based hysteresis model developed by trapezoid equation and the existing discrete hysteresis model were obtained and compared, respectively, with the measured displacement. Since the online estimation method leads to a better identification than the least square method, the parameters in both models were identified by the online estimation method. Figure 3.6 shows the results of output displacement vs. input voltage and the result of error vs. time for the inputs of PWSW200 and SW100. The solid line presents the experimental results and the dash line presents the simulation results calculated by the discrete ARMA-based hysteresis model developed by using trapezoid estimation. Table 3-6 shows a complete comparison of errors for all inputs used. From the results listed above, it can be seen that as the input frequency increases, the estimated error increases. In contrast to the existing discrete hysteresis model, the discrete ARMA-based hysteresis model has less estimation error.

Table 3- 5 Inputs used for model verification

Abbreviation	Input Description	Remarks
PWSW 10	Piecewise continuous combination of different amplitude sinusoidal inputs	10Hz
PWSW 50		50Hz
PWSW 200		200Hz
PWSW 400		400Hz
SW 100	Superposition of four sinusoidal inputs with different frequency, amplitude and phase delay	Highest 100Hz
SW 400		Highest 400Hz
SIN70V 200	70V sinusoidal input	200Hz
SIN70V 300		300Hz
SIN70V 400		400Hz
SIN70V 500		500Hz
SIN70V 600		600Hz

Table 3- 6 Error estimated from the discrete ARMA-based hysteresis model developed by trapezoid equation and the existing discrete model

Inputs	Estimation error (μm) by using Existing discrete hysteresis model	Estimation error (μm) by using Discrete ARMA-based hysteresis model
PWSW 10	0.0946	0.0943
PWSW 50	0.0996	0.0989
PWSW 200	0.1128	0.1112
PWSW 400	0.1627	0.1603
SW 100	0.2212	0.2209
SW 400	0.2683	0.2637
SIN70V 200	0.0309	0.0309
SIN70V 300	0.0570	0.0569
SIN70V 400	0.1293	0.1264
SIN70V 500	0.6041	0.5081
SIN70V 600	1.1037	1.0187

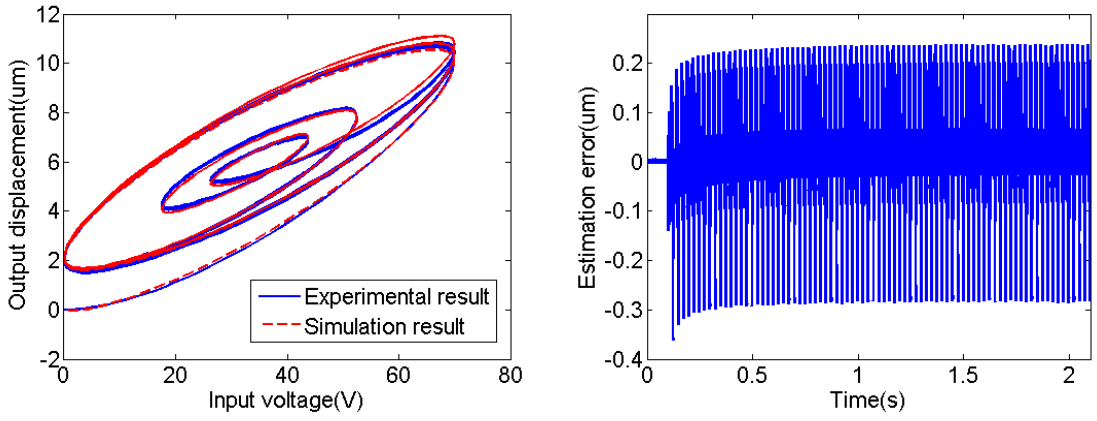

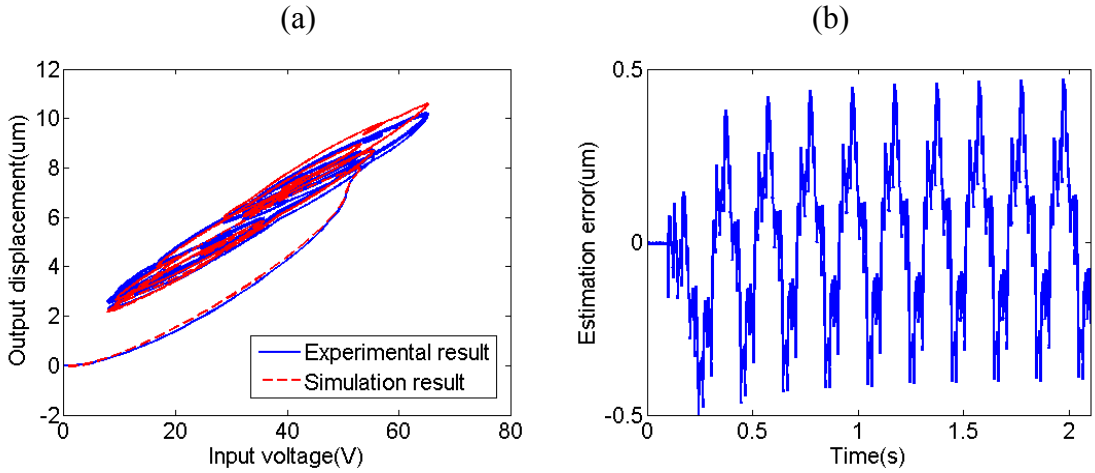

Figure 3. 6 Comparison of experimental results and simulation results and the errors (a) voltage vs. displacement for the PWSW 200 input; (b) estimation error for the PWSW 200 input; (c) voltage vs. displacement for the SW 100 input; and (d) estimation error for to the SW 100 input.

B. Comparison between the discrete ARMA-based hysteresis model developed by trapezoid equation and quadratic equation

The comparison between the discrete ARMA-based hysteresis models developed by using different discrete method was made in order to show the effect of the discrete method with high order polynomial equation. With the identical input, the corresponding outputs were calculated from the discrete ARMA-based hysteresis model developed from the trapezoid equation (3.10)~(3.16) and the quadratic equation (3.21)~(3.24), respectively, and then were compared to the measured output. The error was calculated in terms of the 2-norm of the error vector. Table 3-7 shows the estimation errors of the discrete ARMA based hysteresis model develop by the two different discrete methods. In contrast to the discrete method using trapezoid equation, the use of quadratic equation to develop the discrete ARMA-based hysteresis model can obtain better estimations, especially at high input frequencies. However, at low frequencies, the quadratic equation may be worse due to the error induced by taking inverse of the parameter matrix in Equation (3.18).

Table 3- 7 2-norm error for the discrete ARMA-based hysteresis model developed by using different discrete method

Inputs	Model verification error (μm) Develop from trapezoid estimation	Model verification error (μm) Develop from quadratic estimation
PWSW 10	0.0943	0.1009
PWSW 50	0.0989	0.1003
PWSW 200	0.1112	0.1110
PWSW 400	0.1603	0.1560
SW 100	0.2209	0.2165
SW 400	0.2637	0.2529
SIN70V 200	0.0309	0.0309
SIN70V 300	0.0569	0.0512
SIN70V 400	0.1264	0.1156
SIN70V 500	0.5081	0.4958
SIN70V 600	1.0187	1.0091

3.5.6 Conclusions and Discussions

This paper presents the development of a novel discrete ARMA-based hysteresis model to describe the hysteresis of PEA by using different discrete methods. Both least square method and online estimation method were applied to identify the model parameters. In order to show the effectiveness of the discrete ARMA-based hysteresis model, experiments were carried out and the results obtained were compared to the predictions from both ARMA-based hysteresis model and an existing discrete hysteresis model reported in [68]. It has been shown that the discrete ARMA-based hysteresis model can well predict the hysteresis of the piezoelectric actuator. Moreover, the online estimation method can get better parameter identification for the discrete ARMA-based hysteresis model than the least square method. However, the model shows larger estimation errors at high frequencies than at low frequencies due to the estimation of the integral term in the discrete hysteresis equation. Using a quadratic equation to estimate the integral term can reduce the discrete estimation error at high input frequencies. Therefore, it should be

preferred to use the quadratic equation at high input frequencies.

3.5.7 Acknowledgment

The support to the present study from the China Scholarship Council (CSC) and the Natural Sciences and Engineering Research Council (NSERC) of Canada is acknowledged.

4 Discrete Sliding Mode Control for One-DOF Piezoelectric Actuators

The work presented in this chapter is the one included in the following manuscript appended.

Y. Cao, X. B. Chen and J. Y. Peng, "An Output Tracking Integrated Discrete PID-based Sliding Mode Control on SISO systems," *ASME Journal of Dynamic system, measurement and control*, Submitted as Regular Paper in 2013, under review, manuscript ID: DS-13-1043.

4.1 Introduction and Objectives

SMC is widely employed in control applications due to its excellent performance in disturbance and uncertainty rejection. However, chattering, caused by the discontinuous switching control, can greatly deteriorate its performance. One of the methods to eliminate chattering is to employ a PID regulator instead of the discontinuous switching control, which leads to the development of a novel PID-based SMC recently. As a state tracking control scheme, it has been shown effective in the control of the second order mechanical systems, in which the states can be readily measured. For other systems such as the black box systems whose models are obtained by means of system identification, the states have limited physical meaning and their information might not be available. In such cases, the existing design method is challenged for use due to the lack of system states information. In addition, the existing PID-based SMC is continuous and may not work as expected in digital systems. Due to the unmatched sampling time, zigzag state motion exists, which suggests that the sampling itself also induces chattering. The mean of the zigzag state motion might deviate from the sliding surface, causing steady state

error. Therefore, the appropriate forms of DSMC are desirable to alleviate the aforementioned problems, especially for the applications where the sampling rate is limited. This work is to develop an output tracking based DSMC to compensate the hysteresis and other nonlinear effects of the one-DOF PEAs without chattering.

4.2 Methods

Considering the hysteresis and the other nonlinearities to be uncertainties and disturbance, the performance of the PEA can be described using the general discrete time invariant linear system expressed by the transfer function

$$G(z) = \frac{\sum_{i=0}^{n} \beta_i z^{-i}}{1+\sum_{i=1}^{n} \alpha_i z^{-i}} \tag{4.1}$$

where $\alpha_i, \beta_i (i = 1,2,\cdots,n)$ and β_0 are the parameters. If $\beta_i = 0$ for $i = 1,2,\cdots,n$, the discrete transfer function can be rewritten in a state space form

$$x(k+1) = A_d x(k) + B_d u(k) \tag{4.2}$$

where $x(k) = \begin{bmatrix} y(k-n) & \cdots & y(k-2) & y(k-1) \end{bmatrix}^T \in R^{n\times 1}$ is the state; $u(k) \in R$ is the control input signal; $A_d = \begin{bmatrix} 0_{(n-1)\times 1} & I_{(n-1)\times(n-1)} \\ -\alpha_n & \boldsymbol{\alpha} \end{bmatrix}$ $(\boldsymbol{\alpha} = \begin{bmatrix} -\alpha_{n-1} & -\alpha_{n2} & \cdots & -\alpha_1 \end{bmatrix})$, $B_d = \begin{bmatrix} 0_{(n-1)\times 1} & \beta_0 \end{bmatrix}^T$ are the system matrixes of the discrete state space model. The state vector is represented in terms of the outputs in the past history. As such, the existing CSMC design method can be adopted for the development of the DSMC. However, if $\beta_i \neq 0$ $(i = 1,2,\cdots,n)$, such a state space form does not exist. Therefore, an output tracking based design approach has to be considered. Inspired by this,

the transfer function (4.1) is regarded as the cascade of the nominator $G_1(z)=\sum_{i=0}^{n}\beta_i z^{-i}/\beta_0$ and the denominator $G_2(z)=\beta_0/(1+\sum_{i=1}^{n}\alpha_i z^{-i})$ in this work. It is noted that $G_2(z)$ can be expressed by such a state space model, as shown in Equation (4.2). Thus, $v(z)$, defined as the output of $G_1(z)$ and the input of $G_2(z)$, can be derived by using the nominal SMC design approach. The input u can be obtained by cascading the inverse of the transfer function $G_1(z)$, denoted by G_1^{-1}, to the discrete PID-based SMC which is designed based on $G_2(z)$. It is noted that, due to the imperfection of the plant model, the dynamics of $G_1(z)$ may not be completely inverted by the use of G_1^{-1}. Such an error is considered as an uncertainty provided to the input of the plant and will be compensated by the PID-based SMC, as shown in Figure 4.1.

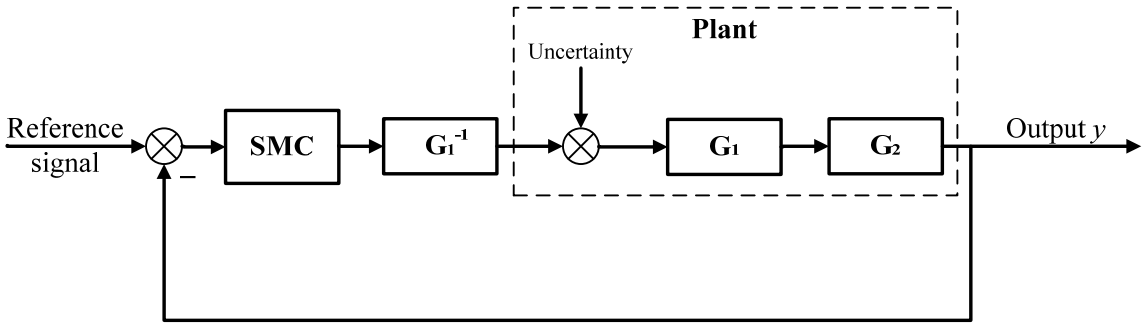

Figure 4. 1 Inversion based approach for the discrete PID-based SMC

Due to the discontinuity of the 'bang-bang' switching control in the nominal SMC design, state switching can occur at high frequency, known as chattering. In order to eliminate chattering, a discrete PID regulator is employed,

$$\Delta v(k) = -[Ps(k) + I\sum_{i=0}^{k} s(i)T + D\frac{s(k) - s(k-1)}{T}] \tag{4.3}$$

where s is the output of the switching function, P, I and D are the proportional, integral and derivative parameters respectively. Such a controller is continuous and thus chattering can be eliminated. Moreover, due to the integral component of the switching control, zero steady state error can be obtained.

4.3 Results

The output tracking based discrete PID-SMC as designed by both the traditional approach and the model reference approach can achieve better tracking performance and as the input frequency increases, the performance improvement with the proposed method becomes more profound. It is noted that the output tracking integrated discrete PID-SMC developed in this work can be used in control applications for proper SISO systems. If the reference signals are not derivable during the designated time period, the model reference approach is recommend in the controller design such that the large overshoot due to the discontinuous properties of the reference input can be eliminated.

4.4 Contributions

The contribution of this paper is the development of an output tracking integrated discrete PID-SMC, in which the system output is integrated in the SMC design such that the proposed method can be employed in the control applications for SISO systems where the system states are not available.

4.5 Paper: An Output Tracking Integrated Discrete PID-based Sliding Mode Control on SISO Systems

Authors: Y. Cao, X. B. Chen, *Member, IEEE* and J. Y. Peng[3]

Index Terms: Discrete time systems, Control systems, Piezoelectric devices, Robustness

4.5.1 Abstract

Sliding mode control (SMC) has been widely employed to compensate for the system uncertainty and disturbance. However, the chattering problem, caused by the discontinuous characteristic of switching function used in traditional SMC, greatly deteriorates the performance of SMC and has become the main limitation for its applications. Also, implementing the SMC in digital systems could make it even worse due to the limited sampling time. Moreover, as a state tracking control scheme, traditional SMC cannot be employed in the applications where the system states are not available. To alleviate these problems, the paper presents the development of a novel control method, so called "the output tracking integrated discrete PID-based SMC", along with the controller design approaches (i.e., the traditional SMC design approach and the model reference approach). Without the need of system states, this novel method allows for eliminating chattering problem and the steady state error that may exists in such control methods

---

Manuscript received October 18, 2012. This work was supported by the China Scholarship Council (CSC) and the Natural Science and Engineering Research Council (NSERC) of Canada.

Y. Cao is with the Department of Mechanical Engineering, 57 Campus Drive, University of Saskatchewan, Saskatoon, SK, S7N 5A9 (e-mail: yuc150@ mail.usask.ca).

X. B. Chen is with the Department of Mechanical Engineering, 57 Campus Drive, University of Saskatchewan, Saskatoon, SK, S7N 5A9 (phone: 1-306-966-1267; e-mail: xbc719@ mail.usask.ca).

J. Y. Peng is with the Department of Mechanical Engineering, 57 Campus Drive, University of Saskatchewan, Saskatoon, SK, S7N 5A9 (e-mail: jip747@ mail.usask.ca).

as the continuous PID-based SMC. In order to demonstrate the effectiveness of the developed method, experiments were carried out on a commercially available piezoelectric actuator with varying sampling times, as compared to the continuous PID-based SMC. The results illustrate that the tracking performance with the proposed method is much better than the continuous PID-based SMC.

4.5.2 Introduction

Sliding model control (SMC) is a form of variable structure control and has been recently drawing considerable attention in the control research community worldwide due to its ability to compensate for the system uncertainties and disturbance [81], [91], [92], [94]. However, because of the discontinuity of SMC switching control, chattering exists and thus excites undesired system high resonance mode to deteriorate the system tracking performance. One solution to the chattering problem is to use the boundary layer control [94], in which a saturation switching control is employed to replace the discontinuous switching control. It is noted that, if the unknown disturbance is profound, a sufficiently-high gain in controller is always required and such a control scheme behaves like a high-gain proportional (P) controller. As a result, steady state error may exist. An alternative way is to enlarge the width of the boundary layer, thus decreasing the effective linear gain for reduced state oscillation around sliding surface. However the state can no longer strictly locate on the ideal sliding surface due to the wider boundary layer and the system does not behave as described by the sliding mode. In [95], a high order sliding surface was used to replace the first order one typically used in the nominal SMC design. With the main advantages of the nominal SMC, the high order sliding mode control (HOSMC) can reduce the chattering effect and improve the accuracy for its realization. The main problem is that it requires increasing sliding information in implementing the HOSMC [97]. Recently, a

new continuous proportional-integral -derivative (PID)-based SMC was developed [98], in which the discontinuous 'bang-bang' switching function is replaced by a PID regulator in order to eliminate the chattering problem. Due to the integral effect of the PID regulator, the steady state tracking error can be eliminated.

As a state tracking control scheme, the PID-based SMC developed in [98] has been shown effective in the control of the second order mechanical systems, in which the states can be readily estimated from the measured output based on its physical model. In some applications, the system states may not be readily, or even be impossibly, obtained [104] due the system complexity. In such cases, the application of the PID-based is challenged due to the lack of information of system states [92].

Furthermore, it is noticed that, if implemented in a digital computer, the continuous SMC (CSMC) may not work as expected [100], [131]. For discrete SMC (DSMC), if the switching time doesn't match the sampling time, the states will not lay on the sliding surface and the trajectory appears like a zigzag motion around the sliding surface, which suggests that the sampling itself also induces the chattering problem in the DSMC. If the mean of zigzag motion deviates from the sliding surface, the steady state error will exist. Therefore, the appropriate forms of discrete SMC are desirable to alleviate the aforementioned problems, especially for the applications where the sampling rate is limited. In [132], a robust DSMC design was proposed for a nonlinear electrical hydraulic actuator system; and the state required was measured by means of a position sensor. In [133], the DSMC design was combined with a state estimator and disturbance observer, which, however, significantly increased the system complexity.

To raise these challenges, this paper presents the development of a novel control method, so called "the output tracking based DSMC", in which the system output is integrated in the SMC

design such that the proposed method can be employed in the applications where the system states are not available. Furthermore, the proposed method is cascaded with the optimal inversion control to further improve the system dynamics, in which the error caused by the imperfect compensation of the optimal inversion is treated as a disturbance and then rejected by the PID-based SMC. In addition, due to the application of the PID regulator in the proposed method, as designed by means of the traditional SMC design approach and the model reference approach, the state zigzag motion, as observed in other DSMCs, is eliminated for improved performance. In order to verify the effectiveness of the proposed method, experiments were carried out on a commercially available piezoelectric actuator (PEA), as compared to the continuous PID-based SMC.

4.5.3 Output Tracking Integrated PID-based Sliding Mode Control

4.5.3.1 Problem statement

Consider a discrete *n*th order single-input-single-output (SISO) system defined by Equation (4.1) where $\alpha_i, \beta_i (i = 1, 2, \cdots, n)$ and β_0 are the parameters and the numerator and denominator are relatively prime polynomials. If $\beta_i = 0$ for $i = 1, 2, \cdots, n$, the discrete transfer function can be rewritten in a state space form $x(k+1) = A_d x(k) + B_d v(k)$, as shown in Equation (4.2), where $x(k) = \begin{bmatrix} y(k-n) & \cdots & y(k-2) & y(k-1) \end{bmatrix}^T \in R^{n\times 1}$ is the state vector; $v(k) \in R$ is the control input signal vector; $A_d = \begin{bmatrix} 0_{(n-1)\times 1} & I_{(n-1)\times(n-1)} \\ -\alpha_n & \boldsymbol{\alpha} \end{bmatrix}$ $(\boldsymbol{\alpha} = \begin{bmatrix} -\alpha_{n-1} & -\alpha_{n-2} & \cdots & -\alpha_1 \end{bmatrix})$, $B_d = \begin{bmatrix} 0_{1\times(n-1)} & \beta_0 \end{bmatrix}^T$ are the system matrixes of the discrete state space model. The state vector is represented in terms of the outputs in the past history. As such, the method introduced in [98]

can be adopted and applied in the design SMC.

For the systems whose model is obtained by means of system identification with $\beta_i \neq 0$ $(i = 1, 2, \cdots, n)$, the aforementioned state space form does not exist and as such, an output tracking based design process has to be employed. For this, the transfer function (4.1) is regarded as the cascade of the nominator $G_1(z) = \sum_{j=0}^{n} \beta_i z^{-j} / \beta_0$ and the denominator $G_2(z) = \beta_0 / (1 + \sum_{i=1}^{n} \alpha_i z^{-i})$, as shown in Figure 4.2.

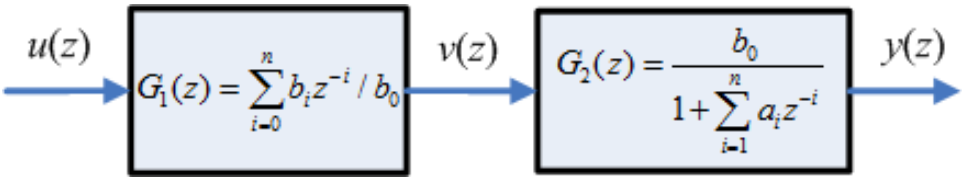

Figure 4. 2 Decomposition of the discrete SISO plant

It is noted that $G_2(z)$ can be expressed by such a state space model, as shown in Equation (4.2). Therefore, the output of $G_1(z)$ or the input to $G_2(z)$, dented by *v*(*z*) in the following, can be derived from the traditional SMC design. The input *u* can be obtained by cascading the inverse of the transfer function $G_1(z)$, denoted by $G_1^{-1}(z)$, to the discrete PID-based SMC which is designed based on $G_2(z)$. It is noted that, due to the imperfection of the plant model, the dynamics of $G_1(z)$ may not be completely inverted by the use of $G_1^{-1}(z)$. Such an error due to the model imperfection is considered as an uncertainty added to the input of the plant and will be compensated by the PID-based SMC, as shown in Figure 4.1.

4.5.3.2 Traditional SMC design

Consider Equation (4.2) with the bounded and matched uncertainties and disturbance

$$x(k+1) = A_d x(k) + B_d v(k) + \varepsilon(k) \tag{4.4}$$

Denote the desired output vector to be $x_d(k) = \begin{bmatrix} y_d(k-n) & \cdots & y_d(k-2) & y_d(k-1) \end{bmatrix}^T \in R^{n\times 1}$. The objective of DSMC is to force the error state $e(k) = x(k) - x_d(k)$, staring from any initial value, to move to the sliding surface and then converge to zero. Equation (4.4) can be rewritten in terms of the dynamics of $e(k)$,

$$e(k+1) = A_d e(k) + B_d v(k) + \varepsilon(k) + A_d x_d(k) - x_d(k+1) \tag{4.5}$$

Similar to the general design approach for the continuous system, the input $v(k)$ can be divided into two parts $v_1(k)$ and $v_{SM}(k)$, i.e.,

$$v_1(k) = -B_d{}^{\dagger}[A_d x_d(k) - x_d(k+1)] \tag{4.6}$$

where $B_d{}^{\dagger}$ is the pseudo inverse of matrix B_d.

Substituting Equation (4.6) into Equation (4.5) yields

$$e(k+1) = A_d e(k) + B_d v_{SM} + \varepsilon(k) + (I - B_d B_d^{\dagger}) A_d x_d(k) - (I - B_d B_d^{\dagger}) x_d(k+1) \tag{4.7}$$

For the system described by Equation (4.4), it can be verified $(I - B_d B_d^{\dagger}) A_d x_d(k) - (I - B_d B_d^{\dagger}) x_d(k+1) = 0$. Thus, Equation (4.7) is reduced to

$$e(k+1) = A_d e(k) + B_d v_{SM} + \varepsilon(k) \tag{4.8}$$

For the sliding function that takes the following form of

$$s(k) = Se(k) \tag{4.9}$$

where S defines the shape of the sliding surface, the control action can be considered consisting two parts, i.e.,

$$v_{SM}(k) = v_{eq}(k) + \Delta v(k) \tag{4.10}$$

where $v_{eq}(k) = -(SB_d)^{-1} SA_d e(k)$ is the equivalent control and $\Delta v(k)$ is the switching control. Substituting Equation (4.10) into Equations (4.8) and (4.9) yields

$$e(k+1) = [I - B_d (SB_d)^{-1} S] A_d e(k) + B_d \Delta v(k) + \varepsilon(k) \tag{4.11}$$

$$s(k+1) = SB_d \Delta v(k) + S\varepsilon(k) \tag{4.12}$$

For the convenience of following discussion, Equations (4.9) and (4.11) are rewritten as

$$e(k+1) = A_p e(k) + B_d \Delta v(k) + \varepsilon(k), \quad s(k) = Se(k) \tag{4.13}$$

where $A_p = [I - B_d (SB_d)^{-1} S] A_d$. The system described by Equation (4.13) is equivalent to a dynamic plant, where $\Delta v(k)$ is the input and $s(k)$ is the output. The aim of the controller design is to force the output of the equivalent plant to be zero. Instead of using the switching control, a PID regulator is employed to generate the control signal in this paper, as shown in Figure 4.3, which is given by Equation (4.3), where P, I and D are parameters of the discrete PID-based SMC; T is the sampling period.

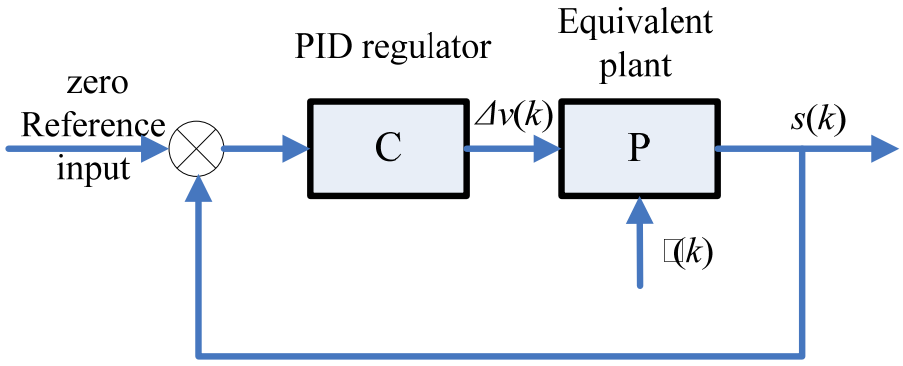

Figure 4. 3 Equivalent plant for the design of $\Delta v(k)$

Theorem 4.1: If the closed-loop system is stable, by using the PID regulator stated in

Equation (4.3), the steady state output of the equivalent plant (4.13) will be zero [134], i.e., $s(\infty) = \lim_{z \to 1} s(z) = 0$.

Theorem 4.2: There exist such parameters *P*, *I* and *D* that the closed-loop control system in Figure 4.3 is stable.

Proof: Substituting Equation (4.3) into (4.12) yields

$$s(k+1) = -(PSB_d + ISB_dT + DSB_d / T)s(k) + (DSB_d / T)s(k-1) - ISB_dT\sum_{i=0}^{k-1} s(i) + S\varepsilon(k) \quad (4.14)$$

Note that

$$ISB_dT\sum_{i=0}^{k-1} s(i) = -s(k) - PSB_d s(k-1) - DSB_d[s(k-1) - s(k-2)]/T + S\varepsilon(k-1) \quad (4.15)$$

Thus, Equation (4.14) can be rewritten as

$$\begin{aligned} s(k+1) = {} & (1 - PSB_d - ISB_dT - DSB_d / T)s(k) + (2DSB_d / T + PSB_d)s(k-1) \\ & + (DSB_d / T)s(k-2) + S\varepsilon(k) - S\varepsilon(k-1) \end{aligned} \quad (4.16)$$

Denoting $\phi(k) = S\varepsilon(k) - S\varepsilon(k-1)$, Equation (4.16) can be re-expressed as a discrete transfer function $s(z)/\phi(z)$ with its characteristic function given by

$$p(z) = z^3 + (1 - PSB_d - ISB_dT - DSB_d / T)z^2 + (2DSB_d / T + PSB_d)z + (DSB_d / T) \quad (4.17)$$

The poles of the transfer function can be arbitrarily allocated by defining the coefficients of the characteristic function

$$\begin{bmatrix} SB_d & SB_dT & SB_d / T \\ SB_d & 0 & 2SB_d / T \\ 0 & 0 & SB_d / T \end{bmatrix} \begin{bmatrix} P \\ I \\ D \end{bmatrix} = \mathbf{H} \begin{bmatrix} P \\ I \\ D \end{bmatrix} = \begin{bmatrix} 1 - \gamma_2 \\ \gamma_1 \\ \gamma_0 \end{bmatrix} \quad (4.18)$$

where γ_0, γ_1 and γ_2 are the coefficients of the characteristic function derived from the desired poles. Matrix **H** is full rank. Therefore, there exist *P*, *I* and *D* such that the closed-loop control system in Figure 4.3 is stable.

The input u can be obtained by an inverse feedforward control, as shown in Figure 4.2.Taking the inverse Z-Transform of the transfer function of $G_1(z)$ yields

$$u(k) = [\beta_0 v(k) - \beta_1 u(k-1) - \cdots - \beta_n u(k-n)] / \beta_0 \tag{4.19}$$

This recursive equation can be readily implemented in digital systems. It is noted in Equation (4.19) that the poles in the transfer function from $v(z)$ to $u(z)$ are the zeros of the plant (4.1). Therefore, the stability of the traditional SMC design approach depends on the location of the zeros of the plant. For the SISO system with zeros locating outside the unit circle, the divergent input u needs to be generated from Equation (4.19). To solve this problem, the optimal inversion, as reported in [6], is adopted and used in the present paper. The objective of the optimal inversion is to develop an input u such that the following cost function is minimized

$$J = [u(k) - u_d(k)]^T Q[u(k) - u_d(k)] + u^T(k) R u(k) \tag{4.20}$$

where $u_d(k) = [\beta_0 v(k) - \beta_1 u(k-1) - \cdots - \beta_n u(k-n)] / \beta_0$, Q and R are weight matrixes, which determine the stability of the optimal inversion. As such, the optimal input is given by

$$u_{opt}(k) = \frac{Q[\beta_0 v(k) - \beta_1 u(k-1) - \cdots - \beta_n u(k-n)]}{\beta_0 (R+Q)} \tag{4.21}$$

4.5.3.3 Model reference design of the output tracking based DSMC

An alternative way to design the output tracking based DSMC is the model reference approach, as shown in Figure 4.4. The objective of the model reference design is to develop a control action which forces the plant dynamics to follow the dynamics of an ideal model. The controller should thus forces the error between the actual output y and the desired output calculated by the reference model y_d to zero as time approaches to infinity.

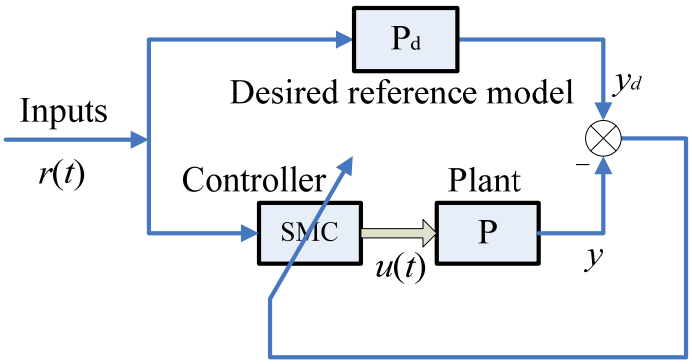

Figure 4. 4 Model reference approach of the SMC design

For the *n*th order discrete SISO system that is described by Equation (4.1) with bounded disturbance and uncertainties, the state space representation is

$$\begin{aligned} x(k+1) &= A_d x(k) + B_d u(k) + \varepsilon(k) \\ y(k) &= C_d x(k) + D_d u(k) \end{aligned} \tag{4.22}$$

It is noted that D_d does not have to be a zero matrix. Suppose the desired state space representation is denoted by

$$\begin{aligned} w(k+1) &= A_m w(k) + B_m r(k) \\ y_d(k) &= C_m w(k) + D_m r(k) \end{aligned} \tag{4.23}$$

where $w(k) \in R^{m\times 1}$ is the state; $r(k) \in R$ is the reference input signal; $y_d(k) \in R$ is the output of the reference system; $A_m \in R^{m\times m}$, $B_m \in R^{m\times 1}$, $C_m \in R^{1\times m}$ and $D_m \in R$ are the system matrixes. The aim of the model reference approach is to force the output of the actual system to follow the output of reference system. Denoting the tracking error as

$$e(k) = y(k) - y_d(k) = C_d x(k) + D_d u(k) + \varepsilon(k) - C_m w(k) - D_m r(k) \tag{4.24}$$

With the denotation of $\delta(k) = [e(k), e(k+1), \cdots, e(k+n-1)]^T$, Equation (4.24) leads to,

$$\begin{aligned} \delta(k) &= A_c x(k) + B_{c0} u(k) + \cdots + B_{c(n-1)} u(k+n-1) \\ &+ \Delta(k) - A_{cm} w(k) - B_{cm0} r(k) - \cdots - B_{cm(n-1)} r(k+n-1) \end{aligned} \tag{4.25}$$

where $\Delta(k)$ represents the effective disturbance and uncertainty of the system,

$$A_c = \begin{bmatrix} C_d \\ C_d A_d \\ C_d A_d{}^2 \\ \vdots \\ C_d A_d{}^{n-1} \end{bmatrix}, B_{c0} = \begin{bmatrix} D_d \\ C_d B_d \\ C_d A_d B_d \\ \vdots \\ C_d A_d{}^{n-2} B_d \end{bmatrix}, B_{c1} = \begin{bmatrix} 0 \\ D_d \\ C_d B_d \\ \vdots \\ C_d A_d{}^{n-3} B_d \end{bmatrix}, \cdots, B_{c(n-1)} = \begin{bmatrix} 0 \\ 0 \\ 0 \\ \vdots \\ D_d \end{bmatrix}, A_{cm} = \begin{bmatrix} C_m \\ C_m A_m \\ C_m A_m{}^2 \\ \vdots \\ C_m A_m{}^{n-1} \end{bmatrix},$$

$$B_{cm0} = \begin{bmatrix} D_m \\ C_m B_m \\ C_m A_m B_m \\ \vdots \\ C_m A_m{}^{n-2} B_m \end{bmatrix}, B_{cm1} = \begin{bmatrix} 0 \\ D_m \\ C_m B_m \\ \vdots \\ C_m A_m{}^{n-3} B_m \end{bmatrix}, \cdots, B_{cm(n-1)} = \begin{bmatrix} 0 \\ 0 \\ 0 \\ \vdots \\ D_m \end{bmatrix},$$

$$\Delta(k) = \begin{bmatrix} 1_{1\times n} \\ C_d \\ C_d A_d \\ \vdots \\ C_d A_d{}^{n-2} \end{bmatrix} \varepsilon(k) + \begin{bmatrix} 0_{1\times n} \\ 1_{1\times n} \\ C_d \\ \vdots \\ C_d A_d{}^{n-3} \end{bmatrix} \varepsilon(k+1) + \cdots + \begin{bmatrix} 0_{1\times n} \\ 0_{1\times n} \\ \vdots \\ 0_{1\times n} \\ 1_{1\times n} \end{bmatrix} \varepsilon(k+n-1),$$ Equation (4.25) leads to

$$\begin{aligned} \delta(k+1) = {} & A_c A_d x(k) + A_c B_d u(k) + B_{c0} u(k+1) + \cdots + B_{c(n-1)} u(k+n) + A_c \varepsilon(k) \\ & + \Delta(k+1) - A_{cm} A_m w(k) - A_{cm} B_m r(k) - B_{cm0} r(k+1) - \cdots - B_{cm(n-1)} r(k+n) \end{aligned} \tag{4.26}$$

It is noted that $A_c \in R^{n\times n}$. Under the assumption that system (4.26) be controllable, i.e., $|A_c| \neq 0$, one has

$$\begin{aligned} x(k) = {} & A_c^{-1}[\delta(k) - B_{c0} u(k) - B_{c1} u(k+1) - \cdots - B_{c(n-1)} u(k+n-1) - \Delta(k) + A_{cm} w(k) \\ & + B_{cm0} r(k) + B_{cm1} r(k+1) + \cdots + B_{cm(n-1)} r(k+n-1)] \end{aligned} \tag{4.27}$$

Substituting Equation (4.27) into Equation (4.26) and denoting $A_e = A_c A_d A_c^{-1} \delta(k)$,

$P = A_c A_d A_c^{-1} A_{cm} - A_{cm} A_m$, $\cdots \Gamma_{n-1} = B_{c(n-2)} - A_c A_d A_c^{-1} B_{c(n-1)}$,

$\bar{\Delta}(k) = A_c \varepsilon(k) + \Delta(k+1) - A_c A_d A_c^{-1} \Delta(k)$, $R_0 = A_c A_d A_c^{-1} B_{cm0} - A_{cm} B_m$,

$R_1 = A_c A_d A_c^{-1} B_{cm1} - B_{cm0}$, $\ldots, R_{n-1} = A_c A_d A_c^{-1} B_{cm(n-1)} - B_{cm(n-2)}$ and $R_n = -B_{cm(n-1)}$, one has the dynamics of the tracking error vector δ given by

$$\begin{aligned} \delta(k+1) = {} & A_e \delta(k) + \Gamma_0 u(k) + \cdots + \Gamma_{n-1} u(k+n-1) \\ & + B_{c(n-1)} u(k+n) + P w(k) + \bar{\Delta}(k) + R_0 r(k) + \cdots + R_n r(k+n) \end{aligned} \tag{4.28}$$

Equation (4.28) has similar form as Equation (4.5). As such the traditional SMC design can be employed to generate the control signal *u*. Following the design as shown in Equation (4.6), one has the control signal consisting of two parts $u(k) = u_1(k) + u_2(k)$. Therefore, Equation (4.28) can be re-written as

$$\delta(k+1) = A_e\delta(k) + Pw(k) + f(u_1) + f(u_2) + \bar{\Delta}(k) + g(r) \tag{4.29}$$

where $f(u_1) = \Gamma_0 u_1(k) + \cdots + \Gamma_{n-1} u_1(k+n-1) + B_{c(n-1)} u_1(k+n)$,

$f(u_2) = \Gamma_0 u_2(k) + \cdots + \Gamma_{n-1} u_2(k+n-1) + B_{c(n-1)} u_2(k+n)$ and

$g(r) = R_0 r(k) + R_1 r(k+1) + \cdots + R_n r(k+n)$.

For a perfect tracking performance, it is required that $\delta(k+1) = 0$. If

$$Pw(k) + f(u_1) + g(r) = 0 \tag{4.30}$$

then Equation (4.29) leads to a nominal SMC problem

$$\delta(k+1) = A_e\delta(k) + f(u_2) + \bar{\Delta}(k) \tag{4.31}$$

In the following passages, $\boldsymbol{u_1}$ will be derived from Equation (4.30). Then the nominal SMC design will be applied to Equation (4.31) and both the equivalent control and the PID regulator will be obtained.

(1) Determination of $\boldsymbol{u_1}$

From Equation (4.30), one has

$$u_1(k+n) = -B_{c(n-1)}^{\dagger}[Pw(k) + \Gamma_0 u_1(k) + \cdots + \Gamma_{n-1} u_1(k+n-1) + R_0 r(k) + \cdots + R_n r(k+n)] \tag{4.32}$$

Substituting Equation (4.32) into Equation (4.30) yields

$$(I - B_{c(n-1)}B_{c(n-1)}^{\dagger})Pw(k) + (I - B_{c(n-1)}B_{c(n-1)}^{\dagger})\Gamma_0 u_1(k) + \cdots + (I - B_{c(n-1)}B_{c(n-1)}^{\dagger})\Gamma_{n-1} u_1(k+n-1) +$$
$$(I - B_{c(n-1)}B_{c(n-1)}^{\dagger})R_0 r(k) + (I - B_{c(n-1)}B_{c(n-1)}^{\dagger})R_1 r(k+1) + \cdots + (I - B_{c(n-1)}B_{c(n-1)}^{\dagger})R_n r(k+n) = 0$$

(4.33)

Equation (4.33) is satisfied for any values of *w* and *r* if and only if

$$\begin{aligned}&(I - B_{c(n-1)}B_{c(n-1)}^{\dagger})P = 0, (I - B_{c(n-1)}B_{c(n-1)}^{\dagger})\Gamma_0 = 0, (I - B_{c(n-1)}B_{c(n-1)}^{\dagger})\Gamma_1 = 0, \cdots, \\ &(I - B_{c(n-1)}B_{c(n-1)}^{\dagger})\Gamma_{n-1} = 0, (I - B_{c(n-1)}B_{c(n-1)}^{\dagger})R_0 = 0, (I - B_{c(n-1)}B_{c(n-1)}^{\dagger})R_1 = 0, \cdots, \\ &(I - B_{c(n-1)}B_{c(n-1)}^{\dagger})R_n = 0\end{aligned} \tag{4.34}$$

Theorem 4.3: For a controllable SISO system described by Equation (4.1), the conditions as given in (4.34) are satisfied if the reference model is selected such that $C_m A_m^{i-1} \neq 0_{1\times m}$ $(i = 1, 2, \cdots, n)$.

Proof: The Equation (4.1) can be rewritten as

$$G(z) = d + \frac{b_{n-1}z^{n-1} + b_{n-2}z^{n-2} + \cdots + b_1 z + b_0}{z^n - a_{n-1}z^{n-1} - a_{n-2}z^{n-2} - \cdots - a_1 z - a_0} \tag{4.35}$$

The state space representation of the above system is similar to Equation (4.22).

Lemma 4.1: If A_c is of rank *n*, then $A_c A_d A_c^{-1}$ can be expressed in terms of its controllable canonical form [135].

Lemma 4.2: For the system of simultaneous equations denoted by $HD = E$, a solution for *D* exists if and only if rank[*H E*] = rank[*H*] [92].

According to Lemma 4.1, $A_c A_d A_c^{-1}$ can be expressed as

$$A_c A_d A_c^{-1} = \begin{bmatrix} N_{11} & N_{12} \\ N_{21} & N_{22} \end{bmatrix} \tag{4.36}$$

where $N_{11} = \begin{bmatrix} 0_{(n-2)\times 1} & I_{(n-2)\times(n-2)} \\ 0 & 0_{1\times(n-2)} \end{bmatrix}$, $N_{12} = \begin{bmatrix} 0_{(n-2)\times 1} \\ 1 \end{bmatrix}$, $N_{21} = \alpha_0$ and

$N_{22} = \tilde{\alpha}^T = \begin{bmatrix} a_1 & a_2 & \cdots & a_{n-1} \end{bmatrix}$.

Thus, $A_c A_d A_c^{-1} A_{cm} = \begin{bmatrix} N_{11}A_{cm1} + N_{12}A_{cm2} \\ N_{21}A_{cm1} + N_{22}A_{cm2} \end{bmatrix}$

where $A_{cm1} = \begin{bmatrix} C_m{}^T & \cdots & (C_m A_m^{n-2})^T \end{bmatrix}$ and $A_{cm2} = C_m A_m^{n-1}$.

Since $N_{11}A_{cm1} + N_{12}A_{cm2} = \begin{bmatrix} 0_{(n-2)\times 1} & I_{(n-2)\times(n-2)} \\ 0 & 0_{1\times(n-2)} \end{bmatrix} A_{cm1} + \begin{bmatrix} 0_{(n-2)\times 1} \\ 1 \end{bmatrix} C_m A_m^{n-1} = A_{cm1}A_m$

Thus, $P = A_c A_d A_c^{-1} A_{cm} - A_{cm}A_m = \begin{bmatrix} N_{11}A_{cm1} + N_{12}A_{cm2} \\ N_{21}A_{cm1} + N_{22}A_{cm2} \end{bmatrix} - \begin{bmatrix} A_{cm1}A_m \\ A_{cm2}A_m \end{bmatrix} = \begin{bmatrix} 0_{(n-1)\times m} \\ N_{21}A_{cm1} + N_{22}A_{cm2} - A_{cm2}A_m \end{bmatrix}$.

Note $C_m A_m^{i-1} \neq 0_{1\times m}$ $(i = 1,2,\cdots,n)$, $Rank(P) = Rank[B_{c(n-1)}] = 1$. According to Lemma 4.2, one has $(I - B_{c(n-1)}B_{c(n-1)}^{\dagger})P = 0$. Let $M_0 = \begin{bmatrix} (C_d B_d)^T & (C_d A_d B_d)^T & \cdots & (C_d A_d{}^{n-2} B_d)^T \end{bmatrix}^T$

$$\begin{aligned} \Gamma_0 &= A_c B - A_c A_d A_c^{-1} B_{c0} \\ &= \begin{bmatrix} M_0 \\ C_d A_d{}^{n-2} B \end{bmatrix} - \begin{bmatrix} 0_{(n-1)\times 1} & I_{(n-1)\times(n-1)} \\ a_0 & \tilde{a}^T \end{bmatrix} \times \begin{bmatrix} d \\ M_0 \end{bmatrix} = \begin{bmatrix} 0_{(n-1)\times 1} \\ C_d A_d{}^{n-2} B_d - a_0 d - \tilde{a}^T M_0 \end{bmatrix} \end{aligned} \tag{4.37}$$

Note $C_d A_d{}^{n-2} B_d - a_0 d - \tilde{a}^T M_0 = C_d A_d{}^{n-2} B_d - a_1 C_d B_d - a_2 C_d A_d B_d - \cdots - a_{n-1} C_d A_d{}^{n-1} B_d - a_0 d$

$= C_d (A^{n-1} - a_{n-1} A_d{}^{n-2} - \cdots - a_1 A^0) B_d - a_0 d = a_0 C_d A_d{}^{-1} B_d - a_0 d = b_0 - a_0 d$

Thus, one has

$$\Gamma_0 = \begin{bmatrix} 0_{1\times(n-1)} & b_0 - a_0 d \end{bmatrix}^T \tag{4.38}$$

Similarly, for $\Gamma_i, (i = 1,2,\cdots,n-1)$ and $R_i, (i = 0,1,\cdots,n)$, one has

$$\Gamma_1 = B_{c0} - A_c A_d A_c^{-1} B_{c1} = B_{c0} - A_d{}^T B_{c1} = \begin{bmatrix} 0_{(n-1)\times 1} \\ C_d A_d{}^{n-2} B_d - \tilde{a}^T M_1 \end{bmatrix} = \begin{bmatrix} 0_{(n-1)\times 1} \\ b_1 - a_1 d \end{bmatrix} \tag{4.39}$$

$$\cdots \Gamma_{n-1} = B_{c(n-2)} - A_d{}^T B_{c(n-1)} = \begin{bmatrix} 0_{(n-1)\times 1} \\ b_{n-1} - a_{n-1} d \end{bmatrix} \tag{4.40}$$

where

$M_1 = \begin{bmatrix} D_d{}^T & B_d{}^T C_d{}^T & \cdots & B_d{}^T (A_d{}^T)^{n-3} C_d{}^T \end{bmatrix}^T$, $M_2 = \begin{bmatrix} 0 & D_d{}^T & B_d{}^T C_d{}^T & \cdots & B_d{}^T (A_d{}^T)^{n-4} C_d{}^T \end{bmatrix}^T$

$\cdots, Rank[\Gamma_i, i = 1,2,\cdots,n-1] = Rank[R_i, i = 0,1,\cdots,n] = Rank[B_{c(n-1)}] = 1$.

Therefore, $(I - B_{c(n-1)}B_{c(n-1)}^{\dagger})\Gamma_i = 0, i = 1,2,\cdots,n-1,\quad (I - B_{c(n-1)}B_{c(n-1)}^{\dagger})R_j = 0, j = 0,1,\cdots,n.$

□

Theorem 4.3 suggests that the model reference approach for the discrete SISO system can be transferred to the nominal DSMC design, as shown in Equation (4.31).

(2) Determination of u_2

Let the sliding surface be

$$s(k) = S\delta(k) = 0 \tag{4.41}$$

Following the nominal SMC design as shown in Equations (4.8) ~ (4.11), one has the control action consisting of two parts, i.e., $u_2(k) = u_{eq}(k) + \Delta u(k)$, where the equivalent control is defined by

$$u_{eq}(k+n) = -(SB_{c(n-1)})^{-1}S[A_e\delta(k) + \Gamma_0 u_2(k) + \Gamma_1 u_2(k+1) + \cdots + \Gamma_{n-1}u_2(k+n-1)] \tag{4.42}$$

and the PID regulator can be given by

$$\Delta u(k) = -[Ps(k) + I\sum_{i=0}^{k} s(i)T + D\frac{s(k) - s(k-1)}{T}] \tag{4.43}$$

(3) Stability analysis

It is noticed that $w(k)$ is a function of $r(k)$, $r(k+1)$, …, $r(k+n)$, substituting Equations (4.39) and (4.40) into Equation (4.32) yields

$$du_1(k+n) + (b_0 - a_0 d)u_1(k) + \cdots + (b_{n-1} - a_{n-1}d)u_1(k+n-1) = g[r(k),\cdots,r(k+n)] \tag{4.44}$$

where $g[r(k),\cdots,r(k+n)] = Pw(k) + R_0 r(k) + \cdots + R_n r(k+n)$.

By taking Z-Transform of Equation (4.44), the transfer function from r to u_1 is given by

$$\frac{u_1(z)}{r(z)} = \frac{g(z)}{dz^n + (b_{n-1} - a_{n-1}d)z^{n-1} + (b_{n-2} - a_{n-2}d)z^{n-2} + \cdots + (b_0 - a_0 d)} \tag{4.45}$$

Compared to Equation (4.35), Equation (4.45) indicates that the poles of the transfer function from *r* to u_1 are the zeros of the plant transfer function. Therefore, location of the zeros of the plant determines the stability in the model reference approach. Particularly, if the zeros of the plant are located outside the unit circle in the complex plane, optimal inversion (4.21) can also be applied.

4.5.4 Experiments

PEAs have been widely used in nanotechnology due to its high precision, fast response and large force generated. However, hysteresis, existing in PEA as a nonlinear effect, can greatly degrade their performance [2], [43]. To improve the performance of PEAs, control and compensation for hysteresis have been drawing considerable attention. In this paper, with the aim of verifying the effectiveness of the discrete PID-based SMC, experiments were designed and carried out on a commercially- available PEA (P-753, Physik Instrumente). The hysteresis nonlinearity existing in the PEA was considered as a disturbance, which was rejected by the proposed discrete PID-based SMC.

The PEA selected for experiments can generate displacement in a range of 15 μm with a resolution of 0.5 nm. For displacement measurements, a built-in capacitive displacement sensor with a resolution of 1 nm was used. Both the actuator and the sensor were connected to a host computer via an I/O board (PCI-DAS1602/16, Measurement Computing Corporation) and controlled via SIMULINK programs. The mass ratio of the stage driven by the PEA to the PEA is 49.8, suggesting that the dynamics of the whole system can be regarded approximately as a second order system [46], [124], [130], [136]. As such, a second order auto-regressive model

was chosen to describe the system dynamics, while the hysteresis exhibited by the actuator is considered as an extra disturbance to the dynamic model, as shown in Eqution (4.46)

$$y(k) = a_1 y(k-1) + a_2 y(k-2) + b_0 x(k) + b_1 x(k-1) + b_2 x(k-2) \tag{4.46}$$

where a_1, a_2, b_0, b_1 and b_2 are the model parameters. As a result, sophisticated models for hysteresis are not required in the implementation of developed control. For the experiments, a 70V white noise input voltage was provided to the PEA and the corresponding output displacements were measured at sampling rate of 1000 Hz, 2000 Hz, 5000 Hz, 10000 Hz, and 20000 Hz, respectively. With the recorded data, the parameters were identified by using the least square method, in which the 2-norm of the difference between the measured data and the estimations was used in the error evaluation. The identified parameters with the error are listed in Table 4-1. It is noted that $\beta_1 \neq 0$ and $\beta_2 \neq 0$, which indicates that the traditional state tracking based DSMC as shown in [132] and [133] are not applicable in this situation.

Table 4- 1 Identified parameters for the dynamic model

Sampling frequency	a_1	a_2	b_0	b_1	b_2	Error (μm)
1000 Hz	0.3212	0.01025	0.003889	0.1189	-0.01765	0.1863
2000 Hz	0.0712	0.12058	0.002944	0.10592	0.01797	0.4224
5000 Hz	0.7567	-0.16145	0.003463	0.01386	0.00447	0.6991
10000 Hz	1.0589	-0.15055	0.002018	0.00075	0.01001	0.7914
20000 Hz	1.6092	-0.6248	0.000778	-0.00041	0.00134	0.3403

4.5.4.1 Output tracking integrated discrete PID-based SMC—Traditional SMC design approach

The output tracking integrated discrete PID-based SMC developed by using the traditional SMC design approach was implemented in the experiments to control the PEA with different

sampling frequencies – 1000Hz and 20000 Hz. A 5 μm step input was provided as the reference signal. The state was designed to be $x = [y, v_y]^{\mathrm{T}}$, where y is the output displacement and v_y is the velocity. The displacement and the velocity were estimated by a α-β filter which is a simplified observer for estimation and filtering. The parameters of the filter was adjust by trails-and-errors as $\alpha = 0.1$, $\beta = 0.0001$ for 20000 Hz sampling rate and $\alpha = 0.3$, $\beta = 0.001$ for 1000 Hz sampling rate. The sliding surface was defined as Equation (4.9) where $S = [m, 1]$. It is noted from Table 4-1 that the zeros of the plant locate outside the unit circle. Therefore, optimal stable inversion (4.21) was integrated in the controller. Parameters in the SMC were adjusted in order to get the best tracking performance. Table 4-2 shows the adjustment results.

Table 4- 2 Parameters adjusted in the proposed method for different sampling rates (traditional SMC design approach)

Sampling frequency	*m*	*P*	*I*	*D*	*Q*	*R*
1000 Hz	1000	0.6	240	0.0005	1	100
20000 Hz	18000	0.001	10	0.000001	1	400

For comparison, a nominal output tracking based DSMC was also implemented to control the PEA. The sliding surface was designed the same as the discrete PID-based SMC. 'Bang-bang' control was applied as the switching control. The parameter K is adjusted to be 1 for 20000 Hz sampling rate and 3 for 1000 Hz sampling rate.

Figure 4.5 and Figure 4.6 show the step tracking performance of PEA controlled by the proposed method derived from the traditional SMC design approach and the nominal output tracking based DSMC, sampled with 20000 Hz rate and 1000 Hz rate respectively. The blue solid line represents the desired displacement while the red dash line corresponds to the output displacement controlled by different methods.

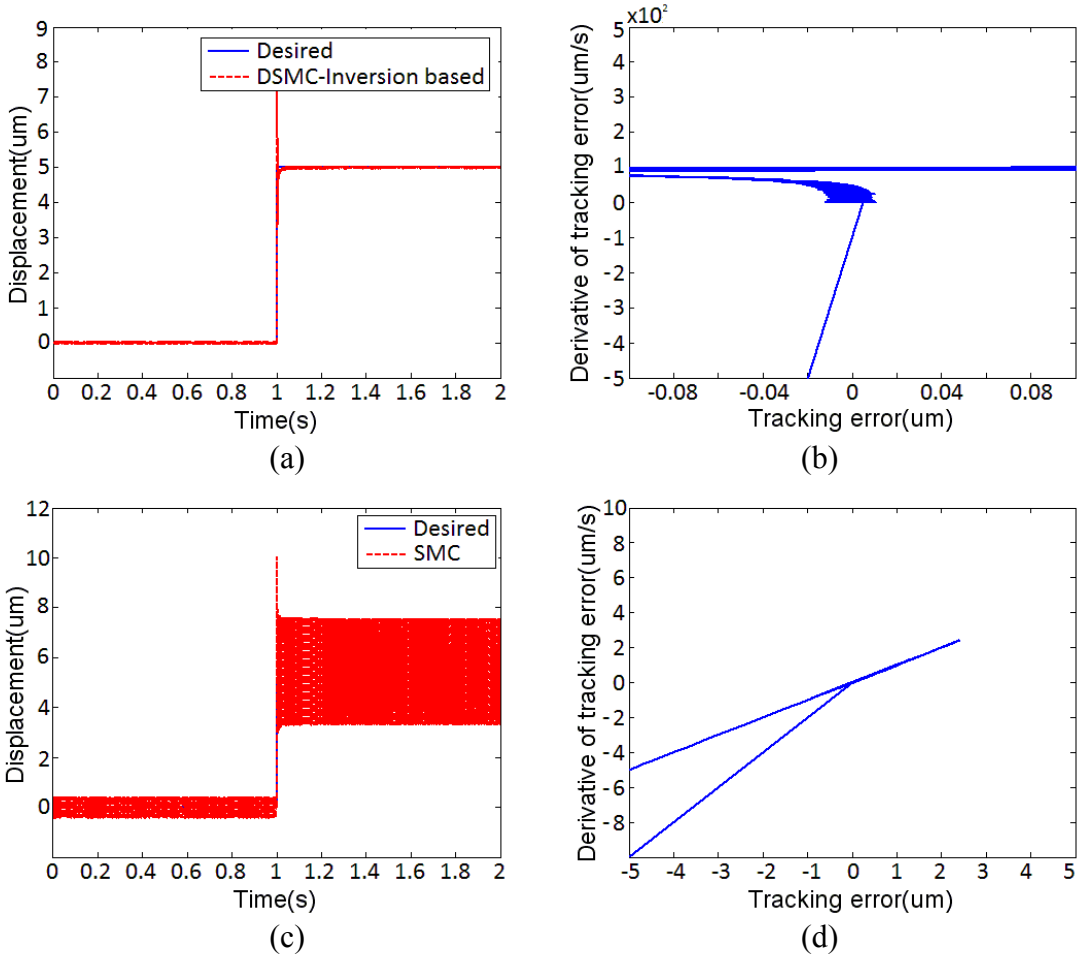

Figure 4. 5 Step tracking performance (20000 Hz sampling rate) of the proposed method designed by the inversion approach
(a) displacement (b) error state track and the ordinary DSMC (c) displacement (d) error state track

It can be seen that serious chattering problem exists in the nominal output tracking based DSMC with 'bang-bang' switching control. The output displacement oscillates from 3.6 μm to 7.6 μm with high frequency. The center of the chattering is 5.6 μm, 0.6 μm offset from the desired displacement, which means that the steady state error exists in the nominal DSMC. By using the PID-based switching control instead of the 'bang-bang' switching, chattering problem and steady state error were eliminated. The error state converges to zero and oscillates around the origin point with its amplitude being 0.015 μm at 20000 Hz sampling rate and 0.006 μm at 1000

Hz sampling rate, which are the noise level of the sensor.

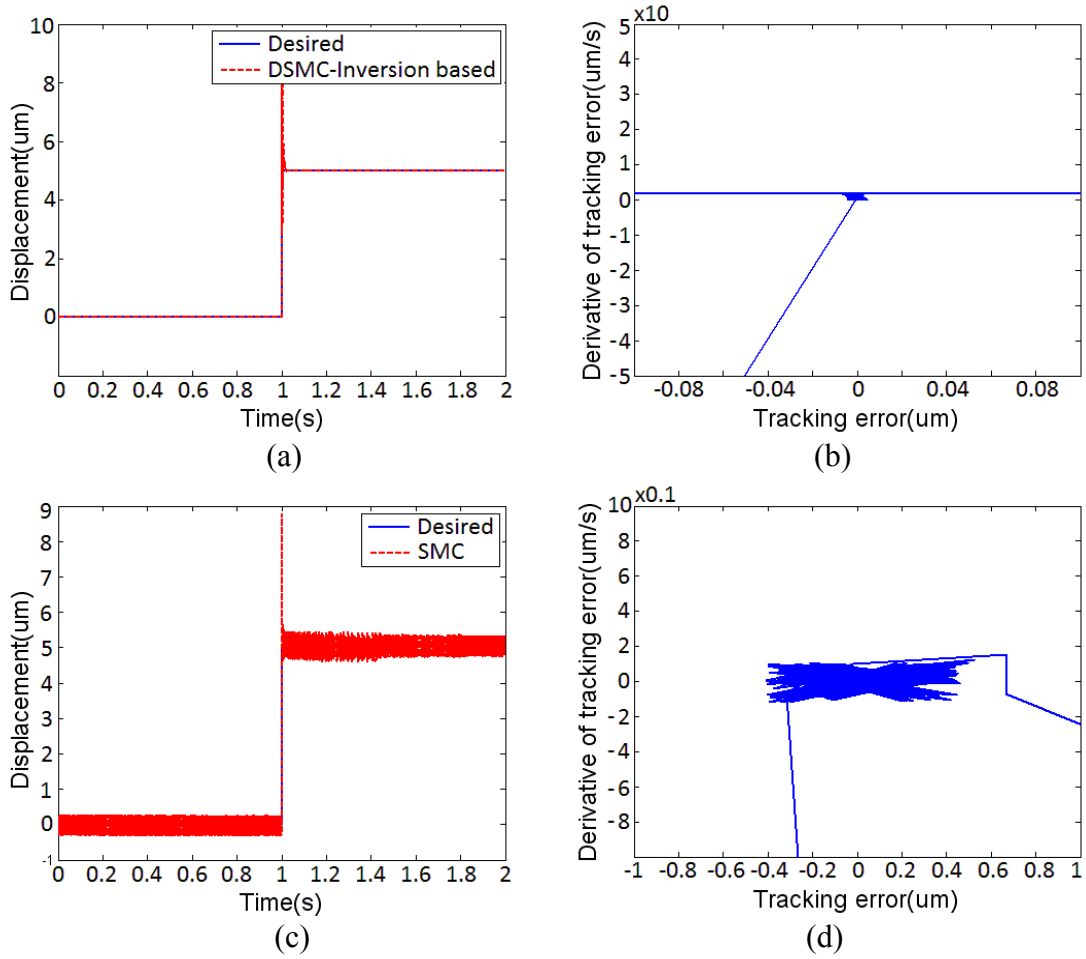

Figure 4. 6 Step tracking performance (1000 Hz sampling rate) of the proposed method designed by the inversion approach
(a) displacement (b) error state track and the ordinary DSMC (c) displacement (d) error state track

Compared with the proposed method designed by using the traditional approach, the error state controlled by the nominal output tracking based DSMC oscillated around the origin region with large amplitude. The oscillation center deviated from the origin point due to the zigzag motion generated by the unmatched switching time. It is noted from the results that the proposed method designed by the traditional approach at both sampling frequencies can achieve good control performance. However, since the reference signal is not derivable at the step time, large

overshoot was observed in the step response.

4.5.4.2 Output tracking integrated discrete PID-based SMC—Model reference approach

In this section, the output tracking integrated discrete PID-based SMC was designed by using the model reference approach. Experiments with both 1000Hz and 20000 Hz sampling rates were carried out. A 5 μm step input was adopted as the reference signal as well. The state was designed to be $x = [y, v_y]^{\mathrm{T}}$ which was estimated by a α-β filter, with the same parameters set as the traditional SMC design approach. The transfer function of the desired second order system was given by

$$G_d(s) = \omega_n^2 / (s^2 + 2\varsigma\omega_n s + \omega_n^2) \tag{4.47}$$

where ς is the desired damping ratio and ω_n is the desired natural frequency. With ς and ω_n being chosen as 0.7 and 1000 rad/s respectively, a step response with 5.7 ms setting time and 4.6% overshoot can be obtained. The optimal stable inversion (4.21) was additionally integrated in the controller. Parameters in the proposed method designed by the model reference approach were adjusted such that the best tracking performance can be achieved. Table 4-3 shows the adjustment results.

Table 4- 3 Parameters adjusted in the proposed method for different sampling rates (model reference approach)

Sampling frequency	*m*	*P*	*I*	*D*	*Q*	*R*
1000 Hz	0.99	4.2	1150	0.001	1	0.5
20000 Hz	0.99	10	25000	0.00002	1	0.001

Figure 4.7 shows the step tracking performance of PEA controlled by the proposed method developed from the model reference approach, sampled at rates of 20000 Hz rate and 1000 Hz,

respectively. The blue solid line represents the output displacement of the reference model while the red dash line corresponds to the output displacement controlled by the proposed method.

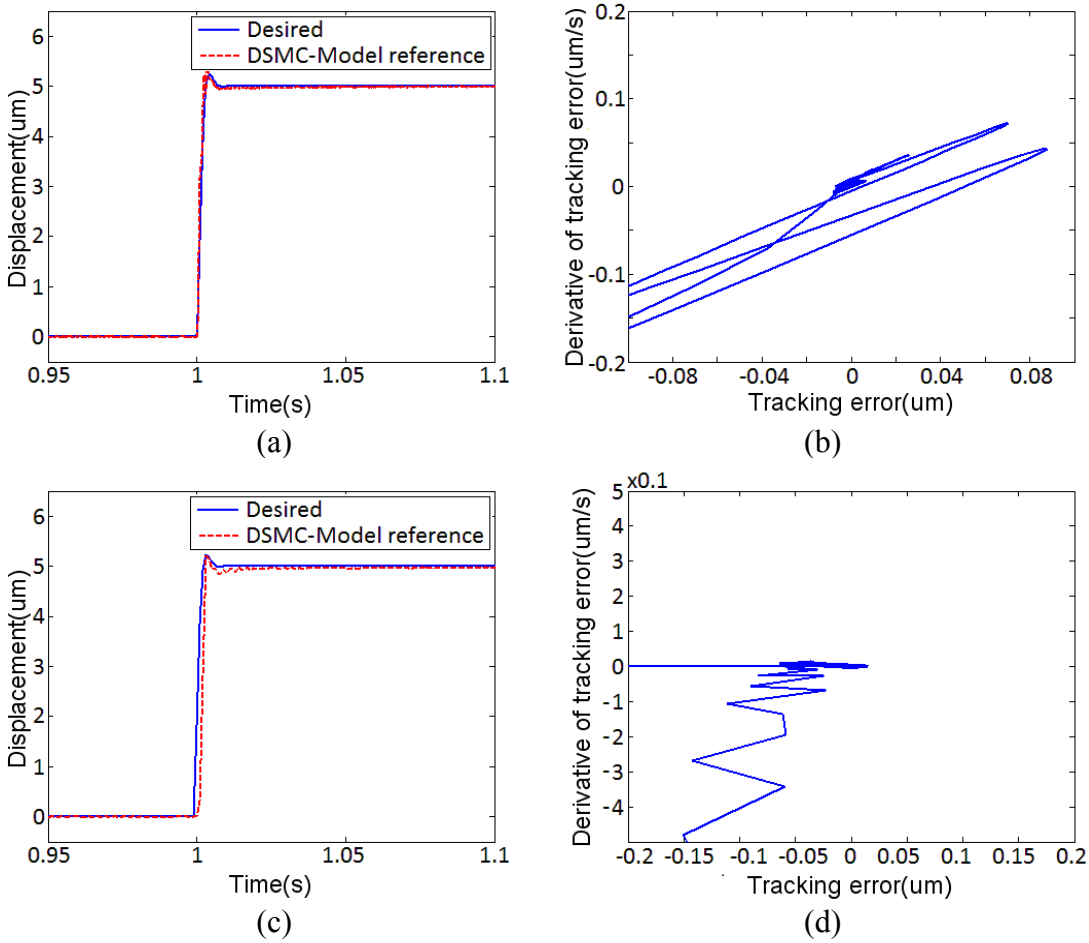

Figure 4. 7 Step tracking performance of the proposed method designed by model reference approach at the 20000 Hz sampling rate
(a) displacement (b) error state track; and at the 1000 Hz sampling rate (c) displacement (d) error state track

The setting time and the overshoot were respectively 5.5 ms and 5.2% for the 20000 Hz sampling rate and 4.2 ms and 4.3% for the 1000 Hz sampling rate. These values are close to that of the reference step response which indicates that the proposed method designed by the model reference approach can achieve a good tracking performance in relation to the reference output at

different sampling frequencies. In contrast with the output tracking integrated discrete PID-based SMC designed by the traditional design approach, less overshoot was observed in the step response because the derivability of the reference signal is not required in the model reference approach.

4.5.4.3 Dynamic tracking performance compared with the continuous PID-based SMC

In order to verify the effectiveness of proposed control method, dynamic tracking experiments with the above sampling frequencies were also carried out on the PEA. Particularly, three types of inputs were used as the reference signal: ① the sinusoidal inputs of an amplitude of 5 μm with different frequencies of 1, 10, 30 and 50 Hz; ② the piecewise continuous combination of different-amplitude sinusoidal inputs with the same frequency (PSWS), as shown in Figure 4.8(a); ③ the superposition of four sinusoidal inputs with different frequencies, amplitudes and phase delays (SW), as shown in Figure 4.8(b) and Equation (4.48).

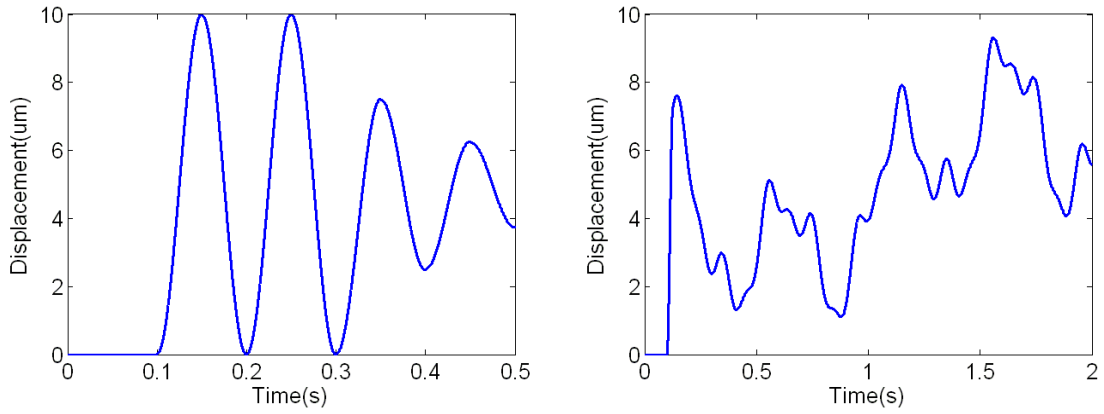

Figure 4. 8 Reference signals in the control verification
(a) piecewise continuous combination of different-amplitude sinusoidal inputs with the same frequency (PSWS) and (b) superposition of four sinusoidal inputs with different frequency, amplitude and phase delay (SW)

$$w = \frac{30}{7}\sin[2\pi \times \frac{f_{\max}}{20}(t-0.1)+\pi] + \frac{25}{7}\sin[2\pi \times \frac{f_{\max}}{5}(t-0.1)+0.5\pi] + \frac{5}{7}\sin[2\pi \times \frac{f_{\max}}{2}(t-0.1)+0.2\pi] + \frac{5}{7}\sin[2\pi \times f_{\max}(t-0.1)] + 5 \quad (4.48)$$

The output tracking integrated discrete PID-based SMC designed by the model reference approach was implemented on the PEA, in which the parameters of the second order reference model were chosen to be $\varsigma = 0.25$ and $\omega_n = 3000 rad/s$. The parameters of the output tracking integrated discrete PID-based SMC were adjusted as shown in Table 4-4. For comparison, the continuous PID-based SMC introduced in [98] was also implemented on the PEA. The parameters of the PID regulator were adjusted by using the Ziegler-Nichols method, leading to P = 0.001, I = 1, and D = 0.0000001 for the 20000 Hz sampling rate, P = 0.002, I = 0.6, and D = 0.0000001 for the 10000 Hz sampling rate, and P = 0.0001, I = 0.03, and D = 0.0000001 for the 5000 Hz sampling rate.

Table 4- 4 Parameters adjusted in the proposed method for different sampling rates (model reference approach)

Sampling frequency	m	P	I	D	Q	R
1000 Hz	0.99	9.6	1500	0.001	1	0.05
2000 Hz	0.99	4	1000	0.00002	1	0.001
5000 Hz	0.99	2	1500	0.00002	1	0.001
10000 Hz	0.99	1.5	3500	0.00002	1	0.001
20000 Hz	0.99	1	12000	0.00002	1	0.001

Figure 4.9 shows the dynamic tracking performance of the output tracking integrated discrete PID-based SMC designed by the model reference approach at 5000 Hz sampling frequency, compared with the continuous PID-based SMC. The tracking error was calculated in terms of the 2-norm of the difference between the desired output and the measured output. More comparison is shown in Table 4-5 and Table 4-6 in detail.

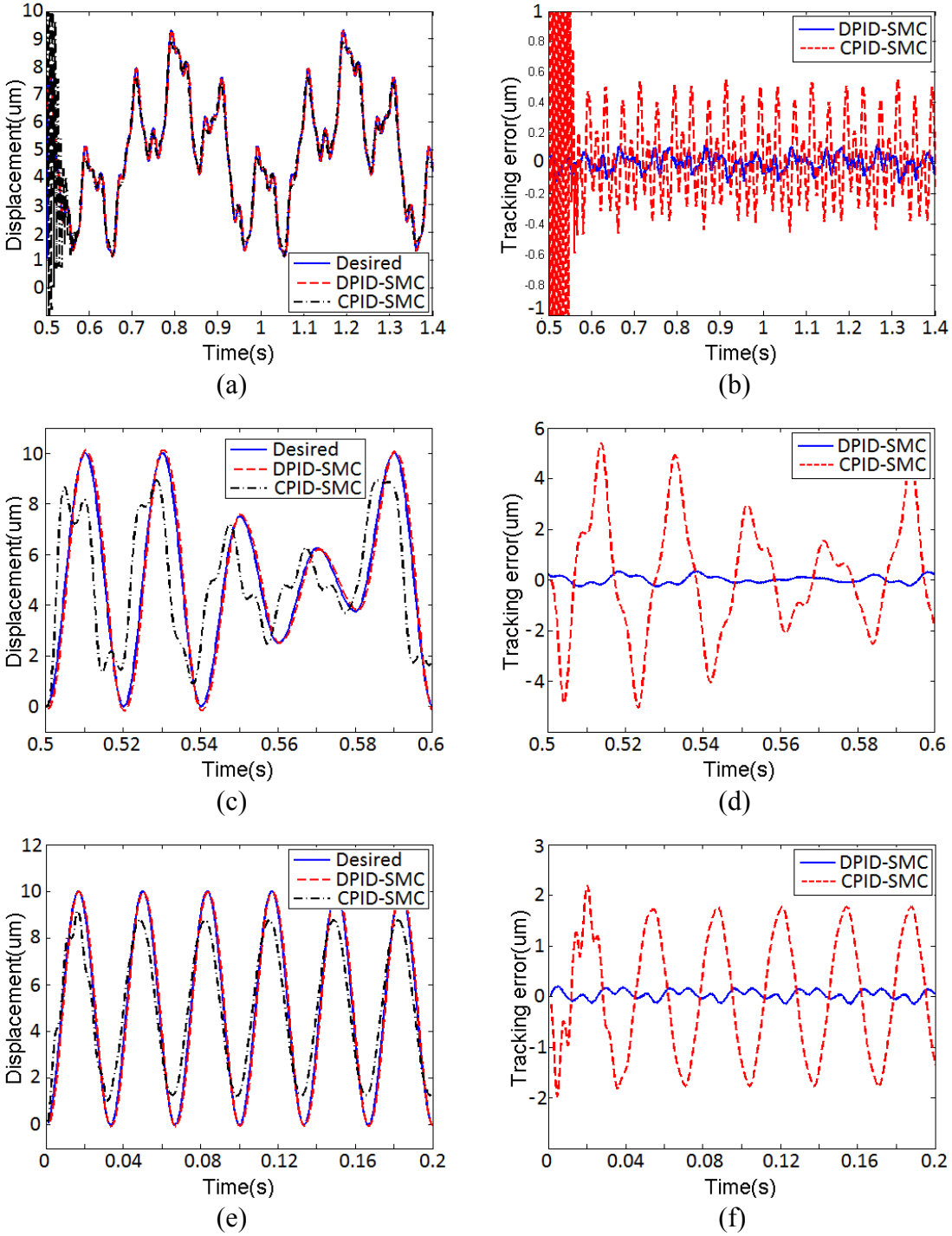

Figure 4. 9 Tracking performance of the proposed method and the continuous PID-based SMC at 5000 Hz sampling rate for different reference signals

SW with its maximum frequency being 50 Hz (a) displacement (b) tracking error; PSWS with its frequency being 50 Hz (c) displacement (d) tracking error; and 30 Hz 5 μm sinusoidal signal (e) displacement (f) tracking error

Table 4- 5 Comparison of the tracking performance between the proposed method and the continuous PID-based SMC at 20000 Hz sampling rate

Reference inputs	Discrete PID-based SMC (Traditional design approach)	Discrete PID-based SMC (Model reference approach)	Continuous PID-based SMC
1 Hz sinusoidal input	0.0117	0.0088	0.0062
10 Hz sinusoidal input	0.0519	0.0383	0.0213
30 Hz sinusoidal input	0.1552	0.1253	0.1001
50 Hz sinusoidal input	0.2641	0.2315	0.2678
SW with f_{max} = 10 Hz	0.0142	0.0106	0.0074
SW with f_{max} = 30 Hz	0.0223	0.0188	0.0169
SW with f_{max} = 50 Hz	0.0313	0.0309	0.0352
PSWS with 10 Hz frequency	0.0393	0.0295	0.0247
PSWS with 30 Hz frequency	0.1188	0.0964	0.0979
PSWS with 50 Hz frequency	0.2000	0.1769	0.1833

Table 4- 6 Comparison of the tracking performance between the proposed method and the continuous PID-based SMC at 5000 Hz sampling rate

Reference inputs	Discrete PID-based SMC (Traditional design approach)	Discrete PID-based SMC (Model reference approach)	Continuous PID-based SMC
1 Hz sinusoidal input	**0.0511**	**0.0283**	**0.0121**
10 Hz sinusoidal input	0.0620	0.0385	0.1535
30 Hz sinusoidal input	0.1600	0.0833	1.2270
50 Hz sinusoidal input	0.3685	0.1865	2.9360
SW with f_{max} = 10 Hz	0.0372	0.0218	0.0479
SW with f_{max} = 30 Hz	0.0635	0.0400	0.1976
SW with f_{max} = 50 Hz	0.0849	0.0541	0.6206
PSWS with 10 Hz frequency	0.0617	0.0384	0.1057
PSWS with 30 Hz frequency	0.1423	0.0812	0.8469
PSWS with 50 Hz frequency	0.2835	0.1430	2.0464

It can be concluded from the comparison that the output tracking integrated discrete PID-based SMC performs similar as the continuous PID-based SMC at high sampling frequencies. For example, the tracking error for 1 Hz 5 μm sinusoidal input controlled by the discrete PID-based SMC developed from the model reference approach is 0.0088 μm which is

only 0.0026 μm more than that controlled by the continuous PID-based SMC, while for 50 Hz sinusoidal input, the tracking error is 0.0363 μm less than that of the continuous PID-based SMC. As sampling frequency decreases, the output tracking integrated discrete PID-based SMC performs much better than the continuous PID-based SMC with one exception at a frequency of 1 Hz, which is bolded in Table 4-6.

At low input frequency, the performance improvement with the proposed method is not apparent. However, as frequency increases, the improvement becomes more profound, for example, showing 91.3% improvement for the 50 Hz SW tracking by using proposed method as designed by means of the model reference approach and 86.3% improvement as designed by the traditional SMC design approach.

It is noted that as compared with the traditional SMC design approach, the model reference approach can achieve better tracking performance. For example, for the 30 Hz sinusoid reference input with 20000 Hz sampling rate, the tracking error by using the model reference approach is 0.1253 μm ─ 0.0301 μm less than that obtained by using the traditional SMC design approach. Moreover, increasing the sampling rate improves the tracking performance of discrete PID-based SMC for both the traditional SMC design approach and the model reference approach.

4.5.4.4 Dynamic tracking under different sampling rates

The improvement of tracking performance with the output tracking integrated discrete PID-based SMC can be further illustrated by experiments with varying sampling rates. Specifically, sinusoidal tracking experiments were implemented on the PEA at sampling rate of 1000 Hz, 2000 Hz, 5000 Hz, 10000 Hz, and 20000 Hz, respectively. Both the discrete PID-based SMCs, as designed by the model reference approach and the continuous PID-based SMC approach, were used to control the PEA with the parameters given in Table 4-4. The parameters

of the continuous PID-based SMC were adjusted to be $P = 0.002$, $I = 0.6$, $D = 0.0000001$ for the case with the 10000 Hz sampling rate. Figure 4.10 shows the tracking error varying with the sampling rates by using these two controllers. The tracking error was evaluated in terms of the 2-norm of the differences between the desired output and the measured output. It can be seen that the discrete PID-based SMC performs better than the continuous one, especially at low sampling rates. It is noted the tracking errors for the continuous PID-based SMC at 1000 Hz and 2000 Hz are not given in Figure 4.10 as they are significantly large.

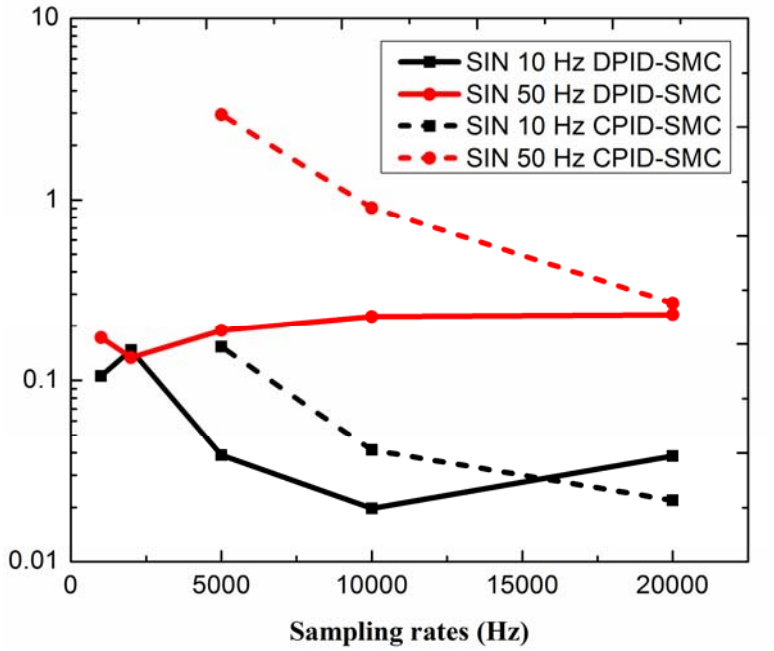

Figure 4. 10 Comparison of tracking errors as controlled by the discrete and continuous PID-based SMC with different sampling rates

4.5.5 Conclusion

This paper presents the development of the output tracking integrated discrete PID-based SMC for SISO system, in which the system output is fed back for generating the control action. As such, it can be employed in the applications where the system states cannot be readily

available. Both the traditional SMC design approach and the model reference approach are employed for the controller design. By applying the PID regulator instead of the 'bang-bang' switching control, chattering, and the zigzag state motion thus the steady state error, were eliminated. In order to verify the effectiveness of the proposed control schemes, experiments were carried out on a commercially available PEA with varying sampling frequencies, as compared to the use of continuous PID-based SMC. The results show that the developed method as designed by both approaches can achieve better tracking performance and that as the input frequency increases, the performance improvement with the developed method becomes more profound. The results also show that due to the non-requirement on the derivability of the reference signal, the developed method designed by the model reference approach has a better performance than the one designed by the traditional SMC design approach.

4.5.6 Acknowledgment

The support to the present study from the China Scholarship Council (CSC) and the Natural Sciences and Engineering Research Council (NSERC) of Canada is acknowledged.

5 Inversion-based Sliding Mode Control and Disturbance Observer based Sliding Mode Control for One-DOF Piezoelectric Actuators

This chapter presents the work that is included in the following manuscript appended.

Y. Cao and X. B. Chen, "Two Modified Discrete PID-Based Sliding Mode Control for Piezoelectric Actuators," *International Journal of Control*, 2012, under review, manuscript ID: TCON-2013-0179.

5.1 Introduction and Objectives

In the previous chapter, the discrete PID-based SMC was developed for the control of PEAs, where hysteresis and other nonlinear effects were considered to be disturbance to the dynamics and rejected by the DSMC. If hysteresis can be completely or partially modeled, the integration of hysteresis models into control schemes may improve the control performance. Inspired by this, discrete inversion based PID-SMC and DOB-based PID-SMC are to be developed in this study, in which the PEA hysteresis is completely and partially predicted, respectively, by using existing models of PEA hysteresis.

5.2 Methods

PEA is commonly modeled as the cascade of the dynamics and the hysteresis, as shown in Figure 5.1. In Chapter 3, a rate independent hysteresis model and a second order auto regressive model were employed to depict the hysteresis and dynamic performance of PEA. The hysteresis nonlinearity can be compensated by cascading an inverse hysteresis prior to the plant, resulting

in a discrete inversion based PID-SMC proposed in this work, as shown in Figure 5.1.

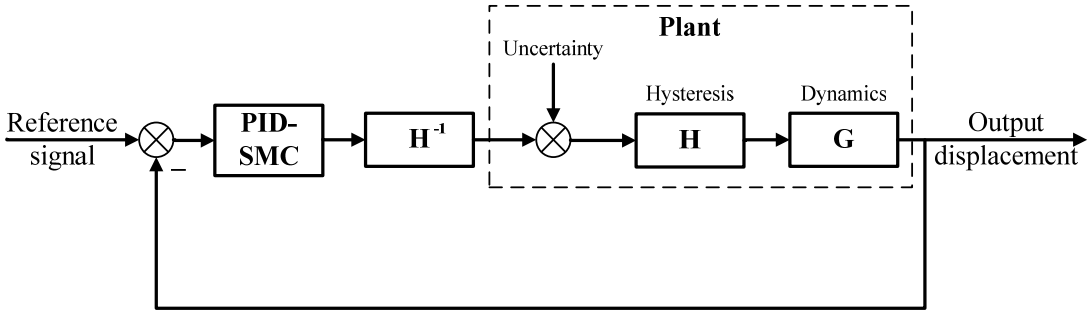

Figure 5. 1 Inversion based PID-SMC

The inverse of the rate independent hysteresis, denoted by H^{-1}, is cascaded to a discrete PID-based SMC to compensate for the nonlinear hysteresis, while the discrete PID-based SMC is designed to improve the dynamics of the PEA. Since the hysteresis is compensated by its inversion, the disturbance to be rejected by the discrete PID-based SMC is reduced. As a result, the tracking error should be less in comparison to the nominal PID-based SMC. Due to the imperfection of the model, the hysteresis may not be completely compensated by the use of H^{-1}. Such a model imperfection is considered to be uncertainty and is provided to the input of the plant which is rejected by the discrete PID-based SMC.

It is reported in the literature that the hysteresis can be considered to be the combination of a linear component and a nonlinear component representing the disturbance. Therefore, DOB might be employed to compensate for the hysteresis, as shown in Figure 5.2, where η is the measurement noise and Q is a low pass filter which is employed to stabilize the DOB. The output of the DOB can be represented as

$$w = -uQ + \frac{Q}{K_e G}(\eta + y) = -uQ + \frac{Q}{K_e G}[\eta + G(K_e u + \delta)] = \frac{Q}{K_e G}\eta + \frac{Q}{K_e}\delta \tag{5.1}$$

where v is the main controller output, u is the control input, δ is the external disturbance, y is the

plant output and η is the sensor noise. w is feedback to the input of the PEA. As a result, the integration of DOB would compensate for the hysteresis which is regarded as disturbance. The discrete PID-based SMC is designed based on the dynamics of the PEA.

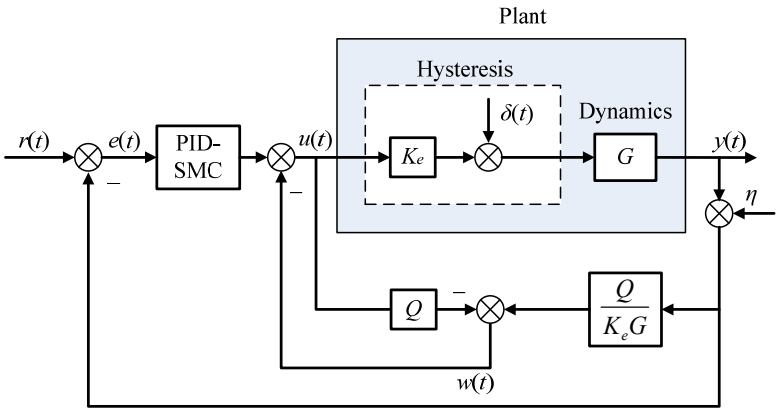

Figure 5. 2 DOB-based PID-SMC

5.3 Results

Integration of the inverse hysteresis and the DOB is more effective in terms of the hysteresis compensation. Therefore, the disturbance, which is rejected by the DSMC, is reduced, thus improving the performance of the discrete PID-based SMC. Based on the examined cases with inputs of varying frequencies, it is recommended that the inversion based discrete PID-SMC should be used if the input frequency is low, while the discrete DOB-based PID-SMC is preferred for applications with higher frequencies.

5.4 Contributions

The contribution of this work was the successful improvement of the discrete PID-based SMC by integrating the inversion feedforward and DOB such that the disturbance to be rejected

by the DSMC is reduced.

5.5 Paper: Two Modified Discrete PID-based Sliding Mode Controllers for Piezoelectric Actuators

Authors: Y. Cao and X. B. Chen, *Member, IEEE*[4]

Index Terms: Disturbance observer, Feedforward control, PID, Sliding mode control, Piezoelectric actuator.

5.5.1 Abstract

Hysteresis is a nonlinear effect that can result in the degraded performance of piezoelectric actuators (PEAs). To counteract the effect, several control methods have been developed and reported in the literature. One promising method for compensation is the use of a proportional-integral-derivative (PID)-based sliding mode control (SMC), in which the PEA hysteresis is treated as an unknown disturbance to the PEA input. If the hysteresis can be modelled or partially modelled, the integration of the hysteresis models into the control schemes may lead to further improved performance. On this philosophy, this paper presents the development of two modified discrete PID-based sliding mode controllers (PID-SMC) for piezoelectric actuators, namely an inversion-based PID-SMC and a disturbance-observer (DOB)-based PID-SMC, in which the PEA hysteresis is predicted or partially predicted through use of existing models for the PEA hysteresis. Experiments were performed to verify the

---

Manuscript received December 16, 2012. This work was supported by the China Scholarship Council (CSC) and the Natural Science and Engineering Research Council (NSERC) of Canada.

Y. Cao is with the Department of Mechanical Engineering, 57 Campus Drive, University of Saskatchewan, Saskatoon, SK, S7N 5A9 (e-mail: yuc150@ mail.usask.ca).

X. B. Chen is with the Department of Mechanical Engineering, 57 Campus Drive, University of Saskatchewan, Saskatoon, SK, S7N 5A9 (phone: 1-306-966-1267; e-mail: xbc719@ mail.usask.ca).

effectiveness of the proposed control schemes. The results were compared to those of the nominal PID-based SMC. By employing the inversion hysteresis and the DOB, the PEA performance was greatly improved.

5.5.2 Introduction

An increasing demand for high accuracy in production manufacturing and other devices has led to rapid development of precision engineering. From its origin in mechanical engineering, it evolved into micro-mechanics and then nanotechnology [1]. Nanotechnology is the study of the control of matter on an atomic and molecular scale. One key requirement imposed on nanotechnology is nano-positioning [2]. Piezoelectric actuators (PEA) have been widely applied to nano-positioning, due to their fast response, high precision, and their ability to generate large forces. However, hysteresis, the main nonlinear effect in PEAs, can greatly degrade the positioning accuracy of PEA-driven systems [61] - [63]. To compensate for the hysteresis effect, the control of PEA has been drawing considerable attention and several methods have been developed. A proportional-integral (PI) controller was used to compensate for the nonlinear effect of hysteresis [23]. The challenge in using PI controllers is maintenance of system stability in the presence of parameter uncertainty and disturbances. Another challenge is the issue of low gain margin in high frequency manipulation due to a rapid loss in phase at the sharp resonant peak [2]. To improve the robustness of control advanced feedback controllers, such as H_∞ and H_2 controllers [137], have been employed for the hysteresis compensation. For example, in [138], the tracking error for a 50 Hz sinusoidal reference input was reduced to 2% of the travelling path by integrating a Smith predictor-based robust H_∞ controller. Inverse feedforward control is also frequently used in PEAs due to its ability to avoid the low gain

margin problem of the feedback control. In [6], the inverse of the Preisach hysteresis model was combined with an optimal control scheme to compensate for PEA hysteresis. The results showed substantial improvements in positioning precision and operational speed. In [139], an inversion-based model predictive controller with an integral-of-error state variable was developed for the piezoelectric actuator control with improved tracking performance under given constraint of the input. Unfortunately, the disturbance and uncertainties were not considered in the aforementioned controller and as a result, the robustness of performance can be degraded by the imperfection of the model used.

Sliding model control (SMC), as a variable structure control method [131], has been widely employed by the control research community worldwide. SMC is recognized for its capacity for rejecting the input disturbance [92]. However, chattering, caused by the discontinuous switching function in SMC, may excite the high frequency resonant vibration, thereby degrading control performance and potentially even damaging the actuators being controlled. To resolve the chattering problem, boundary layer control has been employed by researchers [94], in which a saturation function is used to replace the discontinuous 'bang-bang' switching function. It is noted that if the unknown disturbance to be rejected is significant, a sufficiently high gain in control is needed. To alleviate this problem, one method is to employ a high-order sliding surface instead of the first-order one in the nominal SMC design [95], [96]. It has been shown that the high-order sliding mode control (HOSMC) can reduce the chattering effect, meanwhile improve the control performance [97]. The cost of using HOSMC is the increased sliding information in its implementation, for example, the r-sliding controller keeping $s = 0$ requires $s', s'', \cdots, s^{(r-1)}$ to be available.

A new continuous proportional-integral-derivative (PID) based SMC for PEAs was recently

developed, in which the discontinuous 'bang-bang' switching function is replaced by a PID regulator to eliminate the chattering problem [98]. Experiments were implemented on a commercial available PEA and it was proven that by using a continuous PID-based SMC, the hysteresis existing in the PEA could be effectively compensated, thereby leading to an improved performance. Moreover, due to the integration effect of the PID regulator, zero steady state error was achieved in the tracking performance. If implemented in a digital computer, SMC may lose some properties of its continuous form [100], [101], [131]. For a discrete sliding mode controller (DSMC), if the switching time does not match the sampling rate, the states cannot approach and maintain on the sliding surface. Instead, they follow a zigzag motion around the sliding surface, suggesting that the sampling can also induce chattering in DSMC. Therefore, it is argued in [100] that the discrete form of SMC is essentially needed for its implementation, especially in cases with relatively slow sampling rates. Unfortunately, this issue was not addressed in [98]. In addition, in [98], the hysteresis was regarded as a disturbance and rejected by the PID-based SMC. If the hysteresis can be modeled or partially modeled, the integration of hysteresis models into control schemes may improve the control performance.

In this study, an inversion based discrete PID-SMC and a DOB-based PID-SMC are developed, in which the PEA hysteresis is predicted and partially predicted, respectively, by using existing models of PEA hysteresis. Imperfection of the hysteresis model and other uncertainties are treated as disturbances to be rejected by the discrete PID-based SMC. By using a discrete PID-based SMC, the zigzag motion of the states caused by the mismatch of switching and sampling time can be removed. To verify the effectiveness of the proposed control methods, experiments were performed on a commercially-available PEA. Both the inversion based PID-SMC and the DOB-based PID-SMC was implemented, respectively, and the results were

compared to those of the nominal PID-based SMC reported in [98]. In contrast to the nominal PID-based SMC, compensation for hysteresis is performed more effectively by both inversion based PID-SMC and DOB-based PID-SMC.

5.5.3 Discrete PID-based SMC

Consider a discrete *n*th order single-input-single-output (SISO) system described by

$$G(z)=\frac{\sum_{i=0}^{n} b_i z^{-i}}{\sum_{i=0}^{n} a_i z^{-i}} \tag{5.2}$$

where a_i and b_i $(i=1,2,\cdots,n)$ are the parameters of the transfer function. It can be regarded as a cascade of the nominator $G_1(z)$ and the denominator $G_2(z)$

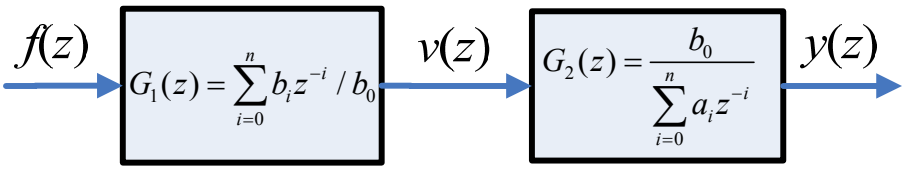

Figure 5. 3 Block diagram of a discrete *n*th order SISO system: *f*(*z*) and *y*(*z*) is the input and output of the dynamics respectively, *v*(*z*) is a middle variable

The system state is defined as

$$x(k)=[y(k),\dot{y}(k),\ddot{y}(k),\cdots,y^{(n-1)}(k)]^{\mathrm{T}} \tag{5.3}$$

where $y^{(n)}(k)$ represents the *n*th order derivative of the output at time *kT*. Then, the transfer function $G_2(z)$ can be written in the discrete state space form as

$$x(k+1)=A_d x(k)+B_d v(k)+\varepsilon(k) \tag{5.4}$$

where $\varepsilon(k)\in R^{n\times 1}$ is the uncertainty at time *kT*; $v(k)$ is the control input signal at time *kT*;

and $A_d \in R^{n\times n}$ and $B_d \in R^{n\times 1}$ represent the system matrixes of the discrete state space model.

Define the error state to be

$$e(k) = x(k) - x_d(k) \tag{5.5}$$

where $x_d(k)$ is the desired state. The objective of the SMC is, via the control action, to force the error state, regardless of its initial value, to move to the sliding surface in a finite amount of time and then converge to zero. If the desired reference state is designed to be

$$x_d(k) = [y_d(k), \dot{y}_d(k), \ddot{y}_d(k), \cdots, {y_d}^{(n-1)}(k)]^{\mathrm{T}} \tag{5.6}$$

where y_d is the desired output and ${y_d}^{(n)}(k)$ represents the *n*th order derivative of y_d. The dynamics of the tracking error state can be derived from Equations (5.4) and (5.6) as

$$e(k+1) = A_d e(k) + A_d x_d(k) - x_d(k+1) + B_d v(k) + \varepsilon(k) \tag{5.7}$$

Considering only the zero order and first order derivatives and neglect the disturbance, a perfect system requires $e(k) = 0$ at any time, yielding

$$A_d x_d(k) - x_d(k+1) + B_d v(k) = 0 \tag{5.8}$$

Equation (5.8) can be satisfied if and only if, according to the study [92]

$$[A_d x_d(k) - x_d(k+1)](I - {B_d}^{\dagger} B_d) = 0 \tag{5.9}$$

where ${B_d}^{\dagger}$ is the pseudo inverse of matrix B_d. Unfortunately, if the state is chosen and given by Equation (5.3) for a discrete SISO system, its state space model (A_d, B_d, C_d, D_d) will not be the controllable canonical form and Equation (5.9) may not be satisfied.

To solve this problem, a linear transform is introduced here, i.e.,

$$x' = Fx \tag{5.10}$$

where $F = [p, pA_d, pA_d^2, \cdots, pA_d^{n-1}]$ and p is a one-by-n vector. If $\bar{e}(k) = Fe(k)$, then, from

Equation (5.4), $\bar{e}(k)$ may be described by

$$\bar{e}(k+1) = FA_d F^{-1}\bar{e}(k) + FB_d v(k) + FA_d F^{-1}x_d(k) - Fx_d(k+1) + F\varepsilon(k) \tag{5.11}$$

As introduced in [98], input *v* can be divided into two components

$$v(k) = v_1(k) + v_2(k) \tag{5.12}$$

where

$$v_1(k) = (FB_d)^{\dagger}[Fx_d(k+1) - FA_d F^{-1}x_d(k)] \tag{5.13}$$

Substituting Equations (5.12) and (5.13) into Equation (5.11) leads to the nominal SMC design problem [92], i.e.,

$$\bar{e}(k+1) = FA_d F^{-1}\bar{e}(k) + FB_d v_2(k) + F\varepsilon(k) \tag{5.14}$$

The sliding surface $s(k)$ is designed to be

$$s(k) = S\bar{e}(k) = 0 \tag{5.15}$$

where matrix *S* defines how the tracking error converges to zero. Combining Equations (5.14) and (5.15) yields

$$SFA_d F^{-1}\bar{e}(k) + SFB_d v_2(k) + SF\varepsilon(k) = 0\,. \tag{5.16}$$

Therefore, $v_2(k)$ can be decomposed into the equivalent control $v_{eq}(k)$ and the switching rule $v_{SM}(k)$, such as

$$v_{eq}(k) = -(SFB_d)^{-1}SFA_d e(k) \tag{5.17}$$

and

$$v_{SM}(k) = -[Ps(k) + I\sum_{i=0}^{k} s(i)T + D\frac{s(k) - s(k-1)}{T}] \tag{5.18}$$

where *P, I,* and *D* are parameters of the discrete PID-based sliding mode control.

As illustrated in the appendix, it can be proved that the state will move towards the sliding

surface and converge to zero, thus eliminating the the steady state error. In addition, according to the transfer function $G_1(z)$, the input f can be derived from v, which is a desired value as calculated from the SMC,

$$f(k) = \frac{[v(k) - b_1 f(k-1) - \cdots - b_n f(k-n)]}{b_0} \tag{5.19}$$

Therefore, $G_1(z)$ yields

$$\frac{f(z)}{v(z)} = \frac{1}{b_0 z^n + b_1 z^{n-1} + \cdots + b_{n-1} z + b_n} \quad . \tag{5.20}$$

Equation (5.20) indicates that the poles of the transfer function from v to f are the zeroes of the plant. As long as the zeroes of the plant are located inside the unit circle, the control is stable. Otherwise, optimal inversion must be applied, as illustrated as follows. The objective of the optimal inversion is to develop a stable input f such that it minimizes the cost function

$$J = [f(k) - f_d(k)]^T Q[f(k) - f_d(k)] + f^T(k) R f(k) \tag{5.21}$$

where $f_d(k) = \frac{v(k)}{b_0} - \frac{b_1}{b_0} f(k-1) - \frac{b_2}{b_0} f(k-2) - \cdots - \frac{b_n}{b_0} f(k-n)$, and Q and R are the weight matrixes which determine the stability of the optimal inversion. For example, if the 2 norm of the weight matrix R is high, the optimization will smooth the input in order to reduce the energy supply to the system. In this case, the output $f(k)$ doesn't tracking the input $f_d(k)$.

To minimize the cost function given in (5.21), it requires

$$\partial J / \partial f(k) = 0 \tag{5.22}$$

The solution of Equation (5.22) leads to the optimal input

$$f_{opt}(k) = \frac{Q[v(k) - \sum_{i=1}^{n} \frac{b_i}{b_0} f(k-i)]}{R + Q} \tag{5.23}$$

Thus, Equation (5.23), together with Equations (5.13), (5.14), (5.18) and (5.19), forms the

discrete PID-based SMC.

5.5.4 Inversion based PID-SMC for Piezoelectric Actuator Hysteresis

A PEA is commonly modeled as the cascade of the dynamics and the hysteresis, as shown in Figure 5.4, in which the input voltage u passes through the hysteresis sub-model, and its output f is the effective mechanical force supplied to the subsequent dynamic model which generates the displacement y. In [136], a rate independent hysteresis model and a second order auto regressive model were employed to describe the hysteresis and dynamic performance of PEA based on our previous research [46], [124], [130].

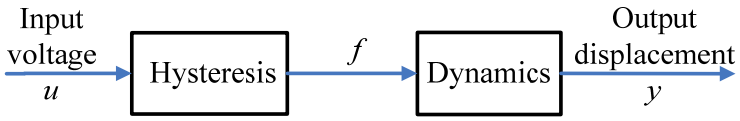

Figure 5. 4 Cascade model of PEA

Adopting this idea, an inversion based PID-SMC is proposed in this study, as shown in Figure 5.1. The inverse of the rate independent hysteresis, denoted by H^{-1}, is cascaded to a PID-based SMC to compensate for the nonlinear hysteresis, while the PID-based SMC is designed to improve the dynamics of the PEA. Since the hysteresis is compensated by its inversion, the disturbance to be rejected by the PID-based SMC is reduced. As a result, the tracking error should be less in comparison to the nominal PID-based SMC introduced in [98]. Due to the imperfection of the hysteresis model, the hysteresis may not be completely compensated by using H^{-1}. Such a model imperfection is considered to be an uncertainty and is added to the input of the plant that is to be compensated by the PID-based SMC. In this study, the inversion of hysteresis developed in [139] is adopted, which is represented by

$$\text{if } f(k+1) > f(k),\ u(k+1) = \frac{-\eta_1 + \sqrt{\eta_1^2 + 4a\varsigma_1}}{2a} \tag{5.24}$$

where $\eta_1 = cf(k+1) + cf(k) + 2b$, $\varsigma_1 = au^2(k) + \eta_1 u(k) + 2[f(k+1) + f(k)]$;

$$\text{if } f(k+1) < f(k),\ u(k+1) = \frac{\eta_2 - \sqrt{\eta_2^2 - 4a\varsigma_2}}{2a} \tag{5.25}$$

where $\eta_2 = -cf(k+1) - cf(k) + 2b$, $\varsigma_2 = -au^2(k) + \eta_2 u(k) + 2[f(k+1) + f(k)]$.

5.5.5 DOB-based PID-SMC for Piezoelectrc Actuator Hysteresis

It is reported in [82] and [98] that the hysteresis can be considered as a combination of a linear component and a non-linear component representing the disturbance, as shown in Figure 5.5, i.e.,

$$F = K_e u + \delta \tag{5.26}$$

where K_e is the effective coefficient of the PEA, δ is the disturbance and $|\delta| \le \delta_{\max}$.

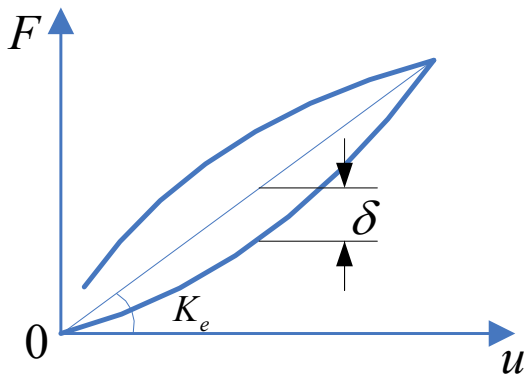

Figure 5. 5 Hysteresis of PEA

It is supposed that the disturbance δ can be compensated by the DOB [81], [82], [140], as shown in Figure 5.2, where η is the measurement noise and Q is a low pass filter employed to

stabilize the DOB. The output of the DOB is given by Equation (5.1) where *w* is feedback to the input of the PEA and as a result, the DOB is able to compensate for the hysteresis that is regarded as the disturbance. The PID-based SMC is Figure 5.2 is designed based on the PEA dynamics.

In [83], three conditions that need to be satisfied for the *Q* filter design are given and restated as follows.

Condition 1: All unstable zeroes of the plant must be zeroes of *Q* such that the output of the DOB *w* is stable;

Condition 2: The relative degree of *Q* must be larger than the relative degree of *G* to ensure reality of the DOB.

Condition 3: To completely compensate for the hysteresis nonlinearity, the steady state gain of the *Q* filter should be 1.

Considering the dynamics of the piezoelectric actuator which is described by a second order transfer function as

$$G(z) = \frac{b_0 z^2 + b_1 z + b_2}{a_0 z^2 + a_1 z + a_2} \tag{5.27}$$

To meet the above conditions, the *Q* filter has be designed with the following transfer function

$$Q(z) = \frac{b_0 z^2 + b_1 z + b_2}{c_0 z^2 + c_1 z + c_2} \tag{5.28}$$

with the following condition

$$\frac{b_0 + b_1 + b_2}{c_0 + c_1 + c_2} = 1 \tag{5.29}$$

The objective of design is to determine the parameters c_0, c_1 and c_2 such that the continuous form of the *Q* filter can be described by the transfer function

$$Q(s) = \frac{D(s)}{N(s)} \tag{5.30}$$

where s is the Laplace operator, $\frac{1}{N(s)} = \frac{1}{(\frac{s}{\omega}+1)^2}$, $D(s)$ is determined by the system parameters and ω is the cut-off frequency. Equation (31) indicates that the amplitude-phase curve of $\frac{1}{N(s)}$ drops at the cut-off frequency with a slope of 40 dB/decade.

Taking a bilinear transform on Equation (5.28), the transfer function of the Q filter can be transformed into a transfer function in the s domain.

$$Q(s) = \frac{\frac{b_0 - b_1 + b_2}{b_0 + b_1 + b_2} T^2 s^2 + \frac{b_0 - b_2}{b_0 + b_1 + b_2} Ts + 1}{\frac{c_0 - c_1 + c_2}{b_0 + b_1 + b_2} T^2 s^2 + \frac{c_0 - c_2}{b_0 + b_1 + b_2} Ts + 1} \tag{5.31}$$

Combining Equations (5.30) and (5.31) with Equation (5.29), one has the parameters c_0, c_1 and c_2 given by

$$\begin{aligned} c_0 &= (\frac{1}{4} + \frac{1}{4\omega^2 T^2} + \frac{1}{\omega T})(b_0 + b_1 + b_2), \\ c_1 &= (\frac{1}{2} - \frac{1}{2\omega^2 T^2})(b_0 + b_1 + b_2) \text{ and} \\ c_2 &= (\frac{1}{4} + \frac{1}{4\omega^2 T^2} - \frac{1}{\omega T})(b_0 + b_1 + b_2). \end{aligned} \tag{5.32}$$

5.5.6 Experiments and Results

Experiments on a commercially-available PEA (P-753, Physik Instrumente), as shown in Figure 5.6, were implemented to verify the effectiveness of the proposed methods. The actuator can generate displacement with a range of 15 μm and a resolution of 0.5 nm. The P-753 PEA has a built-in capacitive displacement sensor for measuring the displacements. The root mean square (RMS) value of the sensor noise is 10~15 nm. Both the actuator and the sensor were connected to a host computer via an I/O board (PCI-DAS1602/16, Measurement Computing Corporation)

and controlled by SIMULINK programs. All displacements were measured with a sampling interval of 0.05 ms. The mass ratio of the stage to the PEA is 49.8, suggesting that the dynamics of the piezoelectric driven stage can be approximately regarded as a second order system according to previous studies [46],[124], [130].

Two experiments were designed and implemented to demonstrate the effectiveness of the proposed control schemes. In the first experiment, the PID parameters and optimal inversion parameters were provided with the same values for all three control schemes, i.e., the inversion based PID-SMC, the DOB-based PID-SMC, and the nominal PID-based SMC, so that their performance could be compared on a common basis. In the second experiment, the PID parameters were adjusted, respectively, for each control scheme to achieve the best tracking performance.

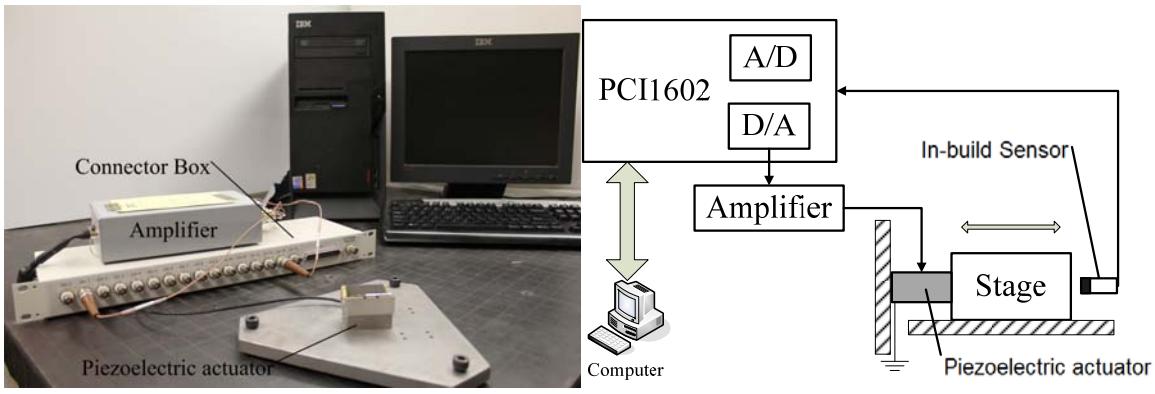

(a) (b)

Figure 5. 6 Experimental settings on the piezoelectric driven stage
(a) picture and (b) schematic diagram.

In both experiments, three types of inputs were used as the reference signal for tracking. The first type was a sinusoidal input with amplitude of 5 μm and frequencies varying from 1 to 50 Hz. The second type was a piecewise continuous function consist of different-amplitude

sinusoidal inputs with the same frequency, as shown in Figure 4.8*a*, where the amplitude is 5 μm for the first and second period of the sinusoidal wave, 2.5 μm for the third period and 0.75 μm for the fourth period. The last type was a superposition of four sinusoidal inputs with different frequencies, amplitudes and phase delays, as shown in Figure 4.8*b* and displacements *w* given by Equation (5.47).

Table 5-1 shows each type of input data and their abbreviation.

Table 5- 1 Inputs in the experiments

Abbreviation	Input Description	Remarks
PWSW10	Piecewise continuous combination of	10 Hz
PWSW30	different amplitude	30 Hz
PWSW50	sinusoidal inputs	50 Hz
SW10	Superposition of four sinusoidal	Maximum 10 Hz
SW30	inputs with different frequency,	Maximum 30 Hz
SW50	amplitude and phase delay	Maximum 50 Hz
SIN1	5 μm sinusoidal input	1 Hz
SIN10		10 Hz
SIN30		30 Hz
SIN50		50 Hz

5.5.6.1 Parameter Identification

First, experiments were performed to identify the parameters, i.e., *a, b* and *c* in the hysteresis model, such that the effective mechanical force *f,* which is the input of the dynamics, can be estimated. Then, the estimated *f* and the measured displacement *y* were used to identify the parameters in the dynamic model.

Since hysteresis dominates in PEA performance under low frequency voltages, a 70V, 1Hz sinusoidal input voltage was applied to the PEA and the corresponding displacement was measured to identify the parameters *a, b* and *c*. Specifically, the continuous hysteresis model

[136] was used and by means of least square method, *a, b* and *c* were given values of 0.0077, 0.1167 and -0.0487, respectively. With these values, the inversion hysteresis model was obtained using Equations (5.24) and (5.25). Figure 5.7 shows an estimation of the hysteresis. The blue solid line is the hysteresis of the PEA for 1Hz input and the red dashed line is the fitted hysteresis. It can be seen that fitting error exists between the measured output and the model output. This error is considered as a disturbance to the PID based. The parameter K_e was 0.1347, as identified in [98].

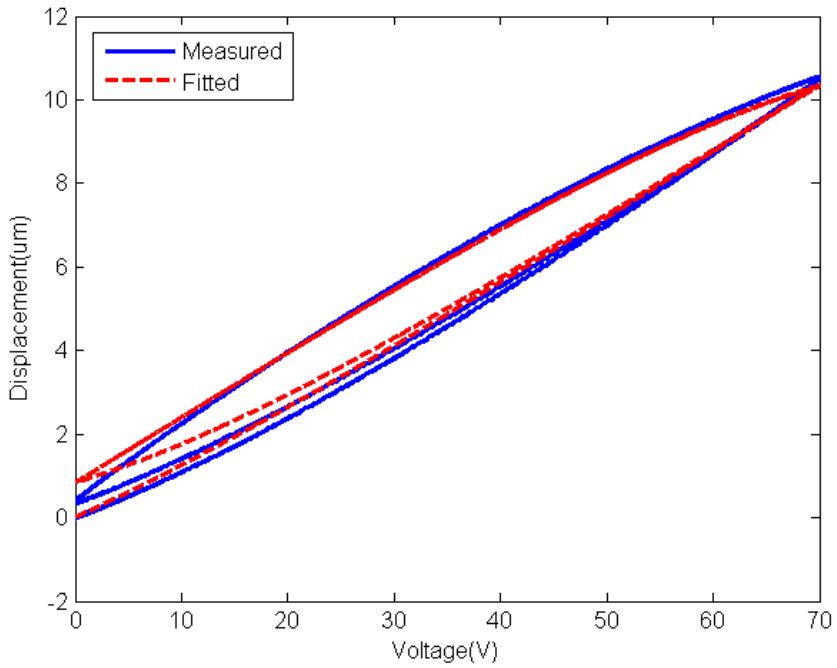

Figure 5. 7 Hysteresis identification

Next, a 70V white noise voltage was provided to the PEA and the corresponding displacement was measured. The input *f* to the dynamic model was estimated by substituting the estimated parameters *a, b* and *c* into the discrete hysteresis model introduced in [136]. With *f* and the measured displacement *y*, the parameters in the dynamic model were identified, leading to

$$y(k) = 1.6035y(k-1) - 0.61995y(k-2) + 0.0050811u(k) - 0.0036354u(k-1) + 0.010553u(k-2) \quad (5.33)$$

Because the proposed methods are to be compared with the nominal PID-based SMC introduced in [98], the dynamic model for the nominal PID-based SMC should be identified as well, which is given by

$$y(k) = 1.6076y(k-1) - 0.61956y(k-2) + 0.00071058u(k) - 0.00047055u(k-1) + 0.0012609u(k-2) \quad (5.34)$$

5.5.6.2 Comparison based on the same PID parameters

To verify the effectiveness of the inversion feedforward compensation and DOB, the control methods were used to control a PEA with a sampling rate of 20 kHz. A comparison was made with the nominal PID-based SMC introduced in [98] based on the same PID parameters. The optimal inversion approach introduced in Section II was applied in the SMC design. The state was designed to be $x = [y, v_y]^T$, where y is the output displacement and v_y is the velocity. The displacement and the velocity were estimated using a α-β filter which is a simplified form of observer for estimation and filtering. The parameters of the filter were determined to be α = 0.1, β = 0.0001 by trials-and-errors. The sliding surface was defined by Equation (5.16) where S = [18000, 1]. For the nominal PID-based SMC, since the zeroes of the plant were located outside the unit circle, the optimal inversion of Equation (5.23) was employed in the controller as well. The parameters of the PID regulator and the optimal inversion were kept the same for the inversion based PID-SMC and the DOB-based PID-SMC. Table 5-2 shows the adjusted parameters. The cutoff frequency in the DOB-based PID-SMC was designed to be 500rad/s.

Table 5- 2 Parameters in the experiments for the first part

Parameters	*P*	*I*	*D*	*Q*	*R*
Value	0.01	30	0.000001	1	100

Table 5-3 compares the tracking errors of the PEA controlled by the nominal PID-based SMC, inversion based PID-SMC and DOB-based PID-SMC. The tracking error is defined by the RMS value of the difference between the output displacement of the PEA and the desired output defined by the reference input. Figure 5.8 shows some of the results for the tracking performance of the PEA controlled by means of different methods.

Table 5- 3 Comparison of the tracking performance controlled by different methods in the experiments for the first part

Inputs	PID-based SMC	Inversion based PID-SMC	DOB-based PID-SMC
SIN 1	0.027	0.0055	0.0063
SIN 10	0.1835	0.0698	0.0516
SIN 30	0.4526	0.2156	0.2016
SIN 50	0.5988	0.3621	0.4588
SW 10	0.044	0.0134	0.0117
SW 30	0.0888	0.0316	0.0365
SW 50	0.1252	0.0494	0.0737
PWSW 10	0.1472	0.0543	0.0403
PWSW 30	0.367	0.1701	0.1599
PWSW 50	0.4823	0.2818	0.3628

Compared to the nominal PID-based SMC, the tracking errors for the inversion based PID-SMC and DOB-based PID-SMC were shown much smaller. For instance, for the 10 Hz SW input, the tracking errors of the piezoelectric actuator controlled by the inversion based PID-SMC and the DOB-SMC are 0.0134 μm and 0.0117 μm, which are 30.4% and 26.6% of that controlled by the nominal PID-based SMC, respectively. This occurred because the use of the inversion hysteresis and DOB has the capacity to compensate for the disturbance rejected by the

PID-SMC. This can also be seen from Figure 5.9, in which the influence of hysteresis is reduced by the inversion feedforward control. Compared to the hysteresis shown in Figure 5.7, the hysteresis here was shown to be reduced 83% by measuring the width of the hysteresis loop at the central input voltage of 35V.

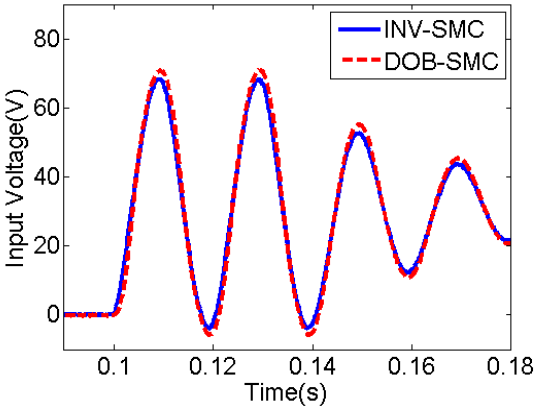

(a)

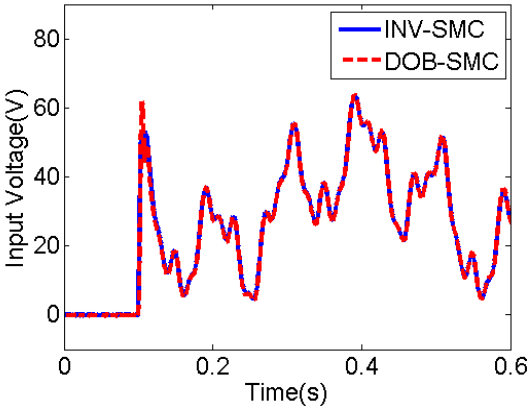

(b)

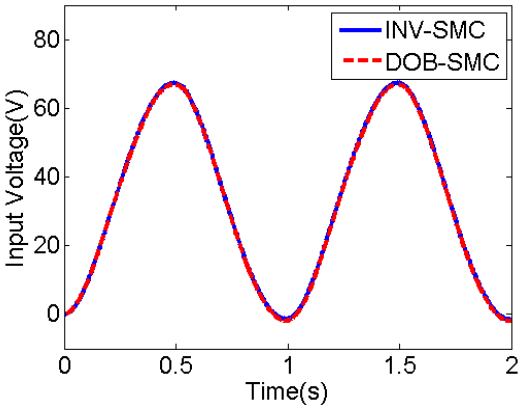

(c)

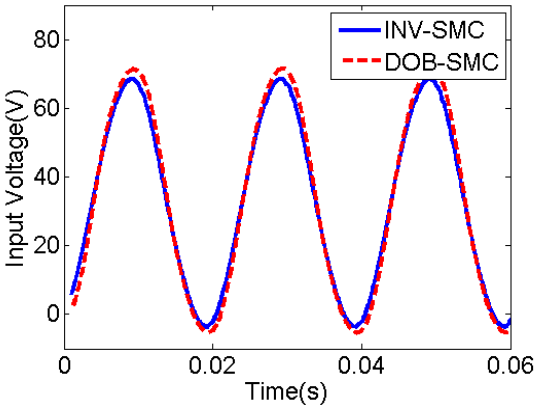

(d)

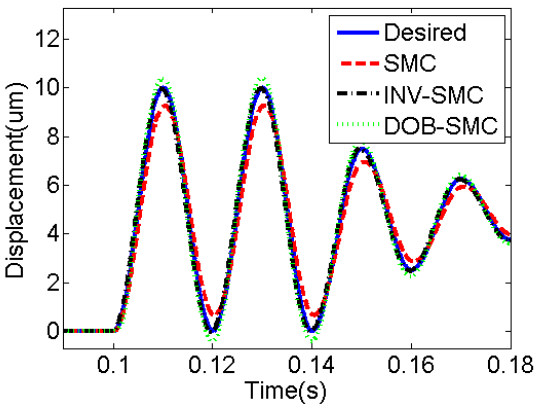

(e)

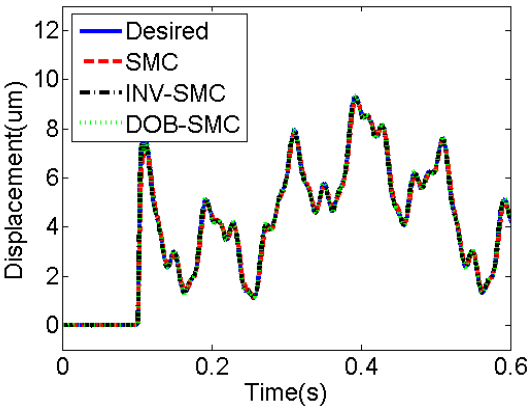

(f)

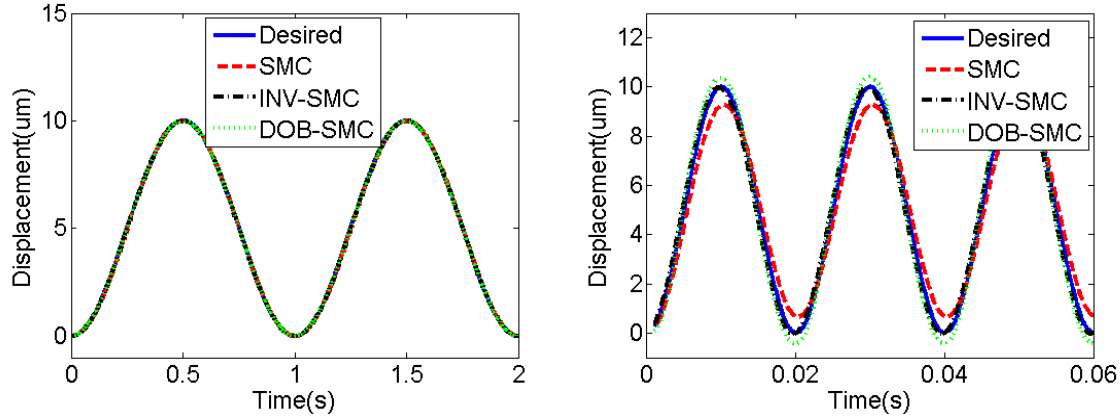

(g) (h)

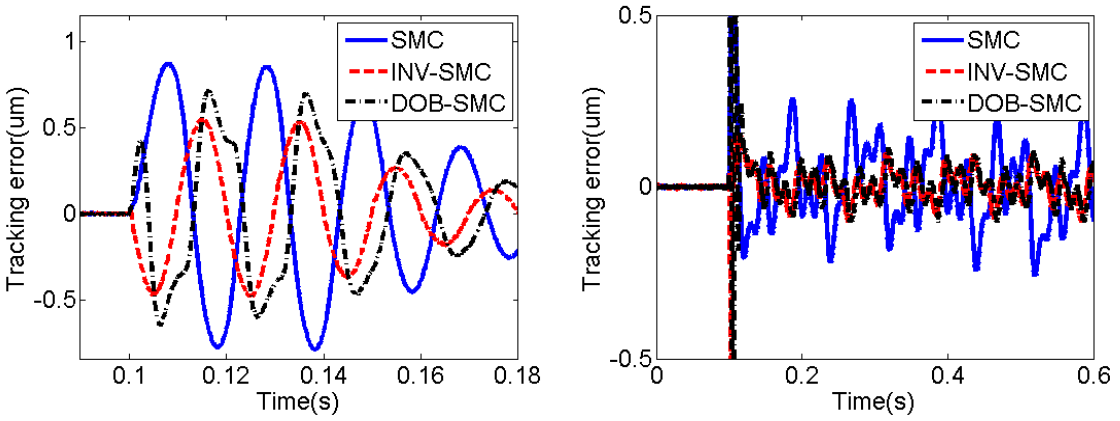

(i) (j)

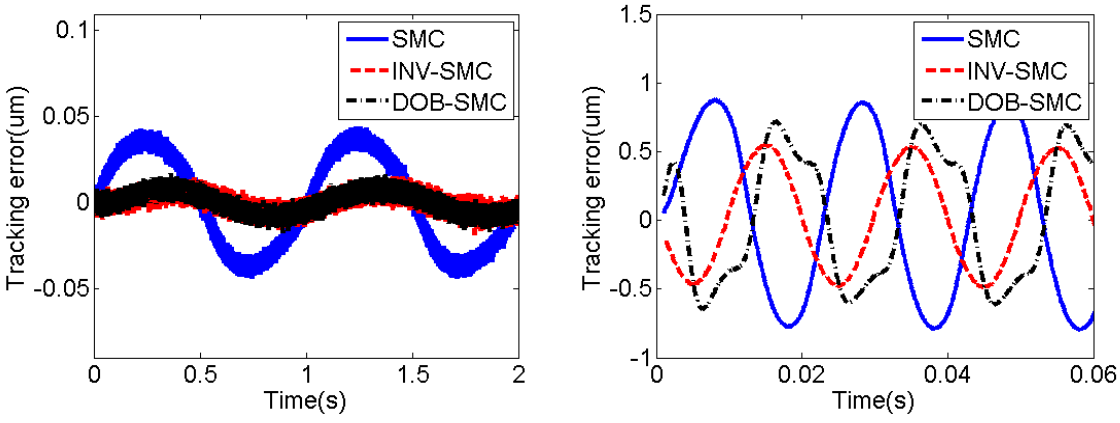

(k) (l)

Figure 5. 8 Comparison of the tracking performance controlled by different methods (a-d) control input for PWSW50, SW50, SIN1 and SIN50 inputs; (e-h) displacements for PWSW50, SW50, SIN1 and SIN50 inputs; (i-l) tracking error for PWSW50, SW50, SIN1 and SIN50 inputs;

At low frequencies, the DOB-based PID-SMC performs better than the inversion based PID-SMC. If the 10 μm 10 Hz sinusoidal signal was applied to the input, the tracking error for the inversion based PID-SMC is 0.0698 μm while the tracking error for the DOB-based PID-SMC is 0.0516 μm. Similar results are also found where PWSW and SW are given as reference inputs. However, an exception exists for the 1Hz sinusoidal input. The tracking error of the PEA controlled by the inversion based PID-SMC is 0.0055 μm which is 87.3% of the tracking error for the DOB-based PID-SMC. At high frequencies, the inversion based PID-SMC performs better, which indicates the high gain margin of the inversion feedforward control. For the SW 50 reference input, for instance, the tracking error for the inversion based PID-SMC is 67% of that for the DOB-based PID-SMC.

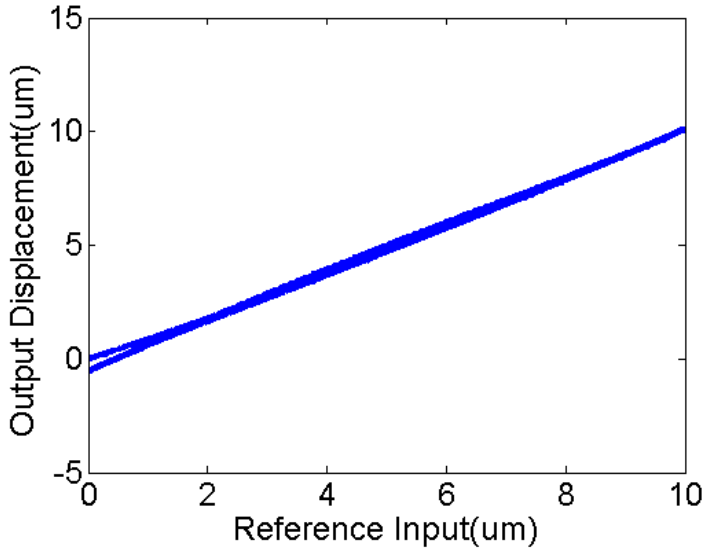

Figure 5. 9 Hysteresis compensation by the inversion feedforward control (Sinusoidal input with 10 um amplitude and 1 Hz frequency)

5.5.6.3 Comparison based on the PID parameters adjusted for the best performance

To verify the effectiveness of the proposed methods, experiments were performed on the

PEA with a 20 kHz sampling rate as well. The PID parameters of the three controllers were adjusted respectively by applying the Ziegler-Nichols method, such that the best tracking performance could be derived. The state was still designed to be $x = [y, v_y]^T$. The displacement and the velocity were estimated by a α-β filter with α = 0.1, and β = 0.0001. The sliding surface was again defined by Equation (5.16), where S = [18000, 1]. The optimal inversion of Equation (5.23) was employed in the controllers for stabilization. Table 5-4 shows the adjusted parameters for each controller. The cutoff frequency in the DOB-based PID-SMC was designed to be 500 rad/s as well.

Table 5- 4 Parameters in the experiments for the second part

Controller	*P*	*I*	*D*	*Q*	*R*
PID-based SMC	0.01	60	0.000001	1	100
Inversion based PID-SMC	0.001	10	0.000001	1	100
DOB-based PID-SMC	0.05	12	0.000001	1	100

Table 5-5 shows the tracking errors of the PEA controlled by the PID-based SMC, inversion based PID-SMC, and DOB-based PID-SMC. The tracking error is represented as described above in section B. From Table 5-5, it can be concluded that both the inversion based PID-SMC and DOB-based PID-SMC performed better than the nominal PID-based SMC. For example, for the PWSW 50 reference input, the tracking errors for the inversion based PID-SMC and the DOB-based PID-SMC are 56.9% and 49.6%, respectively, of the error by the nominal PID-based SMC. This implies that the tracking performance of the PID-based SMC can be improved by reducing the disturbance. At low frequencies, the inversion based PID-SMC performs better than the DOB-based PID-SMC. For example, for the 30 Hz sinusoidal input, the tracking error for the inversion based PID-SMC is 0.0552 μm while the tracking error for the DOB-based PID-SMC is

0.0013 μm more. Similar conclusions can be drawn for the PWSW and SW reference inputs. This differs from the results shown in the last section which indicated the influence of the adjusted PID parameters. At high frequencies, the DOB-based PID-SMC performs better. For the PWSW 50 reference input, the tracking error for the DOB-based PID-SMC is 0.0086 μm less than that of the inversion based PID-SMC.

Table 5- 5 Comparison of the tracking performance controlled by different methods in the experiments for the second part

Inputs	PID-based SMC	Inversion based PID-SMC	DOB-based PID-SMC
SIN1	0.0133	0.0125	0.0137
SIN10	0.0461	0.0368	0.0473
SIN 30	0.0973	0.0552	0.0565
SIN 50	0.1416	0.0867	0.0683
SW 10	0.0161	0.0135	0.0144
SW 30	0.0273	0.0183	0.0205
SW 50	0.0378	0.0223	0.0258
PWSW 10	0.0383	0.0295	0.0373
PWSW 30	0.0832	0.0446	0.0467
PWSW 50	0.1208	0.0687	0.0601

5.5.7 Conclusions and disscussions

PID-based SMC has shown promise in the control of PEA due to its disturbance rejection. In this control scheme, PEA hysteresis is treated as totally-unknown disturbance to the PEA input for compensation. For improvement, this paper presents the development of two modified PID-based SMC, namely, the inversion based PID-SMC and the DOB-based PID-SMC. In the inversion based PID-SMC, the PEA hysteresis is predicted from existing models of PEA hysteresis and then strategically included in the inversion feedforward control for its compensation. In the DOB-based PID-SMC, the PEA hysteresis is partially predicated and

compensated by employing the DOB technique.

To illustrate the effectiveness of the proposed control schemes, experiments were performed and the results were compared with those from the nominal PID-based SMC. It has been shown that by inclusion of the inverse hysteresis and the DOB are more effective in term of the hysteresis compensation. Therefore, the disturbance, which is rejected by the SMC, is reduced, thus improving the performance of the PID-based SMC. Based on the examined cases with inputs of varying frequencies, it is recommended that the inversion based PID-SMC should be used if the input frequency is low, while the DOB-based PID-SMC is preferred for applications with higher frequencies.

5.5.8 Appendix

The state moves towards the sliding surface and converge to zero.

Prove: Divide the switching function into two parts

$$s(k) = s_0 + s_1(k) \tag{5.35}$$

where s_0 is the initial value of the switching function, which depends on the value of the original state.

Substituting Equations (5.19) and (5.35) into Equation (5.16) and considering Equations (5.13)-(5.15), one can derive

$$s_1(k+1) = -[SBP + SBIT(k+1) + 1]s_0 + SF\varepsilon(k) - SB\left[Ps_1(k) + IT\sum_{i=0}^{k} s_1(i) + D\frac{s_1(k) - s_1(k-1)}{T} \right] \tag{5.36}$$

where $B = FB_d$.

Equation (5.36) can be considered as a two-inputs-one-output system, where s_0 and ε re the

inputs. Because Equation (5.36) is linear, it can be divided into two subsystems: the input of one subsystem is s_0 and its corresponding output is s_{11}; the input of the other subsystem is ε and its corresponding output is s_{12}. Therefore,

$$s_1(k) = s_{11}(k) + s_{12}(k) \tag{5.37}$$

Assuming $s_{11}(0) = s_{12}(0) = 0$, the first subsystem can be represented as

$$s_{11}(k+1) = -[SBP + SBIT(k+1) + 1]s_0 - SB\left[Ps_{11}(k) + IT\sum_{i=0}^{k} s_{11}(i) + D\frac{s_{11}(k) - s_{11}(k-1)}{T} \right] \tag{5.38}$$

Taking Z-transform on Equation (5.38), the transfer function from s_0 to s_{11} is given by

$$\frac{s_{11}(z)}{s_0(z)} = \frac{-\left[SBP + SBIT(k+1) + 1 \right]}{z^{-1} + SBP + SBIT\left(z^k + z^{k-1} + \cdots + z^0 \right) + \frac{SBD}{T}(1-z)} \tag{5.39}$$

If s_0 is a step input with its amplitude being s_0, according to the final value theory of the discrete system,

$$s_{11}(\infty) = \lim_{z\to 1}\left(1 - z^{-1}\right)s_{11}(z) = \lim_{z\to 1}\frac{-\left(1 - z^{-1}\right)\left[SBP + SBIT(k+1) + 1 \right]s_0 \frac{z}{z-1}}{z^{-1} + SBP + SBIT\left(z^k + z^{k-1} + \cdots + z^0 \right) + \frac{SBD}{T}(1-z)} = -s_0 \tag{5.40}$$

The second subsystem can be represented as

$$s_{12}(k+1) = -SB\left[Ps_{12}(k) + IT\sum_{i=0}^{k} s_{12}(i) + D\frac{s_{12}(k) - s_{12}(k-1)}{T} \right] + SF\,\varepsilon(k) \tag{5.41}$$

The transfer function from ε to s_{12} is obtained by taking Z-transform on Equation (5.41) as

$$\frac{s_{12}(z)}{\varepsilon(z)} = \frac{SF}{z^{-1} + SBP + SBIT\left(z^k + z^{k-1} + \cdots + z^0 \right) + \frac{SBD}{T}(1-z)} \tag{5.42}$$

Therefore,

$$s_{12}(\infty)=\lim_{z\to 1}\left(1-z^{-1}\right)s_{12}(z)=\lim_{z\to 1}\frac{-\left(1-z^{-1}\right)SF\,\varepsilon(z)}{z^{-1}+SBP+SBIT\left(z^{k}+z^{k-1}+\cdots+z^{0}\right)+\dfrac{SBD}{T}(1-z)}=0 \quad (5.43)$$

Equations (5.37), (5.40), and (5.43) suggest that the value of the switching function *s* is zero as time approaches to infinity. As such the state moves towards the sliding surface and eventually converges to zero.

5.5.9 Acknowledgment

The support to the present study from the China Scholarship Council (CSC) and the Natural Sciences and Engineering Research Council (NSERC) of Canada is acknowledged.

6 Model of the Multi-DOF Piezoelectric Actuators

This chapter presents the work that is included in the following manuscript appended.

Y. Cao and X. B. Chen, "State Space System Identification of three-DOF Piezo-actuator Driven Stages with unknown configuration," *Actuators*, 2, 2013, 1-18.

6.1 Introduction and Objectives

Multi-DOF piezoelectric positioning systems are actuated by PEAs, which are connected through flexible joints. With ingenious design, friction and backlash clearance can be eliminated, leading to improved performance. However, nonlinear effects in the PEAs, such as creep, hysteresis, and the cross-coupling of the parallel mechanism can greatly degrade the positioning accuracy of the stages. In order to develop control schemes for nano-positioning, modeling of piezoelectric stages has been reported in the literature with increasing frequency. This paper aims at developing a dynamic model for the controller design of a three-DOF PEA. Since the detail information with regard to the internal mechanical configuration is not provided by the manufacture, the straightforward modeling method by means of the physical law is not applicable. Instead, a state space model based on the black box system identification is developed for the control of the three-DOF PEA.

6.2 Methods

Considering hysteresis and other nonlinearities to be model uncertainties, the system matrixes in the state space model were derived through singular value decomposition (SVD) of

the Hankel matrix, which was directly identified from a Hankel-Toeplitz model by means of the maximum-a-posteriori (MAP) online estimation.

6.3 Results

The linear state space model can predict the dynamic performance of a piezo-actuator driven stage with improved accuracy. Since MAP estimation utilizes the posteriori parameter information which have the beneficial effect of reduction of variances of parameter estimations, MAP online estimation method performs better in the model identification than the least squares method. Moreover, the identified parameters are updated online if more data is available for the model identification. This provides a starting point from which to adaptively compensate for the dynamics and cross-coupling effects of the piezo-actuator driven stage by means of the mode-based control scheme.

6.4 Contributions

The contribution of this paper is the development of a black box model used to describe the dynamics of 3-DOF piezo-actuator driven stages, which allows investigation of the performance of complicated systems with unknown physical configuration by means of the linear state space model.

6.5 Paper: State Space System Identifcation of three-DOF Piezo-actutator Driven Stages with Unknown Configuration

Authors: Y. Cao and X. B. Chen, *Member, IEEE*[5]

Index Terms: State space model, Hankel matrices, Nano- positioning, System identification, Cross-coupling effect, Dynamics.

6.5.1 Abstract

Due to their fast response, high accuracy and non-friction force, piezo-actuators have been widely employed in multiple degree-of–freedom (DOF) stages for various nano-positioning applications. The use of flexible hinges in these piezo-actuator driven stages allows for eliminating the influence of friction and backlash clearance as observed in other configurations; meanwhile it also causes more complicated stage performance in terms of dynamics and cross-coupling effect between different axes. Based on the system identification technique, this paper presents the development of a model for the 3-DOF piezo-actuator driven stages with unknown configuration, with its parameters estimated from the Hankel matrix by means of the maximum-a-posteriori (MAP) online estimation. Experiments were carried out on a commercially-available piezo-actuator driven stage to verify the effectiveness of the developed model. The results show that the developed model is able to predict the stage performance with improved accuracy, while the model parameters can be well updated online by using the MAP

Manuscript received January 30, 2013. This work was supported by the China Scholarship Council (CSC) and the Natural Science and Engineering Research Council (NSERC) of Canada.

Y. Cao is with the Department of Mechanical Engineering, 57 Campus Drive, University of Saskatchewan, Saskatoon, SK, S7N 5A9 (e-mail: yuc150@ mail.usask.ca).

X. B. Chen is with the Department of Mechanical Engineering, 57 Campus Drive, University of Saskatchewan, Saskatoon, SK, S7N 5A9 (phone: 1-306-966-1267; e-mail: xbc719@ mail.usask.ca).

estimation. These capabilities allow investigation of the complicated stage performance and also provide a starting point from which to apply the mode-based control scheme for an improved stage performance.

6.5.2 Introduction

Piezo-actuator driven stages have advantages of fast response, high precision, and generation of large forces. As such, they have been widely applied in semiconductors, biomedical science, production manufacturing and other devices which require nano- positioning and manipulation [1], [2]. With the ingenious design of flexible hinges, friction and backlash clearance can be eliminated, leading to improved performance. Meanwhile, the use of flexible hinges also caused more complicated stage. Modeling and control for one degree-of-freedom (DOF) piezo-actuator driven stages have drawn considerable attention in the literature [6] – [10]. Due to the cross-coupling effect between different axes, the methods developed for 1-DOF piezo-actuator driven stages cannot be readily extended to multiple-axis ones [11], the research of which is still in its early stage. In [12], a 3-input-3-output state space model was developed for a 3-DOF micro-stage based on the free body force diagram of the stage. Provided with the nominal values and the uncertainty ranges, the parameters were searched so that the resulting physics-based model predicted the displacement outputs with high fidelity. By comparison with experimental data, it was shown that the proposed model was able to predict the performance of the micro-stage. An Auto-Regressive Exogenous (ARX) model was developed in [13] to describe the dynamic performance of a biaxial piezo-stage and the model was then integrated in a feedforward compensator for precision tracking control with experimental verification. However, cross-coupling between the two axes, which might have a negative effect on the performance of the controller, was not considered in the ARX model. In [14], a fourth order linear transfer

function was identified for a piezoelectric stage, where the cross-coupling effect was neglected. As such, a chirp signal was applied to each of the axes independently and with the measurement outputs, the parameters in each transfer function were estimated by using the system identification technique. In [15], the dynamic equations were combined with the Bouc-Wen model for each piezoelectric actuator to describe the performance of a plane-type 3-DOF precision positioning table or stage. The parameters of the model were optimized based on the real-coded genetic algorithm (RGA) method. From the numerical simulations and experimental results, the 3-DOF cross-coupling effect was reduced by the proposed control method and good contour tracking performance was obtained due to successful identification of the dynamic models.

A straightforward modeling method for multi-DOF piezo-actuator driven stages can be based on the internal configuration by means of physics laws, as mentioned above. However, such details with regard to the internal structure are often not provided by the manufactures. Therefore, system identification for multi-DOF piezo-actuator driven stages with unknown configuration is always required for the model development. To meet this need, in this paper we report the model development based on the black box system identification of for 3-DOF piezo-actuator driven stages with unknown configuration. Specifically, a linear discrete state space model $x(k+1) = Ax(k) + Bu(k)$ and $y(k) = Cx(k) + Du(k)$ (A, B, C and D are system matrices) is adopted and applied to describe the dynamics of the piezo-actuator driven stage.

To identify the parameters of the state space model, methods have been reported in the literature [16]-[22]. In [19], a modified frequency domain subspace identification algorithm was developed based on the previous work. The power spectrum estimates was strongly consistent when the measurements were corrupted by bounded random noise. In [20], the numerical

algorithms for subspace state space system identification (N4SID) method was combined with the multivariable output-error state space (MOESP) method for improved performance. The state space model was obtained in [21] by identifying the Markov parameters (a kind of matrix impulse response) that were indirectly calculated from an identified auto-regressive model or transfer function. In [22], the system matrices in the state space model were derived through singular value decomposition (SVD) of the Hankel matrix, which was directly identified from a Hankel-Toeplitz model using the least squares method. The parameters are time-invariant and thus the model cannot be applied if the performance of piezo-actuator driven stage changes with the environmental condition, such as the temperature.

To develop a state space model with updating parameters, the SVD of the Hankel matrix is strategically combined with MAP online estimation in this study. The parameters can be updated as new observations become available. Furthermore, MAP estimation utilizes prior information regarding the parameters and the measurement errors. Inclusion of posteriori parameter information can have the beneficial effect of reducing the variances of parameter estimators. To verify the effectiveness of the state space model identified by using the MAP online estimation, experiments were carried out on a commercially available piezo-actuator driven stage. The estimation errors obtained from the Hankel matrix using online estimation were compared to those reported in [22].

6.5.3 Black Box System Identification

In this section, it is assumed that the configuration or the internal structure of 3-DOF piezo-actuator driven stages is not available or known. Also, it is assumed that the stage is regarded as a linear multiple-input and multiple-output (MIMO) system by ignoring the nonlinearity, which is reasonable as illustrated in the experiments presented later in this paper.

To represent the linear dynamics and cross-coupling effect of the stage, the simplified Hankel-Toeplitz model is adopted and employed in the present study, in which the Hankel matrix is to be identified by implementing the MAP online estimation method.

6.5.3.1 Simplified Hankel-Toeplitz Model

For a linear MIMO system, the discrete state space representation is given by

$$\begin{aligned} x(k+1) &= Ax(k) + Bu(k) + w(k) \\ y(k) &= Cx(k) + Du(k) + v(k) \end{aligned} \tag{6.1}$$

where $A \in R^{n\times n}$, $B \in R^{n\times m}$, $C \in R^{q\times n}$ *and* $D \in R^{q\times m}$ are system matrices, $x \in R^{n\times 1}$ is the state, $u \in R^{m\times 1}$ is the input, $y \in R^{q\times 1}$ is the output, $w \in R^{n\times 1}$ and $v \in R^{q\times 1}$ represent the ignored nonlinearity and uncertainties of the piezo-actuator driven stage, *m* and *q* are the number of inputs and outputs, respectively. By iteration, one has

$$\begin{aligned} x(k+p) &= A^p x(k) + B_p u_p(k) + \Gamma_p w_p(k) \\ y_p(k) &= C_p x(k) + D_p u_p(k) + \Pi_p w_p(k-1) + v_p(k) \end{aligned} \tag{6.2}$$

for any $p \in \{p \mid p \in Z, p > 0\}$, where u_p and y_p are defined as column vectors of the input and output data going *p* steps towards the future,

$$u_p(k) = \begin{bmatrix} u(k) \\ u(k+1) \\ \vdots \\ u(k+p-1) \end{bmatrix}, y_p(k) = \begin{bmatrix} y(k) \\ y(k+1) \\ \vdots \\ y(k+p-1) \end{bmatrix}, \tag{6.3}$$

v_p and w_p are defined as column vectors of the noises and disturbance going *p* steps towards the future, B_p is the controllability matrix, C_p is the observability matrix, D_p is the Toeplitz matrix for the system Markov parameters and

$$B_p = \begin{bmatrix} A^{p-1}B & A^{p-2}B & \cdots & AB & B \end{bmatrix} \in R^{n\times pm}, \Gamma_p = \begin{bmatrix} A^{p-1} & A^{p-2} & \cdots & A & I \end{bmatrix} \in R^{n\times pn},$$
$$C_p = \begin{bmatrix} C^T & (CA)^T & (CA^2)^T & \cdots & (CA^{p-1})^T \end{bmatrix}^T \in R^{pq\times n},$$

$$D_p = \begin{bmatrix} D & 0 & 0 & \cdots & 0 \\ CB & D & 0 & \cdots & 0 \\ CAB & CB & D & \cdots & 0 \\ \vdots & \vdots & \vdots & \ddots & \vdots \\ CA^{p-2}B & CA^{p-3}B & CA^{p-4}B & \cdots & D \end{bmatrix} \in R^{pq \times pm}, \Pi_p = \begin{bmatrix} 0 & 0 & 0 & \cdots & 0 \\ 0 & C & 0 & \cdots & 0 \\ 0 & CA & C & \cdots & 0 \\ \vdots & \vdots & \vdots & \ddots & \vdots \\ 0 & CA^{p-2} & CA^{p-3} & \cdots & C \end{bmatrix} \in R^{pq \times pn}. \tag{6.4}$$

If $pm \geq n$, there exists an interaction matrix **M** such that

$$A^p + \mathbf{M} C_p = 0 \cdot \tag{6.5}$$

Substituting Equation (6.5) into Equation (6.2) yields

$$x(k+p) = (B_p + \mathbf{M} D_p) u_p(k) - \mathbf{M} y_p(k) + \mathbf{M} \Pi_p w_p(k-1) + \mathbf{M} v_p(k) + \Gamma_p w_p(k). \tag{6.6}$$

Combining Equations (6.2) and (6.6) leads to the following equation, which is the so-called simplified Hankel-Toeplitz model

$$\begin{aligned} y_p(k) &= C_p x(k) + D_p u_p(k) + \Pi_p w_p(k-1) + v_p(k) \\ &= C_p (B_p + \mathbf{M} D_p) u_p(k-p) - C_p \mathbf{M} y_p(k-p) + D_p u_p(k) + \Delta(k). \end{aligned} \tag{6.7}$$

where $\Delta(k) = \Pi_p w_p(k-1) + v_p(k) + C_p \mathbf{M} \Pi_p w_p(k-p-1) + C_p \mathbf{M} v_p(k-p) + C_p \Gamma_p w_p(k-p)$.

Using the following denotations

$$\mathbf{\Gamma} = C_p (B_p + \mathbf{M} D_p), \ \mathbf{\Phi} = -C_p \mathbf{M}, \tag{6.8}$$

one has Equation (6.7) rewritten as

$$y_p(k) = \begin{bmatrix} \mathbf{\Gamma} & \mathbf{\Phi} & D_p \end{bmatrix} \begin{bmatrix} u_p(k-p) \\ y_p(k-p) \\ u_p(k) \end{bmatrix} + \Delta(k) \tag{6.9}$$

where $\Delta(k)$ represents the combined model noises and can be regarded as the model estimation error. Define

$$\mathbf{H}_0 \equiv C_p B_p = \mathbf{\Gamma} + \mathbf{\Phi} D_p \ , \tag{6.10}$$

the square matrix $\mathbf{H}_0$ can be estimated without knowing **M**.

Once $\mathbf{H}_0$ is identified, an adjacent $\mathbf{H}_1 \equiv C_p A^p B_p$ can be calculated by using Equation (6.5) such that

$$\mathbf{H}_1 = C_p(-\mathbf{M}C_p)B_p = (-C_p\mathbf{M})C_pB_p = \mathbf{\Phi}\mathbf{H}_0 \tag{6.11}$$

Similarly,

$$\mathbf{H}_i \equiv C_p(A^p)^i B_p = C_p(-\mathbf{M}C_p)\cdots(-\mathbf{M}C_p)B_p = (-C_p\mathbf{M})\cdots(-C_p\mathbf{M})C_pB_p = \mathbf{\Phi}^i\mathbf{H}_0 \tag{6.12}$$

Using $\mathbf{H}_0, \mathbf{H}_1, \cdots$ as building blocks, a Hankel matrix of any size can be constructed. For example,

$$\mathbf{H} = \begin{bmatrix} \mathbf{H}_0 & \mathbf{H}_1 & \cdots & \mathbf{H}_n \end{bmatrix}^T \quad . \tag{6.13}$$

6.5.3.2 Reconstrucion of t the system matrices

The Hankel matrix is arranged with Markov parameters of increasing order going from left of right. Let the Hankel matrices be

$$\bar{\mathbf{H}}(0) = \begin{bmatrix} CB & CAB & \cdots & CA^{n_1}B \\ CAB & CA^2B & \cdots & CA^{n_1+1}B \\ \vdots & \vdots & \ddots & \vdots \\ CA^{n_2}B & CA^{n_2+1}B & \cdots & CA^{n_1+n_2}B \end{bmatrix}, \bar{\mathbf{H}}(1) = \begin{bmatrix} CAB & CA^2B & \cdots & CA^{n_1+1}B \\ CA^2B & CA^3B & \cdots & CA^{n_1+2}B \\ \vdots & \vdots & \ddots & \vdots \\ CA^{n_2+1}B & CA^{n_2+2}B & \cdots & CA^{n_1+n_2+1}B \end{bmatrix} \tag{6.14}$$

where $n_1, n_2 \in \mathbf{Z}$. Comparing Equation (6.14) with Equations (6.4), (6.12) and (6.13), $\bar{\mathbf{H}}(0)$ and $\bar{\mathbf{H}}(1)$ can then be extracted from $\mathbf{H}$ by rearrangement of its elements. The state space matrices are reconstructed from the Hankel matrix by employing the following Lemma 6.1.

Lemma 6.1: An *s*-th order state space model can be reconstructed as

$$A = \Sigma_s^{-\frac{1}{2}} U_s^T \bar{\mathbf{H}}(1) V_s \Sigma_s^{-\frac{1}{2}} \tag{6.15}$$

where B is the first m columns of $\Sigma_s^{\frac{1}{2}} V_s^T$, C is the first q rows of $U_s \Sigma_s^{\frac{1}{2}}$ and $s \le \min\{m(n_1+1), q(n_2+1)\}$, The matrix U_s and V_s are made up of s left and right singular

vectors of $\bar{\mathbf{H}}(0)$, and the diagonal matrix Σ_s is made up of *s* corresponding singular values of $\bar{\mathbf{H}}(0)$ [21].

6.5.3.3 MAP Online estimation

Equation (6.9) can be rewritten as, by ignoring $\Delta(k)$

$$y_p(k) = \boldsymbol{\theta} X + \Delta(k) \tag{6.16}$$

where $\boldsymbol{\theta} = \begin{bmatrix} \boldsymbol{\Gamma} & \boldsymbol{\Phi} & D_p \end{bmatrix}, X = \begin{bmatrix} u_p(k-p) \\ y_p(k-p) \\ u_p(k) \end{bmatrix}$.

By using the least squares method, $\boldsymbol{\theta}$ is identified to be a time-invariant matrix, which might not be able to accurately describe the environment dependent performance of the piezo-actuator drive stage. In order to apply the state space model in the control of piezo-actuator driven stage, the model parameters should be updated as new observation data is available. Therefore, MAP online estimation was employed to identify the parameter matrix in Equation (6.16) instead.

The MAP online estimation method is used to update the parameters as the new observation data points becomes available, which is given by

$$\boldsymbol{\theta}_{i+1} = \boldsymbol{\theta}_i + \mathbf{P}_{i+1}\mathbf{X}_{i+1}^T\boldsymbol{\sigma}_{i+1}^{-1}\mathbf{E}_{i+1} \tag{6.17}$$

where $\mathbf{X}$ has the same definition as the one given in Equation (6.16), $\boldsymbol{\theta}_i$ is the value of identified parameters based on the first *i* groups of data, $\mathbf{P}_i$ is the covariance of identified parameters from the first *i* groups of data, $\boldsymbol{\sigma}_i$ is the variance matrix of measurement errors, and $\mathbf{E}_i$ is the estimation error of the *i*-th group of data. Integration of the prior information regarding the parameters and the information regarding the measurement errors can have the beneficial effect of reduction of variances of parameter estimators. As a result, the parameter

identification could be improved.

Since the Hankel-Toeplitz model is a regression model given the zero initial condition, $\mathbf{E}_i$ was also calculated by using the regression method as

$$\mathbf{E}_{i+1} = y_{pi} - \hat{y}_{pi} \tag{6.18}$$

where y_{pi} is the measurement output of the piezo-actuator driven stage; and $\hat{y}_{pi}$ is the estimation output of the piezo-actuator driven stage calculated through *i*-1 iterations.

6.5.3.4 Model for the 3-DOF Piezo-actuator driven stage

A 3-input-3-output state space model (6.1) is employed for the 3-DOF piezo-actuator drive stage. By implementing the singular value decomposition on the Hankel matrix which is estimated based on the the Hankel-Toeplitz model, as shown in Lemma 6.1, the system matrices of the state space model can be derived.

Since the 3-DOF piezo-actuator driven stage is previously assumed to be linear, the model identification can be implemented on each input channel individually. For example, when an input signal is only provided in one channel $u_i (i = 1,2,3)$, the 3-dimensional output $y_i = [y_{i1} \quad y_{i2} \quad y_{i3}]^T$, can be obtained from the identified one-input-three-output model by applying the method mentioned above

$$\begin{aligned} x_i(k+1) &= A_i x_i(k) + B_i u_i(k) + w_i(k) \\ y_i(k) &= C_i x_i(k) + D_i u_i(k) + v_i(k) \end{aligned} \tag{6.19}$$

where $A_i \in R^{3\times 3}$, $B_i \in R^{3\times 1}$, $C_i \in R^{3\times 3}$ *and* $D_i \in R^{3\times 1}$ are system matrices of the one-input-three-output system.

The states for all three channels in Equation (6.19) may be stacked as

$$\begin{bmatrix} x_1(k+1) \\ x_2(k+1) \\ x_3(k+1) \end{bmatrix} = \begin{bmatrix} A_1 & & \\ & A_2 & \\ & & A_3 \end{bmatrix} \begin{bmatrix} x_1(k) \\ x_2(k) \\ x_3(k) \end{bmatrix} + \begin{bmatrix} B_1 & & \\ & B_2 & \\ & & B_3 \end{bmatrix} \begin{bmatrix} u_1(k) \\ u_2(k) \\ u_3(k) \end{bmatrix} + \begin{bmatrix} w_1(k) & w_2(k) & w_3(k) \end{bmatrix}^T. \quad (6.20)$$

According to the definition of the linear system, the output can be expressed as the sum of $y_i (i = 1,2,3)$, such that

$$y = y_1 + y_2 + y_3 = \begin{bmatrix} C_1 & C_2 & C_3 \end{bmatrix} \begin{bmatrix} x_1(k) \\ x_2(k) \\ x_3(k) \end{bmatrix} + \begin{bmatrix} D_1 & D_2 & D_3 \end{bmatrix} \begin{bmatrix} u_1(k) \\ u_2(k) \\ u_3(k) \end{bmatrix} + v_1(k) + v_2(k) + v_3(k). \quad (6.21)$$

As such, the state space model for the 3-input-3-output system can be expressed as

$$\begin{aligned} x(k+1) &= Ax(k) + Bu(k) + w(k) \\ y(k) &= Cx(k) + Du(k) + v(k) \end{aligned} \quad (6.22)$$

where $A = diag\begin{bmatrix} A_1 & A_2 & A_3 \end{bmatrix}$, $B = diag\begin{bmatrix} B_1 & B_2 & B_3 \end{bmatrix}$, $C = \begin{bmatrix} C_1 & C_2 & C_3 \end{bmatrix}$,

$D = \begin{bmatrix} D_1 & D_2 & D_3 \end{bmatrix}$, $x(k) = \begin{bmatrix} x_1(k) \\ x_2(k) \\ x_3(k) \end{bmatrix}, u(k) = \begin{bmatrix} u_1(k) \\ u_2(k) \\ u_3(k) \end{bmatrix}, w(k) = \begin{bmatrix} w_1(k) \\ w_2(k) \\ w_3(k) \end{bmatrix}$,

$v(k) = v_1(k) + v_2(k) + v_3(k)$.

6.5.4 Experiments and Results

To verify the effectiveness of the state space model and the proposed identification method, experiments were implemented on a commercially-available 3-DOF piezo-actuator driven stage (P-558.TCD, Physik Instrumente), as shown in Figure 6.1a. Driven by four piezoelectric actuators, the P558.TCD can generate linear displacements in the vertical direction *Z*, and rotation around two orthogonal horizontal axes R_x and R_y. Table 6-1 shows the motion range and resolution in each DOF.

For displacement measurements, three capacitive sensors built in the stage are employed. All displacements were measured with a sampling interval of 2 ms in the present study. Both the

actuators and the sensors in the stage are connected to a host computer via a digtital controller (E-761, Physik Instrumente) and controlled by programming in Labview, as shown in Figure 6.1b. During operation, the motion of the four piezoelectric elements must be coordinated to reduce the internal forces generated due to the over actuation, which may cause reduced stiffness and even break or damage the piezo-actuator driven stage. This is realized by a user program interface provided by the manufacturer, which is used to generate the voltage input of each piezoelectric actuator from the user defined reference signal.

Table 6- 1 Motion range and resolution in each DOF

DOF	Z	R_x	R_y
Motion range	50 μm	±250 μrad	±250 μrad
Resolution	0.5 nm	50 nrad	50 nrad

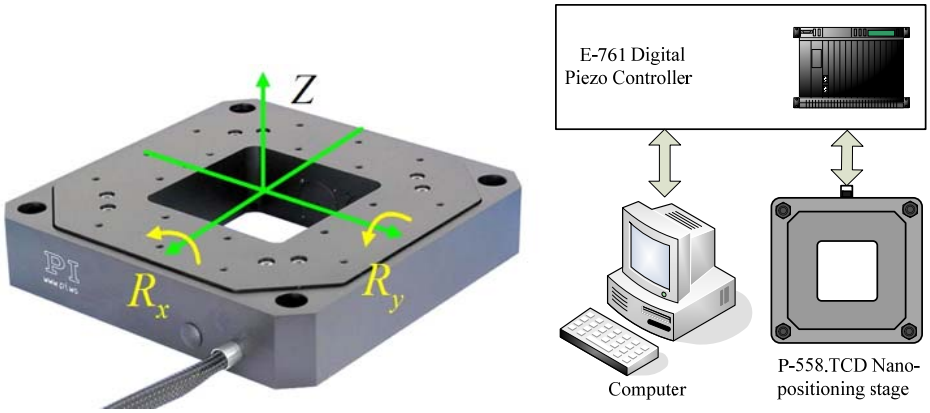

(a) (b)

Figure 6. 1 Experimental settings on the piezo-actuator driven stage
(a) picture and (b) schematic.

6.5.4.1 Linearity of the 3-DOF piezo-actuator driven stage

Examine the linearity of the 3-DOF piezo-actuator driven stage, a case study was conducted

prior to the system identification.

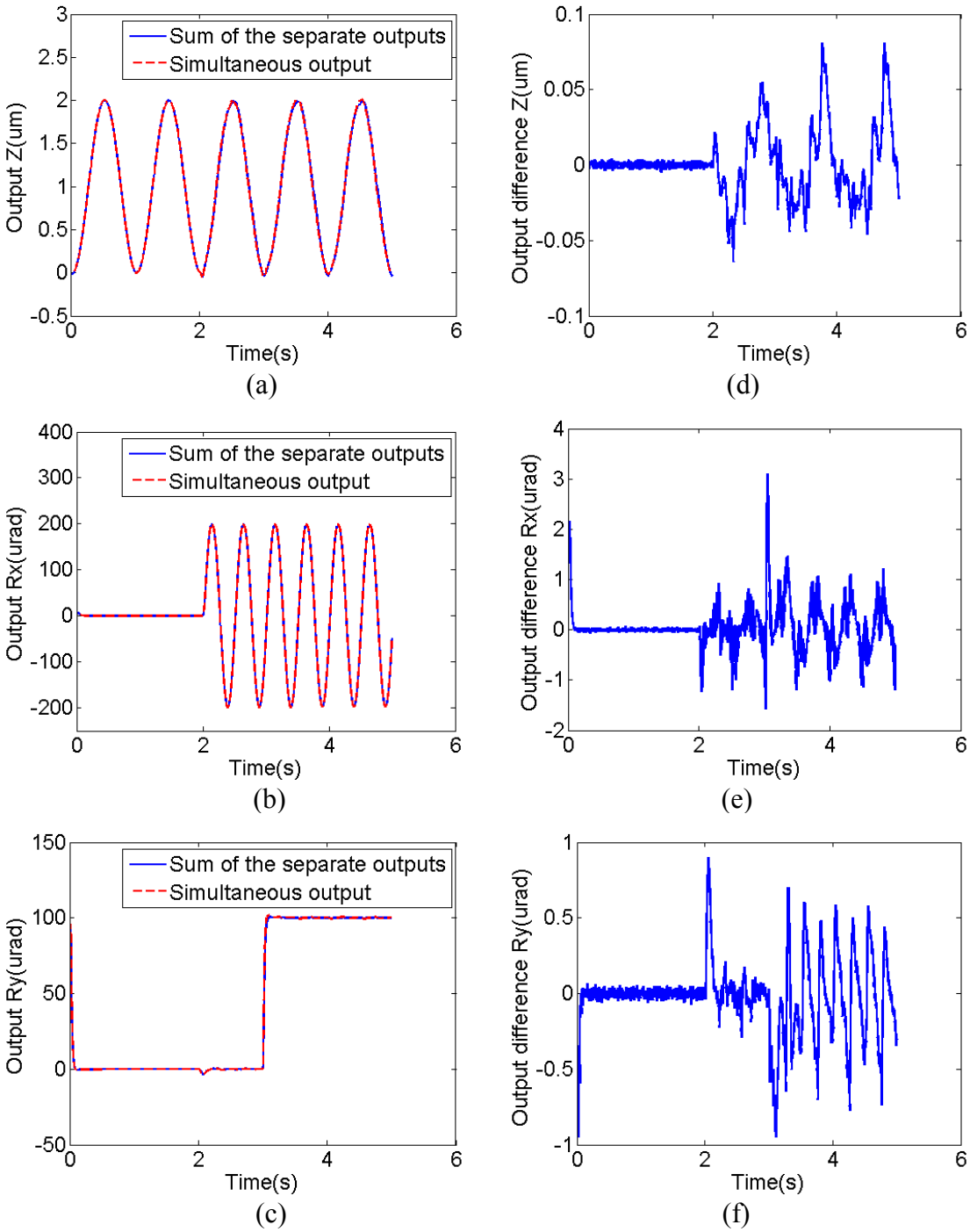

Figure 6. 2 Linearity of the 3-DOF piezo-actuator driven stage
(a-c) comparison between the measured output when the three inputs were provided to the different channels simultaneously and the sum of the outputs when the three inputs were provided separately; (d-f) difference between these two outputs

In particular, a 1 Hz 1 μm sinusoidal reference signal with 1 μm offset, a 2 Hz 200 μm sinusoidal reference signal with 2 s time delay and a 100 μm step reference signal with 3 s time delay were provided to the Z, R_x and R_y channel, respectively, and the corresponding outputs were measured. Then, the stage displacement output as these three signals were applied simultaneously was measured. The criterion used for the linearity examination is that, if the output with three input signals equals or approximately equals to the sum of the outputs when the signals is applied individually, the 3-DOF piezo-actuator driven stage is linear or can be approximately considered to be linear. Figure 6.2 shows the comparison between the two outputs mentioned above.

It can be seen that they overlapped with each other, indicating that the stage can be approximately considered to be a linear system. Differences between the measured output when the three inputs were provided to the different channels simultaneously and the sum of the outputs when the three inputs were provided separately exist. For example, in R_x direction, the maximum difference is approximately 3 μm which is only 1.5% of the amplitude of the reference signal. This difference might be due to the nonlinearities of the 3-DOF piezo-actuator driven stage, which is ignored in the model development presented in this paper.

6.5.4.2 System identification for the 3-DOF piezo-actuator driven stage

Figure 6.3 shows the flow chart of system identification. Since different signals applied in system identification may lead to the difference in the model identified, the effects of applying the random signal and the chirp signal in the parameter estimation were investigated in the signal selection in this study. The two signals were compared and the one with less model prediction error was employed as the input for order selection, in which state space models with different

orders were identified and compared. The one with less model prediction error was employed as the model for the piezo-actuator driven stage.

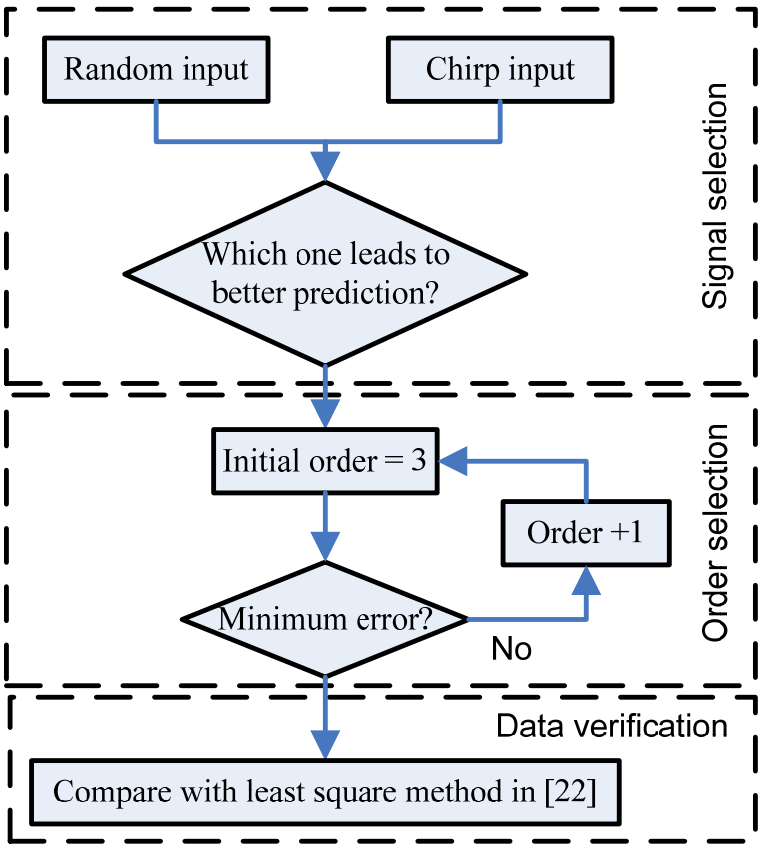

Figure 6. 3 Flow chart of black box system identification

For signal selection, a 20 μm reference chirp signal with 20 μm offset and frequency ranging from 1 to 100 Hz was provided to Channel 1 (Reference Z channel) and the corresponding output in each channel was measured. Based on the empirical knowledge of our previous study on piezoelectric actuators, the order of the state space model was originally set to be 3, and $\boldsymbol{\theta}_0$ in Equation (6.17) was set to be a zero matrix. Since the covariance of the parameters is unknown, $\mathbf{P}_0$ is set to be a diagonal matrix with big covariance designated in the diagonal elements. By

applying online estimation with the identified Hankel matrix, the system matrices of the state space model (Equation (6.19), i=1) were obtained.

The estimation error varied, depending on the values of parameter p in Equation (6.2). Figure 6.4 (a)-(c) shows the estimated error versus the p value. It can be seen that if p=8, the estimation errors in all three output directions approached or reached their individual minimum values. Therefore, it is reasonable to set p=8 as the chirp signal is provided to Channel 1.

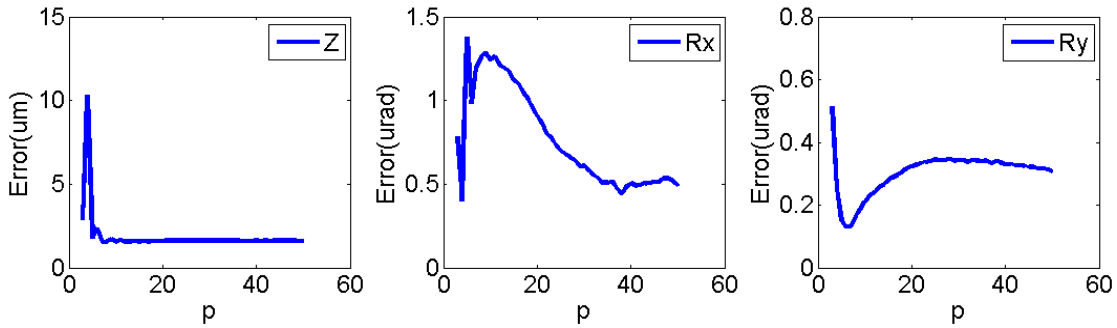

(a) (b) (c)

Figure 6. 4 Estimation error changes with p when reference input was applied in Channel 1 (a) Z direction, (b) Rx direction, (c) Ry direction.

For other two channels, a 200 μrad reference chirp signal with frequency ranging from 1 to 100 Hz was applied. By employing the aforementioned procedure, p was set to 25 and 27 for Channel 2 and 3 respectively. Table 6-2 shows the prediction error in each direction as a 1 Hz sinusoidal reference input was applied to the three channels, respectively. The prediction errors are calculated in terms of the 2-norm of the error vector (Defined as the difference between the measurement and the model prediction). It is seen that the diagonal prediction error is 0.1944 μm, 4.864 μrad and 4.3387 μrad in Z, R_x and R_y direction respectively, which is 0.49%, 2.43% and 2.16% of the desired movement in the individual direction.

Similar to the use of the chirp signal, 40 μm and 200 μrad reference random signals were also

applied to each channel, respectively. The order of each sub-model was chosen to be 3 and p was set to 9, 14 and 13 for the three channels, respectively. The same 1 Hz sinusoidal inputs were provided to difference channels and the output was measured and compared with the model prediction. Table 6-3 illustrate the model prediction error.

Table 6- 2 Model prediction error if chirp inputs were applied

Direction	Z (μm)	R_x (μrad)	R_y (μrad)
1 Hz 20 μm sinusoidal inputs with 20 μm offset in Channel 1	0.1944	0.4030	0.2008
1 Hz 200 μrad sinusoidal inputs in Channel 2	0.0192	4.8640	0.0760
1 Hz 200 μrad sinusoidal inputs in Channel 3	0.0263	0.2060	4.3387

Table 6- 3 Model prediction error if random inputs were applied

Direction	Z (μm)	R_x (μrad)	R_y (μrad)
1 Hz 20 μm sinusoidal inputs with 20 μm offset in Channel 1	0.8670	0.8946	0.2061
1 Hz 200 μrad sinusoidal inputs in Channel 2	0.0542	57.362	0.1020
1 Hz 200 μrad sinusoidal inputs in Channel 3	0.0624	1.0143	45.9597

In contrast to the chirp signal, it can be concluded that the model prediction errors is much bigger when random signals are used in the model identification. For example, when a 1 Hz 200 μrad sinusoidal reference input was provided to Channel 2, the model prediction error in R_x direction reached 57.362 μrad by using the random inputs, which is over 10 times larger than that derived by using the chirp signal. As a result, a chirp signal was employed as the reference input for model identification below.

To determine the order of the state space model, the parameter identification, as described

previously, was repeated with varying values of n (Equation (6.1)) in each channel. Tables 6-4~6-6 show the estimation errors in each channel. Parameter p was chosen to have different values for varying orders based on the method mentioned above. It can be concluded that if the chirp signal was used in Channel 1, the estimation error in the Z direction reached its minimum value of 1.4906 μm with the order of the sub-model being 6 or 7. For the R_y direction, the optimal choice was to set n = 7. Therefore, the sub-model for Channel 1 was considered to be a 7-th order state space system. The system matrices were determined as given in Equation (6.23). Using a similar procedure, the orders of the sub-model for the other two channels were both chosen to be 4 and the system matrices were determined as shown in Equations (6.24) and (6.25).

Table 6- 4 Estimation error from the chirp input in channel 1

Order	p	Estimation error		
		Z (μm)	R_x (μrad)	R_y (μrad)
2	11	1.5635	1.1174	0.1614
3	8	1.5368	1.2597	0.1631
4	11	1.4936	0.8100	0.3496
5	14	1.4914	0.1876	0.1607
6	31	1.4906	0.1184	0.1238
7	38	1.4906	0.1192	0.0908
8	38	1.4907	0.1180	0.1099
9	38	1.4907	0.1202	0.1031
10	30	1.4912	0.1195	0.1251
11	30	1.4913	0.1186	0.1236
12	28	1.4912	0.1266	0.1180

Table 6- 5 Estimation error from the chirp input in channel 2

Order	p	Estimation error		
		Z (μm)	R_x (μrad)	R_y (μrad)
2	47	0.0118	18.0440	0.0565
3	25	0.0106	17.8752	0.0474
4	42	0.0107	17.7877	0.0476
5	47	0.0128	17.7751	0.0483
6	42	0.0129	17.8071	0.0477
7	42	0.0125	17.8073	0.0480
8	47	0.0133	17.8073	0.0477
9	42	0.0118	17.8179	0.0484
10	39	0.0103	17.8363	0.0479
11	42	0.0120	17.8154	0.0475
12	42	0.0119	17.8166	0.0481

Table 6- 6 Estimation error from the chirp input in channel 3

Order	p	Estimation error		
		Z (μm)	R_x (μrad)	R_y (μrad)
2	41	0.0124	1.0996	16.9180
3	27	0.0108	1.0995	16.7524
4	39	0.0111	1.0994	16.5991
5	41	0.0144	1.1006	16.5917
6	39	0.0109	1.0993	16.6212
7	39	0.0111	1.0996	16.6183
8	39	0.0112	1.0996	16.6183
9	39	0.0112	1.0996	16.6177
10	39	0.0111	1.0996	16.6188
11	39	0.0111	1.0993	16.6184
12	39	0.0111	1.0994	16.1686

$$A_1=\begin{bmatrix} 0.9239 & -0.1747 & 0.0057 & -0.0297 & -0.0026 & -0.0045 & -0.0004 \\ 0.1757 & 0.6973 & 0.0604 & -0.2463 & -0.0262 & -0.0333 & -0.0031 \\ 0.0219 & -0.1592 & 0.8761 & -0.0622 & -0.0504 & -0.0266 & 0.011 \\ -0.0291 & 0.2297 & 0.4 & 0.4512 & -0.1 & 0.1691 & 0.0169 \\ -0.0101 & 0.0321 & 0.095 & -0.1506 & 0.9447 & 0.1266 & 0.0155 \\ -0.0068 & 0.0231 & 0.0439 & -0.3232 & -0.1645 & 0.6283 & -0.0277 \\ -0.0044 & 0.0093 & 0.116 & -0.085 & 0.00008 & -0.1766 & 0.8136 \end{bmatrix}, B_1=\begin{bmatrix} 0.3094 \\ -0.2819 \\ -0.0608 \\ 0.0912 \\ 0.0185 \\ 0.0199 \\ 0.0061 \end{bmatrix}$$

$$C_1=\begin{bmatrix} 0.3052 & 0.2798 & -0.0221 & 0.0891 & 0.0073 & 0.0153 & 0.0018 \\ 0.0134 & 0.0259 & 0.0453 & 0.0533 & 0.0381 & -0.0397 & -0.0108 \\ 0.0033 & -0.0215 & 0.0189 & -0.0416 & -0.0061 & 0.0375 & -0.0039 \end{bmatrix}, D_1=\mathbf{0}_{3\times 3} \tag{6.23}$$

$$A_2=\begin{bmatrix} 0.9493 & 0.1175 & 0.0173 & 0.0233 \\ -0.1161 & 0.7929 & -0.1205 & -0.1509 \\ -0.0001 & 0.072 & 0.9273 & -0.2011 \\ 0.0238 & 0.1573 & 0.0285 & 0.7314 \end{bmatrix}, B_2=\begin{bmatrix} 0.2595 \\ 0.2232 \\ -0.0325 \\ -0.0693 \end{bmatrix},$$

$$C_2=\begin{bmatrix} -0.00002 & -0.00001 & -0.00002 & -0.00024 \\ 0.2402 & -0.2215 & -0.0502 & -0.0687 \\ -0.0002 & -0.00053 & -0.00049 & -0.0011 \end{bmatrix}, D_2=\mathbf{0}_{3\times 3} \tag{6.24}$$

$$A_3=\begin{bmatrix} 0.9485 & 0.1204 & -0.0134 & 0.0261 \\ -0.1184 & 0.7981 & 0.0779 & -0.1711 \\ 0.003 & -0.0094 & 0.9656 & 0.1719 \\ 0.0225 & 0.1825 & -0.0783 & 0.711 \end{bmatrix}, B_3=\begin{bmatrix} -0.2574 \\ -0.2229 \\ -0.015 \\ 0.0775 \end{bmatrix},$$

$$C_3=\begin{bmatrix} -0.00002 & -0.00001 & -0.0001 & -0.00022 \\ 0.0043 & -0.0018 & -0.0031 & -0.0028 \\ -0.239 & 0.2205 & -0.0376 & 0.0762 \end{bmatrix}, D_2=\mathbf{0}_{3\times 3} \tag{6.25}$$

6.5.4.3 Model verification for the 3-DOF piezo-actuator driven stage

To illustrate the effectiveness of the MAP online estimation method, 1, 5 and 10 Hz sinusoidal reference inputs were provided to different channels, respectively. As comparison, the estimation method introduced in [22] was implemented, as well. The parameter p was defined as 21, 4 and 7 for the different input channels. Table 6-7 and Table 6-8 show the prediction error in each direction based on the different identification methods. The prediction errors were calculated in terms of the 2-norm of the error vector. It can be concluded that the prediction error

increases with the frequency.

Table 6- 7 Estimation error by applying the online estimation method

Input	Channel	Z (μm)	R_x (μrad)	R_y (μrad)
1 Hz 10 μm	1	0.1468	0.1584	0.0642
1 Hz 200 μrad	2	0.0176	1.0305	0.0742
1 Hz 200 μrad	3	0.0196	0.2574	9.9402
5 Hz 10 μm	1	0.3666	0.3743	0.0956
5 Hz 200 μrad	2	0.0538	2.3801	0.2044
5 Hz 200 μrad	3	0.0510	0.2128	3.1906
10 Hz 10 μm	1	0.5296	0.2699	0.0576
10 Hz 200 μrad	2	0.0530	6.3244	0.3327
10 Hz 200 μrad	3	0.0517	1.1101	5.6707

Table 6- 8 Estimation error by applying the identification method introduced in [16]

Input	Channel	Z (μm)	R_x (μrad)	R_y (μrad)
1 Hz 10 μm	1	1.1124	0.9433	0.3675
1 Hz 200 μrad	2	0.0180	2.2639	0.3403
1 Hz 200 μrad	3	0.0374	0.3065	5.3670
5 Hz 10 μm	1	5.0639	0.9224	0.3974
5 Hz 200 μrad	2	0.0541	4.5928	0.3567
5 Hz 200 μrad	3	0.0608	0.6449	11.349
10 Hz 10 μm	1	6.2860	0.9419	0.4139
10 Hz 200 μrad	2	0.0525	17.785	0.2683
10 Hz 200 μrad	3	0.0543	1.0064	13.497

In contrast to the identification method introduced in [22], the use of posteriori parameter information in MAP online estimation leads to better estimations on the Hankel matrix. For

example, the estimation errors for the 5 Hz, 10 μm sinusoidal inputs to Channel 1 were 0.3666 μm, 0.3843 μrad and 0.0956 in the Z, R_x, and R_y directions, respectively. These results are 7.3%, 40.6% and 24%, respectively of those derived using the identification method introduced in [22].

Figure 6.5 shows the output in each direction as a result of a 10 μm 10 Hz sinusoidal reference input with 10 μm offset in Z direction compared with the model prediction. It can be clearly seen that the identified state space model is able to describe the coupling effect between each axle.

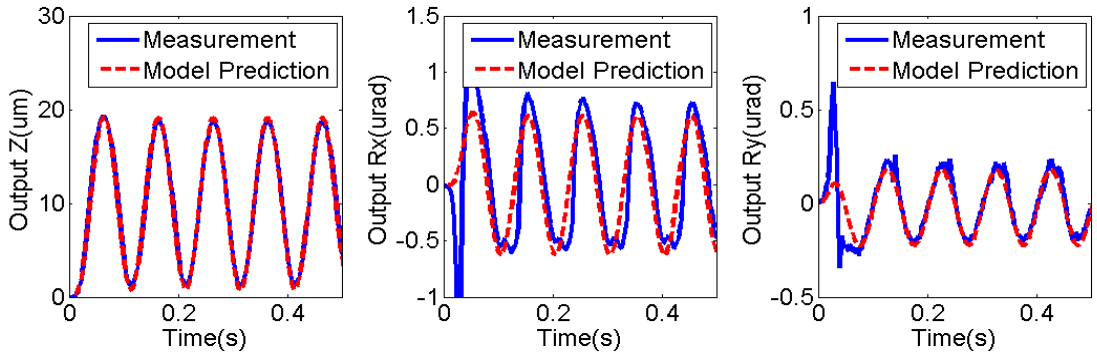

(a) (b) (c)

Figure 6. 5 Comparison of experimental results and model prediction under 10 um 10 Hz sinusoidal input in Channel 1
(a) Z direction; (b) Rx direction; (c) Ry direction

To verify the identified linear state space model three experiments were implemented. In the first experiment, the reference inputs simultaneously applied to the three channels are a 1 Hz and 20 μm sinusoidal reference with 20 μm offset, a 2 Hz and 200 μrad sinusoidal reference with a time delay of 2 seconds, and a 100 μrad step input with a time delay of 3 seconds. The outputs in the three directions were measured and the predicted outputs were obtained according to the identified state space model of Equations (6.23)-(6.25), respectively. In the second experiment, a

1 Hz and 1 μm sinusoidal input with 1 μm offset and a 2 Hz, 0.5 μrad sinusoidal reference input with a 2 s time delay were provided to the piezo-actuator driven stage. The outputs were measured and compared to the predicted outputs.

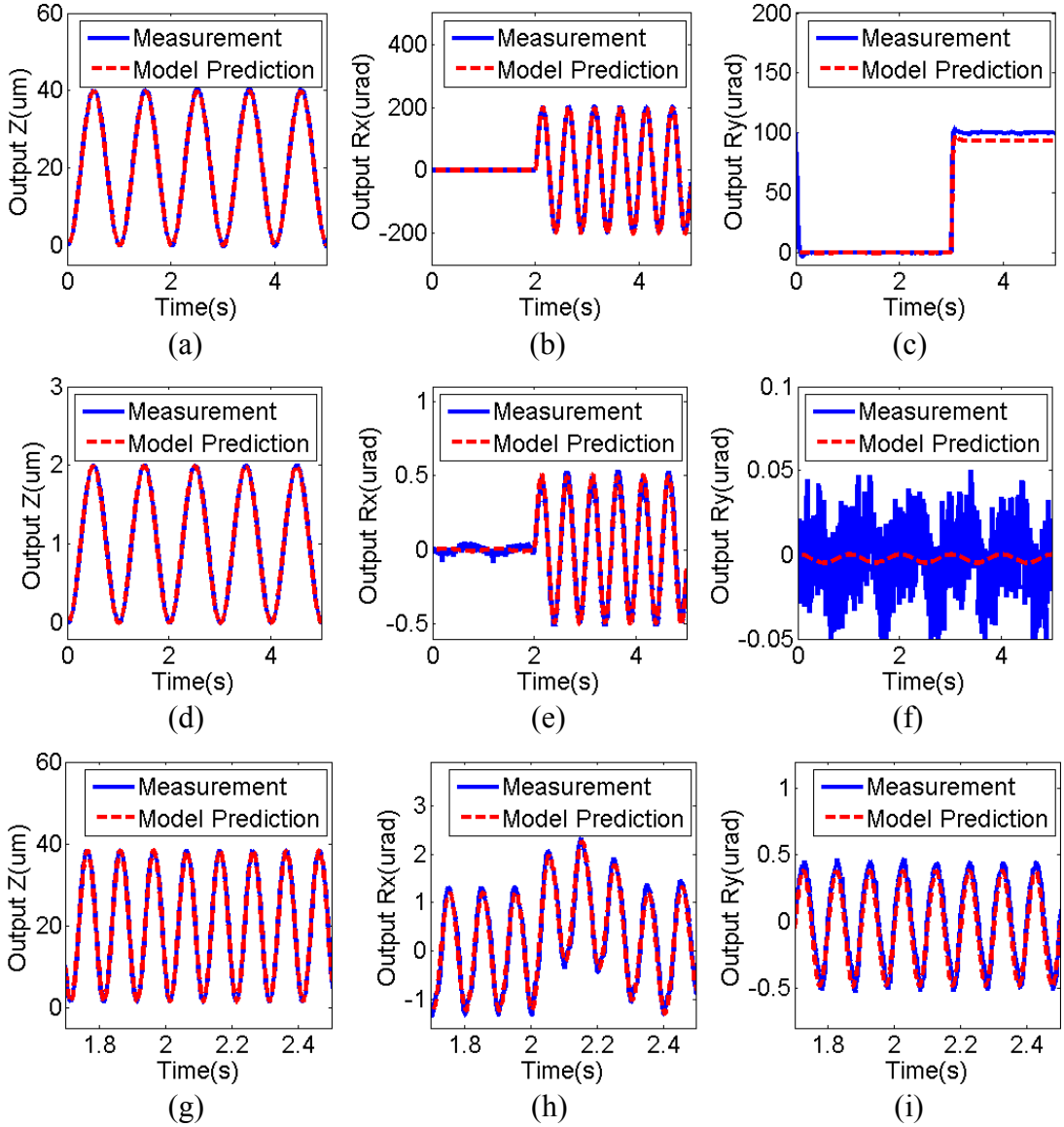

Figure 6. 6 Comparison of experimental results and model prediction from combined inputs to all three channels
in the first experiment (a)-(c); in the second experiments (d)-(f) and in the third experiments (g)-(i).

To validate the model in high frequency, the input of 1 Hz and 2 μm sinusoid in channel 1 was replaced with a 10 Hz 40 μm one in the third experiment. Also, the corresponding outputs in the three directions were measured and compared to the outputs predicted by the identified state space model. The comparison is shown in Figure 6.6, from which it can be concluded that the model is able to describe the performance (both dynamics and cross-coupling effect) of the 3-DOF piezo-actuator driven stage.

6.5.5 Conclusions and Discussions

A straightforward modeling method for multi-DOF piezo-actuator driven stages can be based on the internal configuration by means of physics laws, as mentioned in the literatures. However, such details with regard to the internal structure are often not provided by the manufactures. Therefore, system identification for multi-DOF piezo-actuator driven stages with unknown configuration is always required for the model development.

The contribution of this paper is the development of a black box model used to describe the dynamics of 3-DOF piezo-actuator driven stages with unknown physical configuration, which allows the investigation of the complex system performance with unknown physical configuration by means of the linear state space model. By combining the MAP online estimation methods, the Hankel matrix of the state space model was identified and the model parameters were updated as new observation is available. To show the effectiveness of the proposed estimation method, model verification experiments were carried out on the piezo-actuator driven stage and the outputs obtained were compared to the predictions of the state space model identified using the method introduced in [22]. From the model verification results, it was shown that the linear state space model can predict the dynamic performance of a piezo-actuator driven stage with improved accuracy. Since MAP estimation utilizes the posteriori

parameter information which have the beneficial effect of reduction of variances of parameter estimators, MAP online estimation method performs better in the model identification than the least squares method. Moreover, the identified parameters are updated online if more data is available for the model identification. This provides a starting point from which to adaptively compensate for the dynamics and cross-coupling effects of the piezo-actuator driven stage by means of the mode-based control scheme.

6.5.6 Acknowledgment

Support for the present study from the China Scholarship Council (CSC) and the Natural Sciences and Engineering Research Council (NSERC) of Canada is acknowledged.

7 Discrete Sliding Mode Control for Multi-DOF Piezoelectric Actuators

This chapter presents the work that is included in the following manuscript appended.

Y. Cao and X. B. Chen, "An Output Tracking based Discrete PID-Sliding Mode Control on MIMO systems," *IEEE/ASME Transactions on Mechatroics*, 2013, under review, manuscript ID: TMECH-02-2013-2834.

7.1 Introduction and Objectives

General SMC design, including the PID-based SMC developed recently, is essentially a state tracking control scheme. In some circumstances, it is impossible or prohibitively expensive to obtain all of the required states due to the system complexity. In such cases, the application of the general SMC design method is challenged.

The application of the PID-based SMC can be extended to the control of multi-inputs-multi-output (MIMO) system with one PID-based SMC designed for each pair of input and output independently. However, adjusting controller parameters of one loop affects the performance of another, sometimes even to the extent of destabilizing the entire system. The cross-coupling effects caused by the multivariable interactions accounts for essential difference in design methodologies between single variable and multi-variable control systems, for example, the cross-coupling effects between variables might affect the calculation of the equivalent control, leading to dynamic coupling. The objective of this paper is to extend the application of the output tracking integrated discrete PID-SMC developed in Chapter 4 to the control of MIMO

systems.

7.2 Methods

The application of the discrete PID-based SMC developed in Chapter 4 can be extended to the control of MIMO systems by applying static decoupling in the calculation of the equivalent control. The remaining dynamic decoupling is considered to be disturbance which will be rejected by the PID-based DSMC. By applying the model reference approach, the output tracking problem is transferred to the state tracking problem so that the general SMC design can be applied. Due to the ingenious design of the sliding surface, the coupling effect between variables can be reduced to an acceptable extent.

7.3 Results

By applying the PID based regulator instead of the 'bang-bang' switching control, chattering and the zigzag state motion of the DSMC were eliminated and zero steady state error can be achieved. The verification experiments carried on a commercially available three-DOF PEA showed that the output tracking based discrete PID-SMC as designed by the model reference approach can achieve better tracking performance compared with the nominal PID controller. As the input frequency increases, the advantage of using the discrete PID-based SMC becomes more profound.

7.4 Contributions

The contribution of this work was the development of the discrete output tracking based PID-SMC for MIMO system without measurable model states.

7.5 Paper: An Output Tracking based Discrete PID-Sliding Mode Control on MIMO Systems

Authors: Y. Cao and X. B. Chen, *Member, IEEE* [6]

Index Terms: Control System, Nanotechnology, Piezoelectric devices

7.5.1 Abstract

Sliding mode control (SMC) has been widely employed for control applications in the presence of uncertainty and disturbance due to its ability to reject the disturbance. However, the chattering problem, caused by the discontinuous characteristic of the switching function, greatly deteriorates the performance of SMC and has become the main limitation for its application. Implementing the SMC in black box multi-input-multi-output (MIMO) systems is difficult because of state tracking and coupling effects between the control variables. This paper presents an output tracking based discrete proportional-integral-derivative based SMC (PID-SMC) for a

Manuscript received Febuary 16, 2013. This work was supported by the China Scholarship Council (CSC) and the Natural Science and Engineering Research Council (NSERC) of Canada.

Y. Cao is with the Department of Mechanical Engineering, 57 Campus Drive, University of Saskatchewan, Saskatoon, SK, S7N 5A9 (e-mail: yuc150@ mail.usask.ca).

X. B. Chen is with the Department of Mechanical Engineering, 57 Campus Drive, University of Saskatchewan, Saskatoon, SK, S7N 5A9 (phone: 1-306-966-1267; e-mail: xbc719@ mail.usask.ca).

MIMO system. Using the model reference approach, the output tracking problem is transferred to a sub-state tracking problem on which the general SMC design can apply. Zero steady state error is achieved with the proposed method and the chattering problem is eliminated. To demonstrate the effectiveness of the proposed method, experiments were performed on a commercially available three degrees-of-freedom (DOF) nano-positioning stage as compared to a proportional-integral- derivative (PID) controller.

7.5.2 Introduction

A typical multi-variable system, such as a multiple DOF robot or a temperature and humidity control system, will have several variables that must be controlled [142]. If there is more than one input and the outputs are the controlled variables, the multi-variable system is known as a MIMO system. One of the most important characteristic of a MIMO system is the cross-coupling effect or interaction between variables. For example, one input variable can lead to outputs of all variables. It is common to control each input/output pair separately without considering the coupling effects between variables. However, coupling greatly degrades the performance of the controller in many systems, in particular, parallel mechanics and chemical engineering systems with significant interactions [105]. Since the pioneering research of the early sixties [106], control of MIMO systems has received more and more attention not only in the control research area but also in industry. Generally, controllers for single-input-signal-output (SISO) systems cannot be extended to MIMO systems due to the cross-coupling effect in MIMO systems [107]. Therefore, new controllers must be designed

considering the coupling effect that exists in a MIMO system [108]-[111].

Most decoupled controller design relies on the plant model and is very sensitive to parameter uncertainties. Thus, the emphasis for controller design of MIMO systems should be robust and stable design techniques which can achieve specified decoupling effects under plant uncertainties [142]. In recent decades, SMC, as a form of variable structure control, has drawn considerable attention in the control research community worldwide [84], [92]-[94], [141], [151]-[154] due to its robustness in the presence of system uncertainties and disturbances. However, because of the discontinuous switching control, the states of the actual system are, in fact, switching around the sliding surface rather than staying on it. The switching can occur with high frequency, referred to as chattering. This excites an undesired system high resonance mode which deteriorates the system tracking performance. One solution to the chattering problem is the use of boundary layer control [94], in which a saturation switching control replaces the discontinuous switching control. It is noted that if the unknown disturbance is significant, a sufficiently-high gain in the controller is required and such a control scheme behaves like a high-gain proportional (P) controller. As a result, steady state error may exist. An alternative method for solving the chattering problem is to enlarge the width of the boundary layer and reduce the effective linear gain in order to reduce the state oscillation around the sliding surface. However, the state can no longer strictly locate on the ideal sliding surface due to the wider boundary layer and the system will never behave as described by the sliding mode. Some examples of applying sliding mode controllers to MIMO systems in which the chattering problem was not well solved may be seen in [155]-[157]. In [95], a high order sliding surface was used to replace the first order one

typically used in the nominal SMC design. With the main advantages of the nominal SMC, the high order sliding mode control (HOSMC) can reduce the chattering effect and improve the accuracy for its realization. The main problem is that it requires increasing sliding information in implementing the HOSMC [97].

Recently, a new PID-based SMC was developed [141] in which the discontinuous 'bang-bang' switching function was replaced by a PID regulator to eliminate the chattering problem. Due to the integral effect of the PID regulator, zero steady state error can be achieved in the tracking performance of the plant. The PID-SMC was implemented in the tracking control of a commercially available piezoelectric actuator (PEA) at a 20000 Hz sampling rate, the results of which showed that under the 50 Hz sinusoidal input reference signal the tracking error was reduced by 30% compared to the traditional PID controller.

General SMC design [93], including the PID-SMC developed in [141], is actually a state tracking control scheme. In some circumstances, the system state might not be readily or even be impossibly obtained due to system complexity [104]. In such case, the application of the existing PID-SMC in the control of MIMO systems is challenged due to the lack of system state information. In addition, when implemented in a digital computer, the existing continuous SMC might not work as expected due to quantization error made by data sampling. For discrete SMC, if the switching time doesn't match the sampling time, the state will not stay on the sliding surface and the trajectory appears like a zigzag motion around the sliding surface, which indicates that the sampling itself also induces the chattering in the discrete SMC. Moreover, if the mean of zigzag motion deviates from the sliding surface, steady state error will exist [100],

[101], [131]. Therefore, the output tracking based forms of discrete SMC are desirable to alleviate the aforementioned problems in the control of MIMO systems.

In this study, an output tracking based discrete PID-SMC is developed for the MIMO system. Static decoupling is applied in the equivalent control. The remaining dynamic decoupling is considered as a disturbance which will be rejected by the PID regulator. By applying the model reference approach, the output tracking problem is transferred to the state tracking problem so that the general SMC design can be applied, so called a novel sub-SMC design in this study. Due to the ingenious design of the SMC, the coupling effect between variables can be reduced to an acceptable extent. The first part of this paper focuses on the development of the output tracking based discrete PID-SMC for the MIMO systems based on the model reference approach. To verify the effectiveness of the proposed discrete PID-SMC, experiments were carried out on a commercially available nano-positioning stage which was identified as black box state space model. The results achieved using the proposed design approaches were compared to the traditional PID controller.

7.5.3 Output Tracking based Discrete PID-SMC for MIMO systems

7.5.3.1 Problem statement

Consider a system expressed by the discrete state space model

$$X(k+1) = AX(k) + BU(k) + W(k), Y(k) = CX(k) \tag{7.1}$$

where $X(k) \in R^{n\times 1}$ is the state; $W(k) \in R^{n\times 1}$ is the uncertainty; $U(k) \in R^{q\times 1}$ is the q

dimensional control input signal; $Y(k) \in R^{l\times 1}$ is the l dimensional system output signal; and $A \in R^{n\times n}$, $B \in R^{n\times q}$ and $C \in R^{l\times q}$ are the system matrices. For convenience, only square systems are considered in this study, thus $q = l$ and assume that $n/q = p \in \{\theta \mid \theta \in Z, \theta \geq 1\}$. By applying Lemma 7.1, Equation (7.1) can be transferred to the state space model of the controllable canonical nominal form

$$x(k+1) = A_d x(k) + B_d u(k) + \varepsilon(k), y(k) = C_d x(k) \tag{7.2}$$

where $A_d = FAF^{-1}, B_d = FB, \varepsilon(k) = FW(k), C_d = CF^{-1}$.

Lemma 7.1: If system (A, B, C) is controllable, then matrix A can be transformed into its controllable canonical form by linear transform such that

$$x = FX \tag{7.3}$$

where

$$F = \left[C;\quad CA;\quad CA^2;\quad \cdots;\quad CA^{p-1}\right] \in R^{n\times n} \tag{7.4}$$

Prove: See the appendix.

Let the desired state space model be

$$w(k+1) = A_m w(k) + B_m r(k), y_d(k) = C_m w(k) \tag{7.5}$$

where $w(k) \in R^{m\times 1}$ is the state; $r(k) \in R^{q\times 1}$ is the reference input signal; $y_d(k) \in R^{q\times 1}$ is the output of the reference system; and $A_m \in R^{m\times m}$, $B_m \in R^{m\times q}$ and $C_m \in R^{q\times m}$ are the system matrices of the reference state space model.

Define the tracking error as

$$e(k) = y(k) - y_d(k) = C_d x(k) - C_m w(k) \tag{7.6}$$

The aim of the output tracking based SMC is to force the output of the actual system to follow

the output of the reference system, which indicates $e(k) = 0$.

7.5.3.2 Controller design

By iteration and denoting

$$\delta(k+p-1) = [e^T(k), e^T(k+1), \cdots, e^T(k+p-1)]^T \tag{7.7}$$

Equation (7.6) yields

$$\begin{aligned}\delta(k+p-1) = {} & A_c x(k) + B_{c0}u(k) + \cdots + B_{c(p-2)}u(k+p-2) - A_{cm}w(k) - B_{cm0}r(k) \\ & - \cdots - B_{cm(p-2)}r(k+p-2) + E_{c0}\varepsilon(k) + E_{c1}\varepsilon(k+1) + \cdots + E_{c(p-2)}\varepsilon(k+p-2)\end{aligned} \tag{7.8}$$

where

$$A_c = \begin{bmatrix} C_d \\ C_d A_d \\ C_d {A_d}^2 \\ \vdots \\ C_d {A_d}^{p-1} \end{bmatrix}, B_{c0} = \begin{bmatrix} 0 \\ C_d B_d \\ C_d A_d B_d \\ \vdots \\ C_d {A_d}^{p-2} B_d \end{bmatrix}, B_{c1} = \begin{bmatrix} 0 \\ 0 \\ C_d B_d \\ \vdots \\ C_d {A_d}^{p-3} B_d \end{bmatrix}, \cdots, B_{c(p-2)} = \begin{bmatrix} 0 \\ 0 \\ 0 \\ \vdots \\ C_d B_d \end{bmatrix}, A_{cm} = \begin{bmatrix} C_m \\ C_m A_m \\ C_m {A_m}^2 \\ \vdots \\ C_m {A_m}^{p-1} \end{bmatrix},$$

$$B_{cm0} = \begin{bmatrix} 0 \\ C_m B_m \\ C_m A_m B_m \\ \vdots \\ C_m {A_m}^{p-2} B_m \end{bmatrix}, B_{cm1} = \begin{bmatrix} 0 \\ 0 \\ C_m B_m \\ \vdots \\ C_m {A_m}^{p-3} B_m \end{bmatrix}, \cdots, B_{cm(p-2)} = \begin{bmatrix} 0 \\ 0 \\ 0 \\ \vdots \\ C_m B_m \end{bmatrix}, E_{c0} = \begin{bmatrix} 0 \\ C_d \\ C_d A_d \\ \vdots \\ C_d {A_d}^{p-2} \end{bmatrix}, \cdots,$$

$E_{c(p-2)} = \begin{bmatrix} 0 & 0 & 0 & \cdots & {C_d}^T \end{bmatrix}^T$.

Considering the state space model (7.2), Equation (7.8) becomes

$$\begin{aligned}&\delta(k+p) = A_c A_d x(k) + A_c B_d u(k) + B_{c0}u(k+1) + \cdots + B_{c(p-2)}u(k+p-1) - A_{cm}A_m w(k) - A_{cm}B_m r(k) \\ &- B_{cm0}r(k+1) - \cdots - B_{cm(p-2)}r(k+p-1) + A_c\varepsilon(k) + E_{c0}\varepsilon(k+1) + E_{c1}\varepsilon(k+2) + \cdots + E_{c(p-2)}\varepsilon(k+p-1)\end{aligned} \tag{7.9}$$

Since $A_c \in R^{n\times n}$, if $|A_c| \neq 0$, then Equation (7.8) can be solved for $x(k)$ such that

$$\begin{aligned}x(k) = {} & A_c^{-1}[\delta(k+p-1) - B_{c0}u(k) - B_{c1}u(k+1) - \cdots - B_{c(p-2)}u(k+p-2) + A_{cm}w(k) + B_{cm0}r(k) \\ & + B_{cm1}r(k+1) + \cdots + B_{cm(p-2)}r(k+p-2) - E_{c0}\varepsilon(k) - E_{c1}\varepsilon(k+1) - \cdots - E_{c(p-2)}\varepsilon(k+p-2)]\end{aligned}$$

(7.10)

Prior to further discussions below, it is necessary to list all the notations that will be used in the equations, as shown in Table 7-1.

Table 7- 1 Notations used in the equations

Notation	Equivalent Equation	Notation	Equivalent Equation
A_e	$A_e = A_c A_d A_c^{-1}$	R_2	$R_2 = A_e B_{cm2} - B_{cm1}$
P	$P = A_e A_{cm} - A_{cm} A_m$	⋮	⋮
Γ_0	$\Gamma_0 = A_c B_d - A_e B_{c0}$	R_{p-2}	$R_{p-2} = A_e B_{cm(p-2)} - B_{cm(p-3)}$
Γ_1	$\Gamma_1 = B_{c0} - A_e B_{c1}$	R_{p-1}	$R_{p-1} = -B_{cm(p-2)}$
⋮	⋮	Π_0	$\Pi_0 = A_c - A_e E_{c0}$
Γ_{p-2}	$\Gamma_{p-2} = B_{c(p-3)} - A_e B_{c(p-2)}$	Π_1	$\Pi_1 = E_{c0} - A_e E_{c1}$
R_0	$R_0 = A_e B_{cm0} - A_{cm} B_m$	⋮	⋮
R_1	$R_1 = A_e B_{cm1} - B_{cm0}$	Π_{p-2}	$\Pi_{p-2} = E_{c(p-3)} - A_e E_{c(p-2)}$

Substituting Equation (7.10) into Equation (7.9), the dynamics of the tracking error vector δ is given by

$$\begin{aligned}\delta(k+p) = {} & A_e\delta(k+p-1) + Pw(k) + \Gamma_0 u(k) + \cdots + \Gamma_{p-2}u(k+p-2) + B_{c(p-2)}u(k+p-1) \\ & + R_0 r(k) + \cdots + R_{p-1}r(k+p-1) + \Pi_0\varepsilon(k) + \cdots + \Pi_{p-2}\varepsilon(k+p-2) + E_{c(p-2)}\varepsilon(k+p-1)\end{aligned}$$

(7.11)

Letting $u(k) = u_1(k) + u_2(k)$ and substituting into Equation (7.11), a simplified equation is given by

$$\delta(k+p) = A_e\delta(k+p-1) + Pw(k) + f(u_1) + f(u_2) + \Delta(k) + g(r) \tag{7.12}$$

where $f(u_1) = \Gamma_0 u_1(k) + \cdots + \Gamma_{p-2} u_1(k+p-2) + B_{c(p-2)} u_1(k+p-1)$,

$f(u_2) = \Gamma_0 u_2(k) + \cdots + \Gamma_{p-2} u_2(k+p-2) + B_{c(p-2)} u_2(k+p-1)$,

$g(r) = R_0 r(k) + R_1 r(k+1) + \cdots + R_{p-1} r(k+p-1)$ and $\Delta(r) =$

$\Pi_0\varepsilon(k) + \Pi_1\varepsilon(k+1) + \cdots + \Pi_{p-2}\varepsilon(k+p-2) + E_{c(p-2)}\varepsilon(k+p-1)$. For perfect tracking performance, $\delta(k+p) = 0$. If

$$Pw(k) + f(u_1) + g(r) = 0 \tag{7.13}$$

then Equation (7.12) becomes a nominal SMC problem. Therefore, it is necessary to design u_1 so that Equation (7.13) can be satisfied.

① **Design of u_1**

Lemma 7.2: If A_c is of rank *n*, then A_c can be represented as its controllable canonical form.

$$A_e = \begin{bmatrix} 0_{(p-1)q\times q} & I_{(p-1)q\times(p-1)q} \\ A_0 & \tilde{A}^T \end{bmatrix} \tag{7.14}$$

where $\tilde{A} = \begin{bmatrix} A_1 & A_2 & \cdots & A_{p-1} \end{bmatrix}^T$, $A_0, A_1, \cdots, A_{p-1} \in R^{q\times q}$ are *q* order square matrixes.

Remark 7.1: Lemma 7.2 can be easily proven from Lemma 7.1.

Theorem 7.1: If A_c is of rank *n*, then $P, \Gamma_i (i = 0,1,\cdots,p-2)$, $R_j (j = 0,1,\cdots,p-1), B_{c(p-2)}, \Pi_l (l = 0,1,\cdots,p-2)$ and $E_{c(p-2)}$ are of rank *q*, and their top $(p-1)q$ rows are zero sub-matrices (Proof in the appendix).

Based on Lemma 7.2 and Theorem 7.1, Equation (7.13) can be rewritten as a state space

model

$$\begin{aligned} X_1(k) &= A_{d1}X_1(k) + B_{d1}u_1(k) \\ Y_1(k) &= C_{d1}X_1(k) + D_{d1}u_1(k) \end{aligned} \tag{7.15}$$

where $X_1(k) = \left[u_1{}^T(k) \quad u_1{}^T(k+1) \quad \cdots \quad u_1{}^T(k+p-2) \right]^T$

$Y_1(k) = -P_q w(k) - R_{0q} r(k) - \cdots - R_{(p-1)q} r(k+p-1),$

$$A_{d1} = \begin{bmatrix} 0_{(p-2)q\times q} & I_{(p-2)q\times(p-2)q} \\ 0_{q\times q} & 0_{q\times(p-2)q} \end{bmatrix}, B_{d1} = \begin{bmatrix} 0_{q\times q} \\ \vdots \\ 0_{q\times q} \\ I_{q\times q} \end{bmatrix}, C_{d1} = \begin{bmatrix} \Gamma_0 & \Gamma_1 & \cdots & \Gamma_{p-2} \end{bmatrix}, D_{d1} = B_{c(p-2)}$$

and P_q, R_{0q}, $R_{1q}, \cdots$, $R_{(p-1)q}$ are the last q rows of matrixes P, R_0, $R_1, \cdots$, $R_{(p-1)}$, respectively. The design of u_1 accomplishes the decoupling control of the MIMO system (7.15) where the desired output is

$R_1(k) = -P_q w(k) - R_{0q} r(k) - R_{1q} r(k+1) - \cdots - R_{(p-1)q} r(k+p-1)$ In this study, static decoupling [142] is used in the design of u_1.

Assuming that (A_{d1}, B_{d1}) may be stabilized, the design of a state feedback control

$$u_1(k) = -K_1 X_1(k) + F_1 R_1(k) \tag{7.16}$$

is desired such that the closed-loop discrete transfer function

$$\begin{aligned} T_1(z) &= (C_{d1} - D_{d1}K_1)(zI - A_{d1} + B_{d1}K_1)^{-1} B_{d1}F_1 + D_{d1}F_1 \\ &= [(C_{d1} - D_{d1}K_1)(zI - A_{d1} + B_{d1}K_1)^{-1} B_{d1} + D_{d1}]F_1 \end{aligned} \tag{7.17}$$

has a diagonal and non-singular $T_1(1)$ and the control system is stable.

If such K_1 and F_1 may be found, then

$T_1(0) = [(C_{d1} - D_{d1}K_1)(I - A_{d1} + B_{d1}K_1)^{-1} B_{d1} + D_{d1}]F_1 = I$. Therefore,

$$F_1 = [(C_{d1} - D_{d1}K_1)(I - A_{d1} + B_{d1}K_1)^{-1} B_{d1} + D_{d1}]^{-1} \tag{7.18}$$

as long as K_1 can be found such that $A_{d1} - B_{d1}K_1$ has all its eigenvalues in the unit circle. F_1 is a constant matrix which statically decouples the MIMO system. From Equation (7.17), it may be seen that the term $(C_{d1} - D_{d1}K_1)(zI - A_{d1} + B_{d1}K_1)^{-1}B_{d1}$ determines the dynamic coupling effect of the closed-loop system which can be reduced by the appropriate design of K_1. Denote $\xi(k)$ to be the remaining dynamic coupling effect. Since $P, \Gamma_i (i = 0,1,\cdots, p-2)$, $R_j (j = 0,1,\cdots, p-1)$, $B_{c(p-2)}, \Pi_l (l = 0,1,\cdots, p-2)$ and $E_{c(p-2)}$ are of rank q, $\xi(k)$ is of rank q as well and can be considered to be a matched disturbance which will be rejected by design of u_2.

In this study, the design of K_1 when $p = 3$ will be discussed. Similar design approaches can be employed for other applications.

When $p = 3$, $A_{d1} = \begin{bmatrix} 0_{q\times q} & I_{q\times q} \\ 0_{q\times q} & 0_{q\times q} \end{bmatrix}, B_{d1} = \begin{bmatrix} 0_{q\times q} \\ I_{q\times q} \end{bmatrix}, C_{d1} = \begin{bmatrix} \Gamma_0 & \Gamma_1 \end{bmatrix}, D_{d1} = B_{c1}$. For this specific system, K_1 may be designed as

$$K_1 = \begin{bmatrix} K_{s1} & K_{s1} \end{bmatrix} \tag{7.19}$$

where $K_{s1} \in R^{q\times q}$. Substituting Equation (7.19) into Equation (7.17) and applying matrix transformation gives

$$\begin{aligned}
(C_{d1} - D_{d1}K_1)(zI - A_{d1} + B_{d1}K_1)^{-1}B_{d1} &= \begin{bmatrix} \Gamma_0 - B_{c1}K_{s1} & \Gamma_1 - B_{c1}K_{s1} \end{bmatrix} \begin{bmatrix} zI & -I \\ -K_{s1} & zI - K_{s1} \end{bmatrix}^{-1} \begin{bmatrix} 0 \\ I \end{bmatrix} \\
&= \begin{bmatrix} \Gamma_0 - B_{c1}K_{s1} & \Gamma_1 - B_{c1}K_{s1} \end{bmatrix} \begin{bmatrix} z^{-1}I + z^{-1}(-z^2K_{s1}^{-1} - zI - I)^{-1} & z^{-1}(z^{-1}K_{s1} + K_{s1} + zI)^{-1} \\ (-z^2K_{s1}^{-1} - zI - I)^{-1} & (z^{-1}K_{s1} + K_{s1} + zI)^{-1} \end{bmatrix} \begin{bmatrix} 0 \\ I \end{bmatrix} \\
&= (\Gamma_0 - B_{c1}K_{s1})(K_{s1} + zK_{s1} + z^2I)^{-1} + (\Gamma_1 - B_{c1}K_{s1})(z^{-1}K_{s1} + K_{s1} + zI)^{-1}
\end{aligned} \tag{7.20}$$

If K_{s1} is a lower triangular matrix, then the dynamic terms in Equation (7.20),

$(K_{s1} + zK_{s1} + z^2 I)^{-1}$ and $(z^{-1}K_{s1} + K_{s1} + zI)^{-1}$, are lower triangular matrixes as well. For example, if q = 3, then K_{s1} can be designed as $K_{s1} = \begin{bmatrix} K_{s111} & 0 & 0 \\ K_{s121} & K_{s122} & 0 \\ K_{s131} & K_{s132} & K_{s133} \end{bmatrix}$.

Therefore, $(K_{s1} + zK_{s1} + z^2 I)^{-1} = \begin{bmatrix} K_{s111} + zK_{s111} + z^2 & 0 & 0 \\ K_{s121} + zK_{s121} & K_{s122} + zK_{s122} + z^2 & 0 \\ K_{s131} + zK_{s131} & K_{s132} + zK_{s132} & K_{s133} + zK_{s133} + z^2 \end{bmatrix}^{-1}$.

First, the diagonal elements K_{s111}, K_{s122} and K_{s133} are designed, and then the remainder of the lower triangular elements are designed (Details of the design are given in the next section).

② Design of the equivalent control

By applying Equation (7.16), Equation (7.13) is satisfied and as a result, Equation (7.12) leads to a nominal SMC design such that

$$\delta(k+1) = A_e\delta(k) + \Gamma_0 u_2(k) + \cdots + \Gamma_{p-2} u_2(k+p-2) + B_{c(p-2)} u_2(k+p-1) + \Delta(k) \quad (7.21)$$

In this equation, $\Delta(k)$ includes the model uncertainty and the remaining dynamic coupling effect which is not completely compensated for by the design of u_1. Note that A_e has controllable canonical form.

For the nominal SMC design, u_2 can be divided into the equivalent control and the switching control,

$$u_2 = u_{eq} + u_{sw} \quad (7.22)$$

Let the sliding surface be

$$s(k) = S\delta(k) = 0 \quad (7.23)$$

For ideal sliding motion,

$$S\delta(k+p) = SA_e\delta(k+p-1) + Sf(u_2) + S\Delta(k) = 0 \tag{7.24}$$

Thus, the equivalent control can be designed as

$$u_{eq}(k+n) = -(SB_{c(n-1)})^{-1} S[A_e\delta(k) + \Gamma_0 u_2(k) + \Gamma_1 u_2(k+1) + \cdots + \Gamma_{n-1} u_2(k+n-1)] \tag{7.25}$$

However, Equation (7.25) might not provide a stable solution.

To solve this problem, Equation (7.21) is considered to be a dynamic plant with its output being the tracking error. The objective is to design a controller, called a sub-SMC in this study, that forces the tracking error to approach zero, i.e., $e(k+p) = 0$.

According to Theorem 7.1 and Lemma 7.2, Equation (7.21) can be rewritten as

$$\begin{aligned} e(k+p) = {} & A_0 e(k) + A_1 e(k+1) + \cdots + A_{p-1} e(k+p-1) + B_0 u_2(k) + \cdots + B_{p-2} u_2(k+p-2) \\ & + B_{p-1} u_2(k+p-1) + E_0 \varepsilon(k) + \cdots + E_{p-2}\varepsilon(k+p-2) + E_{p-1}\varepsilon(k+p-1) \end{aligned} \tag{7.26}$$

where $B_0, B_1, \cdots, B_{p-2}, B_{p-1}$ and $E_0, E_1, \cdots, E_{p-2}, E_{p-1}$ are the last q rows of $\Gamma_0, \Gamma_1, \cdots, \Gamma_{p-2}, B_{c(p-2)}$ and $\Pi_0, \Pi_1, \cdots, \Pi_{p-2}, E_{c(p-2)}$ respectively. This is an auto-regressive model which can be represented by a state space model. Applying Lemma 7.1, this state space model can be transferred to the controllable canonical form

$$\begin{aligned} X_2(k+1) &= A_{d2} X_2(k) + B_{d2} u_2(k) + \bar{\Delta}(k) \\ e(k) &= C_{d2} X_2(k) \end{aligned} \tag{7.27}$$

where $C_{d2} = \left[\overbrace{I_{q\times q} \quad 0_{q\times q} \quad \cdots \quad 0_{q\times q}}^{p \text{ block}} \right]$ and $\bar{\Delta}(k)$ is the disturbance. Note that if $X_2(k)$ approaches zero, $e(k)$ will approach zero. Inspired by this, the output tracking SMC design problem (7.21) can be transferred to the state tracking SMC problem.

The sliding surface is designed as

$$s(k) = SX_2(k) = 0 \tag{7.28}$$

where $S = \begin{bmatrix} \Lambda_0 & \Lambda_1 & \cdots & \Lambda_{p-1} \end{bmatrix}$ and $\Lambda_0, \Lambda_1, \cdots, \Lambda_{p-1} \in R^{q \times q}$ are diagonal matrices.

The equivalent control can be designed as

$$u_{eq}(k) = -(SB_{d2})^{-1}(SA_{d2} - \Phi_2 S)X_2(k) \tag{7.29}$$

where Φ_2 is a q-by-q diagonal matrix which stabilizes the SMC.

③ Design of u_{sw}

Substituting Equation (7.22) and Equation (7.29) into Equation (7.28) and considering model (7.27) yields

$$s(k+1) = -\Phi_2 s(k) + SB_2 u_{sw}(k) + S\bar{\Delta}(k) \quad \text{and} \tag{7.30}$$

$$X_2(k+1) = A_p X_2(k) + B_{d2} u_{sw}(k) + \bar{\Delta}(k) \tag{7.31}$$

where $A_p = A_{d2} - B_{d2}(SB_{d2})^{-1}(SA_{d2} - \phi_2 S)$.

Rewrite Equations (7.28) and (7.31) together

$$\begin{aligned} X_2(k+1) &= A_p X_2(k) + B_{d2} u_{sw}(k) + \bar{\Delta}(k) \\ s(k) &= SX_2(k) \end{aligned} \tag{7.32}$$

Equation (7.32) can be considered to be a dynamic plant, where $u(k)$ is the input and $s(k)$ is the output. The goal of the SMC is to force the output of the equivalent plant to track the zero reference input, as shown in Figure 7.1.

Due to the discontinuous characteristics of the 'bang-bang' switching control in Equation (7.21), state switching may occur at a high frequency which leads to a chattering problem. To eliminate chattering, a PID regulator can be employed instead of the discontinuous switching control. This will cause the equivalent control error $s(k)$ to be zero, as provided by Equation

(7.33),

$$u_{sw}(k) = -[Ps(k) + I\sum_{i=0}^{k} s(i)T + D\frac{s(k)-s(k-1)}{T}] \tag{7.33}$$

where P, I and D are matrixes of the discrete PID-based SMC; T is the sampling period.

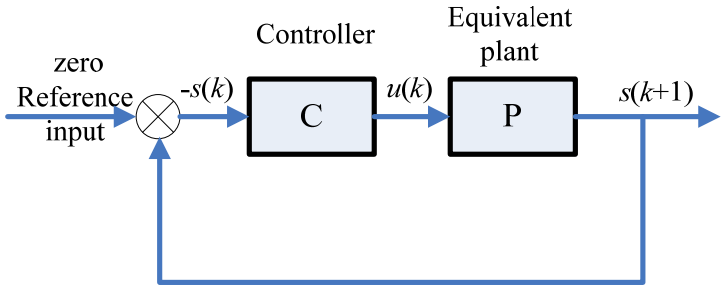

Figure 7. 1 Equivalent plant for SMC

Theorem 7.2: There exist matrices P, I and D such that the closed-loop control system (7.32) is stable.

Proof: Substituting Equation (7.33) into (7.30) yields

$$s(k+1) = -(\phi_2 + SB_{d2}P + SB_{d2}IT + SB_{d2}D/T)s(k) + (SB_{d2}D/T)s(k-1) - SB_{d2}IT\sum_{i=0}^{k-1} s(i) + S\bar{\Delta}(k) \tag{7.34}$$

Note that

$$-SB_{d2}IT\sum_{i=0}^{k-1} s(i) = s(k) + (\phi_2 + SB_{d2}P + SB_{d2}D/T)s(k-1) - (SB_{d2}D/T)s(k-2) + S\bar{\Delta}(k-1) \tag{7.35}$$

Thus, Equation (7.34) can be rewritten as

$$\begin{aligned} s(k+1) = {} & (I - \phi_2 - SB_{d2}P - SB_{d2}IT - SB_{d2}D/T)s(k) + (2SB_{d2}D/T + \phi_2 + SB_{d2}P)s(k-1) \\ & - (SB_{d2}D/T)s(k-2) + S\bar{\Delta}(k) - S\bar{\Delta}(k-1) \end{aligned} \tag{7.36}$$

Denoting $\phi(k+1) = S\bar{\Delta}(k) - S\bar{\Delta}(k-1)$, Equation (7.36) can be re-expressed as a state space model with input being $\phi(k)$ and output being $s(k)$. Its characteristic matrix is given by

$$\bar{A} = \begin{bmatrix} 0_{q\times q} & I_{q\times q} & 0_{q\times q} \\ 0_{q\times q} & 0_{q\times q} & I_{q\times q} \\ \bar{A}_1 & \bar{A}_2 & \bar{A}_3 \end{bmatrix} \tag{7.37}$$

where $\bar{A}_1 = -(SB_{d2}D/T)$, $\bar{A}_2 = 2SB_{d2}D/T + \phi_2 + SB_{d2}P$ and

$\bar{A}_3 = I - \phi_2 - SB_{d2}P - SB_{d2}IT - SB_{d2}D/T$.

The eigenvalues of $\bar{A}$, denoting as $\bar{\lambda}_i (i = 1,2,\cdots,3q)$, can be obtained by

$$\left|\lambda I - \bar{A}\right| = (\lambda - \bar{\lambda}_1)(\lambda - \bar{\lambda}_2)\cdots(\lambda - \bar{\lambda}_{3q}) \tag{7.38}$$

Equation set (7.38) contains $3q$ equations with $3q\times 3q$ unknown parameters. Therefore, there exist matrices P, I and D such that the eigenvalues of $\bar{A}$ can be arbitrarily located, which makes the close-loop system (7.32) stable.

□

Theorem 7.3: If the closed-loop system (7.32) is stable, the zero steady state error can be achieved.

Proof: The switching function may be divided into two parts,

$$s(k) = s_0 + s_1(k) \tag{7.39}$$

where s_0 is the initial vector of the switching function which depends on the position of the original state.

Substituting Equations (7.33) and (7.39) into Equation (7.32) and using the equivalent control (7.29) leads to

$$s_1(k+1) = -[SB_{d2}P + SB_{d2}IT(k+1) + 1 - \Phi_2]s_0 - [(SB_{d2}P - \Phi_2)s_1(k) + SB_{d2}IT\sum_{i=0}^{k} s_1(i) + SB_{d2}D\frac{s_1(k) - s_1(k-1)}{T}] + S\bar{\Delta}(k) \quad (7.40)$$

This is a two inputs one output system where s_0 and $\bar{\Delta}$ are the inputs. Since Equation (7.40) is linear, it can be divided into two subsystems: input s_0 with corresponding output s_{11}; and input $\bar{\Delta}$ with corresponding output s_{12}. Therefore,

$$s_1(k) = s_{11}(k) + s_{12}(k) \quad (7.41)$$

Suppose $s_{11}(0) = s_{12}(0) = 0$, then the first subsystem can be represented as

$$s_{11}(k+1) = -[SB_2P + SB_2IT(k+1) + 1 - \Phi_2]s_0 - [(SB_2P - \Phi_2)s_{11}(k) + SB_2IT\sum_{i=0}^{k} s_{11}(i) + SB_2D\frac{s_{11}(k) - s_{11}(k-1)}{T}] \quad (7.42)$$

Taking a Z-transform of Equation (7.42), the transfer function from s_0 to s_{11} becomes

$$s_{11}(z) = -\Sigma(z)^{-1}\left[SB_2P - \Phi_2 + SB_2IT(k+1) + 1\right]s_0(z) \quad (7.43)$$

where matrix $\Sigma(z) = z^{-1}I_{q\times q} - \Phi_2 + SB_2P + SB_2IT\left(z^k + z^{k-1} + \cdots + z^0\right) + \frac{SB_2D}{T} - \frac{SB_2D}{T}z$. Since, s_0 is a step input with its amplitude being s_0, according to the final value theory of the discrete system,

$$s_{11}(\infty) = \lim_{z\to 1}(1 - z^{-1})s_{11}(z) = \lim_{z\to 1}(1 - z^{-1})\Sigma(z)^{-1}\left[SB_2P - \Phi_2 + SB_2IT(k+1) + 1\right]s_0\frac{z}{z-1} = -s_0 \quad (7.44)$$

The second subsystem can be represented as

$$s_{12}(k+1) = -[(SB_2P - \Phi_2)s_{12}(k) + SB_2IT\sum_{i=0}^{k} s_{12}(i) + SB_2D\frac{s_{12}(k) - s_{12}(k-1)}{T}] + S\bar{\Delta}(k) \quad (7.45)$$

Taking a Z-transform of Equation (7.45), the transfer function from $\bar{\Delta}$ to s_{12} becomes

$$s_{12}(z) = \Sigma(z)^{-1}S\bar{\Delta}(z) \quad (7.46)$$

Therefore,

$$s_{12}(\infty) = \lim_{z \to 1} \left(1 - z^{-1}\right) s_{12}(z) = \lim_{z \to 1} \Sigma(z)^{-1} S \left(1 - z^{-1}\right) \bar{\Delta}(z) = 0 \tag{7.47}$$

Equations (7.33) and (7.47) together with Equation (7.41) indicate that the value of the switching function s is zero when time approaches infinity. This implies that the state will move towards the sliding surface and converge to zero and zigzag motion of the states and the steady state error of the output in the discrete SMC are eliminated.

□

7.5.4 Experiments

Piezoelectric stages have been widely applied to nano-positioning, due to their fast response, high precision, and ability to generate large forces. With ingenious design of flexible hinges, friction and backlash clearance can be avoided which leads to further improvement in their performance. However, nonlinear effects in the piezoelectric actuators, such as creep and hysteresis, can greatly degrade the positioning accuracy of the stages [1], [2], [61]. To improve the performance, control of nano-positioning stages has drawn considerable attention. In this study, with the aim of verifying the effectiveness of a discrete PID-based SMC for a MIMO system, experiments were carried out on the commercially available nano-positioning stage (P-558.TCD, Physik Instrumente) shown in Figure 6.1. Four piezoelectric actuators are used to actuate the stage. It can generate linear displacements in the vertical direction *Z* and rotation around two horizontal directions R_x and R_y. Table 6-1 shows the motion range and resolution of each DOF.

For displacement measurements, three capacitive displacement sensors located inside P-558.TCD are employed. All displacements were measured with a sampling interval of 2 ms in this study. A transform matrix between the sensors' displacements and the outputs Z, R_x and R_y is provied by the manufacturer. Both the actuators and the sensors in the stage are connected to a host computer via a digital piezo controller (E-761, Physik Instrumente) and controlled via Labview programs, as shown in Figure 6.1b. As instructed by its manual, the piezo controller can drive the actuator with a maximum operating frequency of 10-20 Hz if 30-50 V input voltage is applied. The controller can be manipulated in both open-loop mode and closed-loop mode. In open-loop mode, a 4-dimensional voltage signal is generated by the computer and transferred to the controller. Through amplifiers in E-761 board, this signal is received by each piezoelectric actuator. Since there are 4 inputs and 3 outputs, actuation redundancy exists in open-loop manipulation. This might destroy the nano-positioning stage, therefore, manipulation in open-loop mode is not recommended. In closed-loop mode, a 3-dimensional reference signal is forwarded from the computer to the controller and is then processed by the internal PID controllers of the stage and distributed to each piezoelectric actuator. The closed-loop mode may be regarded as a 3-input-3-output system without actuation redundancy and, as a result, it was adopted in this research.

Since the configuration of the nano-positioning stage is unknown, a black-box state space model was applied to describe the dynamic performance. The nonlinearity that exists in the nano-positioning stage is considered to be a disturbance to the dynamics which is rejected by the proposed discrete PID-SMC. Experiments for parameter identification were first carried out to

obtain the state space model. Then, an output tracking based discrete PID-SMC designed using the model reference approach was applied to control the nano-postioning stage for tracking step reference signals. Finally, dynamic tracking control with the proposed methods was implemented and comparison to a PID controller was made.

7.5.4.1 Model identification

In this study, the performance of the nano-positioning stage was described by the state space model

$$x(k+1) = Ax(k) + Bu(k), y(k) = Cx(k) \tag{7.48}$$

where $x(k) \in R^{n\times 1}$ is the state, $u(k) \in R^{3\times 1}$ is the control input, $y(k) \in R^{3\times 1}$ is the system output, and $A \in R^{n\times n}$, $B \in R^{n\times 3}$ and $C \in R^{3\times n}$ are the system matrices. For simplicity, the order of the system was chosen to be nine, thus p = 3. Since the state space model is linear, the model identification may be implemented on each input channel separately. For example, when an input signal is only provided to one channel, i.e., $u_i(i = 1,2,3)$ the three-dimensional output $y_i = \begin{bmatrix} y_{i1} & y_{i2} & y_{i3} \end{bmatrix}^T$ can be obtained by

$$\begin{aligned} x_i(k+1) &= A_i x_i(k) + B_i u_i(k) \\ y_i(k) &= C_i x_i(k) + D_i u_i(k) \end{aligned} \tag{7.49}$$

The states in Equation (7.49) for all three channels may be stacked as

$$\begin{bmatrix} x_1(k+1) \\ x_2(k+1) \\ x_3(k+1) \end{bmatrix} = \begin{bmatrix} A_1 & & \\ & A_2 & \\ & & A_3 \end{bmatrix} \begin{bmatrix} x_1(k) \\ x_2(k) \\ x_3(k) \end{bmatrix} + \begin{bmatrix} B_1 & & \\ & B_2 & \\ & & B_3 \end{bmatrix} \begin{bmatrix} u_1(k) \\ u_2(k) \\ u_3(k) \end{bmatrix} \tag{7.50}$$

According to the definition of the linear system, the output is regarded as the sum of $y_i(i = 1,2,3)$, i.e.,

$$y = y_1 + y_2 + y_3 = \begin{bmatrix} C_1 & C_2 & C_3 \end{bmatrix} \begin{bmatrix} x_1(k) \\ x_2(k) \\ x_3(k) \end{bmatrix} + \begin{bmatrix} D_1 & D_2 & D_3 \end{bmatrix} \begin{bmatrix} u_1(k) \\ u_2(k) \\ u_3(k) \end{bmatrix} \tag{7.51}$$

As such, the system matrices in the state space model for the three-input-three-output system are obtained by

$$A = diag\begin{bmatrix} A_1 & A_2 & A_3 \end{bmatrix}, B = diag\begin{bmatrix} B_1 & B_2 & B_3 \end{bmatrix}, C = \begin{bmatrix} C_1 & C_2 & C_3 \end{bmatrix}, D = \begin{bmatrix} D_1 & D_2 & D_3 \end{bmatrix} \tag{7.52}$$

For parameter identification, a 40 μm reference chirp signal with frequency ranging from 1 to 100 Hz was provided in Channel 1 (Reference *Z* channel) and the corresponding output in each channel was measured. The order of the state space model was originally set to three. By applying the singular value decomposition on the identified Hankel matrix [150], the system matrices of the state space model were obtained.

To identify the state space model in the other two channels, a 200 μrad reference chirp signal with frequency ranging from 1 to 100 Hz was provided. By employing the same aforementioned estimation method, the system matrices of the sub-system were obtained. Equation (7.53) shows the identification results. Table 7-2 gives the prediction error in each direction when a 1 Hz sinusoidal reference input is provided in different channels. The prediction errors are calculated in terms of the 2-norm of the error vector (defined as the difference between the measurement and the model prediction).

$$A_1 = \begin{bmatrix} 0.9235 & 0.1738 & 0.0103 \\ -0.1754 & 0.6964 & -0.0997 \\ 0.024 & 0.1912 & 0.8276 \end{bmatrix}, B_1 = \begin{bmatrix} -0.3125 \\ -0.2797 \\ 0.0717 \end{bmatrix}, \tag{7.53a}$$

$$C_1 = \begin{bmatrix} -0.308 & 0.2794 & 0.0363 \\ -0.0151 & 0.0273 & -0.0456 \\ -0.0028 & -0.0224 & -0.0224 \end{bmatrix}$$

$$A_2 = \begin{bmatrix} 0.9739 & -0.1057 & -0.022 \\ 0.2057 & 0.7501 & -0.1689 \\ 0.024 & 0.5491 & 0.1313 \end{bmatrix}, B_2 = \begin{bmatrix} -0.252 \\ 0.1241 \\ -0.076 \end{bmatrix},$$
$$C_2 = \begin{bmatrix} 0.000057 & 0.00011 & -0.000004 \\ -0.1988 & -0.1714 & -0.0701 \\ 0.0007 & 0.00066 & -0.0011 \end{bmatrix} \quad (7.53b)$$

$$A_3 = \begin{bmatrix} 0.9739 & 0.1063 & 0.0219 \\ -0.2048 & 0.7502 & -0.1684 \\ -0.0235 & 0.5504 & 0.1311 \end{bmatrix}, B_3 = \begin{bmatrix} 0.2534 \\ 0.1251 \\ -0.076 \end{bmatrix},$$
$$C_3 = \begin{bmatrix} -0.00005 & 0.0001 & 0.00005 \\ -0.0015 & 0.0018 & 0.00027 \\ 0.1988 & -0.172 & -0.07 \end{bmatrix} \quad (7.53c)$$

Table 7- 2 Estimation error under chirp inputs in each channel

Direction	Z (μm)	R_x (μrad)	R_y (μrad)
Chirp inputs in Channel 1	0.1944	0.4030	0.2008
Chirp inputs in Channel 2	0.0192	4.8640	0.0760
Chirp inputs in Channel 3	0.0263	0.2060	4.3387

From Table 7-2, it may be seen that the prediction error in the diagonal is only 0.49%, 2.43% and 2.16% of the input amplitude respectively. It is noted in the previous section that the dimension of the state vector should be integral multiple of the number of inputs or output in order to employ the proposed method ($n / q = p \in \{\theta \mid \theta \in Z, \theta \geq 1\}$). This can be guaranteed by choosing the same order in separate identification for each input-output pair. For example, in the aforementioned system identification, the order of each system (A_i, B_i, C_i, D_i, i = 1, 2, 3) is set to be 3 such that the order of the 3-inputs-3-outputs system (A, B, C, D) is 9.

7.5.4.2 Step tracking

The output tracking based discrete PID-SMC for MIMO systems developed using the model reference approach was implemented in experiments to control the nano-positioning stage. The output displacement in each direction was estimated by a α-β filter which is a simplified observer for estimation and filtering. The parameters of the filter were adjusted to be $\alpha = 0.5$, $\beta = 0.002$ using trial-and-error. The sliding surface was defined as given in Equation (7.23) where $S = \begin{bmatrix} m^2 I_{3\times3} & 2mI_{3\times3} & I_{3\times3} \end{bmatrix}$ and $m = -0.7$. The reference model was defined as a second order diagonal transfer matrix as

$$T_m = \begin{bmatrix} \dfrac{\omega_n^2}{s^2 + 2\eta\omega_n s + \omega_n^2} & 0 & 0 \\ 0 & \dfrac{\omega_n^2}{s^2 + 2\eta\omega_n s + \omega_n^2} & 0 \\ 0 & 0 & \dfrac{\omega_n^2}{s^2 + 2\eta\omega_n s + \omega_n^2} \end{bmatrix} \tag{7.54}$$

where η is the desired damping ratio and ω_n is the desired natural frequency. The parameters were adjusted to be $\eta = 0.9$ and $\omega_n = 200$. Then the transfer matrix was transferred to the state space model. For convenience, the PID matrices and stable matrix Φ were chosen to be diagonal matrices. As introduced in Equation (7.19), K_1 in the SMC was selected to be a combination of two lower triangular matrices K_{s1}. To adjust K_1, a diagonal matrix was first applied with its diagonal elements set according to the diagonal outputs. The other elements in the lower triangle were tuned according to the interaction between each axis.

The step tracking experiments were divided into three groups. First, a 10 μm step reference signal was provided in the Z direction. To get the best tracking performance, the first diagonal

elements in the K_{s1}, Φ and PID matrices were set to $K_{s111} = -0.3, \Phi_{11} = 0.9, P_{11} = 1, I_{11} = 60$ and $D_{11} = 0$ Then, a 10 μrad step reference signal was provided in the R_x direction with the other two kept at zero. The second diagonal elements in the K_{s1}, Φ and PID matrices were set to -0.2, 0.5, 4, 500, 0, respectively. To minimize the effect in the Z direction, K_{s121} was set to -0.007. Finally, the same reference signal was provided in the R_y direction with Z and R_x equal to zero. The third diagonal elements were set to $K_{s111} = -0.3, \Phi_{11} = 0.4, P_{11} = 2, I_{11} = 200$ and $D_{11} = 0$. To minimize the effect in the R_x direction, K_{s131} was set to 0.01. The other elements in the matrix K_{s1} were kept at zero.

Figure 7.2 shows the step tracking performance of the nano-positioning stage controlled by the proposed SMC.

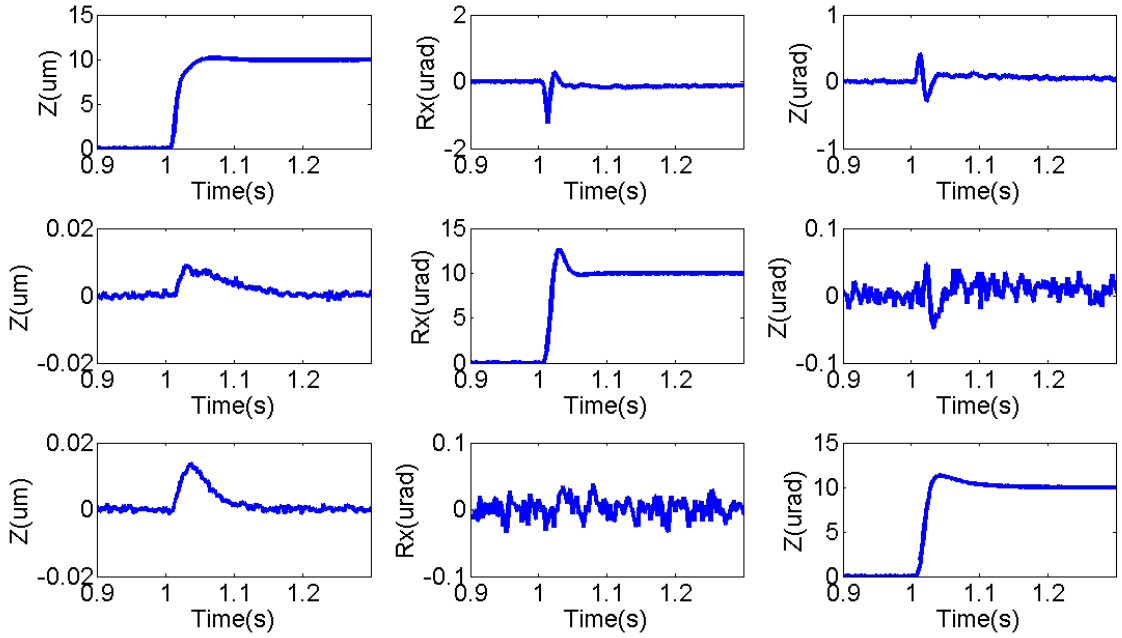

Figure 7. 2 Step tracking performance of the 3-DOF nano-positioning stage

It can be seen that the tracking errors approach to zero through the use of the I component in the PID regulator. This was proven theoretically in the above section. Overshoots exist due to the large control input generated in order to obtain a fast response in each direction.

7.5.4.3 Dynamic tracking performance compared with the PID controller

To verify the effectiveness of the proposed control method, dynamic tracking experiments were carried out on the nano-positioning stage. Three types of inputs were used as the reference signal: ① sinusoidal inputs with different amplitudes and frequencies; ② a piecewise continuous combination of different-amplitude sinusoidal inputs with the same frequency (PWSW), as shown in Figure 4.8a; and ③ the superposition of four sinusoidal inputs with different frequencies, amplitudes and phase delays (SW), as shown in Figure 4.8b and Equation (4.47).

The output tracking based discrete PID-SMC for MIMO systems designed by the model reference approach was implemented on the nano-positioning stage. The same α-β filter, sliding surface, the stable matrix Φ and K_{s1} adjusted for the step reference inputs were employed, as well. To improve the tracking performance, the parameters of the second order reference model were chosen to be $\eta = 0.9$ and $\omega_n = 1000 rad/s$. Thus, the parameters of the PID matrices based on the reference model were readjusted to be $P = diag\begin{bmatrix} 6 & 2 & 3 \end{bmatrix}$, $I = diag\begin{bmatrix} 300 & 50 & 30 \end{bmatrix}$ and $D = 0_{3\times 3}$. For comparison, the PID controller was also implemented on the nano-positioning stage. Table 7-3 shows the PID parameters adjusted by trails-and-errors for the optimal performance.

Table 7- 3 PID parameters adjusted for the PID controller

Channel	P	I	D
Z	1.5	120	0
R_x	2	90	0
R_y	2	100	0

Table 7- 4 Comparison of the tracking performance between the discrete PID-based SMC and PID controller

Reference inputs	Frequency	Discrete PID-based SMC		
		Z	R_x	R_y
10 μm sinusoidal input in Z direction	1 Hz	0.0633	0.0008	0.0008
	5 Hz	0.2912	0.0011	0.0012
	10 Hz	0.7632	0.0025	0.0022
10 μrad sinusoidal input in R_x direction	1 Hz	**0.1184**	0.2707	**0.0285**
	5 Hz	0.2573	1.3789	**0.044**
	10 Hz	0.2666	2.8597	0.0506
10 μrad sinusoidal input in R_y direction	1 Hz	**0.0661**	0.0148	0.2879
	5 Hz	0.0521	0.0197	1.5742
	10 Hz	0.0818	0.034	2.9125
Reference inputs	Frequency	PID controller		
		Z	R_x	R_y
10 μm sinusoidal input in Z direction	1 Hz	0.3658	0.0009	0.0009
	5 Hz	1.7395	0.0012	0.0012
	10 Hz	3.8355	0.0026	0.0026
10 μrad sinusoidal input in R_x direction	1 Hz	0.0909	0.492	0.0148
	5 Hz	0.3095	2.5681	0.0347
	10 Hz	0.5801	5.2104	0.0827
10 μrad sinusoidal input in R_y direction	1 Hz	0.0225	0.077	0.4557
	5 Hz	0.0586	0.024	2.4599
	10 Hz	0.2484	0.0531	5.2334

Table 7-4 compares the tracking performance of the nano-positioning stage controlled by the proposed method and the PID controller. The tracking error was calculated in terms of the 2-norm of the difference between the desired output and the measured output. It can be concluded that the proposed method performs better than the PID controller, especially in the diagonal direction. As frequency increases, the improvement becomes more obvious. For example, if a 1 Hz, 10 μm sinusoidal input is provided in the *Z* direction, the tracking error in the *Z* direction derived by the output tracking based discrete PID-SMC developed with the model reference approach is 0.0633 μm. This is 0.3025 μm less than that derived by the PID controller. For a 10 Hz sinusoidal input in the *Z* direction, the difference increases to 3.0723 μm.

In addition, the coupling effect is reduced when the proposed method is used. For example, consider the 10 Hz, 10 μrad sinusoidal input in the R_y direction. The tracking error in the *Z* direction from the proposed method is 0.0818 μm which is only 32.9% of that from the PID controller. However, at low input frequency, the improvement is not as obvious.

Occasionally, the performance of the output tracking based discrete PID-SMC is worse than the PID controller which has been indicated in bold font in Table 7-4. For example, when a 5 Hz, 10 μrad sinusoidal input is provided in the R_x direction, the tracking error in the R_y direction derived by the proposed method is 0.0093 μm more than that derived by the PID controller. This might be caused by the nonlinear effect that exists in the nano-positioning stage.

To further show the performance of the proposed method, two extra experiments were implemented. In the first experiment, a 2 Hz, 10 μm sinusoidal input was provided in the Z

direction and a 5 Hz, 10 μrad sinusoidal signal was set as the reference input to the R_x direction. There was no reference signal given in the R_y direction. In the second experiment, a 2 Hz, 10 μm PWSW input was provided in the Z direction and a 10 Hz, 50 μrad SW signal was selected as the reference input to the R_y direction, with the other direction kept at zero. Figure 7.3 and Figure 7.4 show the tracking performance.

Compared to the PID controller, the output tracking based discrete PID-SMC for MIMO systems performed better for the combined signals in all three directions. This can be seen from the tracking performance of the second experiment. Using the discrete PID-based SMC instead of the PID controller, tracking errors of 0.1086 μm and 1.1831 μrad were obtained in the *Z* and R_y directions, respectively. This is 0.6151 μm and 1.813 μrad lower than the PID controller. Similar results also occurred in the first experiment.

In terms of the decoupling effect, the advantage of using the proposed method over the PID controller is not as obvious. For example, in the second experiment the tracking error of the nano-positioning stage controlled by the discrete PID-based SMC derived from the model reference approach is 0.0763 μm. This is only 0.009 μm less than the PID controller. But compared with the tracking error without any controller, there is still 51.7% improvement using the discrete PID-based SMC, which can be observed from Figure 7.4(f).

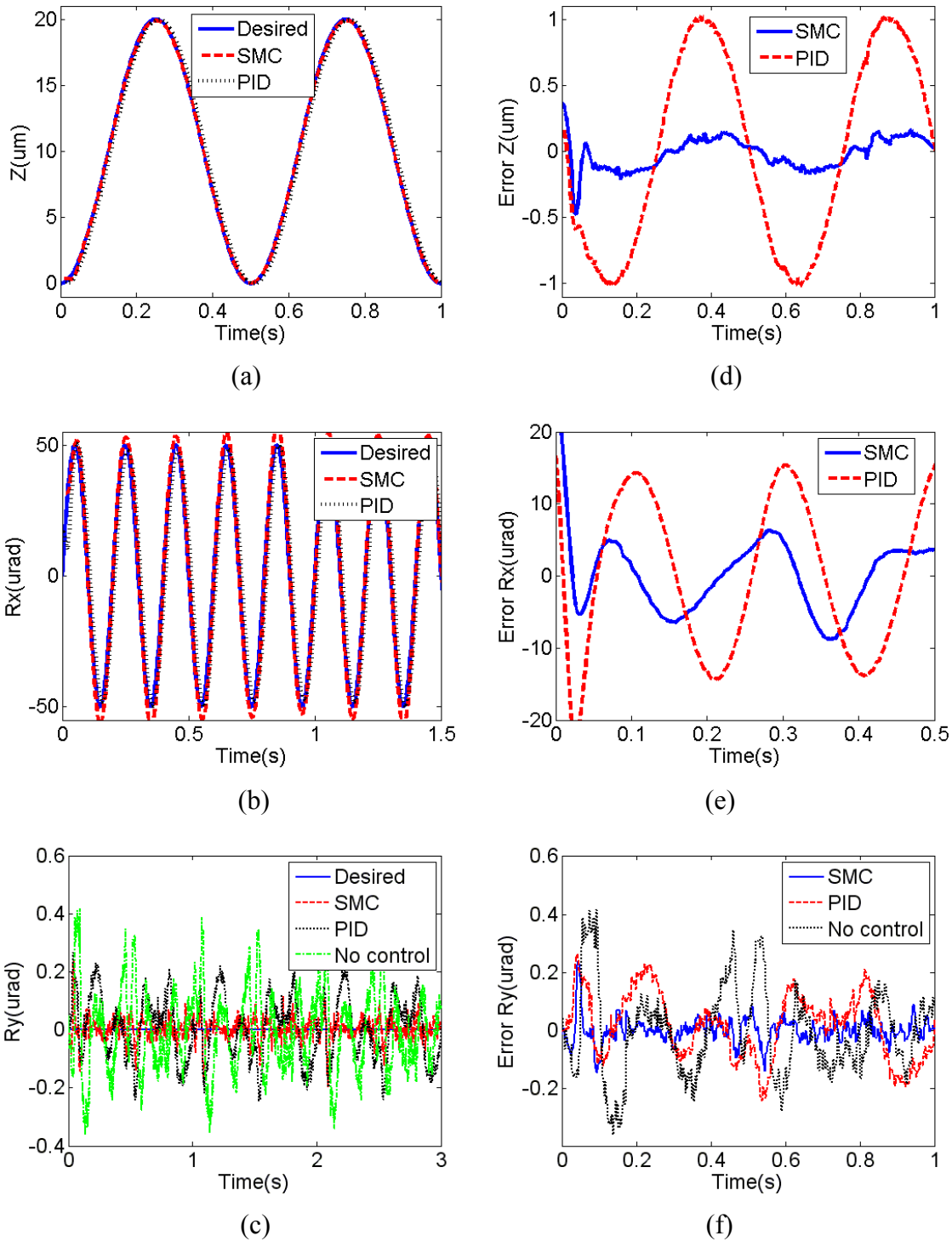

Figure 7. 3 Tracking performance of the discrete PID-based SMC designed by model reference approach for the 2 Hz 10 μm sinusoidal input in Z direction and 5 Hz 50 μrad sinusoidal input in *Rx* direction

output displacement in (a) Z direction, (b) *Rx* direction and (c) *Ry* direction; tracking error in (d) Z direction, (e) *Rx* direction and (f) *Ry* direction;

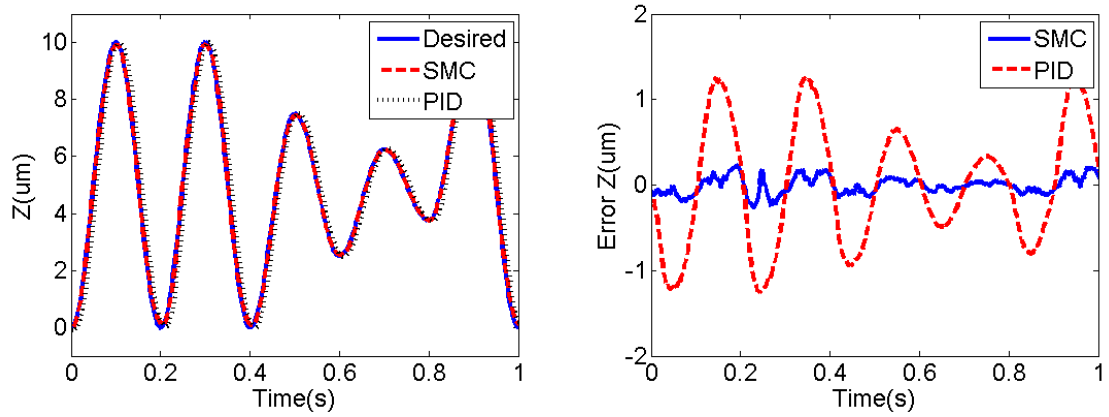

(a)

(d)

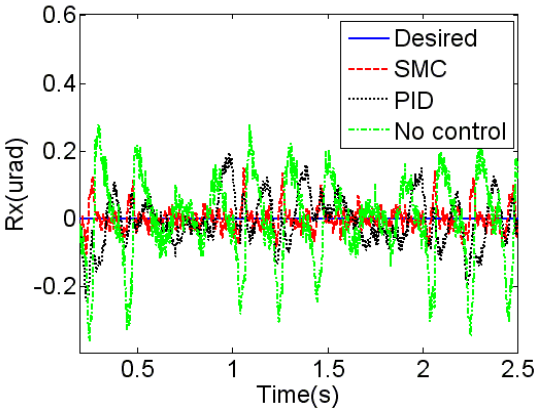

(b)

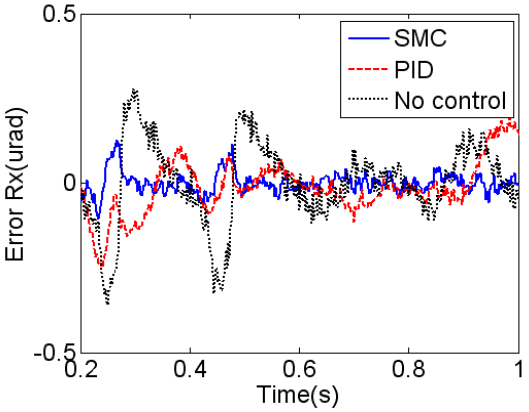

(e)

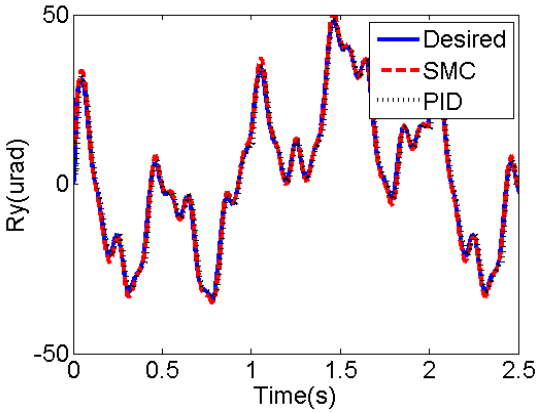

(c)

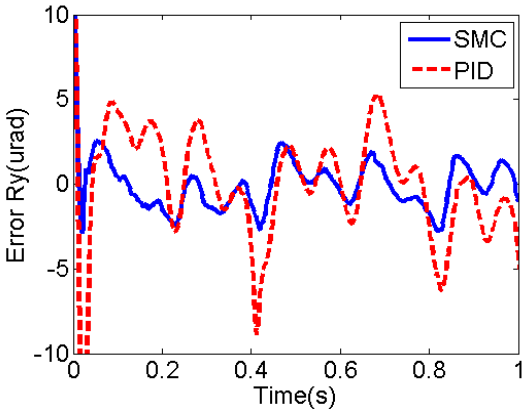

(f)

Figure 7. 4 Tracking performance of the discrete PID-based SMC designed by mode reference approach for the 5 Hz 10 μm PWSW input in Z direction and 10 Hz 50 μrad SW input in *Ry* direction

output displacement in (a) Z direction, (b) *Rx* direction and (c) *Ry* direction; tracking error in (d) Z direction, (e) *Rx* direction and (f) *Ry* direction;

7.5.5 Conclusion

This paper presents the development of an output tracking based discrete PID-SMC for a MIMO system. By applying the model reference approach, the output tracking problem is transferred to a state tracking problem so that the general SMC design method can be applied, so called a novel sub-SMC design in this paper. By applying the PID based switching control instead of the 'bang-bang' switching control, chattering and the zig-zag state motion of the discrete SMC were eliminated. The zero steady state error of the proposed method can be achieved. To verify the effectiveness of the proposed control schemes, experiments were carried out on a commercially available nano-positioning stage using different reference signals given in different directions. A black box state space model was identified to represent the dynamics of the nano-positioning stage such that general SMC design cannot be directly applied. The results obtained were compared with the PID controller. It was shown that the output tracking based discrete PID-SMC designed by the model reference approach can achieve better tracking performance. As the input frequency increases, the advantage of using the proposed method becomes more profound.

7.5.6 Acknowledgment

The support to the present study from the China Scholarship Council (CSC) and the Natural Sciences and Engineering Research Council (NSERC) of Canada is acknowledged.

7.5.7 Appendix

Proof of Theorem 7.1:

Proof: Consider state space model (7.1) and substitute Equation (7.3) into (7.1). Therefore,

$$\dot{x} = FAF^{-1}x + FBu + Fw \tag{7.55}$$

Assume that matrix FAF^{-1} has the controllable canonical form defined as

$$FAF^{-1} = \begin{bmatrix} 0_{m(p-1)\times m} & I_{m(p-1)\times m(p-1)} \\ A_0 & \boldsymbol{\alpha} \end{bmatrix} \tag{7.56}$$

where $\boldsymbol{\alpha} = \begin{bmatrix} A_1 & A_2 & \cdots & A_{p-1} \end{bmatrix}$, $A_0, A_1, \cdots, A_p \in R^{m\times m}$ are the coefficient matrixes.

Substituting Equation (7.4) into Equation (7.56) gives

$$\begin{bmatrix} C \\ CA \\ \vdots \\ CA^{p-1} \end{bmatrix} A = \begin{bmatrix} 0_{m(p-1)\times m} & I_{m(p-1)\times m(p-1)} \\ A_0 & \boldsymbol{\alpha} \end{bmatrix} \begin{bmatrix} C \\ CA \\ \vdots \\ CA^{p-1} \end{bmatrix} \tag{7.57}$$

The first $p\times(m-1)$ rows of Equation (7.57) are satisfied naturally. The last p rows lead to

$$CA^{p-1} = A_0C + A_1CA + A_2CA^2 + \cdots + A_{p-1}CA^{p-1} \tag{7.58}$$

Assume that the elements in these coefficient matrixes are unknown, therefore, Equation (7.58) can be considered to be a group of $m\times n$ linear equations with $m\times n$ unknown parameters which are solvable. Therefore, Equation (7.58) can be satisfied. Moreover, by applying the transform (7.3), the input and output matrices of the new state space model will be, respectively,

$$B' = FB = \begin{bmatrix} B_0; & B_1; & \cdots & B_{p-1} \end{bmatrix} \text{ and} \tag{7.59}$$

$$C' = CF^{-1} = \begin{bmatrix} \overbrace{I_{m\times m} \quad 0_{m\times m} \quad \cdots \quad 0_{m\times m}}^{p \text{ block}} \end{bmatrix} . \tag{7.60}$$

□

Proof of Theorem 7.1:

Proof: According to Lemma 7.2, A_e can be decomposed as

$$A_e = \begin{bmatrix} N_{11} & N_{12} \\ N_{21} & N_{22} \end{bmatrix} \tag{7.61}$$

where $N_{11} = \begin{bmatrix} 0_{(p-2)q\times q} & I_{(p-2)q\times(p-2)q} \\ 0_{q\times q} & 0_{q\times(p-2)q} \end{bmatrix} \in R^{(p-1)q\times(p-1)q}$, $N_{12} = \begin{bmatrix} 0_{(p-2)q\times q} \\ I_{q\times q} \end{bmatrix} \in R^{(p-1)q\times q}$,

$N_{21} = \begin{bmatrix} A_0 & A_1 & \cdots & A_{p-2} \end{bmatrix}$, $N_{22} = A_{p-1}$.

Therefore, $A_e A_{cm} = \begin{bmatrix} N_{11} & N_{12} \\ N_{21} & N_{22} \end{bmatrix} \begin{bmatrix} C_m \\ C_m A_m \\ C_m {A_m}^2 \\ \vdots \\ C_m {A_m}^{p-2} \\ C_m {A_m}^{p-1} \end{bmatrix} = \begin{bmatrix} N_{11}A_{cm1} + N_{12}A_{cm2} \\ N_{21}A_{cm1} + N_{22}A_{cm2} \end{bmatrix}$

where $A_{cm1} = \begin{bmatrix} C_m \\ C_m A_m \\ \vdots \\ C_m A_m^{p-2} \end{bmatrix} \in R^{(p-1)q\times m}$, $A_{cm2} = C_m A_m^{p-1} \in R^{q\times m}$.

$$\because N_{11}A_{cm1} + N_{12}A_{cm2} = \begin{bmatrix} 0_{(p-2)q\times q} & I_{(p-2)q\times(p-2)q} \\ 0_{q\times q} & 0_{q\times(p-2)q} \end{bmatrix} \begin{bmatrix} C_m \\ C_m A_m \\ \vdots \\ C_m A_m^{p-2} \end{bmatrix} + \begin{bmatrix} 0_{(p-2)\times q} \\ I_{q\times q} \end{bmatrix} C_m A_m^{p-1}$$

$$= \begin{bmatrix} C_m A_m \\ C_m {A_m}^2 \\ \vdots \\ C_m {A_m}^{p-2} \\ 0 \end{bmatrix} + \begin{bmatrix} 0 \\ 0 \\ \vdots \\ 0 \\ C_m A_m^{p-1} \end{bmatrix} = A_{cm1}A_m,$$

$$\therefore P = A_e A_{cm} - A_{cm}A_m = \begin{bmatrix} N_{11}A_{cm1} + N_{12}A_{cm2} \\ N_{21}A_{cm1} + N_{22}A_{cm2} \end{bmatrix} - \begin{bmatrix} A_{cm1}A_m \\ A_{cm2}A_m \end{bmatrix} = \begin{bmatrix} 0_{(p-1)q\times m} \\ N_{21}A_{cm1} + N_{22}A_{cm2} - A_{cm2}A_m \end{bmatrix}.$$

$\therefore Rank(P) = Rank[B_{c(p-2)}] = q.$

Next, consider

$$\Gamma_0 = A_c B - A_e B_{c0} = \begin{bmatrix} C_d B_d \\ C_d A_d B_d \\ C_d {A_d}^2 B_d \\ \vdots \\ C_d {A_d}^{p-2} B_d \\ C_d {A_d}^{p-1} B_d \end{bmatrix} - \begin{bmatrix} 0_{(p-1)q\times q} & I_{(p-1)q\times(p-1)q} \\ A_0 & \tilde{A}^T \end{bmatrix} \begin{bmatrix} 0 \\ C_d B_d \\ C_d A_d B_d \\ \vdots \\ C_d {A_d}^{p-3} B_d \\ C_d {A_d}^{p-2} B_d \end{bmatrix} \tag{7.62}$$

Letting $M_0 = \begin{bmatrix} (C_d B_d)^T & (C_d A_d B_d)^T & \cdots & (C_d {A_d}^{p-2} B_d)^T \end{bmatrix}^T$

Equation (7.46) becomes

$$\Gamma_0 = \begin{bmatrix} M_0 \\ C_d {A_d}^{p-2} B \end{bmatrix} - \begin{bmatrix} 0_{(p-1)q\times q} & I_{(p-1)q\times(p-1)q} \\ A_0 & \tilde{A}^T \end{bmatrix} \begin{bmatrix} 0 \\ M_0 \end{bmatrix} = \begin{bmatrix} M_0 \\ C_d {A_d}^{p-2} B_d \end{bmatrix} - \begin{bmatrix} M_0 \\ A_0 d + \tilde{A}^T M_0 \end{bmatrix}$$
$$= \begin{bmatrix} 0_{(p-1)q\times q} \\ C_d {A_d}^{p-2} B_d - \tilde{A}^T M_0 \end{bmatrix}.$$

Similarly, for $\Gamma_i, (i = 1, 2, \cdots, p-2)$,

$$\Gamma_1 = B_{c0} - A_e B_{c1} = \begin{bmatrix} 0_{(p-1)q\times q} \\ C_d {A_d}^{p-2} B_d - \tilde{A}^T M_1 \end{bmatrix} \tag{7.63}$$

$$\Gamma_2 = B_{c1} - A_e B_{c2} = \begin{bmatrix} 0_{(n-1)q\times q} \\ C_d {A_d}^{n-3} B_d - \tilde{A}^T M_2 \end{bmatrix} \tag{7.64}$$

$$\cdots \Gamma_{p-2} = B_{c(p-3)} - A_3 B_{c(p-2)} = \begin{bmatrix} 0_{(n-1)q\times q} \\ C_d B_d - \tilde{A}^T M_{n-1} \end{bmatrix} \tag{7.65}$$

where $M_1 = \begin{bmatrix} 0 & B_d{}^T C_d{}^T & B_d{}^T A_d{}^T C_d{}^T & \cdots & B_d{}^T (A_d{}^T)^{p-3} C_d{}^T \end{bmatrix}^T$,

$M_2 = \begin{bmatrix} 0 & 0 & B_d{}^T C_d{}^T & \cdots & B_d{}^T (A_d{}^T)^{p-4} C_d{}^T \end{bmatrix}^T \cdots$

$\therefore Rank[\Gamma_i, i = 0, 2, \cdots, p-2] = Rank[B_{c(p-2)}] = q.$

Also, it can be proven similarly that $Rank[\Pi_l, l = 0, 1, \cdots, p-2] = Rank[E_{c(p-2)}] = q.$

□

8 Disturbance Observer based Sliding Mode Control for Multi-DOF Piezoelectric Actuators

This chapter presents the work that is included in the following manuscript appended.

Y. Cao and X. B. Chen, "Disturbance Observer based Sliding Mode Control for a three-DOF Nano-positioning Stage," *IEEE/ASME Transactions on Mechatronics*, 2012, under review, manuscript ID: TMECH-09-2012-2566.

8.1 Introduction and Objectives

It is noted in Chapter 5 that if the disturbance and uncertainties can be completely or partially estimated, such estimations should greatly facilitate the hysteresis compensation by means of SMC. Common of the existing studies about the DOB-based control on the multi-DOF nano-positioning stages is that their structures were known and as such physical models can be developed to describe their behaviors. In reality, the challenge is that the commercially-available multi-DOF nano-positioning stages are typically provided without the information regarding the internal structure and as a result, it is difficult or even impossible to build their physical models for the control purpose. To rise to this challenge, this paper is to develop a discrete DOB-based SMC for the multi-DOF nano-positioning stage with unknown configuration.

8.2 Methods

Figure 8.1 shows the proposed control scheme of the discrete DOB-based SMC. Due to the unknown configuration of the nano-positioning stage, the plant was identified as a black box

dynamic system, which is decoupled by the integration of DOB. Each pair of inputs and outputs can be controlled independently by a discrete PID-based SMC designed based on its dynamics. Since the coupling effect is compensated by the use of DOB, the disturbance to be rejected by the PID-based SMC is reduced. Therefore, the tracking error is expected less in comparison to the nominal SMC. Due to the imperfection of the decoupling, integration of the DOB may not completely compensate for the interaction between each pair of inputs and outputs. Such an error is considered to be uncertainty and is estimated based on the desired decoupled system. This error is integrated in the design of the equivalent control of the SMC and rejected by the discrete PID-based SMC.

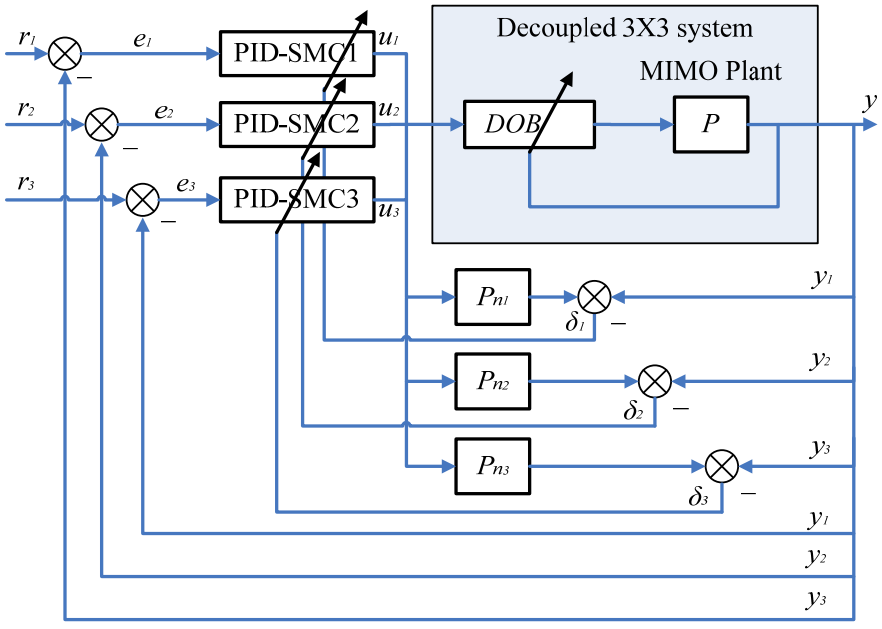

Figure 8. 1 Control scheme of the DOB-based SMC

8.3 Results

By integration of the DOB into the discrete PID-based SMC, the disturbance to be rejected by the feedback control is reduced and the control performance of the three-DOF nano-positioning stage is greatly improved. This improvement becomes more profound as the frequency increases from 1 Hz to 10 Hz in the verification experiments. The developed method may also be employed in the application with a higher frequency, which has not been validated due to the limitation of the experimental settings used in the present study.

8.4 Contributions

The contribution of this work was the successful extension of the application of the discrete DOB-based SMC to the control of multi-DOF piezoelectric actuator without available information regarding the internal mechanical configuration.

8.5 Paper: Disturbance Observer based Sliding Mode Control for a Three-DOF Nano-positioning Stage

Authors: Y. Cao and X. B. Chen, *Member, IEEE*[7]

Manuscript received September 13, 2012. This work was supported by the China Scholarship Council (CSC) and the Natural Science and Engineering Research Council (NSERC) of Canada.

Y. Cao is with the Department of Mechanical Engineering, 57 Campus Drive, University of Saskatchewan, Saskatoon, SK, S7N 5A9 (e-mail: yuc150@ mail.usask.ca).

X. B. Chen is with the Department of Mechanical Engineering, 57 Campus Drive, University of Saskatchewan, Saskatoon, SK, S7N 5A9 (phone: 1-306-966-1267; e-mail: xbc719@ mail.usask.ca).

Index Terms: Control systems, MIMO systems, Observers, Piezoelectric devices, Uncertainty

8.5.1 Abstract

To compensate for the nonlinear effects of nano-positioning stages and their model uncertainties, several control methods have been developed and reported in the literature. One promising method for compensation is the use of a proportional-integral-derivative (PID)-based sliding mode control (SMC), in which the nonlinear effects are treated as an unknown disturbance to the system. If the nonlinearity and the model uncertainties can be completely or partially estimated, integration of their estimations into the control schemes may lead to improved performance. On this basis, this paper presents the development of a disturbance-observer-based (DOB) SMC, in which the nonlinearity of the nano-positioning stage is partially predicted through the use of an observer and then compensated by the PID-based SMC. Experiments were performed to verify the effectiveness of the proposed control schemes, and the results showed that the performance of the nano-positioning stage by employing the DOB-SMC was greatly improved, as compared to the PID-based SMC.

8.5.2 Introduction

An increased requirement for high accuracy in production manufacturing and other devices has led to rapid development of precision engineering. From its origin in mechanical engineering, precision engineering has evolved into micro-mechanics and then nanotechnology

[1]. Nanotechnology is the study on the control or manipulation of matter on an atomic and molecular scale. One key branch of nanotechnology is nano-positioning [2]. Nano-positioning stages have been widely applied in nano-manipulation, due to the fast response, high precision, and large forces generated by their drivers ─ the piezoelectric actuators (PEA). The use of flexure hinges makes it possible to eliminate the friction and clearance issues that exist in a traditional mechanism. However, hysteresis, creep, and other nonlinear effects typically found in nano-positioning stages can greatly degrade the positioning accuracy [3] ─ [5]. As higher performance is required, classical controllers such as the PID controller (which has been widely used in industry), can no longer provide satisfactory results [6]. Therefore, various advanced control methods have been developed [7] – [9].

As a variable structure control method, SMC has recently attracted considerable attention [10] ─ [12] as applied to the control of nano-positioning systems. In [13], SMC was applied in the control of a three degrees-of-freedom (DOF) nanopositioner. Each piezoelectric actuator is considered to be independent and therefore the design of three controllers was required. Due to its ability to reject uncertainties and disturbances, the SMC performed much better than the traditional PID controller. However, chattering, caused by the discontinuous switching function in SMC, may excite the high frequency resonant vibration, thereby degrading control performance and even damaging the actuators being controlled [14]. To solve this problem, in [15] and [16], a high order sliding surface was designed to replace the first order one of the nominal SMC. With the merits of the nominal SMC, the high order sliding mode control (HOSMC) can reduce the chattering effect [17], which, however, is limited by the increased

sliding information for the implementation of HOSMC. In [18], a continuous PID-based SMC for piezoelectric actuators was developed, in which the discontinuous switching function was replaced by a PID regulator to eliminate chattering, while the hysteresis and other nonlinear effects were regarded as an unknown disturbance and were rejected by the PID-based SMC. The experimental results [18] demonstrated that the PID-based SMC can effectively compensate for the hysteresis that exists in a PEA, thus leading to an improved PEA performance.

If disturbances and uncertainties can be completely or partially estimated, such estimations should greatly facilitate their compensation by means of control. In the literature, DOB control schemes were employed [19] ─ [21]; for example, the DOB-SMC was exploited to improve the performance of piezoelectric actuators [22], [23]. Compared to single DOF nano-positioning systems, less research on the control of multi-DOF nano-positioning stages has been reported. In [24], a velocity observer was integrated with SMC to eliminate the coupling effect (i.e., the motion caused to other DOFs when a voltage is applied to one DOF) of a six-DOF motion stage; and the simulations showed that the stage could be manipulated with the same accuracy as that of the position sensors. However, disturbance was neglected in the controller design and was supposed to be rejected by the SMC (which might increase chattering). In addition, experimental verification was not provided in the study [24]. In [25], the sliding mode concept was utilized in the design of a disturbance observer, which decoupled a precision planar motion stage; and the PID control was employed to improve the dynamics of the stage as demonstrated in the experiments. However, the use of discrete switching control may induce serious chattering problems, thereby degrading the controller performance.

Common of the above studies on the multi-DOF nano-positioning stages is that their structures were known and as such physical models can be developed to describe their behaviors. In reality, the challenge is that the commercially-available multi-DOF nano-positioning stages are typically provided without the information on the internal structure and as a result, it is difficult, even impossible, to build their physical models for the control purpose. To rise to this challenge, this paper presents the development of a DOB-SMC for the three-DOF nano-positioning stage with unknown structure. Specifically, the nonlinearity of the nano-positioning stage is estimated through the use of an observer and then compensated by means of the PID-based SMC. The contribution of this paper rests on (1) the development of a novel control scheme that integrates the PID-based SMC with a disturbance observer and (2) the application of the developed control scheme to the three-DOF nano-positioning stage with unknown structure.

8.5.3 DOB-SMC for the Three-DOF Nano-positioning Stage

Figure 8.1 shows the control scheme of the DOB-SMC for the three-DOF nano-positioning stage. Due to the unknown structure of the nano-positioning stage, the plant was identified as a black box dynamic system, which is decoupled by the disturbance observer. By integration with the disturbance observer, the plant can be regarded as a desired decoupled three-input-three-output system, in which each pair of inputs and outputs can be controlled separately by a PID-based SMC. Since the coupling effect is compensated by the disturbance observer, the disturbance to be rejected by the PID-based SMC is reduced. Therefore, the

tracking error is expected to be less in comparison to the three nominal SMC introduced in [13]. Due to the imperfection of decoupling, integration of the disturbance observer may not completely compensate for the interaction between each pair of inputs and outputs. Such an error is considered to be an uncertainty and is estimated according to the desired decoupled system. This error is integrated in the design of the equivalent control of the SMC. Other uncertainties which are not considered in the controller design are treated as the input of the plant and rejected by the PID-based SMC.

8.5.3.1 Design of the disturbance observer

The disturbance observer developed in this section is for the multi-input-multi-output (MIMO) plant with the same number inputs and outputs (so called the square system). Figure 8.2 shows the control scheme with the disturbance observer.

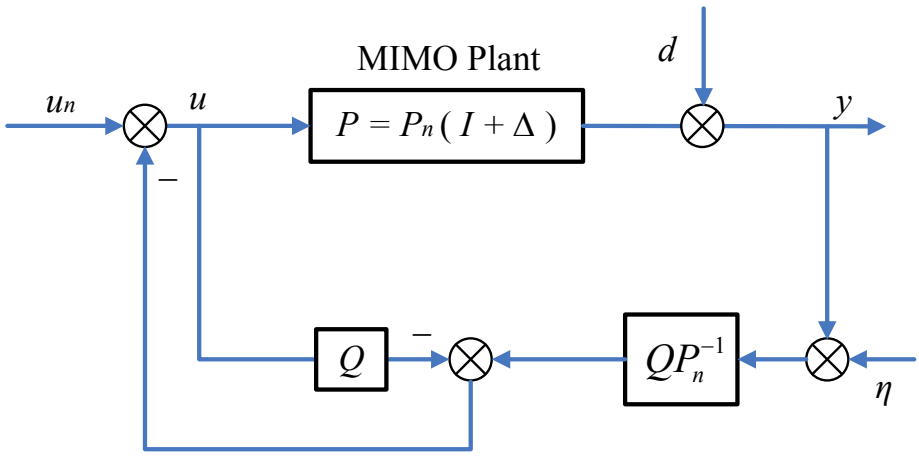

Figure 8. 2 Control scheme with the disturbance observer

Considering the plant P with both multiplicative model error Δ and external disturbance d, its output can be expressed as

$$y = Pu + d = P_n(I + \Delta)u + d \tag{8.1}$$

where $u \in R^m$ is the input to the plant and $y \in R^m$ is the output, m is the size of the square system, and P_n is the nominal or desired model of the plant. Usually, P_n is chosen as a diagonal transfer matrix for the decoupling

$$P_n(s) = diag[P_{n1}(s) \quad P_{n2}(s) \quad \cdots \quad P_{nm}(s)]. \tag{8.2}$$

where s is the Laplace operator and $P_{nj}(j = 1, 2, \cdots, m)$ are the nominal transfer functions for the corresponding pairs of inputs and outputs. The objective of the design is to obtain

$$y = P_n u_n \tag{8.3}$$

as the input-output relation in the presence of the disturbance and uncertainties, where u_n is the command input.

Letting

$$\sigma = y - P_n u \tag{8.4}$$

then,

$$y = P_n u + \sigma\ . \tag{8.5}$$

Substituting Equation (8.5) into Equation (8.3) yields

$$u = u_n - P_n^{-1}\sigma \tag{8.6}$$

where

$$P_n^{-1}(s) = diag[P_{n1}^{-1}(s) \quad P_{n2}^{-1}(s) \quad \cdots \quad P_{nm}^{-1}(s)]. \tag{8.7}$$

Since the inverse of the nominal transfer function $P_{nj}^{-1}(s) \quad (i = 1, 2, \cdots, m)$ may be unstable, in reality it is always multiplied by the diagonal matrix of unity gain low pass filters

$$Q(s) = diag[Q_1(s) \quad Q_2(s) \quad \cdots \quad Q_m(s)] \tag{8.8}$$

such that $QP_n^{-1}(s)$ is causal. Therefore, Equation (7.6) becomes

$$u = u_n - QP_n^{-1}\sigma = u_n - QP_n^{-1}(y + \eta) + Qu \tag{8.9}$$

where η is the sensor noise from the output of the plant. This leads to the control scheme shown in Figure 8.2.

The equation that relates y to u_n, d, and η is

$$y = [I + P(I-Q)^{-1}QP_n^{-1}]^{-1}\{P(I-Q)^{-1}u_n + d - P(I-Q)^{-1}QP_n^{-1}\eta\} = T_{uy}u_n + T_{dy}d + T_{\eta y}\eta \tag{8.10}$$

where $T_{uy} = [I + P(I-Q)^{-1}QP_n^{-1}]^{-1}P(I-Q)^{-1}$ is the transfer function from u_n to y; $T_{dy} = [I + P(I-Q)^{-1}QP_n^{-1}]^{-1}$ is the transfer function from d to y; and $T_{uy} = -[I + P(I-Q)^{-1}QP_n^{-1}]^{-1}P(I-Q)^{-1}QP_n^{-1}$ is the transfer function from η to y.

Since,

$$T_{dy} = [I + P(I-Q)^{-1}QP_n^{-1}]^{-1} = I - P(QP_n^{-1}P + I - Q)^{-1}QP_n^{-1} \quad , \tag{8.11}$$

then Equation (8.11) would be zero if $Q(j\omega) = I$ at low frequencies, indicating that the disturbance has been completely rejected by the disturbance observer.

Similarly, for low frequencies, the transfer function from u_n to y

$$T_{uy} = [I + P(I-Q)^{-1}QP_n^{-1}]^{-1}P(I-Q)^{-1} = [(I-Q)P^{-1} + QP_n^{-1}]^{-1} \tag{8.12}$$

becomes $T_{uy} = P_n$ when $Q(j\omega) = I$. This means that the MIMO system has been regulated as the desired model.

The transfer function from η to y

$$T_{uy} = -[I + P(I-Q)^{-1}QP_n^{-1}]^{-1}P(I-Q)^{-1}QP_n^{-1} \tag{8.13}$$

should be designed to be zero at high frequencies, which requires $Q(j\omega) = 0$. Therefore, the choice of Q as a diagonal matrix of unity gain low pass filters as given in Equation (8.8) fulfills these requirements.

The Q filter is designed for a single-input-single-output (SISO) piezoelectric actuator. Since both Q and P_n are diagonal matrices, Equation (8.9) becomes

$$u_j = u_{nj} - Q_j P_{nj}^{-1}(y_j + \eta_j) + Q_j u_j \quad (j = 1, 2, \cdots, m) \tag{8.14}$$

which means that the Q filter can be designed separately for each input-output pair.

8.5.3.2 Discrete PID-based SMC

The use of disturbance observer, the MIMO plant can be decoupled as desired. However, due to imperfection of the DOB compensation, errors may exist in each output, denoted as $\delta_i (i = 1, 2, \cdots, m)$. This can be estimated as

$$\delta_j = y_j - y_{nj} (j = 1, 2, \cdots, m) \tag{8.15}$$

where $y_{nj} = P_{nj} u_j (j = 1, 2, \cdots, m)$ is the nominal output. This error should be considered in design of the SMC. In this section, the SMC design will be introduced based on the dynamic model for each input-output pair. For convenience, the number j is omitted.

Consider the discrete nominal model described by the pth order transfer function

$$P_p(z) = \frac{\sum_{j=0}^{p} b_j z^{-j}}{1 + \sum_{i=1}^{p} a_i z^{-i}} \tag{8.16}$$

where b_0, a_i and b_i $(i = 1, 2, \cdots, p)$ are parameters of the transfer function. It can be regarded

as a cascade of the numerator $P_1(z)$ and the denominator $P_2(z)$

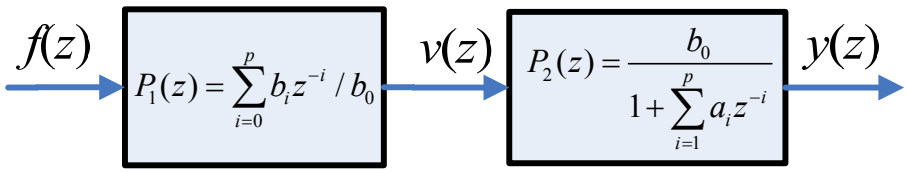

Figure 8. 3 Block diagram of a discrete *n*th order SISO system

f(*z*) and *y*(*z*) are the input and the output of the dynamics, respectively, and *v*(*z*) is an intermediate variable.

Let the nominal state be

$$x_n(k)=[y_n(k-p),\cdots,y_n(k-2),y_n(k-1)]^{\mathrm{T}} \tag{8.17}$$

Then, the transfer function $P_2(z)$ can be written in its discrete state space form as

$$x_n(k+1)=A_d x_n(k)+B_d v(k) \tag{8.18}$$

where $v(k)$ is the control input signal at time kT; and $A_d=\begin{bmatrix}0_{(p-1)\times 1} & I_{(p-1)\times(p-1)}\\ -a_p & \boldsymbol{\alpha}\end{bmatrix}$ $(\boldsymbol{\alpha}=\begin{bmatrix}-a_{p-1} & -a_{p-2} & \cdots & -a_1\end{bmatrix})$ and $B_d=\begin{bmatrix}0_{(p-1)\times 1} & b_0\end{bmatrix}^T$ represent the system matrices of the discrete state space model.

Denoting $x(k)=[y(k-p),\cdots,y(k-2),y(k-1)]^{\mathrm{T}}$ and $\Delta(k)=[\delta(k-p),\cdots,\delta(k-2),\delta(k-1)]^{\mathrm{T}}$, considering Equation (8.15) yields

$$x(k+1)=A_d x(k)+B_d v(k)+\varepsilon(k) \tag{8.19}$$

where

$$\varepsilon(k)=\Delta(k+1)-A_d\Delta(k)\,. \tag{8.20}$$

Equation (8.20) is a non-causal which cannot be implemented in the computer. Therefore,

$\Delta(k+1)$ has to be estimated based on past values. Using trapezoid estimation,

$$\Delta(k+1) = 2\Delta(k) - \Delta(k-1) \tag{8.21}$$

and thus

$$\varepsilon(k) = (2I - A_d)\Delta(k) - \Delta(k-1). \tag{8.22}$$

The error state is defined as

$$e(k) = x(k) - x_d(k) \tag{8.23}$$

where $x_d(k)$ is the desired state. The objective of SMC is to force the error state, regardless of its initial value, to move to the sliding surface in a finite amount of time and then converge to zero. If the desired reference state is designed to be

$$x_d(k) = [y_d(k-p), \cdots, y_d(k-2), y_d(k-1)]^{\mathrm{T}} \tag{8.24}$$

where y_d is the desired output, then the dynamics of the tracking error state can be directly derived from Equations (8.19) and (8.23), i.e.,

$$e(k+1) = A_d e(k) + A_d x_d(k) - x_d(k+1) + B_d v(k) + \varepsilon(k) \tag{8.25}$$

Considering only the zero order and first order derivatives and neglecting the disturbance, a perfect system requires $e(k) = 0$ at any time, which leads to

$$A_d x_d(k) - x_d(k+1) + B_d v(k) = 0 \tag{8.26}$$

Equation (8.26) can be satisfied if and only if [26]

$$[A_d x_d(k) - x_d(k+1)](I - B_d{}^{\dagger} B_d) = 0 \tag{8.27}$$

where $B_d{}^{\dagger}$ is the pseudo inverse of matrix B_d.

As introduced in [18], input *v* can be divided into two components, i.e.,

$$v(k) = v_1(k) + v_2(k) \tag{8.28}$$

where

$$v_1(k) = B_d{}^{\dagger}[x_d(k+1) - A_d x_d(k)] \tag{8.29}$$

It can be verified that for the controllable canonical state space model (8.18) Equation (8.27) is satisfied. Therefore, substituting Equations (8.28) and (8.29) into Equation (8.27) leads to the nominal SMC design problem [26], i.e.,

$$e(k+1) = A_d e(k) + B_d v_2(k) + \varepsilon(k) \quad . \tag{8.30}$$

The sliding surface $s(k)$ is designed to be

$$s(k) = Se(k) = 0 \tag{8.31}$$

where matrix S defines how the tracking error converges to zero.

Combining Equations (8.30) and (8.31) yields

$$SA_d e(k) + SB_d v_2(k) + S\varepsilon(k) = 0 \, . \tag{8.32}$$

Therefore, $v_2(k)$ can be decomposed into the equivalent control $v_{eq}(k)$ and the switching rule $v_{SM}(k)$, where

$$v_{eq}(k) = -(SB_d)^{-1} SA_d e(k) \tag{8.33}$$

and

$$v_{SM}(k) = -[Ps(k) + I\sum_{i=0}^{k} s(i)T + D\frac{s(k) - s(k-1)}{T}] \tag{8.34}$$

and where P, I, and D are parameters of the discrete PID-based sliding mode control.

It can be proved that the state will move towards the sliding surface and converge to zero. Therefore, zigzag motion of the states and the steady state error of the output are avoided.

According to the transfer function $P_1(z)$, the input f can be derived from v, which is a desired value calculated from the SMC, so that

$$f(k) = \frac{[v(k) - b_1 f(k-1) - \cdots - b_n f(k-n)]}{b_0}. \tag{8.35}$$

Therefore, $P_1(z)$ yields

$$\frac{f(z)}{v(z)} = \frac{1}{b_0 z^n + b_1 z^{n-1} + \cdots + b_{n-1} z + b_n} \quad . \tag{8.36}$$

Equation (8.36) indicates that the poles of the transfer function from v to f are the zeroes of the plant. As long as the zeroes of the plant are located inside the unit circle, the control is stable. Otherwise, optimal inversion needs to be applied.

The objective of optimal inversion is to develop a stable input f such that it minimizes the cost function

$$J = [f(k) - f_d(k)]^T Q[f(k) - f_d(k)] + f^T(k) R f(k) \tag{8.37}$$

where $f_d(k) = \frac{v(k)}{b_0} - \frac{b_1}{b_0} f(k-1) - \frac{b_2}{b_0} f(k-2) - \cdots - \frac{b_n}{b_0} f(k-n)$, and Q and R are the weight matrices which determine the stability of the optimal inversion. For example, if the norm of weight matrix R is high, the optimization will smooth the input in order to reduce the energy supply to the system. In this case, the output $f(k)$ does not track the input $f_d(k)$.

Minimizing the cost function given in (8.37) requires that

$$\partial J / \partial f(k) = 0 \tag{8.38}$$

Solution of Equation (8.38) leads to the optimal input

$$f_{opt}(k) = \frac{Q[v(k) - \sum_{i=1}^{n} \frac{b_i}{b_0} f(k-i)]}{R + Q}. \tag{8.39}$$

Thus, Equation (8.39), together with Equations (8.28), (8.29), (8.33) and (8.34), form the discrete

PID-based SMC.

8.5.4 Experiments and Results

Experiments were implemented on a commercially available nano-positioning stage (P-558.TCD, Physik Instrumente), as shown in Figure 6.1, to verify the effectiveness of the proposed methods. In this stage, four piezoelectric actuators are used to actuate the stage, generating linear displacements along the vertical direction Z and two rotations around the horizontal axes of R_x and R_y. Table 6-1 shows the motion range and resolution of each DOF.

For displacement measurements, three capacitive displacement sensors built in the actuator were employed. All displacements were measured with a sampling interval of 2 ms in this study. The relationship between the sensors' displacements and the outputs Z, R_x and R_y is supplied by the manufacturer. Both the actuators and the sensors in the stage are connected to a host computer via a digital piezo controller (E-761, Physik Instrumente) and controlled via Labview programs, as shown in Figure 6.1b. As instructed by its manual, the piezo controller can drive the actuator with a maximum operating frequency of 10-20 Hz if 30-50 V input voltage is applied. The controller can be manipulated in both open-loop and closed-loop modes. In the open-loop mode, a four- dimensional voltage signal is generated by the computer and transferred to the controller, where the voltage signal is amplified and applied to each piezoelectric actuator. Since there are 4 inputs and 3 outputs, actuation redundancy exists in the open-loop manipulation, which might destroy the nano-positioning stage if they are not properly coordinated. Therefore, the operation of the stage in the open-loop mode is not recommended by the manufacturer. In the

closed-loop mode, a three-dimensional reference signal is generated in the computer and then sent to the controller, where the PID scheme is applied to generate the control action or voltage to each piezoelectric actuator. The closed-loop mode can be regarded as a 3-input-3-output system without actuation redundancy, which was employed for the experiments presented in this paper.

Since only the nominal plant model is required in the disturbance observer design, to account for the unknown structure of the nano-positioning stage three auto-regressive models (ARX) were identified to describe the dynamics for each input-output subsystem. The coupling effects among the axles are considered to be disturbances which are rejected by the proposed method. Experiments was performed to identify the parameters of the nominal plant model and then, the DOB-SMC, as designed based on the nominal model, was used to control the nano-positioning stage for tracking sinusoidal reference signals. Also, dynamic tracking control with the proposed methods was implemented and the results were compared to the three nominal SMC introduced in [13] using a PID regulator instead of the boundary layer control.

8.5.4.1 Parameter Identification

Experiments were performed to identify the model parameters for the nano-positioning stage. Since a diagonal nominal plant model is needed in the design of a DOB-SMC and as such the transfer function from each input channel to the corresponding output was identified. Due to the unknown structure of the nano-positioning stage, in this study three ARX models were employed to describe the dynamics of each input and output subsystem. Based on our previous research

[27] - [30], the dynamics order was chosen as two. For model identification, a 40 μm reference chirp signal with frequency ranging from 1 to 100 Hz was applied to Channel 1 (Reference *Z* channel) and the corresponding output in the *Z* direction was measured. From the results obtained, the model parameters were identified using the least squares method, giving the model

$$y(k) = 1.699y(k-1) - 0.7394y(k-2) - 0.004917u(k-1) + 0.04512u(k-2) \quad (8.40)$$

For the other two input and output subsystems in rotation, 200 μrad reference chirp signals with frequency ranging from 1 to 100 Hz were applied to the R_x and R_y channels and the corresponding outputs were measured. Using the same estimation method, the ARX models for the sub-systems were obtained as well, given by

$$y(k) = 1.796y(k-1) - 0.8122y(k-2) - 0.001969u(k-1) + 0.03962u(k-2) \quad (8.41)$$

and

$$y(k) = 1.832y(k-1) - 0.847y(k-2) - 0.001185u(k-1) + 0.02997u(k-2) \quad (8.42)$$

8.5.4.2 Results of experimental verification

In the verification experiments, three types of inputs were used as the reference signals for tracking. The first type of inputs was sinusoidal signals with different amplitudes and frequencies varying from 1 to 10 Hz. The second type of inputs was a piecewise continuous function consisting of different-amplitude sinusoidal signals with the same frequency (PWSW), as shown in Figure 4.8*a*. The amplitudes of the second, third and fourth period of the sinusoidal signals were 100%, 50% and 15% of the amplitude of the first period, respectively. The last type, shown in Figure 4.8*b*, was a superposition of four sinusoidal singals with different frequencies,

amplitudes and phase delays (SW), and displacements w given by Equation (4.47).

The DOB-based SMC for MIMO systems developed in this paper was then implemented on the nano-positioning stage. The output displacement in each direction was estimated by an α-β filter which is a simplified observer for estimation and filtering. The parameters in the α-β filter were adjusted by trial-and-error, leading to $\alpha = 0.5$ and $\beta = 0.002$. The sliding surface was defined by Equation (8.33) with S being [0.2, 1]. The cut-off frequency in the DOB-SMC was selected to be 30 Hz. To improve tracking performance, the parameters of the PID-based SMC were adjusted based on the tracking performance in each inputs and output subsystem. For comparison, the nominal PID-based controller was also implemented on the nano-positioning stage. Table 8-1 shows the PID parameters that were adjusted for optimal performance. Table 8-2 and Table 8-3 show the tracking performance of the nano-positioning stage, obtained by means of the developed method as compared to the nominal PID-based SMC. The tracking error was calculated in terms of the 2-norm of the difference between the desired and measured outputs.

Table 8- 1 PID parameters adjusted for the DOB-based SMC and nominal SMC

Parameters	Channel	P	I	D	R	Q
DOB-based SMC	1	0.3	0.5	0	0.1	1
	2	0.1	0.3	0	0.05	1
	3	0.05	0.1	0	0.05	1
Nominal PID-based SMC	1	0.1	0.6	0	0.1	1
	2	0.2	0.3	0	0.05	1
	3	0.05	10	0	0.05	1

Table 8- 2 Tracking error by means of the DOB-based SMC

Reference inputs	Frequency	Z (μm)	$R_x(\mu rad)$	$R_y(\mu rad)$
10 μm sinusoidal inputs in Z direction	1 Hz	0.2435	0.0384	**0.0208**
	5 Hz	1.1848	0.2586	0.046
	10 Hz	2.7955	0.4356	0.1012
10 μrad sinusoidal inputs in R_x direction	1 Hz	0.0008	0.1399	**0.0682**
	5 Hz	0.0011	1.1099	0.0215
	10 Hz	0.0024	2.4265	0.0386
10 μrad sinusoidal inputs in R_y direction	1 Hz	0.0009	0.018	0.1378
	5 Hz	0.0011	0.0245	0.7901
	10 Hz	0.0022	0.0717	2.0945

Table 8- 3 Tracking error by means of the nominal PID-based SMC

Reference inputs	Frequency	Z (μm)	$R_x(\mu rad)$	$R_y(\mu rad)$
10 μm sinusoidal inputs in Z direction	1 Hz	0.4481	0.055	0.0179
	5 Hz	2.2843	0.2601	0.0574
	10 Hz	4.4031	0.5002	0.1782
10 μrad sinusoidal inputs in R_x direction	1 Hz	0.0008	0.6204	0.0133
	5 Hz	0.0012	2.235	0.0251
	10 Hz	0.0025	3.3913	0.0445
10 μrad sinusoidal inputs in R_y direction	1 Hz	0.0009	0.0184	0.3133
	5 Hz	0.0012	0.0358	2.3295
	10 Hz	0.0025	0.0789	3.3418

From Table 8-2 and Table 8-3, it can be seen that the developed method performs much better than the nominal PID-based SMC controller, especially in the diagonal direction. Moreover, as the frequency increases, the performace improvement becomes more obvious. For

example, when a 1 Hz, 10 μm sinusoidal input was applied to the *Z* direction, the tracking error in the *Z* direction which occurred using the DOB-SMC was 0.2435 μm, which is 0.2046 μm less than that of the nominal PID-based SMC controller. In comparison, for a 10 Hz sinusoidal input in the *Z* direction, the difference increased to 1.6076 μm.

Also, it can be seen that the coupling effect was reduced by means of the developed method. For example, for the 10 Hz, 10 μrad sinusoidal input in the R_y direction, the tracking error in the *Z* direction using the proposed method was 0.0022 μm, which is 88% less than the error by using the nominal PID-based SMC controller. In the other hand, it is also noted that there are two data bolded in Table 8-2, showing the error with the DOB-SMC is slightly bigger than the one with PID-based SMC. Both of them are the coupling effects in the R_y direction when a sinusoidal input of 1 Hz was applied to the *Z* and R_y directions, respectively. Given their small values, the authors would not see specific reasons behind their difference.

To further show the performance of the proposed method, two more experiments were designed and implemented on the nano-positioning stage. In the first experiment, a 2 Hz, 10 μm sinusoidal input was applied to the Z direction and a 5 Hz, 50 μrad sinusoidal signal was set as the reference input to the R_x direction, while the zero reference signal was given in the R_y direction. In the second experiment, a 2 Hz, 10 μm PWSW input was applied to the *Z* direction and a 10 Hz, 50 μrad SW signal was selected as the reference input to the R_y direction, with the other direction input kept at zero. Figures 8.4 and 8.5 show the tracking performance.

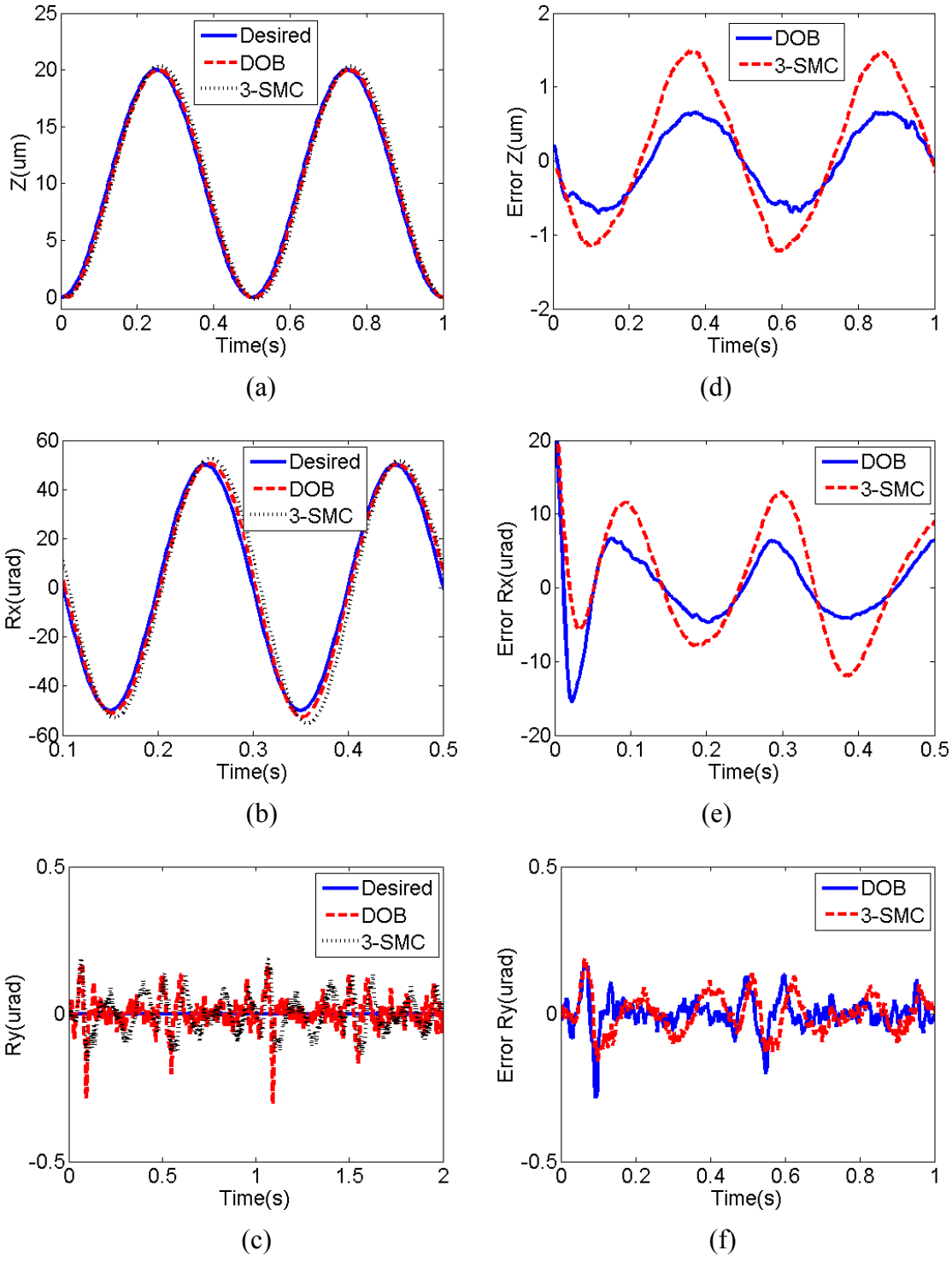

Figure 8. 4 Tracking performance of the discrete PID-based SMC designed by model reference approach as compared with the three nominal PID-based SMC (stated as 3-SMC) introduced in [13] for a 2 Hz, 10 μm sinusoidal input in the Z direction and 5 Hz, 50 μrad sinusoidal input in the *Rx* direction: output displacement in (a) Z direction, (b) *Rx* direction and (c) *Ry* direction; tracking error in (d) Z direction, (e) *Rx* direction and (f) *Ry* direction;

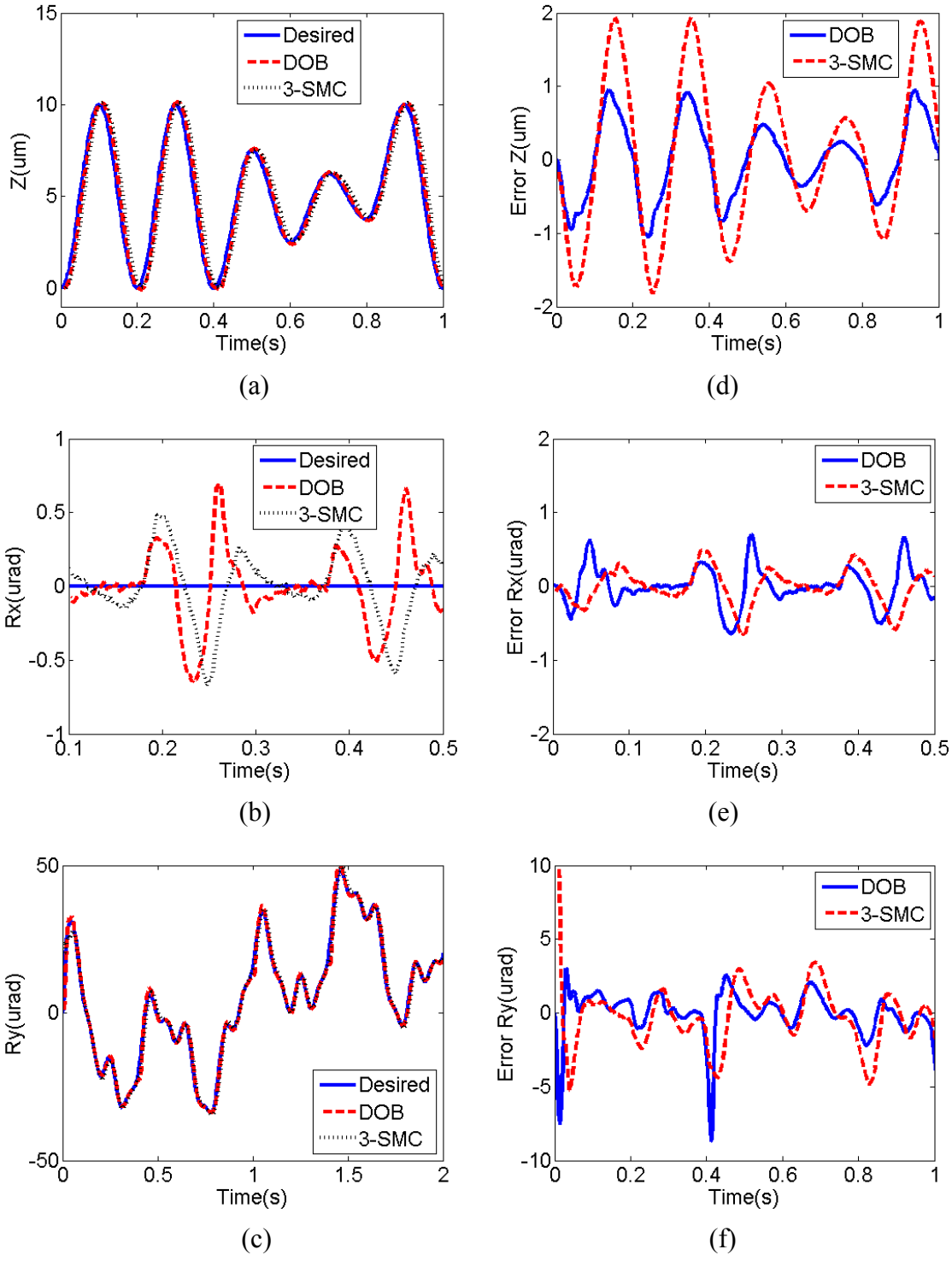

Figure 8. 5 Tracking performance of the discrete PID-based SMC designed by model reference approach as compared with the three nominal PID-based SMC (3-SMC) introduced in [13] for the 5 Hz 10 μm PWSW input in Z direction and 10 Hz 50 μrad SW input in *Ry* direction: output displacement in (a) Z direction, (b) *Rx* direction and (c) *Ry* direction; tracking error in (d) Z direction, (e) *Rx* direction and (f) *Ry* direction;

Compared to the nominal PID controller, the DOB-SMC for MIMO systems performed better for the combined signals in all three directions, as seen from the tracking performance of the second experiment. Using the DOB-SMC, the tracking errors are 0.6861 μm and 1.7618 μrad in the Z and R_y directions, respectively, which were 0.3361 μm and 0.7141 μrad lower than the nominal PID-based SMC. Similar results also obtained in the first experiment. However, since a low frequency component existed in the input signal, it is not easy to determine the advantage on the decoupling effect of using the proposed method over the PID-based SMC. For example, in the first experiment, the tracking error of the nano-positioning stage controlled by the DOB-based SMC was 0.0507 μm which is only 0.0118 μm less than that of the nominal PID-based SMC.

8.5.5 Conclusions and Discussion

PID-based SMC has shown promise in the control of nano-positioning systems due to its disturbance rejection. In this control scheme, all nonlinear effects and the model uncertainty are treated as unknown disturbances to the nano-positioning system. For improvement, this paper presents the development of the DOB-SMC, in which the nonlinear effects of the three-DOF nano-positioning stage and model uncertainties are partially predicted and then compensated by the PID-based SMC. To illustrate the effectiveness of the proposed control schemes, experiments were performed and the results were compared with those from the nominal PID-based SMC. It has been shown that by integration of the disturbance observer into the PID-based SMC, the disturbance to be rejected by the feedback control is reduced and the control performance of the

three-DOF nano-positioning stage is greatly improved. This improvement becomes more profound as the frequency increases from 1 Hz to 10 Hz. The developed method may also be employed in the application with a higher frequency, which has not been validated due to the limitation of the experimental settings used in the present study.

8.5.6 Acknowledgment

The support to the present study from the China Scholarship Council (CSC) and the Natural Sciences and Engineering Research Council (NSERC) of Canada is acknowledged.

9 Conclusions and Future Work

PEAs have been widely employed in various nano-positioning applications. However, hysteresis and other nonlinear effects greatly degrade the performance of PEAs. To exploit the full potential of PEAs in nano-positioning applications, this work presents the development of the model and its corresponding control schemes for both the one-DOF PEAs and three-DOF PEAs.

The control schemes developed to improve the performance of one-DOF PEAs can be generally divided into two categories. If modeling of hysteresis is not considered, the hysteresis together with other nonlinearities can be regarded as disturbances and rejected by the robust controller. This leads to the development of the discrete PID-based SMC, with details introduced in Chapter 4. If hysteresis can be completely or partially modeled, the integration of hysteresis models into control schemes will improve the control performance (Chapter 5). Based on the fact that PEAs are commonly modeled as the cascade of the dynamics and hysteresis, as stated in Chapter 3, an inverse hysteresis model can be employed to compensate for the hysteresis nonlinearity. Combined with the PID-based SMC, it is experimentally verified that the performance of the PEA can be further improved. Alternatively, by applying DOB, the hysteresis information can be estimated and integrated in the design of the PID-based SMC, leading to the development of the DOB-based SMC.

A straightforward modeling method for multi-DOF PEAs can be based on the internal configuration by means of physics laws. However, such details with regard to the internal structure are often not provided by the manufactures. In this situation, a state space model is developed in Chapter 6, based on which the output tracking based SMC can be designed and implemented in the control of multi-ODF PEA (Chapter 7). Integration of DOB into the SMC will further improve the performance of the multi-DOF PEA, as illustrated in Chapter 8.

9.1 Concluding Remarks

The aim of this research work is to develop a feedforward or DOB based SMC to improve the PEA performance and implementing it digitally. The main conclusions of this research are summarized as follows.

1. The discrete ARMA-based hysteresis model can predict the hysteresis of the PEA with acceptable accuracy. Online estimation allows better parameter identification for the discrete ARMA-based hysteresis model than the least square method. However, the model shows larger errors at high frequencies due to the estimation of the integral term in the discrete hysteresis equation. Using a quadratic equation to estimate the integral term can reduce the discrete estimation error at high input frequencies. Therefore, it should be preferred to use the quadratic equation at high input frequencies.

2. By applying the discrete PID regulator instead of the discontinuous switching control, such problems as the chattering, zigzag state motion and steady state error, which

are typically observed in the DSMC, are eliminated. The output tracking integrated discrete PID-SMC developed from both the traditional design approach and the model reference approach can achieve better tracking performance, especially at low sampling rates. As the input frequency increases, the performance improvement with the proposed method becomes more profound. Due to the non-requirement on the derivability of the reference signal, the output tracking integrated discrete PID-SMC designed by the model reference approach has a better performance than the one designed by the traditional approach.

3. Inclusion of the inverse hysteresis and DOB in the DSMC design are more effective in terms of the hysteresis compensation. It has been shown that the disturbance, which is rejected by the switching control of DSMC, is reduced, thus improving the performance of the discrete PID-based SMC. Based on the examined cases with inputs of varying frequencies, it is recommended that the discrete inversion based PID-SMC should be used if the input frequency is low, while the discrete DOB-based PID-SMC is preferred for applications with higher frequencies.

4. By combining the MAP online estimation methods, the Hankel matrix of the state space model is identified and the model parameters can be updated as new observation is available. Since MAP estimation utilizes the posteriori parameter information which have the beneficial effect of reduction of variances of parameter estimators, MAP online estimation method performs better in the model identification than the least squares method.

5. The application of the discrete PID-based SMC designed for SISO systems are successfully extended to the control of MIMO system. The discrete output tracking based PID-SMC developed from the model reference approach can achieve better tracking performance. As the input frequency increases, the advantage of using the proposed method becomes more profound.

6. By integration of the DOB in the discrete PID-based SMC design, the disturbance, which is rejected by the DSMC, is reduced and the performance of the discrete PID-based SMC is greatly improved. This improvement becomes more profound as the frequency increases and thus the developed method is also expected to be employed in the application with a higher frequency.

9.2 Future Work

It is worth explicitly stating the limitations of the methods used in the present study so that future work based upon this research moves forward successfully.

First, the shape functions are considered to be linear in the development of the discrete ARMA based hysteresis model proposed in Chapter 3. Better parameter identification is expected by applying special designed nonlinear shape functions in the hysteresis model.

Second, the optimal inversion control is integrated in the discrete PID-based SMC in Chapter 4 to compensate for the numerator of the plant. If the zeros of the plant locate outside the unite circle in the complex plane, compensation error exists in the optimal

inversion control since the inverse numerator of the plant is unstable. Although, this compensation error is considered to be disturbance and rejected by the DSMC, it has a negative effect on the tracking performance of the discrete PID-based SMC.

Finally, the output tracking based discrete PID-SMC developed in Chapter 7 is only applicable in the control of square MIMO systems.

Based upon the work presented in this dissertation, a number of studies can be considered for the future work along the similar direction.

1. The discrete inversion feedforward based PID-SMC can be further improved by integration of the inverse Preisach model, which is shown to have a high accuracy in the parameter estimations in the literature. However, compared with the discrete ARMA based hysteresis model, the inverse Preisach model has more rigorous requirement in the digital implementation. That might challenge its application with high sampling rates.

2. Extend the application of the output tracking integrated discrete PID-SMC developed in Chapter 7 to the control of non-square multi-DOF actuators. If the number of inputs is more than the number of outputs, actuation redundancy exists and thus the control of each actuator should coordinate with each other so as to avoid the deformation or internal stress of the system. To alleviate this problem, control allocation might be employed, which distribute the control signal to different actuators based on certain rules to prevent actuation redundancy.

3. There are two different approaches to implement DSMC in the control of complicated MIMO system without measurable states. The first one is to design a state

tracking based DSMC combined with the state estimation. The second one is to design an output tracking based DSMC as presented in Chapter 7. Comparison between these two approaches has not been reported in the literature.

4. It is expected that the discrete PID-based SMCs developed in Chapters 7 and 8 would also be employed in the applications with high frequency, such as fast steering mirrors. This will further verify the effectiveness of the proposed control methods on multi-DOF PEA-driven positioning systems.

References

[1] P. R. Ouyang, R. C. Tjiptoprodjo, W. J. Zhang and G. S. Yang, Micro-motion Devices Technology: The State of Arts Review, International Journal of Advance Manufacture Technology (2008) 38: 463-478

[2] S. Devasia and S. O. R. Moheimani, A Survey of Control Issues in Nano-positioning, IEEE Transactions on Control System Technology, Vol.15, No.5, Sep.2007, 802-823

[3] D. Chapman, W. Thomlinson, R. E. Johnston and D. Washburn, Diffraction Enhanced X-Ray Imaging, Physics in Medicine and Biology (1997) 42: 2015-2025

[4] A. Sebastian and S. M. Salapaka, Design Methodologies for Robust Nano-Positioning, Transactions on Control System Technology, Vol.13, No.6, Nov.2005, 868-876

[5] M. Ishitobi, M. Nishi and M. Miyachi, A Survey of Recent Innovations in Vibration Damping and Control Using Shunted Piezoelectric Transducers, IEEE Transactions on Control System Technology, Vol.11, No.4, July 2003, 482-494

[6] D. Corft, G. Shed and S. Devasia, Creep, Hysteresis, and Vibration Compensation for Piezoactuators: Atomic Force Microscopy Application, ASME Journal of Dynamic Systems Measurement and Control, Vol. 123, Mar. 2001, 35-43

[7] K. K. Leang and S. Devasia, Feedback-Linearized Inverse Feedforward for Creep, Hysteresis, and Vibration Compensation in AFM Piezoactuators , IEEE Transactions on

Control System Technology, Vol.15, No.5, Sep.2007, 927-935

[8] G. Schitter, P. Menold and H. F. Knapp et. al. High Performance Feedback for Fast Scanning Atomic Force Microscopes, Review of Scientific Instruments Vol.72, No. 8 Aug.2001, 3320-3327

[9] S. C. Tien, Q. Z. Zou and S. Devasia, Iterative Control of Dynamics-Coupling-Caused Errors in Piezoscanners During High-Speed AFM Operation, IEEE Transactions on Control System Technology, Vol.13, No.6, Nov.2005, 921-931

[10] K. K. Leang and S. Devasia, Hysteresis, Creep, and Vibration Compensation for Piezo-actuators: Feedback and Feedforward Control, Proceedings of 2nd IFAC Conference on Mechatronic System, 2002, 283-289

[11] A. Visintin, Differential Models of Hysteresis, Springer-Verlag Berlin Heidelberg, 1994

[12] S. Bashash and N. Jalili, Intelligence Rules of Hysteresis in the Feedforward Trajectory Control of Piezoelectrically-Driven Nanostagers, Journal of Micromachanics and Microengineering (2007) 17: 342-349

[13] Y. Tian, B. Shirinzadeh and D. Zhang, Design and Dynamics of a Three-DOF Flexure-based Parallel Mechanism for Micro/Nano Manipulation, Microelectronic Engineering (2010) 87: 230-241

[14] Y. K. Yong, S. S. Aphale and S. O. R. Moheimani, Design, Identification and Control of a Flexure-based Stage for Fast Nanoscale Positioning, IEEE Transactions on

Nanotechnology, Vol.8, No.1, January 2009, 46-54

[15] H. S. Kim and Y. M. Cho, Design and Modeling of a Novel Three-DOF Precision Micro-stage, Mechatronics (2009) 19: 598-608

[16] P. Gao and S. M. Swei, A Six-Degree-of-Dreedom Micro-manipulator based on Piezoelectric Actuator, Nanotechnology (1999) 10: 447-452

[17] C. Hui, Dynamics and Control of Parallel Manipulators with Redundant Actuation, Msc. Thesis, Electrical and Electronic Engineering at the Hong Kong University of Science and Technology, May, 2001

[18] S. Kock and W. Schumacher, A Parallel X-Y Manipulator with Actuation Redundancy for High-Speed and Active-Stiffness Applications, Proceedings of the 1998 IEEE International Conference on Robotics & Automation, Leuven, Belgium, May. 1998

[19] J. Kim, F. C. Park, S. J. Ryu, J. Kim, J. C. Hwang, C. Park and C. C. Iurascu, Design and Analysis of a Redundantly Actuated Parallel Mechanicsm for Rapid Machining, IEEE Transactions on Robotics and Automation, Vol.17, No.4, Aug. 2001, 423-434

[20] R. Kurtz and V. Hayward, Multiple-Goal Kinematic Optimization of a Parallel Spherical Mechanical with Actuator Redundancy, IEEE Transactions on Robotics and Automation, Vol.8, No.5, Oct. 1992, 644-651

[21] I. D. Walker and S. I. Marcus, Subtask Performance by Redundancy Resolution for Redundant Robot Manipulators, IEEE Journal of Robotics and Automation, Vol.4, No.3,

June 1988, 350-354

[22] X. Du, R. Dixon, R. M. Goodall and A. C. Zolotas, Modelling and Control of a High Redundancy Actuator, Mechatronics (2010) 20: 102-112

[23] H. Jung, J. Y. Shim and D. Gweon, New Open-loop Actuating Method of Piezoelectric Actuators for Removing Hysteresis and Creep, Review of Scientific Instruments, Vol.71, No.9, Sep. 2000, 3436-3440

[24] H. Jung and D. Gweon, Creep Characteristics of Piezoelectric Actuators, Review of Scientific Instruments, Vol.71, No.4, Apr. 2000, 1896-1900

[25] J. H. Zhong, Modeling and Control Piezoceramic Actuator for Nanopositioning, Master Thesis of Department of Mechanical and Aerospace Engineering, North California State University, Aug. 2003

[26] R. Ben Mrad and H. Hu, Dynamic Modeling of Hysteresis in Piezoceramics, 2001 IEEE/ASME International Conference on Advanced Intelligent Mechatronics Proceedings, Como, Italy, July 8-12, 2001

[27] A. Telba and W. G. Ali, Hysteresis Modeling in a Piezoelectric Nanopositioner Stage, Proceedings of the World Congress on Engineering 2011, Vol. 2, WCE 2011, London, U. K., July 6-8, 2011

[28] O. Henze and W. M. Rucker, Identification Procedures of Preisach Model, IEEE Transactions on Magnetics, Vol. 38, No. 2, Mar. 2002, 833-836

[29] I. D. Mayergoyz, Mathematical Models of Hysteresis, Physical Review Letters, Vol. 56, No. 15, Apr. 14, 1986, 1518-1521

[30] S. H. Lee, T. J. Royston and G. Friedman, Modeling and Compensation of Hysteresis in Piezoceramic Transducers for Vibration Control, Journal of Intelligent Material Systems and Structures, Vol. 11, Oct. 2000, 781-790

[31] S. H. Lee and T. J. Royston, Modeling Piezoceramic Transducer Hysteresis in the Structural Vibration Control Problem, Journal of the Acoustical Society of America, 108 (6), Dec. 2000, 2843-2855

[32] H. Hu and R. Ben Mrad, On the Classical Preisach Model for Hysteresis in Piezoceramic Actuators, Mechatronics (2003) 13: 85-94

[33] K. K. Leang and S. Devasia, Design of Hysteresis-Compensating Iterative Learning Control for Piezo-positioners: Application to Atomic Force Microscopes, Mechatronics (2006) 16: 141-158

[34] K. Kuhnen and H. Janocha, Inverse Feedforward Controller for Complex Hysteretic Nonlinearities in Smart-material Systems, Control and Intelligent Systems, Vol. 29, Issue 3, 2001, 74-83

[35] J. H. Oh and D. S. Bernstein, Semilinear Duhem Model for Rate-Independent and Rate-Dependent Hysteresis, IEEE Transactions on Automatic Control, Vol.50, No.5, May 2005, 631-645

[36] J. H. Oh and A. K. Padthe et. al. Duhem Models for Hysteresis in Sliding and Presliding Friction, Proceedings of the 44th IEEE Conference on Decision and Control, and the European Control Conference 2005, Seville, Spain, Dec.12-15, 2005

[37] A. K. Padthe and D. S. Bernstein, A Delay Duhem Model for Jump Resonance

Hysteresis, Proceedings of the 46th IEEE conference on Decision and Control, New Orleans, LA, USA, Dec.12-14, 2007

[38] F. IKhouane, V. Manosa and J. Rodellar, Dynamic Properties of the Hysteretic Bouc-Wen Model, Systems & Control Letters (2007) 56: 197-205

[39] O. G. Bellmunt, F. Ikhouane and D. M. Miracle, Control of Bouc-Wen Hysteretic Systems: Application to a Piezoelectric Actuator, Proceedings of Power Electronics and Motion Control Conference, Sep. 1-3 2008

[40] J. Song and A. Der Kiureghian, Generalized Bouc-Wen Model for Highly Asymmetric Hysteresis, Journal of Engineering Mechanics, Jun. 2006, 610-618

[41] O. G. Bellmunt, F. Ikhouane, P. C. Vilanova and J. B. Jane, Modeling and Validation of a Piezoelectric Actuator, Electrical Engineering (2007) 89: 629-638

[42] C. J. Lin and S. R. Yang, Modeling of a Piezo-actuated Positioning Stage based on a Hysteresis Observer, Asian Journal of Control, Vol. 7, No. 1, 73-80, Mar. 2005, 73-80

[43] H. J. M. T. A. Adriaens, W. L. de Koning, and R. Banning, Modeling Piezoelectric Actuators, IEEE/ASME Transactions on Mechatronics, Vol. 5, No. 4, Dec. 2000, 331-341

[44] R. Banning and W. L.de Koning et.al. State-space Analysis and Identification for a Class of Hysteresis System, Automatica (2001) 37: 1883-1892

[45] G. M. Clayton, S. Tien and A. J. Fleming et. al. Inverse-feedforward of Charge-controlled Piezopositioners, Mechatronics (2008) 18: 273-281

[46] X. B. Chen, Q. S. Zhang, D. Kang, and W. J. Zhang, On the Dynamics of

Piezoelectric Positioning Systems, Review of Scientific Instrument 79. 116101, 2008

[47] S. Salapaka, A. Sebastian, J. P. Cleveland and M. V. Salapaka, High Bandwidth Nano-positioner: A Robust Control Approach, Review of Scientific Instruments, Vol.73, No.9, Sep.2002, 3232-3241

[48] B. Bhikkaji, M. Ratnam, A. J. Fleming and S. O. R. Moheimani, High-Performance Control of Piezoelectric Tube Scanners, IEEE Transactions on Control System Technology, Vol.15, No.5, Sep.2007, 853-866

[49] G. M. Clayton, S. Tien and A. J. Fleming, Hysteresis and Vibration Compensation in piezoelectric actuators by Integrating Charge Control and Inverse Feedforward, Proceedings on 4th IFAC Symposium on Mechatronic Systems, 2006

[50] G. Schitter and A. Stemmer, Identification and Open-Loop Tracking Control of a Piezoelectric Tube Scanner for High-Speed Scanning-Probe Microscopy, IEEE Transactions on Control System Technology, Vol.12, No.3, May. 2004, 449-454

[51] D. Croft and S. Devasia, Vibration Compensation for High Speed Scanning Tunnelling Microscopy, Review of Scientific Instruments, Vol.70, No.12, Dec.1999, 4600-4605

[52] L. Deng and Y. H. Tan, Modeling Hysteresis in Piezoelectric Acuators Using NARMAX Models, Sensors and Actuators (2009) A149: 106-112

[53] D. Song and C. J. Li, Modeling of Piezo Actuator's Nonlinear and Frequency Dependent Dynamics, Mechatronics (1999): 391-410

[54] X. L. Zhang, Y. H. Tan and M. Y. Su, Modeling of Hysteresis in Piezoelectric

Actuators using Neural Networks, Mechanical Systems and Signal Processing (2009) 23: 2699-2711

[55] X. J. Dang and Y. H. Tan, An Inner Product-based Dynamic Neural Network Hysteresis Model for Piezoceramic Actuators, Sensors and Actuators (2005) A121: 535-542

[56] Z. Tong, Y. H. Tan and X. W. Zeng, Modeling Hysteresis using Hybrid Method of Continuous Transformation and Neural Networks, Sensors and Actuators (2005) A119: 254-262

[57] C. J. Chiena, F. S. Lee and J. C. Wang, Enhanced Iterative Learning Control for a Piezoelectric Actuator System using Wavelet Transform Filtering, Journal of Sound and Vibration (2007) 299: 605-620

[58] E. Lin, Generalized Wavelet Formulation of Hysteresis Models for Smart Material Systems, Hysteresis Modeling and Micromagnetics – NIST, Gaithersburg, Maryland, USA, 2009

[59] Y. H. Yu, Z. C. Xiao, E. B. Lin and N. Naganathan, Analytic and Experimental Studies of a Wavelet Identification of Preisach Model of Hysteresis, Journal of Magnetism and Magnetic Materials (2000) 208: 255-263

[60] T. Fett and G. Thun, Determination of room-temperature tensile creep of PZT, Journal of Materials Science Letters (1998) 17: 1929-1931

[61] P. Ge and M. Jouaneh, Tracking Control of a Piezoceramic Actuator, IEEE Transactions on Control Systems Technology, Vol.4, No.3, May 1996, 209-216

[62] K. K. Leang and S. Devasia, Design of Hysteresis Compensating Iterative Control for Piezo-positioners: Application on Atomic Force Microscopes, Mechatronics (2006) 16: 141-158

[63] C. J. Lin and S. R. Yang, Precise Positioning of Piezo-actuated Stages using Hysteresis-Observer based Control, Mechatronics (2006) 16: 417-426

[64] C. Y. Lin and P. Y. Chen, Precision tracking control of a biaxial piezo stage using repetitive control and double-feedforward compensation, Mechatronics (2011) 21: 239-249

[65] F. C. Wang, Y. C. Tsai, C. H. Hsieh, L. S. Chen and C. H. Yu, Robust Control of a Two-Axis Piezoelectric Nano-positioning Stage, Preprints of the 18th IFAC World Congress Milano, Italy, Aug. 28-Sep. 2, 2011

[66] R. F. Fung and W. C. Lin, System Identification and Contour Tracking of a Plane-Type 3_DOF (X, Y, θz) Precision Positioning Table, IEEE Transactions on Control Systems Technology, Vol. 18, No. 1, Jan. 2010, 22-34

[67] T. W. Chen and B. Francis, Optimal Sampled-Data Control Systems, Springer-Verlag Berlin Heidelberg, 1995

[68] J. Vörös, Modeling and Identification of Hysteresis using Special Forms of the Coleman-Hodgdon Model, Journal of Electric Engineering, Vol.60, No.2, 2009, 100-105

[69] R. H. Comstock and W. Acton, Charge Control of Piezoelectric Actuators to Reduce the Hysteresis Effects, United State Patent, Apr.21th, 1981

[70] A. J. Fleminga and S. O. R. Moheimani, A Grounded-load Charge Amplifier for

Reducing Hysteresis in Piezoelectric Tube Scanners, Review of Scientific Instruments 76, 073707 (2005)

[71] A. J. Fleming and S. O. R. Moheimani, Improved Current and Charge Amplifiers for Driving Piezoelectric Loads, and Issues in Signal Processing Design for Synthesis of Shunt Damping Circuits, Journal of Intelligent Material Systems and Structures 2004, Vol. 15, Feb. 2004, 77-92

[72] M. S. Tsai and J. S. Chen, Robust Tracking Control of a Piezoactuator Using a New Approximate Hysteresis Model, Transactions of the ASME, Vol.125, Mar.2003, 96-102

[73] J. M. Cruz-Hernández and V. Hayward, Phase Control Approach to Hysteresis Reduction, IEEE Transactions on Control System Technology, Vol.9, No.1, Jan.2001, 17-26

[74] X. B. Tan and J. S. Baras, Adaptive Identification and Control of Hysteresis in Smart Materials, IEEE Transactions on Automatic Control, Vol.50, No.6, June 2005, 827-839

[75] G. Tao and P. V. Kokotović, Adaptive Control of Plants with Unknown Hysteresis, IEEE Transactions on Automatic Control, Vol.40, No.2, Feb. 1995, 200-212

[76] Y. Wu and Q. Z. Zou, Iterative Control Approach to Compensate for Both the Hysteresis and the Dynamics Effects of Piezo Actuators, IEEE Transactions on Control System Technology, Vol.15, No.5, Sep.2007, 936-944

[77] H. S. Ahn, Y. Q. Chen and K. L. Moore, Iterative Learning Control: Brief Survey and Categorization, IEEE Transactions on Systems, Man and Cybernetics-Part C:

Applications and Reviews, Vol.37, No.6, Nov. 2007, 1099-1121

[78] J. Ghosh and B. Paden, Iterative Learning Control for Nonlinear Nonminimum Phase Plants, Journal of Dynamic Systems, Measurement, and Control, Vol.123, Mar. 2001, 21-30

[79] D. A. Bristow, M. Tharayil and A. G. Alleyne, A Survey of Iterative Learning Control, IEEE Control Systems Magazine, Vol. 26, No. 3, June 2006, 96-114

[80] J. R. Ryoo, T. Y. Doh, M. J. Chung, Robust Disturbance Observer for the Track-Following Control System of an Optical Disk Drive, Control Engineering Practice (2004) 12: 577-585

[81] Y. J. Choi, K. J. Yang, W. K. Chung, H. R. Kim and H. Suh, On the Robustness and Performance of Disturbance Observers for Second-Order Systems, IEEE Transactions on Automatic Control, Vol.48, No.2, Feb. 2003, 315-320

[82] S. Chang, J. G. Yi and Y. T. Shen, Disturbance Observer based Hysteresis Compensation for Piezoelectric Actuators, 2009 American Control Conference, Hyatt Regency Riverfront, St. Louis, Mo, USA, June 10-12, 2009

[83] A. Tesfaye, H. S. Lee and M. Tomizuka, A Sensitivity Optimization Approach to Design of a Disturbance Observer in Digital Motion Control Systems, IEEE/ASME Trans. Mechatronics, Vol. 5, No. 1, Mar. 2000, 32-38

[84] H. C. Liawa, B. Shirinzadeh and J. Smith, Enhanced Sliding Mode Motion Tracking Control of Piezoelectric Actuators, Sensors and Actuators (2007) A138: 194–202

[85] A. Woronko, J. Huang and Y. Altintas, Piezoelectric Tool Actuator for Precision Maching on Conventional CNC Turning Centers, Precision Engineering (2003) 27: 335-345

[86] C. L. Hwang and C. Jan, State Estimator based Feedback Control for a Class of Piezoelectric Systems with Hysteresis Nonlinearity, IEEE Transactions on Systems, Man and Cybernetics-Part A: Systems and Humans, Vol.35, No.5, Sep. 2005, 654-664

[87] S. Khan, M. Elitas, E. D. Kunt and A. Sabanovic, Discrete Sliding Model Control of Piezo Actuator in Nano-Scale Range, IEEE International Conference on Industrial Technology, Dec. 15-17, 2006

[88] X. Xue and J. Tang, Robust and High Precision Control using piezoelectric actuator Circuit and Integral Continuous Sliding Mode Control Design, Journal of Sound and Vibration (2006) 293: 335-359

[89] K. Abidi, A. Sabanovic and S. Yesilyurt, Sliding Mode Control based Disturbance Compensation and External Force Estimation for a piezoelectric actuator, The 8th IEEE International Workshop on Advanced Motion Control, Mar. 25-28, 2004

[90] S. H. Yu, B. Shirinzadeh, G. Alici and J. Smith, Sliding Mode Control of a Piezoelectric Actuator with Neural Network Compensation Rate-dependent Hystersis, Proceedings of the 2005 IEEE International Conference on Robotics and Automation, Barcelona, Spain, Apr. 2005

[91] S. Wang, S. Habibi and R. Burton, Sliding Mode Control for an Electrohydraulic Actuator System with Discontinuous Nonlinear Friction, Proc. IMechE, Vol.222 Part I: J.

Systems and Control Engineering

[92] C. Edwards and S. K. Spurgeon, Sliding Mode Control-Theory and Applications, Taylor & Francis Ltd. 1998

[93] S. Wang, R. Burton and S. Habibi, Filtering Controller in Sliding Mode: From the Estimation to Control, Proc. IMechE, Vol.223 Part I: J. Systems and Control Engineering

[94] K. D. Young, V. I. Utkin and Ü. Özgüner, A Control Engineer's Guide to Sliding Mode Control, IEEE Transactions on Control Systems Technology, Vol.7, No.3, May 1999, 328-342

[95] A. Levant, Homogeneity Approach to High-order Sliding Mode Design, Automatica (2005) 41: 823-830

[96] A. Rhif, A High Order Sliding Mode Control with PID Sliding Surface: Simulation on a Torpedo, International Journal of Information Technology, Control and Automation, Vol. 2, No. 1, Jan. 2012, 1-13

[97] L. Fridman and A. Levant, Higher Order Sliding Modes, In W. Perruquetti and J. P. Barbot, Sliding Mode Control in Engineering, New York: Marcel Dekker, 2002, 53-101

[98] J. Y. Peng and X. B. Chen, PID-based Sliding Mode Control for Piezoelectric Actuators, Mechatronics, Submitted for Possible Publication, Jul. 2011

[99] N. Rafee, T. W. Chen and O. P. Malik, A Technique for Optimal Digital Redesign of Analog Controllers, IEEE Transactions on Control Systems Technology, Vol.5, No.1, Jan. 1997, 89-99

[100] W. B. Gao, Y. F. Wang and A. Homaifa, Discrete-Time Variable Structure Control Systems, IEEE Transactions on Industrial Electronics, Vol.42, No.2, April 1995, 117-122

[101] G. Monsees, Discrete-time Sliding Mode Control, PhD Thesis, Delft University of Technology, 2002, 182 pages, ISBN: 90-77017-83-6

[102] A. Bartoszewicz, Discrete-time Quasi-sliding Mode Control Strategies, IEEE Transaction on Industrial Electronics, Vol.45, No.4, Aug. 1998, 633-637

[103] J. Daafouz, P. Riedinger and C. Iung, Stability Analysis and Control Synthesis for Switched System: A Switched Lyapunov Function Approach, IEEE Transactions on Automatic Control, Vol.47, No.11, Nov. 2002, 1883-1887

[104] N. S. Nise, Control System Engineering, 6th edition, John Wiley & Sons, Inc. 2011

[105] A. Bentayeb, N. Maamri and J. C. Trigeassou, Design of PID Controller for Delayed MIMO Plants using Moments Based Approach, Journal of Electrical Engineering, Vol. 57, No. 6, 2006, 318-328

[106] B. S. Morgan, The Synthesis of Linear Multivariable Systems by State Variable Feedback, IEEE Transactions on Automatic Control, AC-9, 1964, 404-411

[107] W. H. Wang, Z. S. Hou and S. T. Jin, Model-free Indirect Adaptive Decoupling Control for Nonlinear DiscreteTime MIMO Systems, Joint 48th IEEE Conference on Decision and Control and 28th Chinese Control Conference, Shanghai, P.R. China, Dec. 16-18, 2009

[108] M. H. Amin and M. Moness, Design of precompensators via infinite-zero structure for dynamic decoupling of linear invertible systems, International Journal of Control, Vol. 47, No. 4, 1988, 993-1009

[109] M. Moness and M. H. Amin, Minimal-order precompensators for decoupling linear multivariable systems S (A, B, C, E), International Journal of Control, Vol. 47, No. 6, 1988, 1925-1936

[110] C. A. Lin and C. M. Wu, Block Decoupling Control of Linear Multivariable Systems, Asian Journal of Control, Vol. 1, No. 3, Sep. 1999, 146-152

[111] K. J. Astrom, K. H. Johansson and Q. G. Wang, Design of Decoupled PID Controllers for MIMO Systems, Proceedings of the American Control Conference 2001, Arlington, VA, USA, 2015-2020

[112] O. Härkegård, Resolving Actuator Redundancy-Control Allocation vs. Linear Quadratic Control, ECC' 03, Cambridge, UK, Feb. 2004

[113] O. Härkegård and S. Torkel Glad, Resolving Actuator Redundancy-Optimal Control vs. Control Allocation, Automatica (2005) 41: 137-144

[114] R. Brinkerhoff and S. Devasia, Output Tracking for Actuator Deficient/Redundant Systems: Multiple Piezoactuator Example, J. Guidance, Vol.23, No.2: Engineering Notes, Oct. 1999

[115] D. Liberzon and A. S. Morse, Basic Problems in Stability and Design of Switched Systems, IEEE Control System Magazine, Vol.19, No.5, Oct. 1999, 59-70

[116] M. S. Branicky, Stability of Switched and Hybrid Systems, Proceedings of the 33rd

Conference on Decision and Control, Lake Buena Vista, FL, Dec. 1994

[117] H. Ishii and B. A. Francis, Stabilizing a Linear System by Switching Control with Dwell Time, Proceedings of the American Control Conference, Arlington, VA, June 25-27, 2001

[118] H. Lin and P. J. Antsaklis, Stability and Stabilizablility of Switched Linear Systems: A survey of Recent Results, IEEE Transactions on Automatic Control, Vol.54, No.2, Feb. 2009, 308-322

[119] W. W. Shang, S. Cong and S. L. Jiang, Coordination Control of Parallel Manipulators with Actuation Redundancy, Joint 48th IEEE Conference on Decision and Control and 28th Chinese Control Conference, Shanghai, P.R. China, December 16-18, 2009

[120] R. Garrido and D. Torres-Cruz, On PD Control of Parallel Robots with Redundant Actuation, 1st International Conference on Electrical and Electronics Engineering, 2004

[121] L. Zaccarian, On Dynamic Control Allocation for Input-Redundant Control Systems, Proceedings of the 46th IEEE Conference on Decision and Control, New Orleans, LA, USA, Dec. 12-14, 2007

[122] T. I. Fossen, A Survey of Control Allocation Methods for Ships and Underwater Vehicles, 14th Mediterranean Conference on Control and Automation, Ancona, Italy, June 2006

[123] M. Rakotondrabe, Y. Haddab and P. Lutz, Development, Modeling and Control of a Micro-/Nano-positioning 2-DOF Stick-Slip Device, IEEE/ASME Transactions on

Mechatronics, Vol.14, No.6, Dec. 2009, 733-745

[124] J. W. Li, X. B. Chen and W. J. Zhang, A New Approach to Modeling System Dynamics ─ In the Case of a Piezoelectric Actuator with a Host System, IEEE/ASME Transactions on Mechatronics, Vol.15, No.3, June 2010, 371-379

[125] S. Bashash and N. Jalili, Robust Adaptive Control of Coupled Parallel Piezo-Flexural Nano-positioning Stages, IEEE/ASME Transactions on Mechatronics, Vol. 14, No. 1, Feb. 2009, 11-20

[126] U. X. Tan, T. L. Win, Y. S. Cheng, C. N. Riviere and T. A. Wei, Feedforward Controller of III-Conditioned Hysteresis Using Singularity-Free Prandtl-Ishlinskii Model, IEEE/ASME Transactions on Mechatronics, Vol. 14, No. 5, Oct. 2009, 598-605

[127] F. Ikhouane, J. E. Hurtado and J. Rodellar, Variation of the Hysteresis Loop with the Bouc-Wen model Parameters, Nonlinear Dynamic (2007) 48:361-380

[128] O. G. Bellmunt and F. Ikhouane, Modeling and Verification of a Piezoelectric actuator, Electrical Engineering (2007) 89: 629-638

[129] R. F. Fung and W. C. Lin, System identification of a novel 6-DOF precision positioning table, Sensors and actuators (2009) A150: 286-295

[130] J. Y. Peng and X. B. Chen, Modeling Piezoelectric-Driven Stick-Slip Actuators, IEEE/ASME Transactions on Mechatronics, Vol.16, No.2, April 2011, 394-399

[131] A. Bartoszewicz, Discrete-Sliding Mode Control Strategies, IEEE Transactions on Industrial Electronics, Vol.45, No.4, Aug. 1998, 633-637

[132] Y. Lin, Y. Shi and R. Burton, Modeling and Robust Discrete-time Sliding Mode

Control Design for a Fluid Power Electrohydraulic Actuator System, IEEE/ASME Transactions on Mechatronics, Vol. 18, No. 1, Feb. 2013, 1-10

[133] J. L. Chang, Combing State Estimator and Disturbance Observer in Discrete-time Sliding Mode Controller Design, Asian Journal of Control, Vol. 10, No. 5, Sep. 2008, 515-524

[134] Y. Cao and X. B. Chen, Integrated Inversion-Feedforward and PID-based Sliding Mode Control for Piezoelectric Actuators, American Control Conference, Montreal, Canada, Jun. 27-29, 2012

[135] S. S. Hu, Principles of Automatic Control, National Defence Industry Press of China, Third-edition, 1994

[136] Y. Cao and X. B. Chen, A Novel Discrete ARMA-based Model for Piezoelectric Actuator Hysteresis, IEEE Transactions on Mechatronics, Vol. 17, No. 4, Aug. 2012, 737-744

[137] H. Zhang, Y. Shi, A. S. Mehr and H. Huang, Robust H-infinity PID control for multivariable networked control systems with disturbance/noise attenuation, International Journal of Robust and Nonlinear Control, Vol. 22, No. 2, Jan. 2012, 183-204

[138] J. Y. Peng and X. B. Chen, H_2 optimal Digital Control of Piezoelectric Actuators, Proceedings of the 8th World Congress on Intelligent Control and Automation, Jinan, China, July 6-9, 2010

[139] Y. Cao, L. Cheng, X. B. Chen and J. Y. Peng, An inversion-based model predictive

control with an integral-of-error state variable for piezoelectric-actuators, IEEE Transactions on Mechatronics, Vol. 18, No. 3, June 2013, 895-904

[140] B. K. Kim and W. K. Chung, Advanced Disturbance Observer Design for Mechanical Positioning Systems, IEEE Transactions on Industrial Electronics, Vol. 50, No. 6, Dec. 2003, 1207-1216

[141] J. Y. Peng and X. B. Chen, Integrated PID-based Sliding Mode State Estimation and Control for Piezoelectric-actuators, IEEE/ASME Transactions on Mechatronics, Accepted for publication.

[142] Q. G. Wang, Decoupling Control, Springer, 2003

[143] H. S. Kim and Y. M. Cho, Design and modeling of a novel 3-DOF precision micro-stage, Mechatronics (2009) 19: 598-608

[144] R. Banning, W. L. de Koning, H. J. M. T. A. Adriaens and R. K. Koops, State-Space Analysis and Identification for a Class of Hystersis Systems, Automatica (2001) 37: 1883-1892

[145] R. Johansson, A. Robertsson, K. Nilsson and M. Verhaegen, State-Space System Identification of Robot Manipulator Dynamics, Mechatronics (2001) 10: 403-418

[146] M. Viberg, Subspace-based State-Space System Identification, Circuits Systems Signal Processing, Vol. 21, No. 1, 2002, 23-37

[147] Hüseyin Akçay, Frequency Domain Subspace-based Identification of Discrete-time Power Spectra from Uniformly Spaced Measurement, Automatica (2011) 47: 363-367

[148] S. D. M. Borjas and C. Garcia, Subspace Identification for Industrial Process, TEMA Tend. Mat. Apl. Comput., 12, No. 3, 2011, 183-194

[149] J. N. Juang, M. Phan, L. G. Horta and R. W. Longman, Identification of Observer/Kalman Filter Markov Parameters: Theory and Experiments, NASA Technical Memorandum 104069

[150] R. K. Lim, M. Q. Phan and R. W. Longman, State-Space System Identification with Identified Hankel Matrix, Department of Mechanical and Aerospace Engineering Technical Report No. 3045, Princeton University, Princeton, NJ, Sep. 1998

[151] A. Woronko, J. Huang and Y. Altintas, Piezoelectric Tool Actuators for Precision Maching on Conventional CNC Turning Centers, Precision Engineering (2003) 27: 335-345

[152] L. Hsu, R. R. Costa and J. P. V. S. da Cunha, Model-reference Output-feedback Sliding Mode Controller for a Class of Multivariable Nonlinear Systems, Asian Journal of Control, Vol. 5, No. 4, Dec. 2003, 543-556

[153] B. C. Toledo, S. D. Gennaro, A. Loukianov and J. R. Dominguez, Sliding Mode Output Regulation for Induction Motors, Proceedings of the 13th Mediterranean Conference on Control and Automation, Limassol, Cyprus, Jun. 27-29, 2005

[154] J. L. Chang, Robust Output Regulation using Error Feedback Dynamic Sliding Mode Control, Proceedings of 2006 CACS Automatic Control Conference, St. John's University, Tamsui, Taiwan, Nov. 10-11, 2006

[155] J. Mozaryn, J. E. Kurek, Design of Decoupled Sliding Mode Control for the

PUMA 560 Robot Manipulator, Proceedings of the Third International Workshop on Robot Motion and Control, Warszawa, Poland, Nov. 9-11, 2002

[156] B. B. Goeree, E. D. Fasse, M. J. L. Tiernego and J. F. Broenink, Sliding Mode Control of Spacial Mechanical Systems Decoupling Translation and Rotation, Proceedings of the ASME Dynamics Systems and Control Division, ASME DSC, Vol. 61, 545-554

[157] J. C. Shen, W. U. Jywe, C. H. Liu, Y. T. Jian and J. Yang, Sliding Mode Control of a Three-Degrees-of-Freedom Nanopositioner, Asian Journal of Control, Vol. 10, No. 3, May 2008, 267-276

[158] B. J. Kenton and K. K. Leang, Design and Control of a Three-Axis Serial-Kinematic High-Bandwidth Nanopositioner, IEEE Transactions on Mechatronics, Vol.17, No. 2, Apr. 2012, 356-369

[159] R. Merry, M. Uyanik, R. van de Molengraft, R. Koops, M. van Veghel and M. Steinbuch, Identification, Control and Hysteresis Compensation of A three-DOF Metrological AFM, Asian Journal of Control, Vol. 11, No. 2, Mar. 2009, 130-143

[160] K. Abidi, Sliding Mode Control for High Precision Motion Control Systems, Master Thesis, Sabanci University, Spring 2004

[161] J. Y. Dong, S. M. Salapaka and P. M. Ferreira, Robust MIMO Control of a Parallel Kinematics Nano-positioner for High Resolution High Bandwidth Tracking and Repetitive Tasks, Proceedings of the 46th IEEE Conference on Decision and Control, New Orleans, LA, USA, Dec. 12-14, 2007

[162] Y. Wu and Q. Z. Zou, Robust Inversion-based 2DOF Control Design for Output Tracking: Piezoelectric Actuator Example, Proceedings of the 46th IEEE Conference on Decision and Control, New Orleans, LA, USA, Dec 12-14 2007

[163] T. H. Ho and K. K. Ahn, Speed Control of a Hydraulic Pressure Coupling Drive Using an Adaptive Fuzzy Sliding Mode Control, IEEE/ASME Transactions on Mechatronics, Vol. 17, No. 5, Oct. 2012, 976-986

[164] X. Song and Z. Sun, Pressured-Based Clutch Control for Automotive Transmissions Using a Sliding Mode Controller, IEEE/ASME Transactions on Mechatronics, Vol.17, No. 3, Jun. 2012, 534-546

[165] W. Wu and Z. M. Bai, Sliding Mode Control based on Disturbance Observer for Servo System, The 2nd International Conference on Computer and Automation Engineering (ICCAE), Feb. 26-28, 2010

[166] B. A. Güvenç, L. Güvenç and S. Karaman, Robust MIMO Disturbance Observer Analysis and Design with Application to Active Car Steering, International Journal of Robust and Nonlinear Control (2010) 20: 873-891

[167] K. Abidi and A. Šabanovic, Sliding Mode Control for High-Precision Motion of a Piezostage, IEEE Transactions on Industrial Electronics, Vol.53, No.6, Dec. 2006, 1-9

[168] D. F. Li and H. Gutierrez, Observer-based Sliding Mode Control of a 6-DOF Precision Maglev Positioning Stage, The 34th IEEE Annual Conference on Industrial Electronics, Nov. 10-13, 2008

[169] S. Y. Dian, Y. Arai and W. Gao, Dynamic Compensation of Modeling

Uncertainties and Disturbance of a Precision Planar Motion Stage based on Sliding Mode Observer, International Journal of Advanced Manufacturing Technology (2010) 46: 899-912

Copyright permission

The papers in this thesis have been submitted for for review. At the time of the publication of this thesis, the papers "A Novel Discrete ARMA-based Model for Piezoelectric Actuator Hysteresis" and "State Space System Identification of three-DOF Piezo-actuator Driven Stages with Unknown Configuration" have been accepted for final publication, but contents of the remaining manuscripts will change in accordance to the reviewers' comments and hence will not necessarily be in the same form as appears here. Regardless, permission to include these submitted manuscripts has been sought and responses from the publishers are appended. Where copyright issues have been raised, permission to include in the thesis, the paper has been given.

The permissions by E-mail responses from each publisher are included as follows:

Dear Dr. Cao,

Thanks for your inquiry. Actuators is an open access journal and does not hold the copyright of published paper but only has license granted by the authors to publish papers. The authors of Actuators hold the copyright and do not need permission to reuse the material in the paper.

Kind regards,

Mary Fan

Managing Editor

On 3/20/2013 3:08 AM, Yu Cao wrote:

Dear Editor,

I am writing my Ph.D dissertation. Could you give me the permission to add this paper to one of the charpters in the thesis? I will appreciate it very much.

Regards,

Yu Cao

On 3/4/2013 2:44 AM, Mary Fan wrote:

Dear Dr. Cao,

We are pleased to inform you that the following paper has been officially accepted for publication:

Manuscript ID: actuators-30019

Type of manuscript: Article

Title: System Identification of 3-DOF Piezo-actuator Driven Stages with Unknown Configuration

Authors: Yu Cao *, Xiongbiao Chen

Received: 28 January 2013

E-mails:yuc150@mail.usask.ca,xbc719@mail.usask.ca

Submitted to special issue: Human Centered Actuators,

http://www.mdpi.com/journal/actuators/special_issues/human-centered-actuators/

We will now edit and finalize your paper which will then be returned to

you for your approval within the next couple of days.

Kind regards,

Mary Fan

Assistant Editor

Email:mary.fan@mdpi.com

MDPI Branch Office, Beijing

Actuators Editorial Office

Tel.: +86 10 6280 0830

E-mail:actuators@mdpi.com

http://www.mdpi.com/journal/actuators/

MDPI AG

Kanderstrasse 25, CH-4057 Basel, Switzerland

Tel. +41 61 683 77 34; Fax +41 61 302 89 18

http://www.mdpi.com/

This is not a problemjust put a reference to your submision as Submitted

Sincerely

Eric Rogers

Editor-in-Chief

International Journal of Control

On Tue, 19 Mar 2013 13:14:24 -0600, Yu Cao <yuc150@mail.usask.ca> wrote:

Dear Editor,

I am Yu Cao, the author of the following paper in the International Journal of Control under review:

Y. Cao and X. B. Chen, “Two Modified Discrete PID-Based Sliding Mode Control for Piezoelectric Actuators,” International Journal of Control, 2013, Manuscript ID: TCON-2013-0179

I am writing my Ph.D dissertation. Could you give me the permission to add this paper to one of the charpters in the thesis? I will appreciate it very much.

Regards,

Yu Cao

These are your thesis research. There is no problems using them for your thesis; however, please cite them as there are other authors listed in the papers

From: "Yu Cao" <yuc150@mail.usask.ca>

To: "kokmeng lee" <kokmeng.lee@me.gatech.edu>

Sent: Wednesday, March 20, 2013 3:16:30 AM

Subject: Permission to use

Dear Editor,

I am Yu Cao, the author of the following four papers in IEEE/ASME Transactions on Mechatronics:

Y. Cao and X. B. Chen, "A Novel Discrete ARMA-based Model for Piezoelectric Actuator Hysteresis," IEEE/ASME Transactions on Mechatronics, Vol. 17, No. 4, August 2012, 737-744

Y. Cao, L. Cheng, X. B. Chen and J. Y. Peng, An inversion-based model predictive control with an integral-of-error state variable for piezoelectric-actuators, IEEE/ASME Transactions on Mechatronics, Vol. 18, No. 3, June 2013, 895-904

Y. Cao and X. B. Chen, "An Output Tracking based Discrete PID-Sliding Mode Control on MIMO systems," IEEE/ASME Transactions on Mechatroics, 2013, Under Review, Manuscript ID: TMECH-02-2013-2834

Y. Cao and X. B. Chen, "Disturbance Observer based Sliding Mode Control for a three-DOF Nano-positioning Stage," IEEE/ASME Transactions on Mechatronics, 2012, Under Review, Manuscript ID: TMECH-09-2012-2566.R1

I am writing my Ph.D dissertation. Could you give me the permission to add these papers to four of the chapters in the thesis? I will appreciate it very much.

Regards,

Yu Cao